THE UNIVERSITY OF MICHIGAN

INDUSTRY PROGRAM OF THE COLLEGE OF ENGINEERING

THE EFFECT OF AXIAL TURBULENCE PROMOTERS ON HEAT TRANSFER AND PRESSURE DROP INSIDE A TUBE

Lawrence B. Evans

A dissertation submitted in partial fulfillment
of the requirements for the degree of
Doctor of Philosophy in the
University of Michigan
Department of Chemical and Metallurgical Engineering
1962

June, 1962

IP-570

ACKNOWLEDGMENTS

The author wishes to express his appreciation to the following individuals and organizations for their contributions.

Professor Stuart W. Churchill, chairman of the committee, for his interest, encouragement, and for his wholehearted and prompt cooperation on every occasion.

Professor John A. Clark for his many suggestions concerning the experimental technique and for his generously allowing the complete use of the facilities of the Heat Transfer and Thermodynamics Laboratory of the Department of Mechanical Engineering.

Dr. Robert R. White (Atlantic Refining Company) for initially suggesting the topic and serving as chairman of the committee during the first part of the investigation.

The other members of the doctoral committee for their advice, encouragement, and willingness to be of help at any time.

Professor Julius T. Banchero for serving on the committee during the early phases of the work.

The staff of the Department of Chemical and Metallurgical Engineering and the staff of the Heat Transfer and Thermodynamics Laboratory of the Department of Mechanical Engineering for their assistance during all phases of the work.

The Industry Program of the College of Engineering for the preparation of the dissertation.

The Procter and Gamble Company for their fellowship during the academic year 1956-57.

The Continental Oil Company for their fellowship during the academic year 1957-58.

The University of Michigan for its fellowship during the academic year 1958-59.

TABLE OF CONTENTS

	Page
ACKNOWLEDGMENTS	ii
LIST OF TABLES	vi
LIST OF FIGURES	vii
NOMENCLATURE	xiii
ABSTRACT	xxii
INTRODUCTION	1
THEORETICAL CONSIDERATIONS AND PREVIOUS WORK	5
Mathematical Statement of the General Problem	5
Dimensional Analysis	6
Pressure Drop of Turbulence Promoters Based on Drag of a Single Bluff Body	7
Review of Previous Work	9
EXPERIMENTAL APPARATUS AND PROCEDURE	26
Description of the Equipment	26
Description of Turbulence Promoters	33
Description of the Procedure	40
Method of Calculating Heat Transfer Coefficients	44
Method of Calculating Friction Factors	47
EXPERIMENTAL RESULTS AND DISCUSSION OF RESULTS	50
Empty Tube	50
Solid Rod in the Center of the Tube	55
Disks Evenly Spaced and Centered in the Tube	65
Streamline Shapes Evenly Spaced and Centered in the Tube	88
Reliability of the Data for all Geometries	102
ECONOMICS	111
Mathematical Model of a Heat Exchanger	111
Factors Which Affect the Economics	114
Procedure for Designing the Optimum Heat Exchanger	116
Example Design of a Typical Heat Exchanger	123
Conclusions Regarding the Economics of Using Turbulence Promoters	130
SUMMARY AND CONCLUSIONS	139
BIBLIOGRAPHY	143

TABLE OF CONTENTS (continued)

	Page
APPENDICES.	146
APPENDIX A - DESCRIPTION OF COMPUTER TECHNIQUES FOR PROCESSING DATA.	146
APPENDIX B - DERIVATIONS.	168
APPENDIX C - ORIGINAL AND PROCESSED DATA.	202
APPENDIX D - CALCULATIONS REQUIRED FOR EXAMPLE HEAT EXCHANGER DESIGN.	217

LIST OF TABLES

Table		Page
I	FUNCTIONS F(d), G(d), AND H(d) USED IN EQUIVALENT FRICTION FACTOR CORRELATIONS FOR ANNULI..................	14
II	POSITION OF THERMOCOUPLES ON TEST SECTION RELATIVE TO OTHER ITEMS..	32
III	BLUFF-BODY TURBULENCE PROMOTER COMBINATIONS USED IN THIS INVESTIGATION..	39
IV	THERMOCOUPLE EMF vs. DEGREES CENTIGRADE FOR COPPER-CONSTANTAN THERMOCOUPLES................................	147
V	FIRST THREE ROOTS λ_i OF EQUATION (B-72) AND ASSOCIATED VALUES OF ξ_i FOR b/a = 1.100, 1.2418, AND 1.5000.........	187
VI	THE FUNCTION $\Lambda(\lambda_n, r/a)$ FOR b/a = 1.100, 1.2418, AND 1.500 AS A FUNCTION OF (r - a)/(b - a)..................	188
VII	SUMMARY OF EXPERIMENTAL CONDITIONS......................	205
VIII	CONSTANTS C(s,d) AND n(s,d) USED IN FRICTION FACTOR CORRELATION EQUATION (64) FOR INDIVIDUAL PROMOTER COMBINATIONS..	206
IX	CONSTANTS C(s,d) AND n(s,d) USED IN CORRELATION EQUATION (65) OF EFFECTIVE DRAG COEFFICIENT FOR INDIVIDUAL PROMOTER COMBINATIONS..........................	207
X	CONSTANTS C(s,d) AND n(s,d) USED IN CORRELATION EQUATION (67) OF MEAN HEAT TRANSFER COEFFICIENTS FOR INDIVIDUAL PROMOTER COMBINATIONS..........................	208
XI	PRESSURE DROP RESULTS....................................	209 210 211
XII	INTEGRATED RESULTS FROM HEAT TRANSFER MEASUREMENTS.......	212
XIII	LOCAL HEAT TRANSFER MEASUREMENTS.........................	213 214 215 216

LIST OF FIGURES

Figure		Page
1	Cross-Section of Tube with Bluff Body Turbulence Promoter Inserted to Illustrate the Difference Between Disk and Streamline Shape........................	4
2	Comparison of Friction Factor Correlations for Annuli, Ratio of ΔP Predicted by Correlations to ΔP Calculated Using Blasius Equation and Hydraulic Radius vs. Diameter Ratio d, for Re = 10,000, 20,000 and 40,000..	16
3	Photograph of Overall View of Equipment.................	27
4	Photograph of Closeup of Test Section...................	27
5	Photograph of Thermocouple Switches and Recording Potentiometer..	27
6	Schematic Diagram of the Apparatus......................	28
7	Diagram of the Test Section.............................	30
8	Diagram of Disk and Streamline Shape Showing Relative Dimensions and Method of Mounting........................	36
9	Photograph of Individual Turbulence Promoter Shapes Used...	37
10	Photograph of a String of Disks and a String of Streamline Shapes......................................	37
11	Friction Factor for the Empty Tube as a Function of Reynolds Number, f vs. Re...............................	51
12	Sample Values of the Local Heat Transfer Coefficients for the Empty Tube as a Function of Longitudinal Position, h(z) vs. z..................................	52
13	Nusselt Number for the Empty Tube as a Function of Reynolds Number, $Nu/(Pr^{1/3}(\mu/\mu_w)^{0.14})$ vs. Re.............	54
14	Friction Factor for the Tube with a Solid Rod in the Center as a Function of Reynolds Number, f vs. Re, with Parameters of d..................................	56
15	Friction Factor for the Tube with a Solid Rod in the Center as a Function of Reynolds Number, Based on Equivalent Diameters, f* vs. Re*.......................	57

Figure Page

16 Sample Values of the Local Heat Transfer Coefficient for a Tube with a Threaded Rod in the Center as a Function of Longitudinal Position, h(z) vs. z, for d = 0.250 59

17 Sample Values of the Local Heat Transfer Coefficient for a Tube with a Solid Rod in the Center as a Function of Longitudinal Position, h(z) vs. z, for d = 0.625 60

18 Sample Values of the Local Heat Transfer Coefficient for a Tube with a Solid Rod in the Center as a Function of Longitudinal Position, h(z) vs. z, for d = 0.750 61

19 Nusselt Numbers for the Tube with a Solid Rod in the Center as a Function of Reynolds Number, Nu vs. Re, with Parameters of d 63

20 Nusselt Number for the Tube with a Solid Rod in the Center as a Function of Reynolds Number Based on Equivalent Diameters, $Nu^*/Pr^{1/3}[\mu/\mu_w]^{0.14}$ vs. Re* 64

21 Friction Factor for Disks as a Function of Reynolds Number, f vs. Re, for s = 2 with Parameters of d 66

22 Friction Factor for Disks as a Function of Reynolds Number, f vs. Re, for s = 4 with Parameters of d 67

23 Friction Factor for Disks as a Function of Reynolds Number, f vs. Re, for s = 8 with Parameters of d 68

24 Friction Factor for Disks as a Function of Reynolds Number, f vs. Re, for s = 12 with Parameters of d 69

25 Effective Drag Coefficient for Disks as a Function of Reynolds Number, f_D vs. Re, for s = 12, 8, 4, and 2 with Parameters of d 71

26 Effective Drag Coefficient for Disks as a Function of Free Area, f_D vs. A_f, for s = 12, 8, 4, and 2 with Parameters of Re 72

27 Effective Drag Coefficient for Disks as a Function of Spacing, f_D vs. s, for d = 0.625, 0.750, and 0.875 and Any Reynolds Number 73

LIST OF FIGURES (continued)

Figure		Page
28	Test of Effective Drag Coefficient Correlation, f_D Values Predicted by Correlation vs. Values Measured Experimentally for Disks and Streamline Shapes	75
29	Sample Values of Local Heat Transfer Coefficient Ratio for Disks as a Function of Longitudinal Position from Disk with Reynolds Number Approximately 10,000, h/h_0 vs. x, for d = 0.625, 0.750, and 0.875	77
30	Overall Mean Heat Transfer Coefficient Ratio for Disks as a Function of Reynolds Number, h_m/h_0 vs. Re, for s = 12, 8, 4, and 2 with Parameters of d	80
31	Overall Mean Heat Transfer Coefficient Ratio for Disks as a Function of Free Area, h_m/h_0 vs. A_f, for s = 12, 8, 4, and 2 with Parameters of Re	82
32	Overall Mean Heat Transfer Coefficient Ratio for Disks as a Function of Spacing, h_m/h_0 vs. s, for Re = 10,000, 20,000, and 40,000 with Parameters of d	83
33	Test of Heat Transfer Correlation, h_m/h_0 Ratios Predicted by Correlation vs. Values Measured Experimentally for Disks and Streamline Shapes	85
34	Friction Factor for Streamline Shapes as a Function of Reynolds Number, f vs. Re, for s = 4 with Parameters of d	89
35	Friction Factor for Streamline Shapes as a Function of Reynolds Number, f vs. Re, for s = 8 with Parameters of d	90
36	Friction Factor for Streamline Shapes as a Function of Reynolds Number, f vs. Re, for s = 12 with Parameters of d	91
37	Effective Drag Coefficient for Streamline Shapes as a Function of Reynolds Number, f_D vs. Re, for s = 12, 8, and 4 with Parameters of d	93
38	Effective Drag Coefficient for Streamline Shapes as a Function of Free Area, f_D vs. A_f, for s = 12, 8, and 4 with Parameters of Re	94

LIST OF FIGURES (continued)

Figure		Page
39	Effective Drag Coefficient for Streamline Shapes as a Function of Spacing, f_D vs. s, for d = 0.625, 0.750, and 0.875 with Parameters of Re..................	95
40	Sample Values of Local Heat Transfer Coefficient Ratio for Streamline Shapes as a Function of Longitudinal Position from Shape with Reynolds Number Approximately 10,000, h/h_0 vs. x, for d = 0.625, 0.750, and 0.875....	97
41	Overall Mean Heat Transfer Coefficient Ratio for Streamline Shapes as a Function of Reynolds Number, h_m/h_0 vs. Re, for s = 12, 8, 4, and 0 with Parameters of d..	98
42	Overall Mean Heat Transfer Coefficient Ratio for Streamline Shapes as a Function of Free Area, h_m/h_0 vs. A_f, for s = 12, 8, 4, and 0 with Parameters of Re...	100
43	Overall Mean Heat Transfer Coefficient Ratio for Streamline Shapes as a Function of Spacing, h_m/h_0 vs. s, for Re = 10,000, 20,000, and 40,000 with Parameters of d..	101
44	Frequency Distribution of Heat Balance Errors...........	107
45	Frequency Distribution of Difference Between Local Angular ΔT and Mean ΔT for all Three Angles for Streamline Shapes..	109
46	Frequency Distribution of Difference Between Local Angular ΔT and Mean ΔT for all Three Angles for Disks...	109
47	Illustration of Heat Exchanger Costs for a Given Geometry and Tube Diameter as a Function of Nusselt Number...	121
48	Fixed Cost, Pumping Cost, and Total Cost per BTU as a Function of Nusselt Number for Example Heat Exchanger Design Using an Empty Tube Geometry, Parameters of d..	126
49	Fixed Cost, Pumping Cost, and Total Cost per BTU as a Function of Nusselt Number for Example Heat Exchanger Design Using Turbulence Promoters with D = 0.50 inch..	129

Figure		Page
50	Ratio of Pumping Cost for Disks to Pumping Cost for Empty Tube as a Function of Nusselt Number, $(E/Q)/(E/Q)_{ET}$ vs. Nu for s = 12, 8, 4, and 2 with Parameters of d.	131
51	Ratio of Pumping Cost for Streamline Shapes and Solid Rod to Pumping Cost for Empty Tube as a Function of Nusselt Number, $(E/Q)/(E/Q)_{ET}$ vs. Nu for s = 12, 8, 4, and 0 with Parameters of d.	132
52	Flow Rate as a Function of Rotameter Reading, GPM vs. Reading, for Rotameters 1, 2, 3, and 4	149
53	Sample Raw Data Sheet for Pressure Drop Measurements	152
54	Listing of Data Cards for Pressure Drop Measurements of Sample Problem	154
55	Computer Analysis of Pressure Drop Data for Sample Problem	155
56	Raw Data Sheet for Heat Transfer Measurements	157
57	Listing of Data Cards for Heat Transfer Measurements of Sample Problem	159
58	Computer Analysis of Heat Transfer Data for Sample Problem, Pages I, II, III, and IV	160 161
59	Boundary Conditions for Solution of Conduction Equation Considering Axial Conduction into the Non-Heat-Generating Portion of the Tube	179
60	Dimensionless Form of Solution for Axial Conduction into the Non-Heat-Generating Portion of the Tube, Showing that the End Effect is Negligible	186
61	Damping Function Defined by Equation (B-80) as a Function of the Parameter na/S, δ(na/S, b/a) vs. na/S, for b/a = 1.24	190
62	Sample Hypothetical Values of Fluid Temperature and Inside Wall Temperature as a Function of Longitudinal Position, $T_f(y)$ and $T_a(y)$ vs. y for Rapidly Varying Inside Wall Temperature	192

LIST OF FIGURES (continued)

Figure		Page
63	Effect of Neglecting Damping of Outside Wall Temperature When Inside Wall Temperature is Rapidly Varying with Longitudinal Position	192
64	Frequency Distribution of Error Introduced by AZAR Recorder	197

NOMENCLATURE

a	Inside radius of tube, ft.
$\tilde{a}$	Dimensionless inside radius of tube (2a/L) used only in Part 4 of Appendix B
$a_0 \cdots a_3$	Arbitrary constants used in Part 4 of Appendix B and as coefficients of polynomial in Equation (A-17)
A	Total heat transfer surface inside the tubes in a heat exchanger, ft^2
A	Rate of heat generation per unit volume of tube wall, $BTU/hr\text{-}ft^3$
A_0	Expression defined by Equation (53), i.e., rate of heat generation in the tube wall at 0 deg. F, $BTU/hr\text{-}ft^3$
A_2	Term defined by Equation (A-13) used in calculating $\Delta T_{generation}$
A_3	Term defined by Equation (A-14) used in calculating $\Delta T_{generation}$
A_4	Term defined by Equation (A-15) used in caclulating $q(z)$
A_f	Fraction free area at point of maximum radius of promoter, dimensionless
$\tilde{A}_n$	Coefficient in orthogonal function expansion of $g(\tilde{r})$ used only in Part 4 of Appendix B
A_{tube}	Cross-sectional area of the tube, ft^2
A_p	Projected area of the promoter, ft^2
b	Outside radius of tube, ft.
$\tilde{b}$	Dimensionless outside radius of tube (2b/L) used only in Part 4 of Appendix B
b_1, b_2	Arbitrary constants used in Part 4 of Appendix B
$B_1 \cdots B_3$	Expressions defined by Equations (112), (113), and (114) used to obtain E/Q as a function of Nusselt number from correlations
B_n	Coefficient in Fourier series expansion of hypothetical periodic inside wall temperature, deg. F
c	Heat capacity of fluid, BTU/lb_m - deg. F

NOMENCLATURE (continued)

$C_1 \cdots C_n$	Various constants used in correlations, dimensionless
$C(s,d)$	Constant used in correlations of friction factor, effective drag coefficient, and mean heat transfer coefficient ratio for individual promoter combinations, dimensionless
C_E	Cost per unit pumping energy, dollars/BTU
C_F	Fixed cost proportionality constant (fixed cost = $C_F A^m$), dollars/ ft^{2m}
C_W	Cost of working fluid in heat transfer equipment, dollars/lb_m
d	Ratio of diameter of bluff-body turbulence promoter (at point of maximum diameter) to diameter of tube, dimensionless
D	Inside diameter of tube, ft.
D*	Equivalent tube diameter used in correlations for an annulus, ft.
$\tilde{D}_n$	Coefficient in orthogonal function expansion defined by Equation (B-61) used only in Part 4 of Appendix B
D_p	Diameter of bluff-body promoter at point of maximum diameter, ft.
E	Energy expended in pumping, BTU/hr
E	Electrical potential, volts
E/Q	Ratio of pumping energy to total rate of heat transfer for a specified heat exchanger with specified inside tube geometry (function of Nusselt number), dimensionless
$(E/Q)_{ET}$	Ratio of pumping energy to total rate of heat transfer for a specified heat exchanger using an empty tube geometry (function of Nusselt number), dimensionless
f	Friction factor based on inside tube diameter and superficial velocity as defined by Equation (22), dimensionless
f*	Friction factor based on equivalent diameter D* and true mean velocity in tube, dimensionless
f_0	Friction factor calculated for an empty tube as a function of mass flow rate using Equation (15), dimensionless
f_D	Effective drag coefficient for a single bluff body, dimensionless

$F(d)$	Function used for interpolating graphical equivalent friction factor correlation of Lohrenz and Kurata
$g(\vec{r}), g(y)$	Any arbitrary function
g_c	Gravitational constant, lb_m - ft/lb_f - sec^2
$G(d)$	Function used in friction factor correlation of Meter and Bird, dimensionless
h	Local inside heat transfer coefficient including resistance of tube wall, BTU/hr - deg. F - ft^2
h'	Effective outside heat transfer coefficient including resistance of tube wall, BTU/hr - deg. F - ft^2
h_0	Mean inside heat transfer coefficient for empty tube as calculated from Sieder-Tate equation, BTU/hr - deg. F - ft^2
h_c	Convection coefficient from Fiberglas insulation to air, BTU/hr - deg. F - ft^2
h_m	Mean inside heat transfer coefficient, BTU/hr - deg. F - ft^2
h_m/h_0	Ratio of mean heat transfer coefficient for any inside tube geometry to coefficient for empty tube at same mass flow rate
$h(z)_{est}$	Estimate of local heat transfer coefficient for empty tube geometry or tube with solid rod which considers change in physical properties of fluid. Defined by Equation (63), BTU/hr - deg. F - ft^2
$H(d)$	Function used in friction factor correlation of Meter and Bird, dimensionless
I	Electric current, amps
$I_0(x)$	Modified Bessel function of the first kind and order zero
$I_1(x)$	Modified Bessel function of the first kind and order one
J	Electric current density in tube wall, amps/ft^2
$J_0(x)$	Bessel function of the first kind and order zero
$J_1(x)$	Bessel function of the first kind and order one
J_c	Conversion factor (777.5 ft - lb_f/BTU)

k	Thermal conductivity of fluid, BTU/hr - deg. F - ft
K	Thermal conductivity of tube wall, BTU/hr - deg. F - ft
K_0	Thermal conductivity of tube wall at 0 deg. F, BTU/hr - deg. F - ft
K_b	Thermal conductivity of tube wall evaluated at the outside wall temperature, BTU/hr - deg. F - ft
K_{fg}	Thermal conductivity of Fiberglas insulation, BTU/hr - deg. F - ft
K_{mica}	Thermal conductivity of mica insulation, BTU/hr - deg. F - ft
$K_0(x)$	Modified Bessel function of the second kind and order zero
$K_1(x)$	Modified Bessel function of the second kind and order one
L	Length of heated portion of tube, ft
L_p	Distance between pressure taps for experimental apparatus, ft
m	Slope of steady temperature increase in fluid and inside wall temperature ($m = Q/WcL$), deg. F/ft
m	Exponent of inside surface area such that fixed heat exchanger cost is proportional to A^m, dimensionless
$n(s,d)$	Exponent used in correlations of friction factor, effective drag coefficient, and mean heat transfer coefficient ratio for individual promoter combinations, dimensionless
n_1, n_2	Exponents used in various correlations, dimensionless
n_p	Number of individual bluff bodies contained in string of turbulence promoters, dimensionless
N_{tube}	Number of tubes in parallel in a shell and tube heat exchanger, dimensionless
Nu	Nusselt number, dimensionless
Nu^*	Nusselt number based on equivalent diameter, dimensionless
$Nu_{optimum}$	Value of Nusselt number for which the total cost of a heat exchanger is lowest, dimensionless

p	Exponent of Nusselt number defined by Equation (111) used to obtain (E/Q) as a function of Nu from correlations, dimensionless
P	Local fluid pressure, lb_f/ft^2
ΔP	Longitudinal pressure drop between pressure taps, lb_f/ft^2
ΔP_{form}	Pressure drop due to form drag of individual bluff body which would be present if there were no drag on the tube wall, lb_f/ft^2
ΔP_{total}	Total pressure drop caused by both form drag and drag of the tube wall, lb_f/ft^2
ΔP_{tp}	Pressure drop occurring along length (n_pS) occupied by string of turbulence promoters (estimated by Equation (61)), lb_f/ft^2
ΔP_{ET}	Pressure drop due to drag on the tube wall that would be present without turbulence promoters, lb_f/ft^2
Pr	Prandtl number, dimensionless
Pr_m	Overall mean value of Prandtl number obtained by integrating local Prandtl number Pr_z over length of tube, dimensionless
Pr_z	Prandtl number of fluid flowing in tube evaluated at local mixed-mean fluid temperature, dimensionless
q	Local rate of heat transfer per unit area, BTU/hr - ft^2
q_L	Heat loss per unit area of outside tube wall through insulation, BTU/hr - ft^2
Q	Total rate of heat transfer, BTU/hr
Q_{in}	Total rate of heat input to tube by generation in tube wall as calculated using Equation (70), BTU/hr
Q_{out}	Total rate of heat removal by water as calculated using Equation (71), BTU/hr
r	Radial distance from center of tube, ft.
$\tilde{r}$	Dimensionless radial distance (2r/L) used only in Part 4 of Appendix B
r_{ins}	Outside radius of Fiberglas insulation, ft.
R	Electrical resistance, ohms

NOMENCLATURE (continued)

R_p	Radius of turbulence promoter, ft.
Re	Reynolds number, dimensionless
Re_m	Overall mean value of Reynolds number obtained by integrating local Reynolds number Re_z over length of tube, dimensionless
Re_z	Reynolds number of fluid flowing in tube evaluated at local mixed-mean fluid temperature, dimensionless
Re*	Reynolds number based on equivalent diamter and true mean velocity, dimensionless
$\mathcal{R}, \mathcal{R}_+, \mathcal{R}_-, \mathcal{R}_0$	Dummy variables used only in Part 4 of Appendix B
s	Ratio of spacing between promoters to tube diameter, dimensionless
S	Spacing between turbulence promoters, ft.
t_{mica}	Thickness of mica insulation, ft.
T	Temperature, deg. F
$\tilde{T}$	Dimensionless temperature ($4KT/L^2A_0$) used only in Part 4 of Appendix B
$\tilde{T}_I$	Solution in Region I (the heat-generating zone) of the conduction equation which accounts for axial conduction into the non-heat-generating portion of the tube, dimensionless
$\tilde{T}_{II}$	Solution in Region II (the non-heat-generating zone) of the conduction equation which accounts for axial conduction into the non-heat-generating portion of the tube, dimensionless
T_a	Temperature at inside tube wall, deg. F
T_{amb}	Ambient air temperature, deg. F
T_b	Temperature at outside radius of tube, deg. F
T_{inlet}	Mixed-mean temperature of the fluid at Z = 0, the inlet of the test section (actually measured at the inlet to the equipment), deg. F
T_f	Mixed-mean temperature of the fluid, deg. F

T_{outlet}	Mixed-mean temperature of the fluid at Z = L, the outlet of the test section (actually measured at the outlet of the equipment), deg. F
T_{tc}	Temperature measured by outside wall thermocouple at outside edge of mica sheet, deg. F
T_{wall}	Temperature at the inside tube wall, deg. F
$\Delta T_{generation}$	Temperature difference between inside and outside wall caused by internal generation of heat, deg. F
ΔT_m	Mean temperature difference which provides driving force for heat transfer, deg. F
ΔT_{max}	Maximum difference between inside wall temperature and fluid temperature for hypothetical, periodic inside wall temperature distribution, deg. F
ΔT_{mean}	Mean difference between inside wall temperature and fluid temperature for hypothetical, periodic inside wall temperature distribution, deg. F
ΔT_{min}	Minimum difference between inside wall temperature and fluid temperature for hypothetical, periodic inside wall temperature distribution, deg. F
$\Delta T_{periodic}$	Hypothetical periodic inside wall temperature, deg. F
$\Delta T'_{periodic}$	Damped component of hypothetical periodic inside wall temperature which would be measured at outside wall, deg. F
u	True mean velocity of fluid, ft/sec
U	Superficial mean velocity of fluid, ft/sec
U_{max}	Mean fluid velocity at point of minimum free area, ft/sec
U_{oa}	Overall heat transfer coefficient defined by Equation (74), BTU/hr - deg. F - ft^2
dV	Infinitesimal volume of tube wall, ft^3
$\tilde{V}, \tilde{V}_1, \tilde{V}_2$	Dummy variables used only in Part 4 of Appendix B, dimensionless
V_r	Local fluid velocity in the radial direction, ft/hr
V_z	Local fluid velocity in the longitudinal direction, ft/hr

NOMENCLATURE (continued)

W	Mass flow rate of fluid, lb_m/hr
x	Ratio of distance from point of maximum diameter of promoter to diameter of tube, dimensionless
X	Distance from first point of maximum radius of turbulence promoter, ft.
y	Distance from center of heated section of tube, ft.
$\tilde{y}$	Dimensionless axial distance from center of heated section (2y/L), used only in Part 4 of Appendix B
y_1, y_2	Two arbitrary longitudinal positions along tube, between which the hypothetical periodic inside wall temperature is expanded in a Fourier series, ft.
$Y_0(x)$	Bessel function of the second kind and order zero
$Y_1(x)$	Bessel function of the second kind and order one
$\mathcal{Y}, \mathcal{Y}_+, \mathcal{Y}_-, \mathcal{Y}_0$	Dummy variables used only in Part 4 of Appendix B
z	Ratio of longitudinal distance from beginning of heating to diameter of tube, dimensionless
Z	Longitudinal distance from beginning of heating, ft.
Z_0	Reference value of longitudinal position at which temperature, pressure, and velocities are known in statement of theoretical problem, ft.
α	Ratio of equivalent diameter to inside diameter of tube (used in correlations for an annulus), dimensionless
β	Rate of change of thermal conductivity of tube wall with temperature, 1/deg. F
γ	Rate of change of electrical resistivity of tube wall with temperature, 1/deg. F
$\delta(na/S, b/a)$	Damping function defined by Equation (B-80), dimensionless
η	Ratio of heat flux at inside wall to heat flux at outside wall of an annulus (in the limiting case of two parallel plates) used in theoretical analysis of Barrow, dimensionless

NOMENCLATURE (continued)

λ_n	Eigenvalues defined by Equation (B-72), dimensionless
$\tilde{\lambda}_n$	Dummy Eigenvalue defined by Equation (B-49) and used only in Part 4 of Appendix B
$\Lambda(\lambda_n, r/a)$	Set of orthogonal functions associated with eigenvalue λ_n and defined by Equation (B-53), dimensionless
μ	Dynamic viscosity of fluid, $lb_m/ft - hr$
μ_w	Viscosity of fluid in tube evaluated at the inside wall temperature, $lb_m/ft - hr$
$(\mu/\mu_w)_m$	Overall mean value of viscosity ratio obtained by integrating local viscosity ratio $(\mu/\mu_w)_z$ over length of tube, dimensionless
$(\mu/\mu_w)_z$	Viscosity ratio of fluid inside tube evaluated at local mixed-mean fluid temperature, dimensionless
ξ_n	Parameter associated with eigenvalue λ_n and defined by Equation (B-73)
ρ	Density of fluid, lb_m/ft^3
$\bar{\rho}$	Electrical resistivity of tube wall, ohm-ft.
$\bar{\rho}_m$	Mean electrical resistivity of tube wall, ohm-ft.
$\bar{\rho}_o$	Electrical resistivity of tube wall at 0 deg. F, ohm-ft
ϕ	$(1 + \gamma T_b)/(1 + \beta T_b)$
$\phi(d)$	Function used in friction factor correlation for annuli by Meter and Bird, dimensionless

INTRODUCTION

In recent years the problem of improving the rate of heat transfer to a fluid flowing in a tube has been a subject of increasing importance. The advent of the nuclear reactor with its large heat flux requirements has demanded the development of improved technique for obtaining high heat transfer rates. The rapid expansion of the chemical process industry has made it necessary to improve the performance of existing equipment for exchanging heat in order to keep plants already built from becoming o bsolete. The exploration of space has created requirements for heat transfer equipment which must both be compact and must consume a minimum of power for operation.

One technique for improving the rate of heat transfer is to insert devices commonly referred to as "turbulence promoters" inside the tube to disturb the flow, enhance the mixing, and thus reduce the resistance to heat transfer. Many types of devices have been suggested for this service including such things as roughening elements attached to the tube wall, twisted metal strips to impart a swirling motion to the fluid, bluff objects in the center of the tube, and packing material.

Unfortunately, any insert which improves the rate of heat transfer by enhancing the mixing also increases the pressure drop, and more energy is required to pump the fluid through the tube. Therefore, in order to determine the economic feasibility of turbulence promoters in a given heat transfer application it is necessary to be able to predict quantitatively the rate of heat transfer and the pressure drop as a function of flow rate, tube diameter, geometry of the turbulence promoters, physical properties of the fluid, and temperature boundary condition at the tube wall.

At the present time the information concerning the effect of turbulence promoters is of insufficient scope and reliability for design purposes. One of the main difficulties in studying turbulence promotion is the large number of possible geometrical configurations. The only promoters that have been systematically varied are twisted metal strips and roughening elements attached to the tube wall.

In particular, little data exist for the effect of bluff objects inside a tube on the pressure drop and the rate of heat transfer from the tube wall to the fluid. There is a particular scarcity of data for local heat transfer coefficients and for fluids other than air. Apparently no previous investigation has considered the effect of streamlining a bluff-body turbulence promoter.

The purpose of this investigation was, therefore, to obtain experimental values of the pressure drop and local rates of heat transfer for bluff-body turbulence promoters, including streamline shapes, in water.

Because of the large number of independent variables, those which were expected to be less significant were fixed. Thus, only one fluid (water); only one tube diameter (one inch inside diameter); and one boundary condition (constant wall heat flux) were utilized. This reduced the problem to a consideration of the geometry of the promoter (shape, diameter, spacing) and flow rate of the fluid. To further simplify the consideration of geometry, only promoters centered in the tube, symmetric about the axis and at uniform spacing were studied.

Thus, the variables considered in this investigation were: flow rate of the fluid, shape of the promoter, ratio of promoter diameter to inside tube diameter, and the ratio of promoter spacing to inside tube diameter. The effect of promoter shape was studied by considering two dissimilar shapes: disks and a streamline body as shown in Figure 1. These shapes represent the two extremes of no streamlining and a great deal of streamlining. Data were also obtained for a solid rod in the center of the tube in an attempt to find out what happens in the limiting case of promoters at zero spacing. Data were obtained with the empty tube for comparison.

An attempt was made to obtain data of sufficient scope and accuracy to enable it to be used for the following purposes:

1. Determine whether bluff-body turbulence promoters can be used economically to improve the rate of heat transfer to a fluid flowing in a tube.

2. Determine whether there is an optimum geometry for the promoter.

3. Obtain correlations to permit the design of turbulence promoters for the most promising geometries.

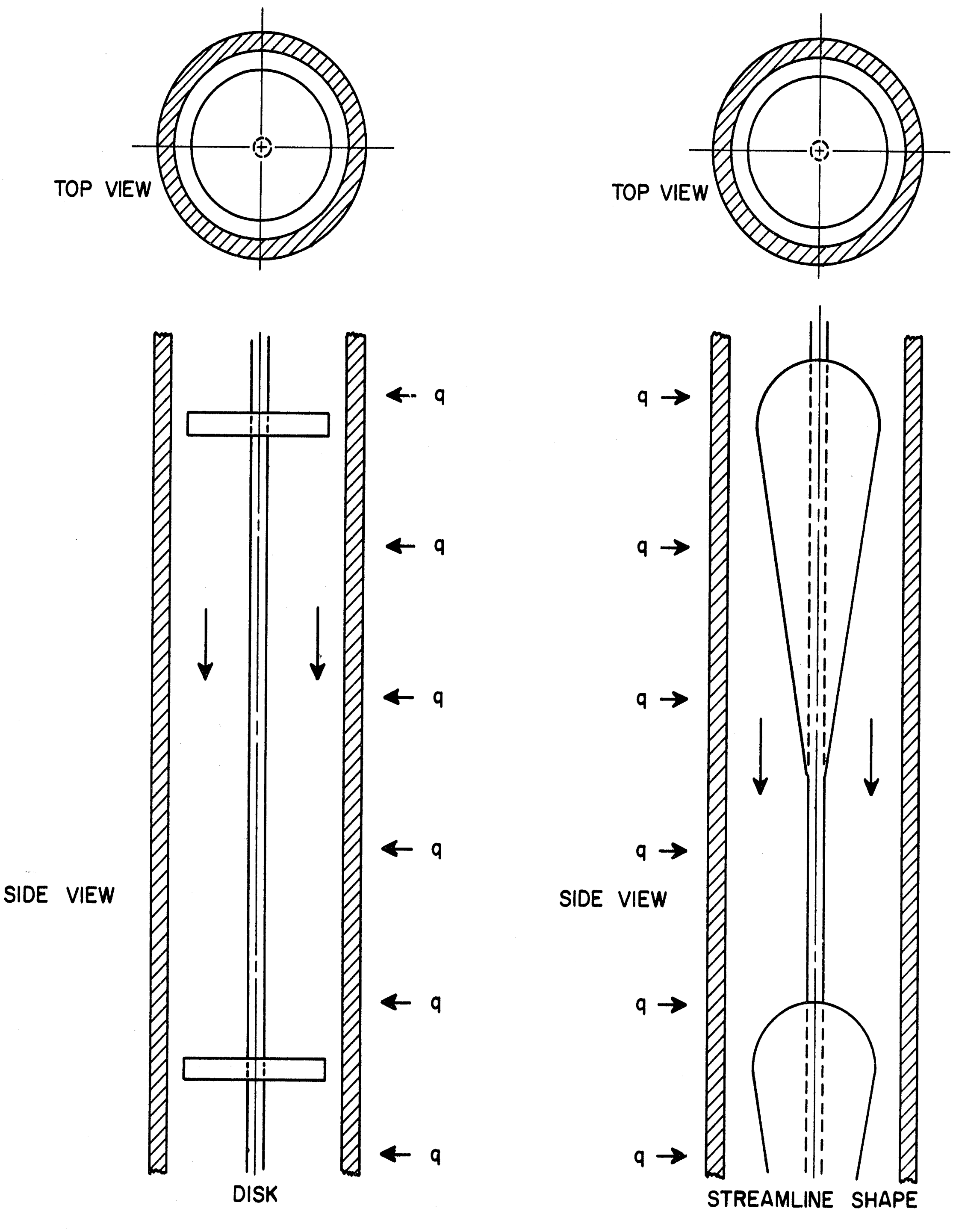

Figure 1. Cross-Section of Tube with Bluff Body Turbulence Promoter Inserted to Illustrate the Difference Between Disk and Streamline Shape.

THEORETICAL CONSIDERATIONS AND PREVIOUS WORK

Mathematical Statement of the General Problem

The mathematical statement of the general problem studied in this investigation is as follows:

A fluid is flowing under steady-state conditions in a cylinder of diameter D in which there are a series of obstructions, symmetric about the axis, evenly spaced at distance S apart. The obstructions as shown below are defined by the equation

$$R_p = R_p(X) \tag{1}$$

where R_p is the radius of the promoter and X is the distance from the first point of maximum radius of the promoter.

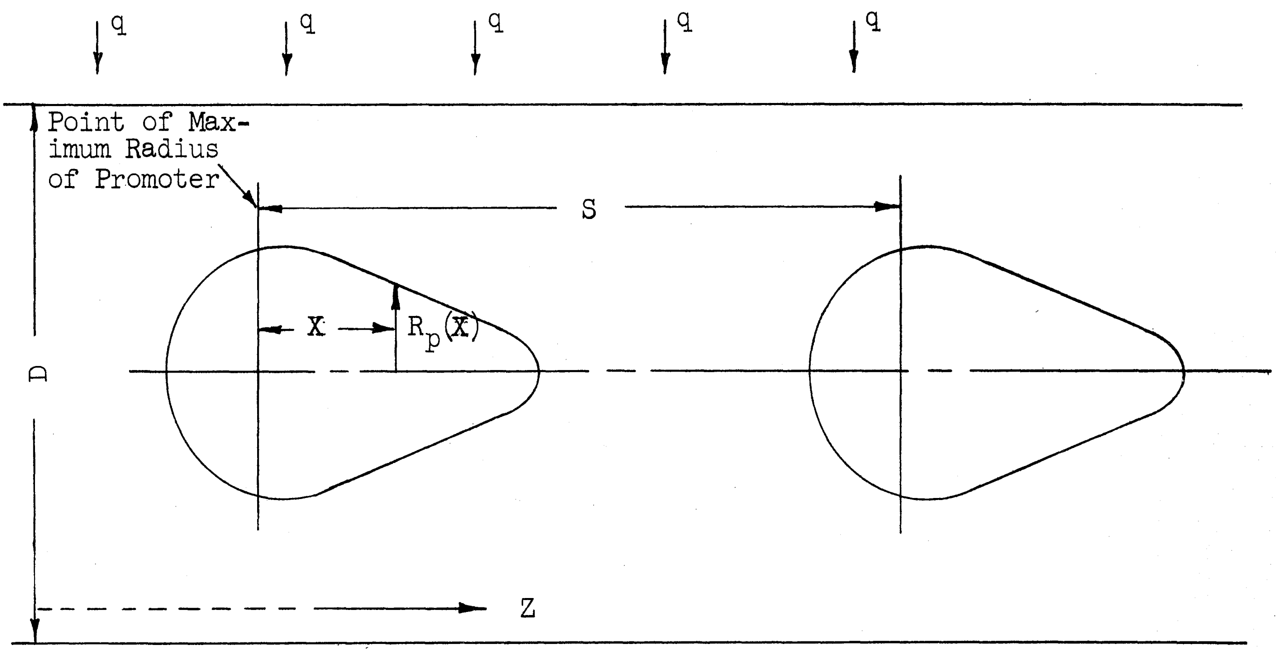

Boundary conditions are specified by giving the velocity of the fluid in the longitudinal and radial directions, temperatures, and pressures at some reference point, Z_0, i.e. $V_z(r,Z_0)$, $V_r(r,Z_0)$, $T(r,Z_0)$, and $P(r,Z_0)$ are specified, where Z is the longitudinal distance down the cylinder. In addition the wall temperature distribution $T_{wall}(Z)$ (or using the same notation, $T(D/2,Z)$) must be given for Z greater than Z_0.

The problem is to determine the velocities, temperature, and pressure at any point: $V_z(r,Z)$, $V_r(r,Z)$, $T(r,Z)$, and $P(r,Z)$. This, in turn, will either enable the rate of heat transfer and pressure drop to be calculated or will eliminate the need for such information.

The solution of the Navier-Stokes equations together with the energy equation subject to the boundary conditions just described should--in theory--provide the answer. Unfortunately, there is no known, general solution to these equations for turbulent flow in even an empty tube--much less one in which bluff objects have been introduced. The complex, little-understood nature of turbulent flow makes this approach impossible at the present time.

Dimensional Analysis

In dimensionless form the rate of heat transfer can be expressed in terms of the Nusselt number

$$Nu = hD/k \tag{2}$$

where the heat transfer coefficient h is defined as

$$h = \frac{q}{T_{wall} - T_f} \tag{3}$$

The overall pressure drop can be expressed in terms of the following dimensionless ratio called the friction factor

$$f = \frac{g_c\ D}{2\rho\ U^2} \left[\frac{-\Delta P}{L_p}\right] \tag{4}$$

For a given set of boundary conditions, a given shape of bluff body, and a fluid whose physical properties can be assumed to be independent of temperature, the specification of the rate of heat transfer and pressure drop should be a function of the following dimensionless variables:

1. Dimensionless flow rate, $Re = D\rho U/\mu$
2. Prandtl number, $Pr = c\mu/k$
3. Ratio of promoter diameter to tube diameter, $d = D_p/D$
4. Ratio of promoter spacing to tube diameter, $s = S/D$

Pressure Drop of Turbulence Promoters Based on Drag of a Single Bluff Body

One approach to the problem of predicting the pressure drop for a combination of bluff body turbulence promoters is to assume that the pressure drop for a series of bluff body promoters is composed of two parts: 1) drag on the tube wall which would be present even if there were no bluff body, and 2) form drag of the bluff body.

The pressure drop due to drag on the tube that would be present in a length S of the empty tube containing a single bluff body is

$$-\Delta P_{ET} = \frac{2f_0\ \rho\ U^2\ S}{g_c\ D} \tag{5}$$

$$= \frac{2f_0\ \rho\ U^2\ s}{g_c} \tag{6}$$

The pressure drop due to the form drag of the body may be expressed

$$-\Delta P_{form} = \frac{f_D \rho U_{max}^2 A_p}{2 g_c A_{tube}} \tag{7}$$

$$= \frac{f_D \rho}{2 g_c} \quad \frac{U^2 d^2}{(1 - d^2)^2} \tag{8}$$

where A_p = projected area of the promoter

A_{tube} = cross-sectional area of the tube

U_{max} = mean superficial velocity at point of minimum free area

f_D = effective drag coefficient

The total pressure drop is

$$-\Delta P_{total} = \frac{2 f \rho U^2 s}{g_c} \tag{9}$$

where f = friction factor for turbulence promoters based on the inside tube diameter and the mean velocity in the empty tube

Since

$$\Delta P_{total} - \Delta P_{ET} = \Delta P_{form} \tag{10}$$

then

$$\frac{2 f \rho U^2 s}{g_c} - \frac{2 f_0 \rho U^2 s}{g_c} = \frac{f_D \rho U^2 d^2}{2 g_c (1-d^2)^2} \tag{11}$$

$$\left[\frac{f}{f_0} - 1\right] = \frac{1}{4 s} \left[\frac{f_D}{f_0}\right]\left[\frac{d^2}{(1-d^2)^2}\right] \tag{12}$$

The preceding analysis is quite simplified. One would not expect f_D above to have the same value as the drag coefficient measured in an infinite fluid of uniform velocity. Furthermore, f_D should be a function of spacing s , since as the promoters get closer and closer together, their wakes will start interfering with each other and the drag coefficient should decrease. The coefficient f_D should also be a function of the diameter ratio d since it involves or includes a wall effect. For these reasons the coefficient f_D will, henceforth, be referred to as an "effective drag coefficient".

If the fraction free area A_f is defined as

$$A_f = (1-d^2) \tag{13}$$

then a trial correlation for the rate of momentum transfer might be made by plotting the effective drag coefficient

$$f_D = \frac{4 A_f^2 s}{d^2} \left[f - f_0 \right] \tag{14}$$

versus s, d, and Reynolds number.

Review of Previous Work

Empty Tube--the Limiting Case of Infinite Promoter Spacing or Zero Promoter Diameter

When the spacing becomes infinite or the diameter of the promoter goes to zero, the geometry reduces to the case of an empty tube. This case has been the subject of a very large number of theoretical and experimental investigations which are well summarized by McAdams[28] and Knudsen and Katz[22].

A generally accepted empirical correlation for the friction factor in a smooth tube is that given by Nikuradse[33].

$$\frac{1}{\sqrt{f}} = 4.0 \log_{10} (\text{Re } f^{1/2}) - 0.40 \tag{15}$$

This is the quantity used throughout this dissertation when referring to the friction factor f_0 for the empty tube.

In addition, correlations for the friction factor in an empty tube which are useful because of their explicit nature include that of Blasius[5]

$$f = 0.079\ Re^{-0.25} \tag{16}$$

and that of Colburn[10] based upon the j-factor

$$f = 0.046\ Re^{-0.20} \tag{17}$$

The generally accepted empirical correlation for the Nusselt number is that given by Sieder and Tate[38]

$$Nu = C_2\ Re^{0.8}\ Pr^{1/3}\ (\mu/\mu_w)^{0.14} \tag{18}$$

valid for $Re > 10{,}000$ and $Pr > 0.70$.

Sieder and Tate give a value of 0.027 for C_2, Bird, Stewart, and Lightfoot[4] suggest 0.026, McAdams[28] recommends 0.023, and Drexel and McAdams[14] correlated data for air with a constant of 0.021.

Tube with a Solid Rod in the Center--the Limiting Case of Promoters at Zero Spacing

When the promoter spacing goes to zero, the geometry reduces to the case of flow in an annulus. Data for an annulus are generally correlated with Nusselt numbers, friction factors, and Reynolds numbers defined on the basis of the velocity in the annulus and some equivalent diameter. This leads to confusion when compared with results for an empty tube or a tube with a set of turbulence promoters whose spacing is not equal to zero. In this later case data are generally correlated on the basis of the superficial velocity in the empty tube and the inside tube diameter. In the interest of clarity the following conventions will be adopted for this presentation.

1. The terms Re, f, Nu, and D will refer to values evaluated using the inside tube diameter D and the superficial velocity U based on flow in the empty tube. In other words,

$$U = \frac{4\ W}{\rho\ \pi\ D^2} \tag{19}$$

$$Re = \frac{D\ \rho\ U}{\mu} \tag{20}$$

$$= \frac{4\ W}{\mu\ \pi\ D} \tag{21}$$

$$f = \frac{g_c\ D}{2\ \rho\ U^2} \left[\frac{-\Delta P}{L_p}\right] \tag{4}$$

$$= \frac{g_c\ \pi^2 \rho D^5}{32\ W^2} \left[\frac{-\Delta P}{L_p}\right] \tag{22}$$

$$Nu = \frac{h\ D}{k} \tag{2}$$

2. The terms Re*, f*, Nu*, and D* will refer to values evaluated using an <u>equivalent</u> diameter D* and the mean velocity u in the annulus. In other words,

$$u = \frac{4\ W}{\rho\ \pi\ D^2\ (1-d^2)} \tag{23}$$

$$\alpha = D^*/D \tag{24}$$

$$Re^* = \frac{D^*\ \rho\ u}{\mu} \tag{25}$$

$$= \frac{4\ D^*\ W}{\mu\ \pi\ D^2\ (1-d^2)} \tag{26}$$

$$= \frac{\alpha \; Re}{(1-d^2)} \tag{27}$$

$$f^* = \frac{g_c \; \rho \; \pi^2 \; (1-d^2) \; D^4 \cdot D^*}{32 \; W^2} \left[\frac{-\Delta P}{L_p} \right] \tag{28}$$

$$= (1-d^2)^2 \; \alpha \; f \tag{29}$$

$$Nu^* = \frac{h \; D^*}{k} \tag{30}$$

$$= \alpha \; Nu \tag{31}$$

Various correlations have been proposed for pressure drop in an annulus. Knudsen and Katz[22] recommend

$$f^* = 0.076 \; Re^{*-0.25} \tag{32}$$

with

$$\alpha = 1 - d \tag{32a}$$

Davis[12] gives

$$f^* = 0.055 \; (1-d)^{-0.10} \; Re^{*-0.20} \tag{33}$$

with

$$\alpha = 1 - d \tag{33a}$$

Whalker, Whan, and Rothfus[42] present

$$f^* = 0.079 \; Re^{*-0.25} \tag{34}$$

$$\alpha = 1 + \frac{(1-d^2)}{2 \ln d} \tag{34a}$$

Lohrenz and Kurata[26] have recently presented a graphical correlation of f* vs. Re* based on

$$\alpha = \left[1 + d^2 + \frac{(1-d^2)}{\ln d} \right]^{1/2} \tag{35}$$

Their definition of equivalent diameter (i.e. α) has the advantage that, when plotted on logarithmic coordinates, all friction factors for laminar flow fall on the same straight line defined by

$$f^* = \frac{16}{Re^*} \tag{36}$$

and the critical Reynolds number where flow deviates widely from laminar behavior occurs at Re* = 2300. For fully developed turbulent flow, however, (Re* > 10,000) this correlation yields a family of lines, each corresponding to a different diameter ratio d. Lohrenz and Kurata present lines only for the limiting values of d = 0 and d = 1.0 and one intermediate value corresponding to d = 0.33. In order to compare their graphical correlation quantitatively with other correlations for annuli, it is necessary to have an equation for interpolation. The following is suggested for the equivalent Reynolds number range 10,000 < Re* < 40,000.

$$f^* = 0.079\ F(d)\ Re^{*-0.25} \tag{37}$$

where F(d) is a tabulated function of d given in Table I.

Meter and Bird[29] propose on semi-theoretical grounds the following equation

$$\frac{1}{\sqrt{f^*}} = G(d)\ \log_{10}\left[\phi(d) Re^* \sqrt{f^*}\right] - H(d) \tag{38}$$

with

$$\alpha = 1 - d \tag{38a}$$

and

$$\phi(d) = \frac{1}{(1-d)^2}\left[1 + d^2 + \frac{(1-d^2)}{\ln d}\right] \tag{38b}$$

where G(d) and H(d) are complicated functions of d whose values are tabulated in Table I.

Because of the different definitions of equivalent diameter used by different investigators, it is difficult to compare directly the various correlations of f* vs. Re*. This difficulty can be eliminated, however, by converting all of the equivalent friction factor correlations of the form f* vs. Re* to the type ordinarily used in empty tubes,

TABLE I

FUNCTIONS F(d), G(d), AND H(d) USED IN EQUIVALENT FRICTION FACTOR CORRELATIONS FOR ANNULI

d	F(d)	G(d)	H(d)
0.00	0.918	4.000	0.400
0.05	0.918	3.747	0.293
0.10	0.910	3.736	0.239
0.15	0.903	3.738	0.208
0.20	0.881	3.746	0.186
0.30	0.853	3.771	0.154
0.40	0.830	3.801	0.131
0.50	0.817	3.833	0.111
0.60	0.807	3.866	0.093
0.70	0.798	3.900	0.076
0.80	0.779	3.933	0.060
0.90	0.771	3.967	0.046
1.00	0.762	4.000	0.031

f vs. Re, by using the relations

$$Re^* = \frac{\alpha \, Re}{1-d^2} \tag{27}$$

$$f = \frac{f^*}{(1-d^2)^2 \alpha} \tag{39}$$

In other words, for a given mass flow rate of fluid in the annulus the Reynolds number may be calculated using

$$Re = \frac{4 \, W}{\mu \, \pi \, D} \tag{21}$$

Then, using any particular correlation for which α is specified, Re* may be calculated, f* may be obtained as a function of Re* from the correlation, and the value converted to f for comparison with other correlations.

This was done for each of the five correlations, using various values of diameter ratio d and Reynolds number Re. In addition, the friction factor was calculated using the Blasius equation (16) and the hydraulic radius. In effect, this is simply one more correlation of the form

$$f^* = 0.079 \, Re^{*-0.25} \tag{40}$$

with

$$\alpha = 1 - d \tag{40a}$$

The comparison is shown in Figure 2. To eliminate the wide variation of f with d at a given Reynolds number, the ratio of the friction factor f obtained using each of the five correlations to that obtained using Equation (40) is plotted. This is the same as plotting the ratio of the pressure drop (for flow through the annulus at a given

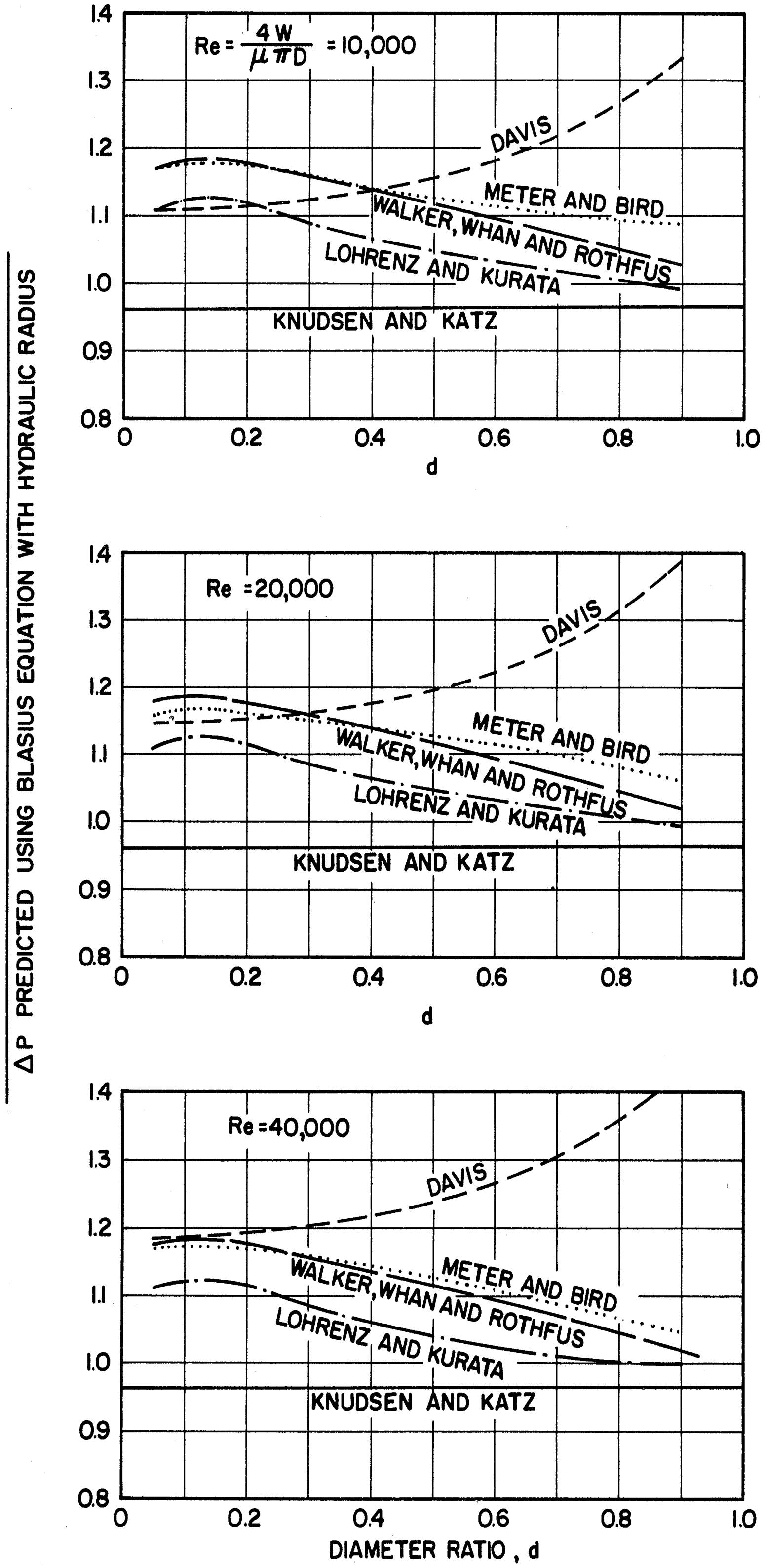

Figure 2. Comparison of Friction Factor Correlations for Annuli, Ratio of ΔP Calculated Using Blasius Equation and Hydraulic Radius vs. Diameter Ratio d, for Re = 10,000, 20,000, and 40,000.

mass flow rate) predicted by each correlation to that predicted by Equation (40). It can be seen that the correlation of Walker, Whan, and Rothfus[42] agrees very well with that of Meter and Bird[29]. The correlation of Lohrenz and Kurata[26] predicts pressure drops about ten per cent lower than that of Walker, Whan, and Rothfus, but this could well be due to the difficulty in interpolating their plot for different values of d. Considering the reliability of the data, any of the three correlations is probably acceptable.

Lohrenz and Kurata's choice of equivalent diameter has the advantage of correlating all diameter ratios with a single curve in the laminar region and of predicting a single value of the equivalent Reynolds number Re^* for transition from laminar flow, but it has the disadvantage of producing separate lines for each diameter ratio in the turbulent region and the correlation suffers from lack of an analytic expression for calculating the friction factor. Walker, Whan, and Rothfus' correlation on the other hand, has the advantage of producing a single curve for all diameter ratios in the fully developed turbulent region, but of producing separate lines in the laminar region and separate transition equivalent Reynolds numbers Re^* for each different value of d.

Much less has been done on the study of heat transfer to a fluid flowing in an annulus than on pressure drop. This is particularly true for heat transfer to the <u>outside</u> wall of the annulus.

Barrow[2] made a theoretical study of convection heat transfer coefficients for turbulent flow between parallel plates in which the heat flux at each wall was arbitrary. The assumptions were: 1) constant eddy diffusivity of heat over the channel, and 2) the thermal diffusivity was negligible compared with the eddy diffusivity.

He defined q as the rate of heat transfer at one plate and ηq as the rate of heat transfer at the other plate and obtained the following expressions for the Nusselt number

$$Nu = \frac{0.1986\ Re^{7/8}\ Pr}{5.03\ (2 + \eta)\ Re^{1/8} + 9.74\ [Pr - (2 + \eta)]} \qquad (41)$$

at the plate where the rate of heat transfer is q, and

$$Nu = \frac{0.1986\ Re^{7/8}\ Pr}{5.03\ (2 + 1/\eta)\ Re^{1/8} + 9.74\ [Pr - (2 + 1/\eta)]} \qquad (42)$$

at the plate where the rate of heat transfer is ηq.

For $\eta = -1$, corresponding to symmetrical heating or cooling (i.e. equal rate of heat transfer at each wall), the Nusselt numbers are the same and agree well with

$$Nu^* = 0.023\ Re^{*0.8}\ Pr^{0.4} \qquad (43)$$

where $\alpha = 1 - d$.

However, with $\eta = 0$ (corresponding to heat transfer at one wall only, which is the case of interest in this study) the Nusselt number predicted by Equation (41) is about 30 per cent lower than the value given by Equation (43) at a $Re^* = 10,000$ and 40 per cent lower at $Re^* = 40,000$.

Only one set of data for heat transfer to the outside wall of an annulus could be found in the literature: that of Monrad and Pelton[30] for a solid rod in the center of a tube with a diameter ratio d of 0.541. On the basis of their data they propose

$$Nu^* = 0.023 \; Re^{*0.8} \; Pr^n \qquad (44)$$

with $\alpha = 1 - d$ (44a)

and $n = 0.3$ for cooling

$n = 0.4$ for heating

Turbulence Promoters

In this section a review of previous experimental studies of different types of turbulence promoters will be presented in chronological order. The work done by Koch[23] which will be described in its place is the only extensive work done on bluff-body turbulence promoters.

Because of the extensive work done with rough tubes, and because roughening elements are usually placed in a different class from other types of turbulence promoters, no attempt is made to review the experiments on the effect of roughness of the tube wall. A complete summary of previous work done in this field, however, is provided by Nunner[34].

Royds' work[36] reported in 1921 is apparently the earliest. His equipment consisted of a horizontal, double-tube heat exchanger. Hot air on the inside was cooled by water on the outside. The inside diameter of the inside tube was 2-5/8 in. The length of the test section was about 7 ft; no hydrodynamic entry length was provided.

The turbulence promoters (or retarders as he called them) for which results were presented consisted of twisted metal strips of different pitch. The strips were 1-15/16 in. by 0.10 in. Apparently they rested on the bottom of the tube.

The experimental data were not presented, but overall heat transfer coefficients were plotted. In the pressure drops reported, the change in kinetic energy due to the change in temperature of the air was not taken into account.

Royds' general conclusion was that his retarders increased the rate of heat transfer, but were slightly less efficient when the energy required for pumping is compared with that for plain tubes.

Colburn and King[9] presented their results in 1931. Their test section was a 3 ft. horizontal length of 2-5/8 in. steel tube through which hot air was passed. The air was cooled by water flowing through a 1/4 inch copper coil soldered around the tube.

Ten turbulence promoters of the following designs were tested:

2 large twisted steel strips
3 small twisted steel strips
2 copper wire spirals
1 propeller-shaped brass baffle
1 set of copper wire spirals

Although it is not clear how the turbulence promoters were supported in the tube, it is most likely that they rested on the bottom of the tube.

Data were obtained and overall heat transfer coefficients determined for a Reynolds number range of about 3,000 to 10,000. No hydrodynamic entry length was provided; the air entered the test section directly from a mixing chamber.

The general conclusions were: 1) heat transfer coefficients can be materially increased by the use of baffles, etc. 2) values for almost any type of packing of baffle lie on the same curve of heat transfer vs. pressure drop, so that if the pressure drop for a new baffle is known, the heat transfer coefficient can be estimated.

Nagaoka and Wantanabe[31] also published their results in 1931. The equipment consisted of a horizontal, double-tube heat exchanger in which water on the inside was heated by hot transformer oil on the outside.

The inside tube had an inside diameter of 1.06 in. and a length of 5.37 ft. A hydrodynamic entry length of 3.28 ft. was provided.

Twenty-two different turbulence promoters were tested. Each consisted of wires of various shapes wound in spiral coils such that the outside diameter of the coil was the same as the inside diameter of the tube. Approximately five flow rates were tried with each promoter, covering a range of Reynolds number of 4,000 to 20,000. Overall heat transfer coefficients were given.

Colburn(11) reviewed in 1942 the data and results of both his earlier work with King and the work of Nagaoka and Wantanabe.

Seigel reported his work(39) (which primarily concerned applications to air-conditioning and refrigerating coils) in 1946. Data were taken for heating water in a 5/8 inch outside diameter horizontal copper tube. The water was heated by passing an electric current through the tube.

Three types of promoters were tested:

1. twisted copper strips 0.02 inches thick
2. spiral wire spring
3. 3/8 inch copper tube with sealed ends

The test section was 10 ft. long with no hydrodynamic entry length. No data on the pressure drop were reported; overall heat transfer coefficients were plotted as a function of water flow rate in GPM.

The general conclusion of Seigel was that spiral springs gave the biggest increase in heat transfer and the pressure drop was least when the distance between turns was largest.

Measurements made by Evans and Sarjant[15] for cooling of high temperature gases were reported in 1951. Air, heated electrically, was cooled by water flowing through copper tubes coiled around the tube. Turbulence promoters tested were:

1. a two inch solid rod centered in the tube for one set of data and resting on the bottom for another
2. twisted metal strips 2-1/2 inch by 3/32 inch (pitches of 1/7, 1/9, 1/12, and 1/14)

The solid rods did not extend for the complete length of the test section. This uncertainty in the geometry as well as the complications of high temperature makes it very difficult to compare their results with the results of others.

Margolis[27] obtained data in 1957 using two different fluids: water and air; his data are presented and discussed by Kreith and Margolis[24,25]. The equipment consisted of a horizontal, single-pass heat exchanger in which the fluid was heated in the tube by condensing steam on the outside. Two inside diameters of tubes were tested (0.53 in. and 1.12 in.).

The test section was 42 inches long with no hydrodynamic entry length between the mixing chamber and the test section. Overall heat transfer coefficients were obtained for nine different turbulence promoters consisting of the following:

3 twisted strips of metal
6 wire coils

About seven flow rates were tried for each promoter covering a range of Reynolds number from 1,000 to 10,000.

Some of the conclusions were: 1) the rate of heat transfer per unit area in vortex flow is considerably larger than in axial flow through straight tubes and ducts; 2) a qualitative difference exists between the results for air and water which is difficult to explain; 3) the effect is due largely to the centrifugal force which is present.

Koch[23] published in 1958 data for turbulence promoters using the same equipment which Nunner[34] used to study the effect of roughness. The equipment consisted of a horizontal tube in which air was heated by condensing steam on the outside of the tube. The test section was 3.21 ft. long and the tube had an inside diameter of 1.97 in. A hydrodynamic entry length of 8.19 ft. was provided.

Overall heat transfer coefficients were determined for the following types of turbulence promoters:

14 orifices
10 disks
4 propeller devices
2 rings
3 twisted strips of metal
4 types of packing material

In addition, some velocity distributions and wall shear stress measurements were made for a few orifices.

The general conclusion was that twisted metal strips, orifices, and propellers were most effective. The use of turbulence promoters is economical in some cases.

In 1960 Gambill, Bundy, and Wansbrough[17,18] reported the results of a comprehensive study of the effect of twisted metal strips on heat transfer and pressure drop to water flowing in a tube. Data were taken for non-boiling heat transfer, boiling heat transfer, and burnout.

A series of inside tube diameters ranging from 0.136 to 0.249 inches was studied over a Reynolds number range of 10,000 to 200,000. No special entry length was provided for the twisted tapes.

In 1962 Gambill and Bundy[19] presented additional heat transfer results obtained using the same equipment as for their previous work, but with ethylene glycol as the working fluid. An overall correlation was obtained for predicting heat transfer rates and friction factors for any tube containing twisted metal strips using any fluid with Prandtl number greater than that of air.

Miscellaneous Related Studies

This section presents a review of several investigations which, although they did not study directly the effect of turbulence promoters on the rate of heat transfer and pressure drop to a fluid flowing in a tube, have results which pertain in part to the problem.

Kemeny and Cyphers[21] presented experimental data on the rate of heat transfer and pressure drop from water to the inside tube of an annulus with surface spoilers. The surface spoilers consisted of both semi-circular protrusions and depressions wound helically around the tube. A very good presentation of the economics of artificially increasing the heat transfer at the expense of pressure drop is given.

Sundstrom and Churchill[40] and Zartman and Churchill[43] as part of separate studies of heat transfer from gas flames in a cylindrical burner measured local rates of heat transfer from hot air to cold water flowing outside the tube. The flow was disturbed by the presence of a single, disk-shape bluff-body flame holder centered in the burner.

Sundstrom and Churchill's tube was one inch in inside diameter, the flame holder provided 48 per cent free area and the Reynolds number varied from 5,000 to 20,000. Zartman and Churchill's tube was five inches in inside diameter; data were taken for several holders with free areas less than 10 per cent. The Reynolds number was at 14,000 for each case.

Boelter, Young, and Iverson[6] determined local heat transfer rates to air in the entrance region of a tube for a wide variety of hydrodynamic entrances, some of which might be classed as turbulence promoters.

Faruqui and Knudsen[16] measured heat transfer rates in short tubes in which the flow upstream had been obstructed by orifices.

EXPERIMENTAL APPARATUS AND PROCEDURE

The apparatus was designed to obtain accurate local convective heat transfer coefficients and values of the overall pressure drop for water flowing in a tube. The equipment was constructed in a manner to allow any arbitrary devices to be easily inserted in the center of the tube. A vertical direction of flow was chosen to provide symmetry about the axis.

Description of the Equipment

The essential parts of the equipment are: 1) water supply and metering system, 2) electrically heated test section, 3) thermocouples and accessories, and 4) manometer assembly.

Figure 3 is a photograph of the overall view of the equipment showing the rotameters, manometers, and control panel. Figure 4 is a closeup of the test section. Figure 5 is a closeup of the thermocouple switches and recording potentiometer. Each part of the equipment will be described in turn.

Water Supply and Metering System

The best illustration of the water supply and metering system is given by Figure 6, the schematic diagram of the apparatus. Water enters the apparatus from the city water lines and is metered by one of four rotameters. It then flows through the vertical test section from top to bottom and is discharged into the city drain lines. The flow rate and gage pressure are regulated by valves at the inlet and outlet of the equipment.

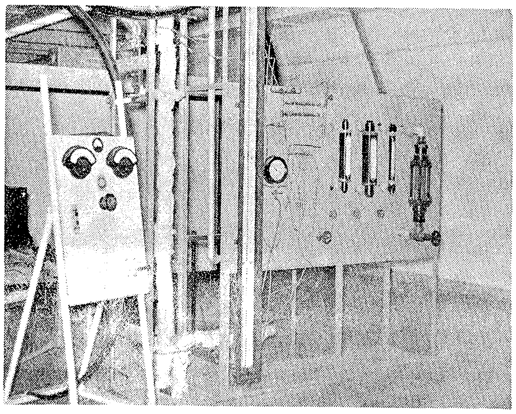

Figure 3. Photograph of Overall View of Equipment.

Figure 4. Photograph of Closeup of Test Section.

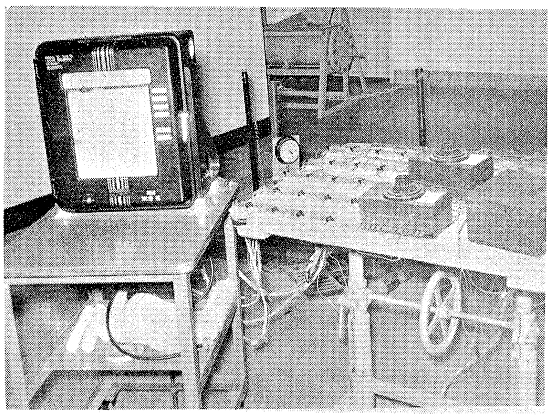

Figure 5. Photograph of Thermocouple Switches and Recording Potentiometer.

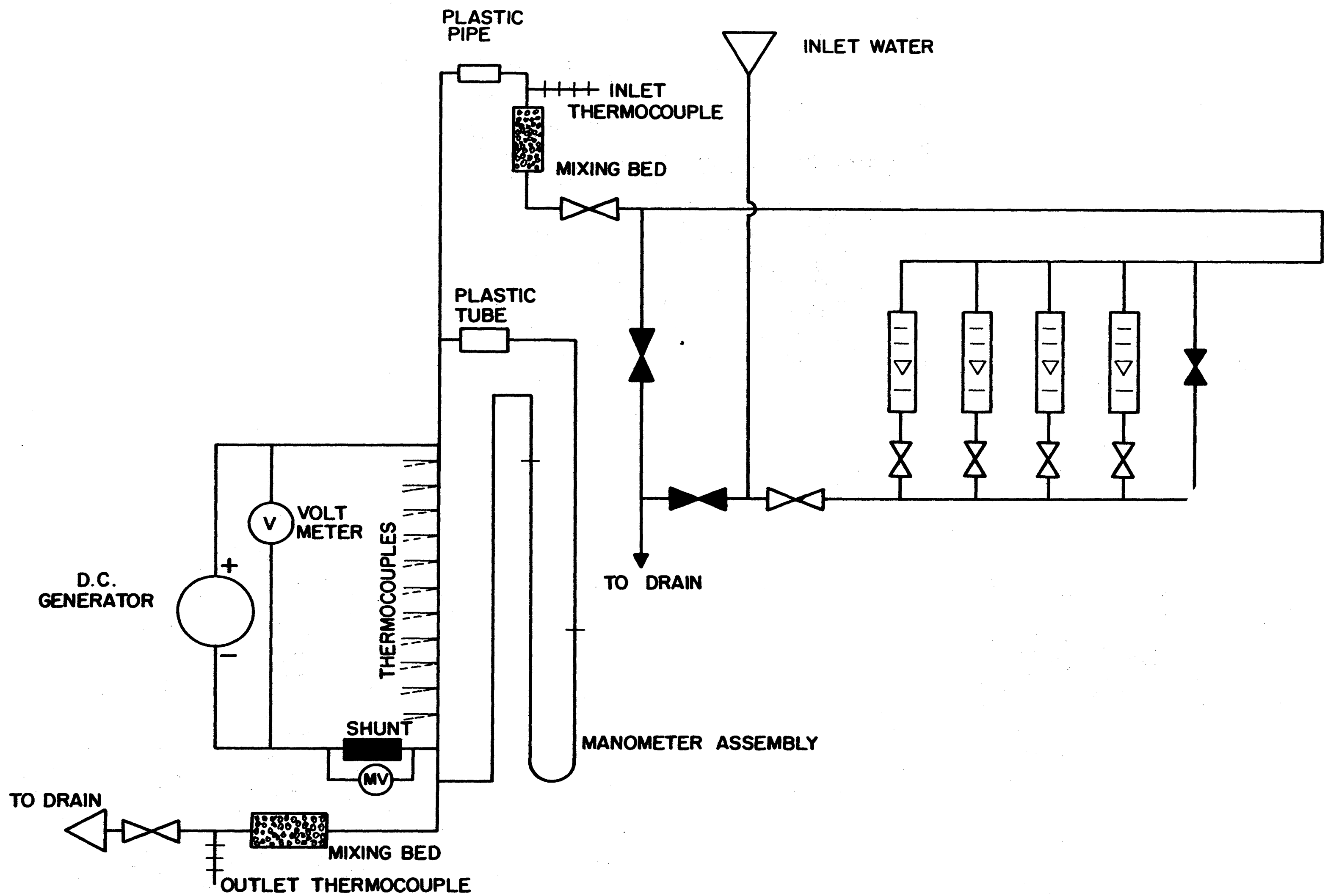

Figure 6. Schematic Diagram of the Apparatus.

The rotameters were calibrated by measuring the time required for a given weight of water (weighed on scales) to pass through the equipment at several flow rates. Calibration curves and their equations are given in Appendix A.

The inlet and outlet water temperatures are measured with thermocouples immediately before and after the test section. In each case, prior to having its temperature measured, the water flows through a packed bed 2 inches x 10 inches filled with 3/8 inch Raschig rings to insure good mixing.

Electrically Heated Test Section

Figure 7 is a diagram of the test section which consists of a stainless steel tube 119.88 inches in length with an inside diameter of 1.005 inches and an outside diameter of 1.240 inches. The first 49.69 inches serve as a hydrodynamic calming section. The next 64.34 inches are the heating section. The final 5.85 inches act as an outlet section. The test section is connected to the water supply and metering system by two 1-1/4 inch tube connectors.

Heat is generated electrically in the heating section by passing an electric current through the tube wall. The current is generated by a 12 volt, 3000 amp d.c. generator whose output can be varied from 4 to 36 kilowatts. The electrical terminals at the extremes of the heating section are copper bus bars 4 inches wide and 3/4 inches thick. Holes were drilled in the center of the bus bars approximately two inches from each end and the steel tube was silver soldered to the bus bars. As can best be seen from the detailed diagram in Figure 7 the bus bars were

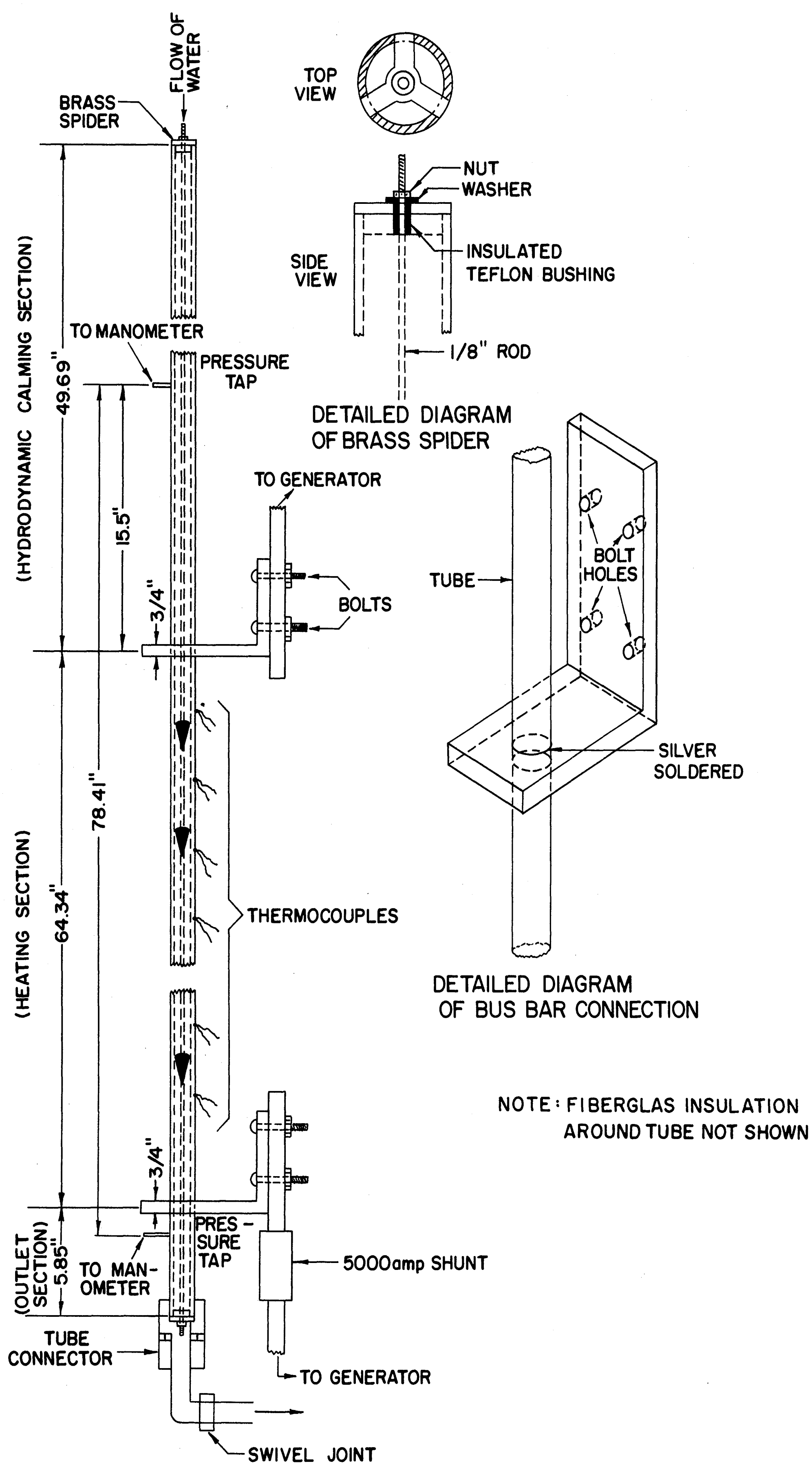

Figure 7. Diagram of the Test Section.

bent at right angles and provided with bolts so that the test section could be easily disconnected from the generator.

The heating section is insulated electrically from the water supply and metering system by a one foot length of 1-1/4 inch plastic pipe which serves as the final section of the inlet water pipe.

The entire test section from the measurement of the inlet water temperature to the measurement of the outlet water temperature is thermally insulated with Fiberglas insulation 1-1/2 inches thick.

The electric current through the heating section is measured by noting the emf (in millivolts) across a 5000 amp shunt. This emf is measured with a Leeds and Northrup 8662 precision portable potentiometer. The voltage across the heating section is measured with a d.c. voltmeter.

<u>Thermocouples and Accessories</u>

The outside wall temperature of the heating section is measured at 22 axial stations at one angular position with copper-constantan thermocouples. In addition at three of the 22 axial stations temperatures are measured at two other angular positions, each 120 degrees apart. A list of the locations of the thermocouples relative to the other items comprising the test section is given in Table II.

The thermocouples are held in place by an epoxy resin and are insulated electrically from the heating section by a thin (0.002 inch) sheet of mica.

The thermocouple emfs may be measured one of two ways: First, by the 8662 potentiometer; or second, by a Leeds and Northrup 20 point AZAR Speedomax recording potentiometer with arbitrary zero and arbitrary

TABLE II

POSITION OF THERMOCOUPLES ON TEST SECTION
RELATIVE TO OTHER ITEMS

Item	Longitudinal Position (Tube Diameters)	Angular Position (Degrees)
Top of Tube	-49.44	--
Pressure Tap	-12.35	--
Bus Bar (Beginning of Heating)	0.00	--
Thermocouple 1R	1.49	0
Thermocouple 2R	5.41	0
Thermocouple 3R	9.42	0
Thermocouple 4R	13.40	0
Thermocouple 5R	17.41	0
Thermocouple 6R	22.17	0
Thermocouple 7R	25.34	0
Thermocouple 8R	29.32	0
Thermocouple 9R	33.30	0
Thermocouple 20L	34.30	0
Thermocouple 19L	35.30	0
Thermocouple 18L	36.29	0
Thermocouple 10R	37.28	0
Thermocouple 17L	38.28	0
Thermocouple 16L	39.28	0
Thermocouple 15L	40.28	0
Thermocouple 11R	41.20	0
Thermocouple 12R	45.27	0
Thermocouple 13R	49.22	0
Thermocouple 14R	53.26	0
Thermocouple 15R	57.28	0
Thermocouple 16R	62.47	0
Thermocouple 14L	34.30	120
Thermocouple 13L	36.29	120
Thermocouple 12L	38.28	120
Thermocouple 11L	34.30	240
Thermocouple 10L	36.29	240
Thermocouple 9L	38.28	240
Bus Bar (End of Heating)	64.02	--
Pressure Tap	65.67	--
Bottom of Tube	69.84	--

range. By use of 20 double-pole-double-throw knife switches, the AZAR recorder is able to record up to 40 thermocouple emfs.

The thermocouples were calibrated prior to use using a constant temperature oil bath and precision thermometers calibrated by the U. S. Bureau of Standards over the range from 40 deg. F to 250 deg. F. The calibration agreed with that appearing in the International Critical Tables[32].

Manometer Assembly

Pressure taps are located 12.41 inches before and 1.66 inches after the heating section making a total distance between taps of 78.41 inches. The holes are 1/16 inch in diameter; connections to the manometer assembly are made with 1/4 inch copper tubing silver soldered to the outside of the test section. The manometer assembly is insulated electrically from the heating section by using a 12 inch piece of plastic tubing for the connection in place of the copper tubing at one point in the system.

The manometers consist of two vertical, 100 inch, single-tube, King manometers. The first contains mercury as the indicating fluid; the second used an organic oil of specific gravity 1.750 (referred to as Purple Fluid). A pressure gage is connected to measure the gage pressure at either the inlet or outlet to the heating section. With the apparatus pressure drops from 0.02 to 60 psi could be measured with reasonable accuracy.

Description of the Turbulence Promoters

Easy insertion of arbitrary devices in the center of the tube required the following features: 1) that it be easy to disconnect the test section from the rest of the equipment; and, 2) that there be a relatively simple method of centering the devices in the tube.

In order to disconnect the test section, the following steps were necessary:

A. All water to the system was turned off and the drain valve opened to drain water from the apparatus.

B. The tube connector at the top of the stainless steel tube was disconnected.

C. Both pressure tap connections were disconnected.

D. Four bolts were removed from the bus bar connectors at the top and bottom of the heating section.

E. The test section was swung down into a horizontal position on the floor where the bottom tube connector was disconnected and the test section moved away. A swivel joint was provided at the floor just below the test section so that the test section could be rotated down.

This whole procedure could be done in less than 30 minutes. Reassembly of the equipment also required approximately 30 minutes and consisted of doing the opposite of the above steps in reverse order.

Provision was made for centering a 1/8 inch rod in the tube and keeping it in tension. Thus, any arbitrary device could be mounted in the tube so long as it could be attached to the 1/8 inch rod.

Two brass spiders were provided at each end of the stainless steel tube as shown in the detailed diagram of Figure 7. The 1/8 inch rod (usually made of brass) was threaded at each end and could be put in tension in the center of the tube by passing each end through the spider and tightening the nuts on the end. A teflon bushing in the spider and use of rubber washers made certain that the rod was insulated electrically from the heating section.

Since the 1/8 inch rod was mounted vertically, centered at each end of the tube, and held in tension, any device centered on the rod was centered in the tube when the rod was in place. Each of the three types of devices: disks, streamline shapes, and solid rods will now be described and the method of mounting them on the rod will be explained.

Disks

Disks were prepared having diameters of 5/8, 3/4, and 7/8 inches and a thickness of 1/8 inch. They were machined from nylon rod and a hole slightly larger than 1/8 inch was drilled in the center of each. The disks were held in place on the centering rod with two aluminum collars, 1/4 inch in diameter, before and after each disk. The collars were held in place with a small set screw. A diagram of the disk and method of mounting it on the rod is shown in Figure 8.

Streamline Shapes

The shapes, while resembling teardrops, were actually composed of a cone tangent to a sphere. This is illustrated in Figure 8 with the important relative dimensions noted.

The shapes were machined from nylon rod and had diameters (at the point of maximum diameter) of 5/8, 3/4, and 7/8 inches. A hole slightly larger than 1/8 inch was drilled in the center of each shape so that it could be mounted on the rod. Each shape was held in place on the rod by a small set screw. As an added precaution to insure that the devices

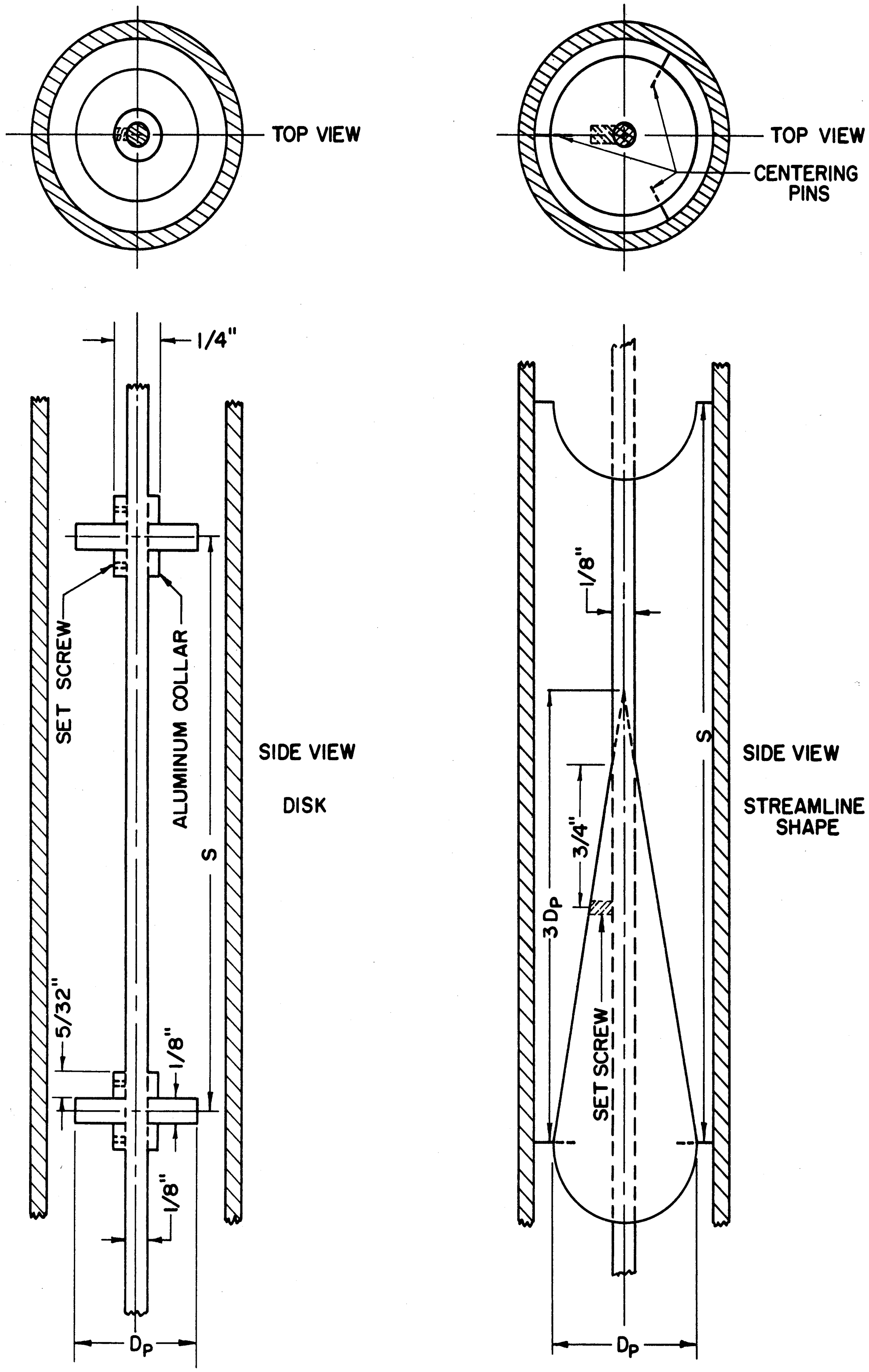

Figure 8. Diagram of Disk and Streamline Shape Showing Relative Dimensions and Method of Mounting.

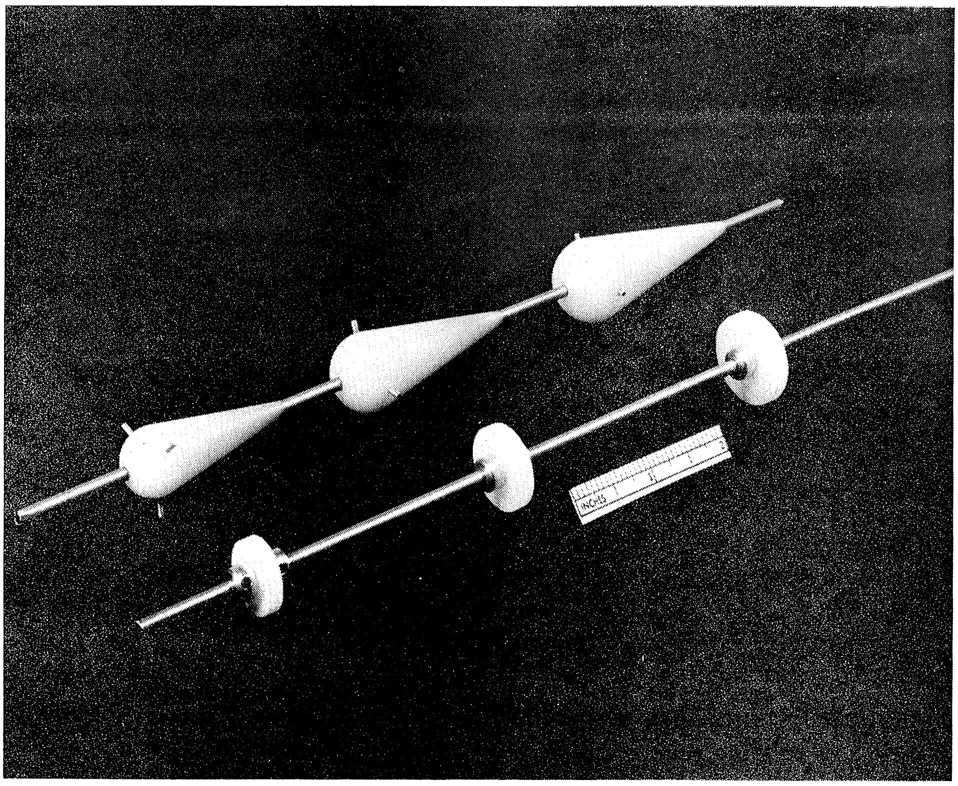

Figure 9. Photograph of Individual Turbulence Promoter Shapes Used.

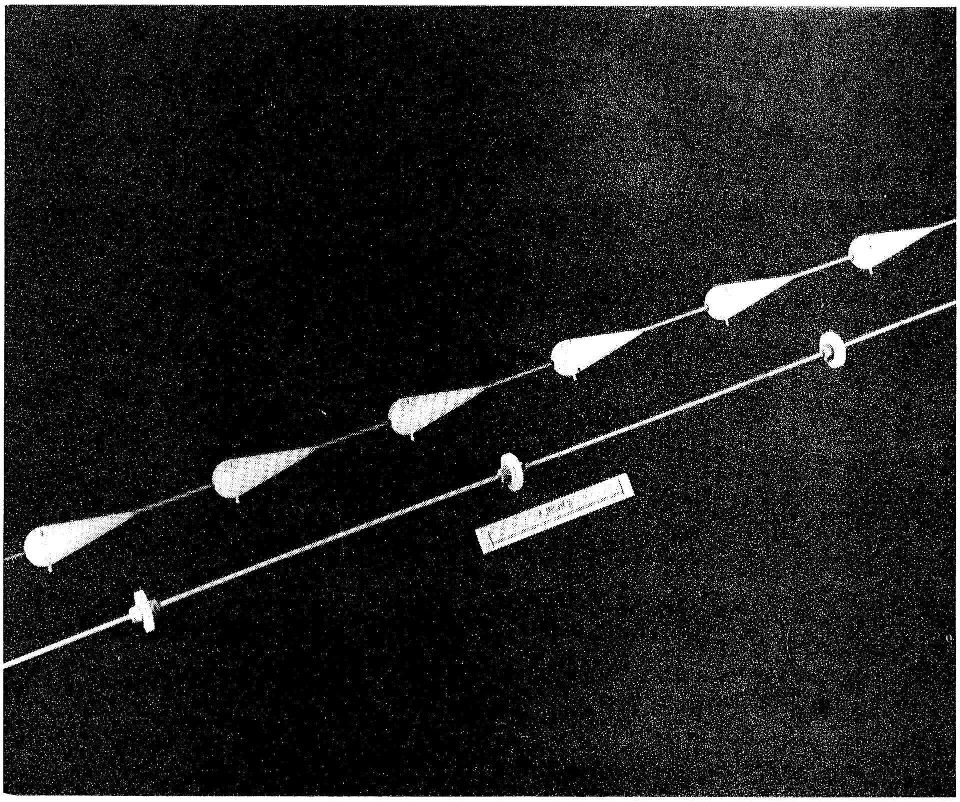

Figure 10. Photograph of a String of Disks and a String of Streamline Shapes.

were centered, three aluminum pins (3/32 inches in diameter) were installed at the point of maximum diameter of the shape. The pins were 120 degrees apart, extending far enough so that when the shape was mounted on the rod in the tube, the pins just touched the tube wall, holding the device in place.

Figure 9 is a photograph of the six individual bluff-body turbulence promoters (i.e. disks of three diameters and streamline shapes of three diameters) utilized in this investigation. One turbulence promoter combination, by definition, consists of a string of individual bluff bodies all of the same shape and diameter spaced an equal distance apart. An illustration of a combination of disks and a combination of streamline shapes is shown in the photograph of Figure 10.

The 21 different bluff-body turbulence promoter combinations used in this investigation are itemized in Table III. An attempt was made to choose the number of promoters such that the total length of the string of promoters was 48 inches (which is almost exactly the same as 48 tube diameters). For various reasons, however, as noted in the footnotes to Table III it was necessary to use a shorter string of promoters in some cases. The variation in the length of the string of promoters used in the experimental measurements in no way impairs the usefulness or generality of the data. Since local heat transfer coefficients were measured, the total length of the string is immaterial; it is necessary only to obtain data near one representative promoter or group of promoters. As will be shown later, the variation in length of the string of promoters was corrected for in the calculation of friction factors.

TABLE III

BLUFF-BODY TURBULENCE PROMOTER COMBINATIONS USED
IN THIS INVESTIGATION

Shape	d	s	n_p	Length of String
Disk	0.625	12	4	48
Disk	0.750	12	4	48
Disk	0.875	12	4	48
Disk	0.625	8	6	48
Disk	0.750	8	6	48
Disk	0.875	8	6	48
Disk	0.625	4	12	48
Disk	0.750	4	12	48
Disk	0.875	4	8	32*
Disk	0.625	2	11	22**
Disk	0.750	2	11	22**
Disk	0.875	2	8	16*
Streamline Shape	0.625	12	4	48
Streamline Shape	0.750	12	4	48
Streamline Shape	0.875	12	4	48
Streamline Shape	0.625	8	6	48
Streamline Shape	0.750	8	6	48
Streamline Shape	0.875	8	6	48
Streamline Shape	0.625	4	6	24**
Streamline Shape	0.750	4	6	24**
Streamline Shape	0.875	4	6	24**

* Total length of string of promoters shortened because of excessive pressure drop which would result, reducing maximum flow rate which could be obtained.

** Total length of string of promoters shortened to save the expense and effort of fabricating a large number of shapes.

Solid Rods

The first type of solid rod tested was simply the 1/8 inch brass rod used to mount the disks and streamline shapes.

The second type of solid rod tried was a 1/4 inch threaded brass rod. The rod was mounted (not in tension) using a special spider at the top only and centered with three teflon centering spiders, each held in place with nuts threaded on the rod. These tests were originally made with the idea of using a threaded rod to mount the disks and streamline shapes. Although this proved impractical, the data fall in the same class as the other data for solid rods and seem worthy of presentation.

The third type of solid rod tested consisted of 5/8 and 3/4 inch brass rods. At each end of the rods 1/8 inch holes were drilled in the center and threaded so that studs could be screwed into the rod and used with the brass spiders to center the rod at each end of the tube. At two points along the rod (dividing the rod approximately into thirds) two 1/8 inch holes were drilled perpendicular to the axis of the rod, each of the two holes being 1/2 inch apart and perpendicular to each other. Nylon rod segments 1/8 inch in diameter (each one inch long) were inserted through the holes so that they protruded the same distance on each side of the rod. The nylon rod segments were held in place by small set screws perpendicular to each rod. Thus, when the brass rod was in the tube, it was centered at two points in addition to the ends.

Description of the Procedure

The procedure used to obtain heat transfer and pressure drop data will be described for a typical situation.

The first step (assuming that the equipment was still set up from a previous run) was to remove the test section from the rest of the equipment as described in the description of the turbulence promoters. The centering rod on which the turbulence promoter combination from the previous run was mounted was removed and, if a different diameter or shape device was to be tested, the old devices were removed from the centering rod and new ones installed. If the same shape and diameter devices were to be tested again, but at a different spacing, they were simply loosened. In either case, the devices were moved to the desired position and the necessary set screws were tightened to hold the objects in place on the rod.

The distance from the end of the rod to each object was then measured and recorded on a data sheet. The centering rod was inserted in the spiders at each end of the tube, the nuts on the end of the rod were tightened, and the distance from the top of the tube to the end of the centering rod was measured and recorded. Thus, the distance from the top of the tube to each turbulence promoter could be determined from the measurements.

The test section was then reconnected to the water supply and metering system; the electrical terminals were connected; the pressure taps were connected and the water was turned on to the system. The water was always discharged directly to the drain (bypassing the test section) at maximum flow rate for about 15 minutes to remove any foreign material that may have accumulated in the pipes.

The manometer lines were bled to remove any air and the equipment was ready for taking data. Pressure drop data were usually taken first, by varying the flow rate and recording the rotameter reading, the manometer scale being used, the manometer reading, and the temperature. The flow rate was controlled by a valve at the outlet of the equipment so that back pressure was always maintained on the test section, thus, assuring that the tube was full of water.

The procedure for taking heat transfer data was more involved. The first step was to adjust the flow rate of the water through the test section to the desired value. The d.c. generator was then started and the voltage set so as to give the desired rate of heat input.

The temperatures throughout the system were observed (either using the 8662 potentiometer or the AZAR Speedomax recording potentiometer to record the thermocouple emfs) at intervals of about five minutes until steady-state conditions were attained (i.e. until the temperatures did not change). For the first run of a session about two hours were usually required for the system to come to steady state because it took a long time for the generator and electrical leads to heat up to their equilibrium temperatures. For subsequent runs less than 15 minutes were usually required to achieve a steady state.

When steady state was achieved, the zero and range of the AZAR recorder were adjusted so that the minimum wall temperature of the tube was at zero on the recorder and the maximum wall temperature was at about 90 per cent of full scale. Two 8662 portable potentiometers were set so that they provided reference emfs which recorded at about 0 and 80 per cent of full scale on the AZAR recorder.

At this point the data taking commenced. The following items were recorded on a data sheet: 1) the rotameter number and reading, 2) the manometer scale and manometer reading, 3) the voltmeter scale and voltage across the test section, 4) the number of millivolts across the 5000 amp shunt (i.e. the current through the test section), 5) the inlet water thermocouple reading, 6) the outlet water thermocouple reading, 7) the value of the two reference emfs supplied by the 8662 potentiometer, and 8) one or more randomly selected wall temperatures. Items 4, 5, 6, and 8 were obtained using one of the 8662 potentiometers.

The AZAR recorder was then started with all the knife switches set in the same position. As soon as 20 points had been recorded, twelve of the knife switches (for the twelve channels which had two thermocouples attached to them) were thrown to give additional temperature readings. After the next 20 points (eight of which were the same) had been recorded, the knife switches were returned to their original positions. This was repeated four times so that the 32 different emfs were recorded four times.

At this time the original 8 items of data (i.e. rotameter readings, manometer readings, etc.) were measured again and recorded. This terminated a run and the generator was turned off, the water rate adjusted to a new value and the whole procedure repeated for a new run.

Generally, five flow rates were used (or, in other words, five heat transfer runs were made) for each turbulence promoter combination.

Data were almost always taken in the evening to minimize any variation in the water pressure caused by other users in the building turning water on and off. A complete set of pressure drop data and heat transfer data at five flow rates could usually be obtained in one evening.

Method of Calculating Heat Transfer Coefficients

The local convective heat transfer coefficient is defined as

$$h(z) = \frac{q(z)}{T_{wall}(z) - T_f(z)} \tag{45}$$

where z = longitudinal distance from beginning of heating (tube diameters)

$h(z)$ = local heat transfer coefficient (BTU/hr - deg F - ft^2)

$q(z)$ = local rate of heat transfer per unit area (BTU/hr - ft^2)

$T_{wall}(z)$ = temperature of the inside tube wall (deg F)

$T_f(z)$ = mixed mean temperature of the fluid (deg F)

The general procedure for obtaining these local heat transfer coefficients from the experimental measurements is as follows:

1. $q(z)$ is determined by measuring the electric current and knowing the electrical resistance of the tube.

2. $T_f(z)$ is obtained from an energy balance. The heat added to the water is integrated from the beginning of the tube to z.

3. $T_{wall}(z)$ is obtained by measuring the outside wall temperature and calculating the inside wall temperature from solutions of the conduction equation.

When the electric current passes through the tube wall, generating heat, a temperature gradient is developed so that the heat will flow to the inside wall. The differential equation (usually referred to as the conduction equation which describes this process is

$$\frac{1}{r}\frac{\partial}{\partial r}\left[r\,K\,\frac{\partial T}{\partial r}\right] + \frac{\partial}{\partial y}\left[K\,\frac{\partial T}{\partial y}\right] + A = 0 \qquad (46)$$

where T = temperature (deg F)

r = radius (ft)

y = longitudinal distance (ft)

A = rate of heat generation per unit volume of tube wall (BTU/hr - ft^3)

K = thermal conductivity of the tube wall (BTU/hr - deg F - ft)

The rate of heat generation A as derived in Appendix B is

$$A = \frac{3.41276\, I^2 \bar{\rho}_m^{\,2}}{\bar{\rho}_o\,(1+\gamma T)\pi^2\,(b^2-a^2)^2} \qquad (47)$$

where $\bar{\rho}$ = electrical resistivity of the tube wall, assumed to be a linear function of temperature (ohm-ft)

$$\bar{\rho} = \bar{\rho}_o\,(1+\gamma T) \qquad (48)$$

and

$$\bar{\rho}_m = \frac{\bar{\rho}_o\,(b^2-a^2)}{2\displaystyle\int_a^b \frac{b\ r\ dr}{1+\gamma T(r)}} \qquad (49)$$

The symbol $\bar{\rho}$ for electrical restivity will always be written with a bar over it to distinguish it from the fluid density ρ .

Equation (46) which is a non-linear partial differential equation can be simplified considerably and reduced to a non-linear ordinary differential equation by considering that axial conduction is not important. Axial conduction, however, can arise and influence the solution of (46) in one of two ways: 1) by conduction of heat into the non-heat-generating portion of the tube; and, 2) by presence of a non-constant axial temperature gradient at the inside wall. Each of these possibilities is considered in Appendix B and shown to produce a negligible effect.

Therefore, neglecting axial conduction ($\frac{\partial T}{\partial y}$ = constant) and letting

$$K = K_0 \; (1 + \beta T) \tag{50}$$

then the conduction equation becomes

$$\frac{d^2T}{dr^2} + \frac{1}{r}\frac{dT}{dr} + \frac{\beta}{1+\beta T}\left[\frac{dT}{dr}\right]^2 + \frac{3.41276 \; I^2 \; \bar{\rho}_m^{\;2}}{\pi^2 \; K_0 \; \bar{\rho}_0 \; (1+\gamma T)(1+\beta T)(b^2 - a^2)^2} = 0 \tag{51}$$

with the boundary conditions

$$T'(b) = 0 \tag{52a}$$

$$T(a) = T_a \tag{52b}$$

Define

$$A_0 = \frac{3.41276 \; I^2 \bar{\rho}_m^{\;2}}{\bar{\rho}_0 \; \pi^2 \; (b^2 - a^2)^2} \tag{53}$$

The solution as suggested by Clark[8] is

$$T(b) - T(a) = \frac{A_0}{2\,K_b}\left[b^2 \ln \frac{b}{a} - \frac{(b^2 - a^2)}{2}\right] + \left[\frac{A_0}{2\,K_b}\right]^2 \left[\frac{3\beta + \gamma + 4\gamma\beta\, T_b}{6(1 + \gamma T_b)(1 + \beta T_b)}\right](b - a)^4 \tag{54}$$

where, of course, T(a) is the value T_{wall} which is required and T(b) is the outside wall temperature which is measured.

The difference between T(b) and T(a) caused by generation of heat in the tube wall is often referred to as $\Delta T_{generation}$.

The rate of heat transfer to the fluid at the inside wall is found by

$$q(z) = \frac{1}{a}\int_a^b A \; r \; dr \tag{55}$$

$$= \frac{3.41276\ \bar{\rho}_o(1 + \gamma T_b(z))I^2}{2\pi^2\ (b^2 - a^2)\ a} \qquad (56)$$

The mean fluid temperature is given by

$$T_f = T_{inlet} + \frac{2\pi\ a \int_a^Z q(Z)\ dZ}{W\ c} \qquad (57)$$

or, since q(Z) is very nearly constant

$$T_f = T_{inlet} + \frac{Z}{L}\ (T_{outlet} - T_{inlet}) \qquad (58)$$

Thus, in practice, Equation (56) was used to obtain q(z); Equation (54) was used to obtain T_{wall} and Equation (58) was used to obtain $T_f(Z)$. All data processing was performed on the IBM 704. A detailed description of the computational method and the numerical values of the constants in the preceding equations is given in Appendix A.

Method of Calculating Friction Factors

The friction factor is defined as

$$f = \frac{g_c\ D}{2\ \rho\ U^2} \left[\frac{-\Delta P}{L_p}\right] \qquad (4)$$

$$= \frac{g_c\ \pi^2\ \rho\ D^5}{32\ W^2} \left[\frac{-\Delta P}{L_p}\right] \qquad (22)$$

since $$U = \frac{4\ W}{\pi \rho D^2} \qquad (19)$$

with L_p = distance between pressure taps (ft)

ΔP = pressure drop (lb_f/ft^2)

As explained previously, the use of the superficial velocity U and the inside diameter of the tube D allows the same definition of f to apply for the empty tube, the tube with turbulence promoters, and the tube with a solid rod in the center.

It is tacitly assumed, however, that the geometry of the tube is the same for the entire distance L_p between pressure taps. This is certainly true for the empty tube and for the tube with a solid rod in the center. But for the turbulence promoters the string of promoters occupied only part of the distance between pressure taps. This is illustrated below.

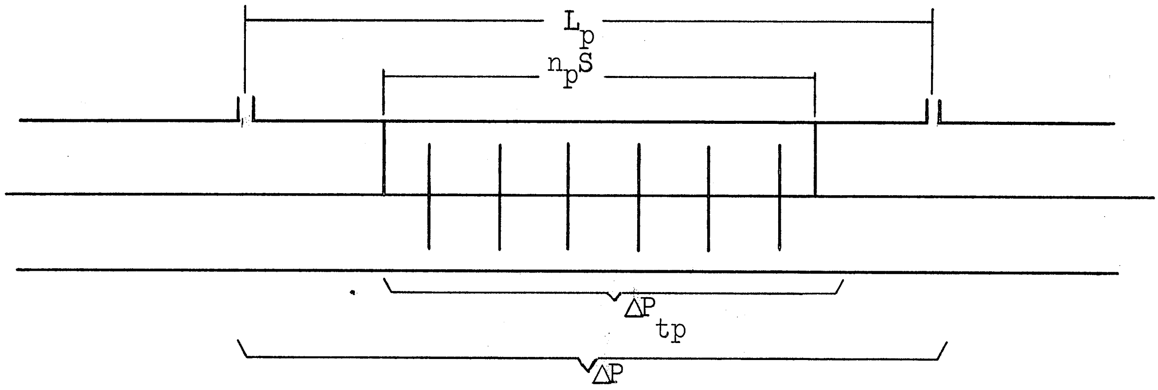

The desired friction factor for the tube with turbulence promoters is defined as

$$f = \frac{g_c \; D}{2 \; \rho \; U^2} \left[\frac{-\Delta P_{tp}}{n_p \; S} \right] \tag{59}$$

$$= \frac{g_c \; \pi^2 \rho \; D^5}{32 \; W^2} \left[\frac{-\Delta P_{tp}}{n_p \; S} \right] \tag{60}$$

This friction factor takes into account only the pressure loss due to drag of the bluff-bodies and drag of the tube wall for the length of tube occupied by the string of uniformly spaced turbulence promoters.

Unfortunately ΔP_{tp} could not be measured, but instead only the overall pressure drop ΔP was obtained. An attempt at correcting this difficulty, however, was made by estimating the pressure drop due to the tube wall between the pressure taps and string of turbulence promoters and subtracting it from ΔP to obtain ΔP_{tp}. Thus,

$$\Delta P_{tp} \cong \Delta P - \frac{32 \; W^2 \; f_0}{g_c \; \pi^2 \; \rho \; D^5} \; (L_p - n_p \; S) \tag{61}$$

where f_0 is the friction factor for empty tubes as calculated using Nikuradse's correlation equation (15) for smooth tubes. This, of course, neglects the pressure loss due to drag on the 1/8 inch rod (on which the promoters were mounted) in the length of tube for which there were no promoters. As will be shown later, the difference between the friction factor for a smooth tube and that for a tube with a 1/8 inch rod in the center is very small. For almost all geometries, the difference between ΔP_{tp} and ΔP is a very small per cent of ΔP. Substituting Equation (61) into Equation (59) an expression for the friction factor for bluff-body turbulence promoters which do not occupy the complete distance between pressure taps is obtained.

$$f = \left[\frac{g_c \; \pi^2 \; \rho \; D^5}{32 \; W^2}\right] \left[\frac{-\Delta P}{L_p}\right] \frac{L_p}{n_p \; S} - f_0 \left[\left(\frac{L_p}{n_p \; S}\right) - 1\right] \tag{62}$$

Equation (22) was used to calculate friction factors for the empty tube and the tube with a solid rod in the center and Equation (62) was used to calculate friction factors for a string of turbulence promoters. A description of the computer program used to process the pressure drop data as well as specific values of the constants in the preceding equations is given in Appendix A.

EXPERIMENTAL RESULTS AND DISCUSSION OF RESULTS

Empty Tube

Pressure Drop

Data were obtained for the empty tube primarily for use as a check on the reliability of the experimental apparatus and procedure. Friction factors are plotted versus Reynolds number in Figure 11. They agree well with the accepted correlation for smooth tubes, Equation (15), of Nikuradse[33].

Heat Transfer

Sample values of the local heat transfer coefficient $h(z)$ are presented in Figure 12 as a function of z for the empty tube to illustrate the local variation. The integrated mean value for each case is indicated by the solid line. A definite thermal entrance region is observed extending from 5 to 15 diameters from the beginning of heating.

In some cases the heat transfer coefficient increases gradually throughout the heated section. Both of these effects were noted by Hartnett[20] in his experimental study of the entrance region. Although Hartnett could not account for the gradual increase in the heat transfer coefficient along the tube, the most logical explanation seems to be the favorable change in the physical properties of the water (particularly the viscosity) as it is heated. An estimate of the local heat transfer coefficient, taking into account the change in physical properties of the fluid is given by

$$h(z)_{est} = (h_m) \frac{Re_z^{0.8} \; Pr_z^{1/3} \; (\mu/\mu_w)_z^{0.14}}{Re_m^{0.8} \; Pr_m^{1/3} \; (\mu/\mu_w)_m^{0.14}} \qquad (63)$$

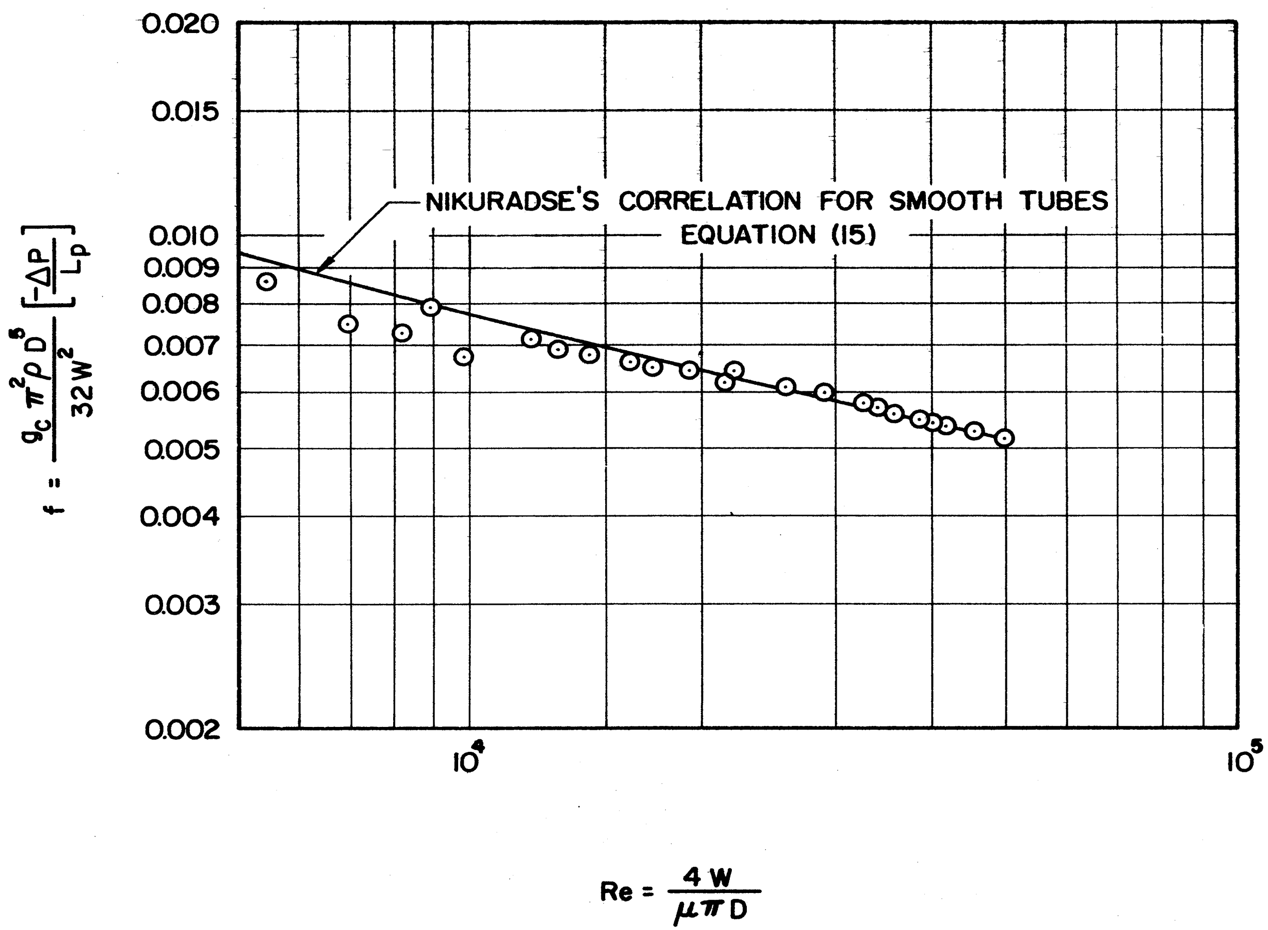

Figure 11. Friction Factor for the Empty Tube as a Function of Reynolds Number, f vs. Re.

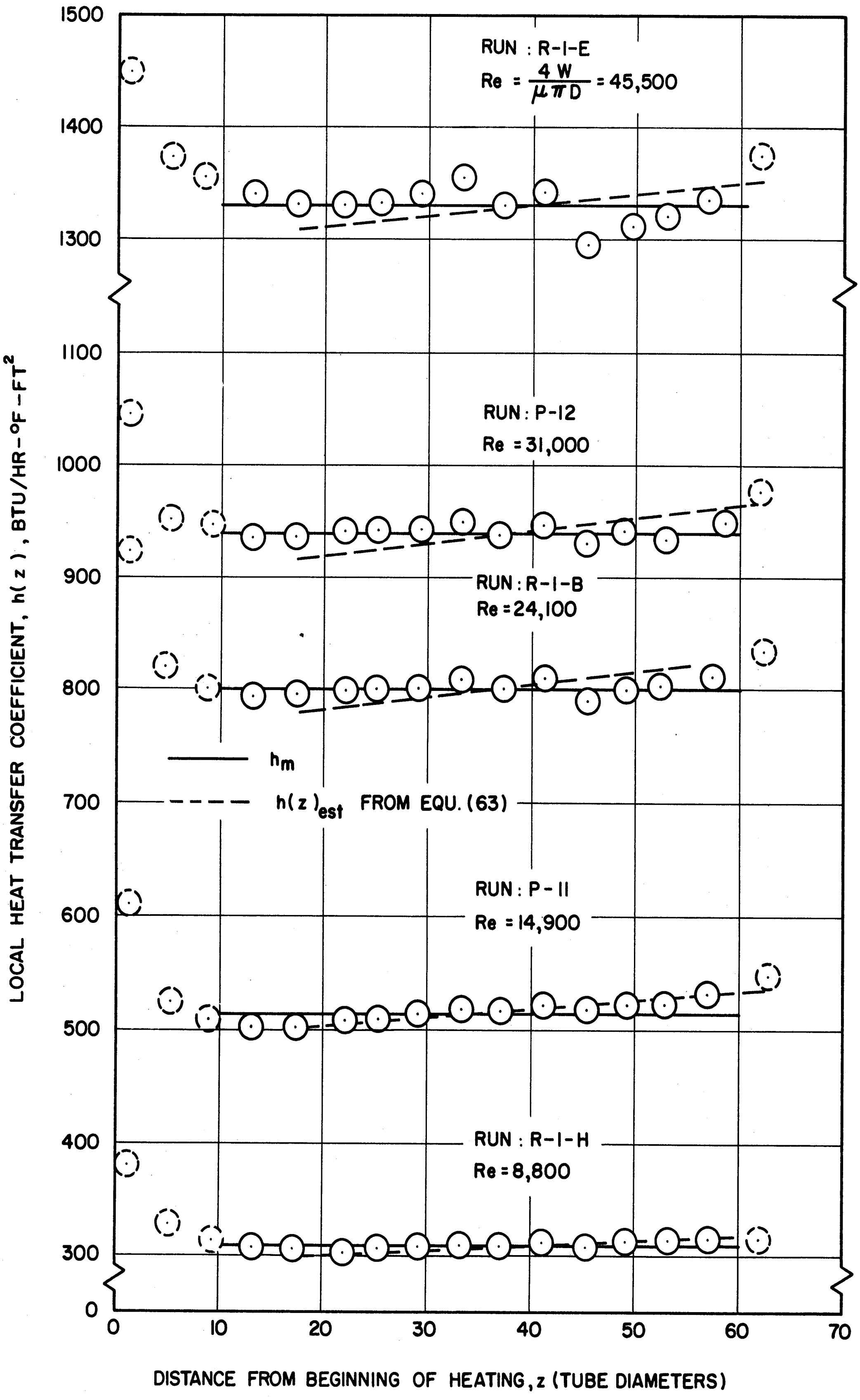

Figure 12. Sample Values of Local Heat Transfer Coefficients for the Empty Tube as a Function of Longitudinal Position, h(z) vs. z.

The subscript z indicates that the quantity is a local value evaluated at the local mixed-mean fluid temperature $T_f(z)$. The subscript m indicates that the quantity is a mean value and has been obtained by integrating the local value over the entire length of the heated section (with the exception of the first fifteen tube diameters). The term h_m is the integrated mean value of the measured local heat transfer coefficients $h(z)$.

The longitudinal distribution of the heat transfer coefficient due to change in the physical properties of the fluid as it was heated was estimated using Equation (63) and plotted as a dashed line in Figure 12. It can be seen that Equation (63) satisfactorily explains the gradual increase in local heat transfer coefficient with increasing fluid temperature. The solid line in Figure 12 is the value of h_m.

It should be noted that in order to use Equation (63) it is necessary to know the value of h_m which must be obtained from the data. The form of Equation (63) is such that when $h(z)_{est}$ is integrated, the resulting mean value is forced to have a value of h_m.

In some cases the local heat transfer coefficients "scatter" slightly. This scatter appears to be random and is probably due to errors in reading thermocouples.

Nusselt numbers based on the overall integrated mean heat transfer coefficients are presented in Figure 13 versus Reynolds number. The values have been divided by $Pr^{1/3}(\mu/\mu_w)^{0.14}$ to reduce the effect of physical property variation. It is seen that the results agree well with the Sieder-Tate equation[38] in the region of Reynolds number greater

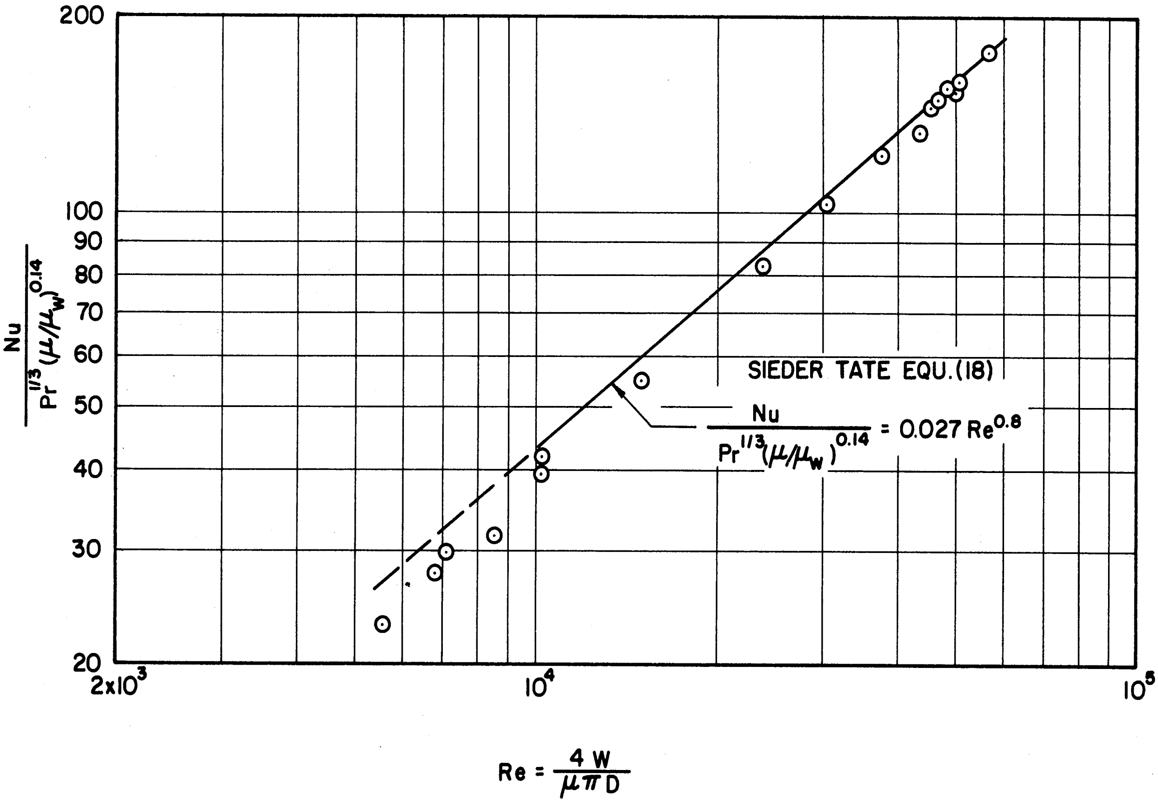

Figure 13. Nusselt Number for the Empty Tube as a Function of Reynolds Number, $\frac{Nu}{Pr^{1/3}\ (\mu/\mu_w)^{0.14}}$ vs. Re.

than 10,000 for which the Sieder-Tate equation is valid. As would be expected, in the Reynolds number range Re < 10,000 corresponding to the transition region of flow for heat transfer the data points fall below a line extrapolating Equation (18).

Solid Rod in the Center of the Tube

Pressure Drop

Friction factors defined by Equation (22) are plotted in Figure 14 as a function of the Reynolds number ($4W/\mu \pi D$). This method emphasizes the variation in pressure drop with geometry at the same mass flow rate. The rod with $d = 0.75$ gives a pressure drop over 20 times that of the empty tube, while the rod with $d = 0.125$ increases the pressure drop by only about fifteen per cent.

In Figure 15 the results are compared with the equivalent friction factor correlation for annuli recommended by Lohrenz and Kurata[26]. In this case the friction factors and Reynolds numbers are based on an equivalent diameter and the mean velocity of the fluid in the annulus. In other words,

$$f^* = (1-d^2)^2 \alpha f \tag{29}$$

$$Re^* = \frac{\alpha Re}{(1-d^2)} \tag{27}$$

$$\alpha = \left[1 + d^2 + \frac{(1-d^2)}{\ln d}\right]^{1/2} \tag{35}$$

The data fall between the lines corresponding to the limiting cases of $d = 0$ and $d = 1$ and are well within the reliability of the correlation as stated by Lohrenz and Kurata[26]. The effect of roughness

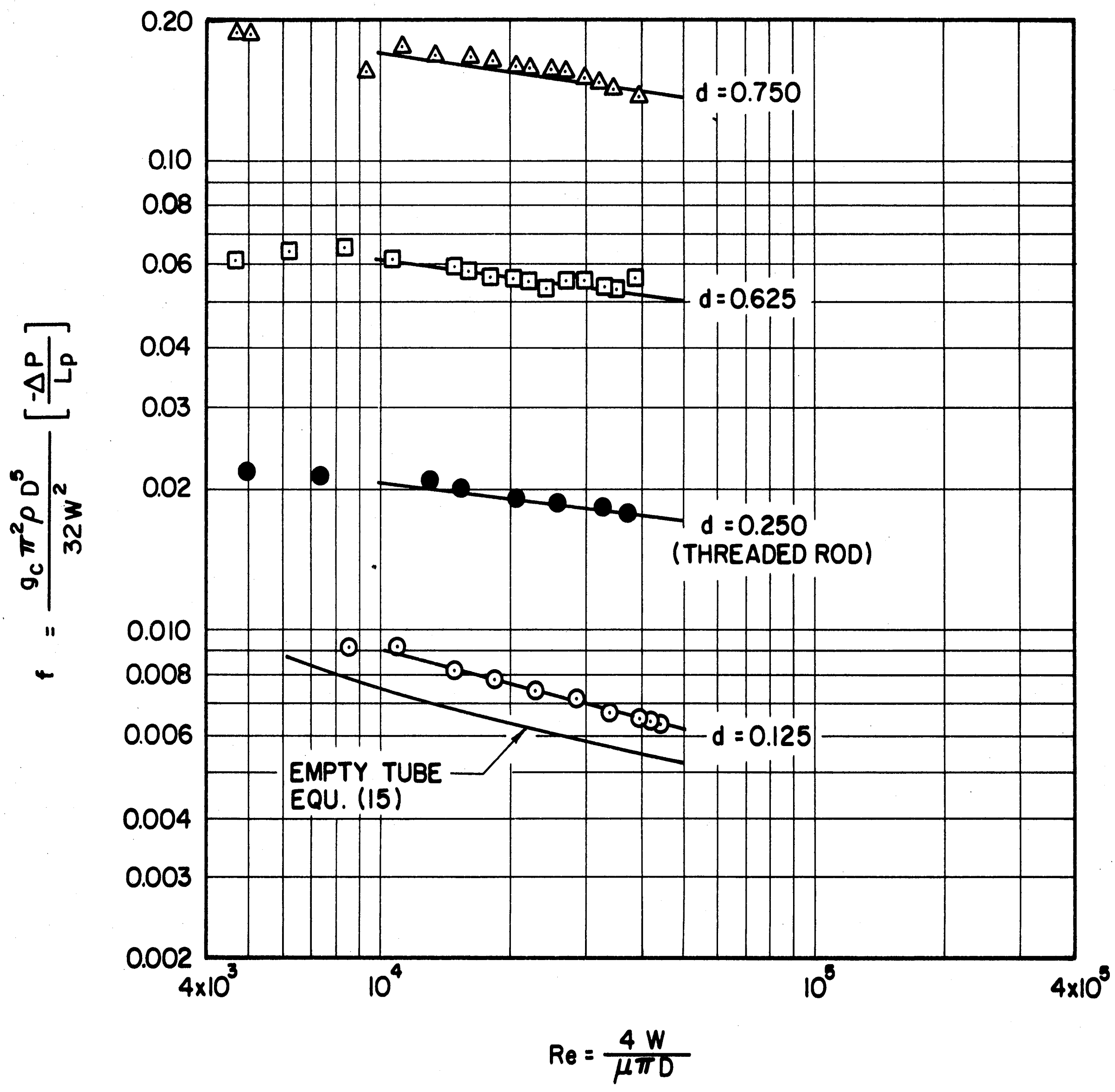

Figure 14. Friction Factor for the Tube with a Solid Rod in the Center as a Function of Reynolds Number, f vs. Re, with Parameters of d.

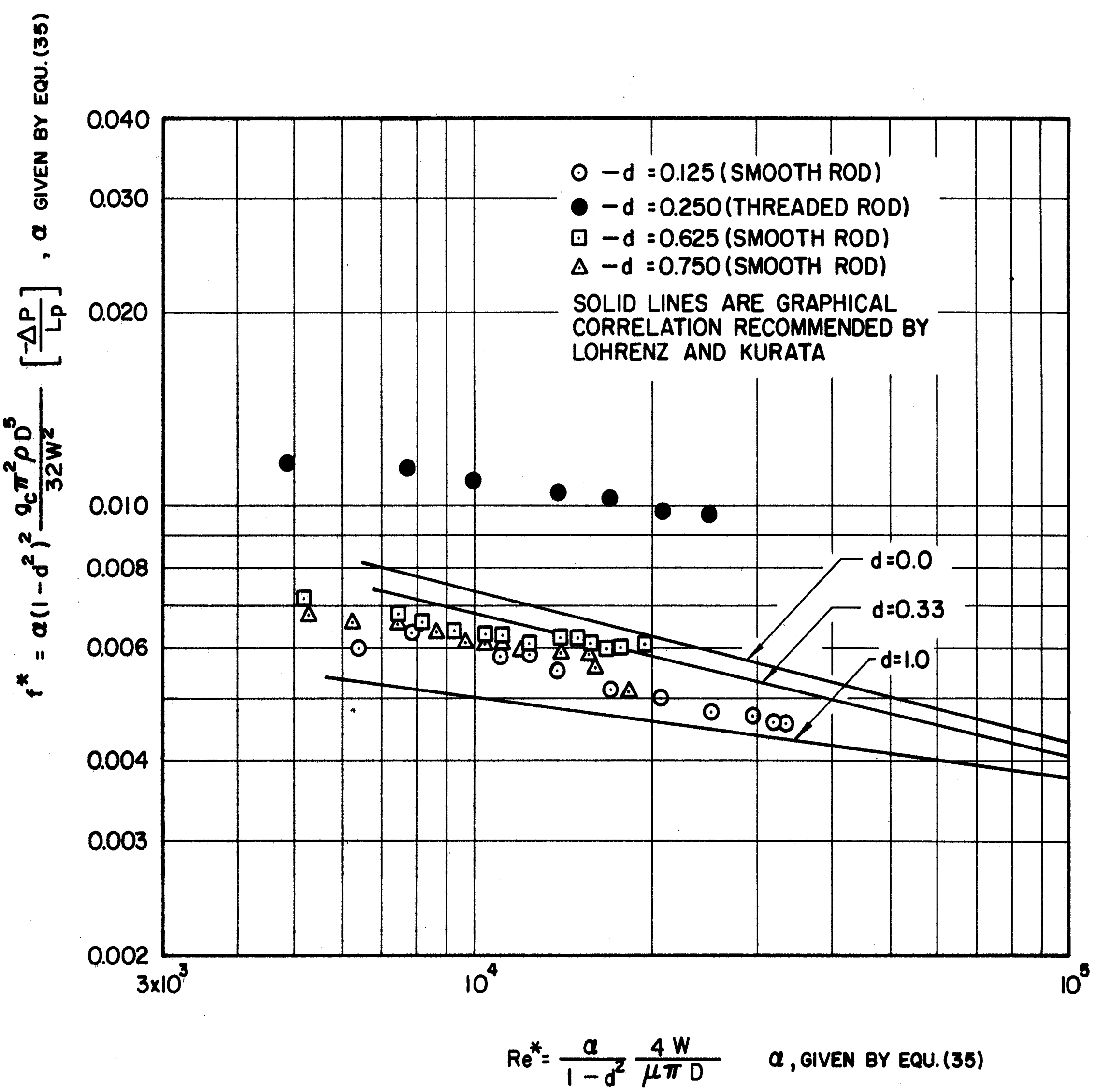

Figure 15. Friction Factor for the Tube with a Solid Rod in the Center as a Function of Reynolds Number Based on Equivalent Diameters, f* vs. Re*.

on the results for the threaded rod is quite noticeable in this method of presentation.

Heat Transfer

Sample values of the local heat transfer coefficients are plotted in Figures 16, 17, and 18 for the solid rods. For each of these rods there were at least two centering supports: one located before the heated section and one located somewhere within the heated section. Some of the local values of h are not considered representative because they are in the thermal entrance region or because they were increased due to disturbances in the flow near a centering support. These points are indicated by dashed circles and were not used in computing the mean value indicated by the solid line.

Some of the same features are noted in the plots of h(z) vs. z that were noted in the results for the empty tube--particularly the increase in h as the fluid is heated.

In many cases the effect is accentuated because the change in physical properties may cause a variation in the local Reynolds number such that the flow at the outlet of the heated section is in the fully developed region of flow ($Re^* > 10,000$) while the local Reynolds number at the inlet is in the transition region ($2300 < Re^* < 10,000$).

Equation (63) can not predict the effects of a change in regime of flow caused by a change in the physical properties of the fluid. The reason is that Nu^* is roughly proportional to Re^* in the transition region of flow, while it is proportional to $Re^{*0.8}$ in fully developed turbulent flow. Accordingly, it is noticed that the biggest

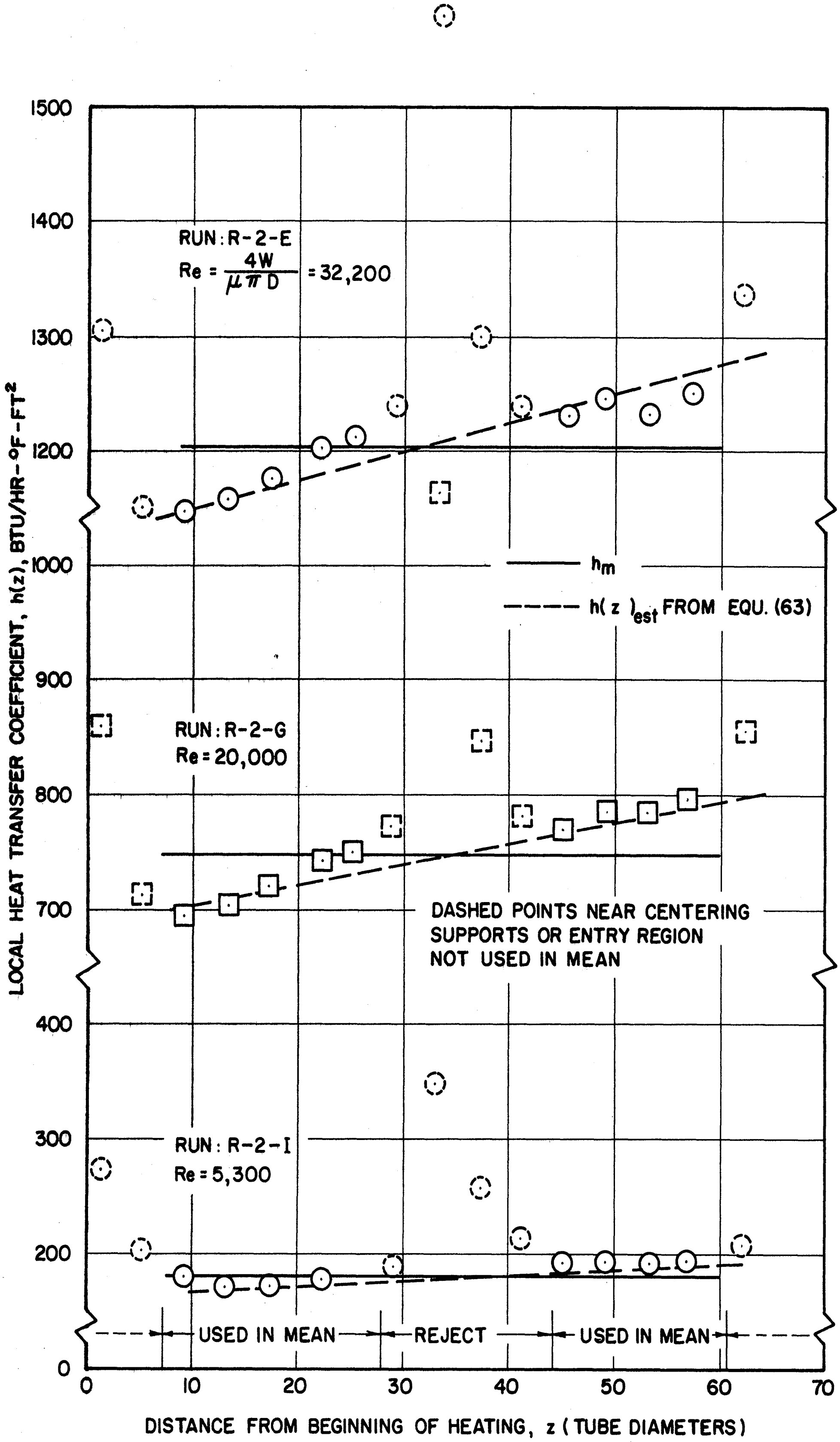

Figure 16. Sample Values of the Local Heat Transfer Coefficient for a Tube with a Threaded Rod in the Center as a Function of Longitudinal Position, h(z) vs. z, for d = 0.250.

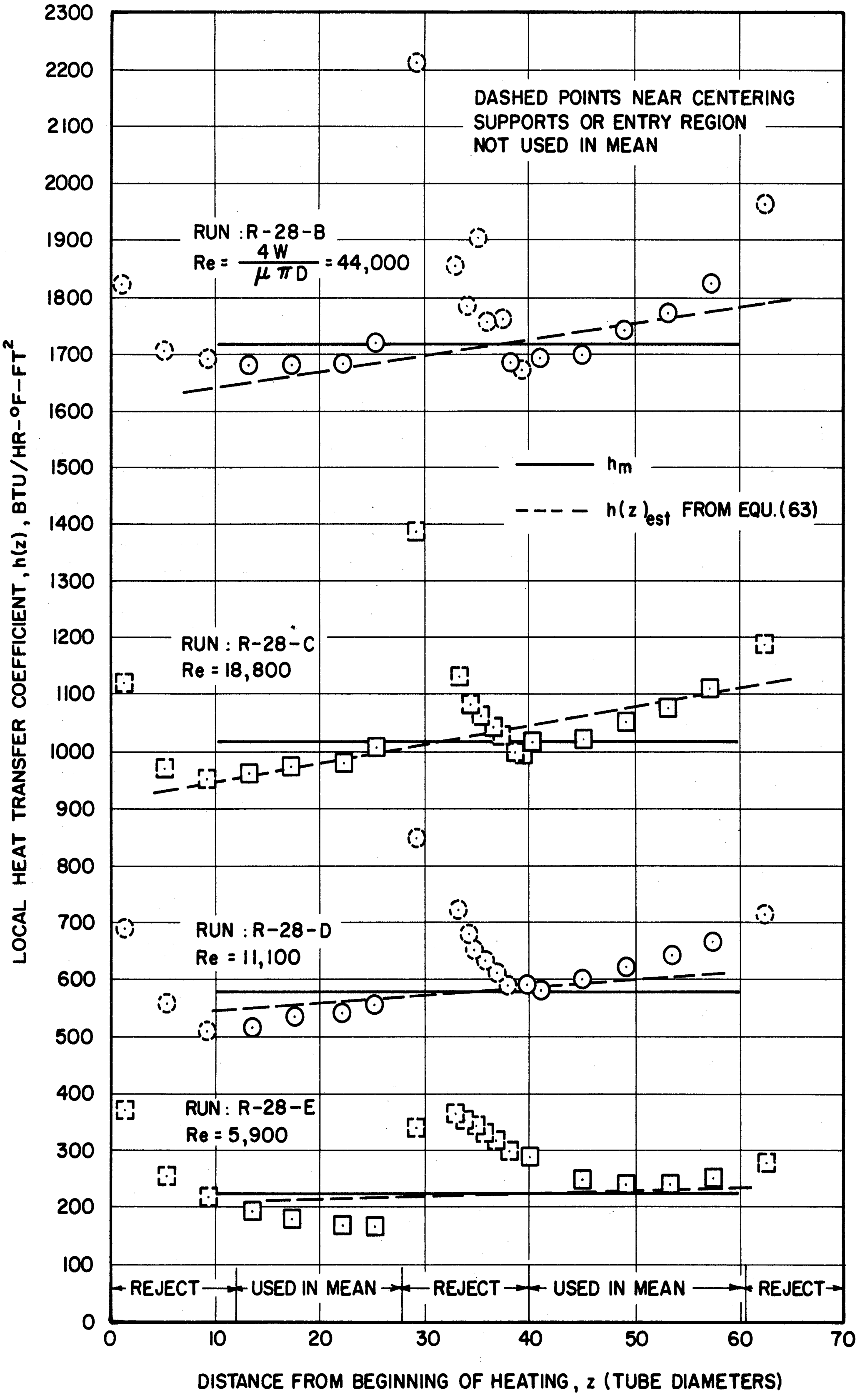

Figure 17. Sample Values of the Local Heat Transfer Coefficient for a Tube with a Solid Rod in the Center as a Function of Longitudinal Position, h(z) vs. z, for d = 0.625.

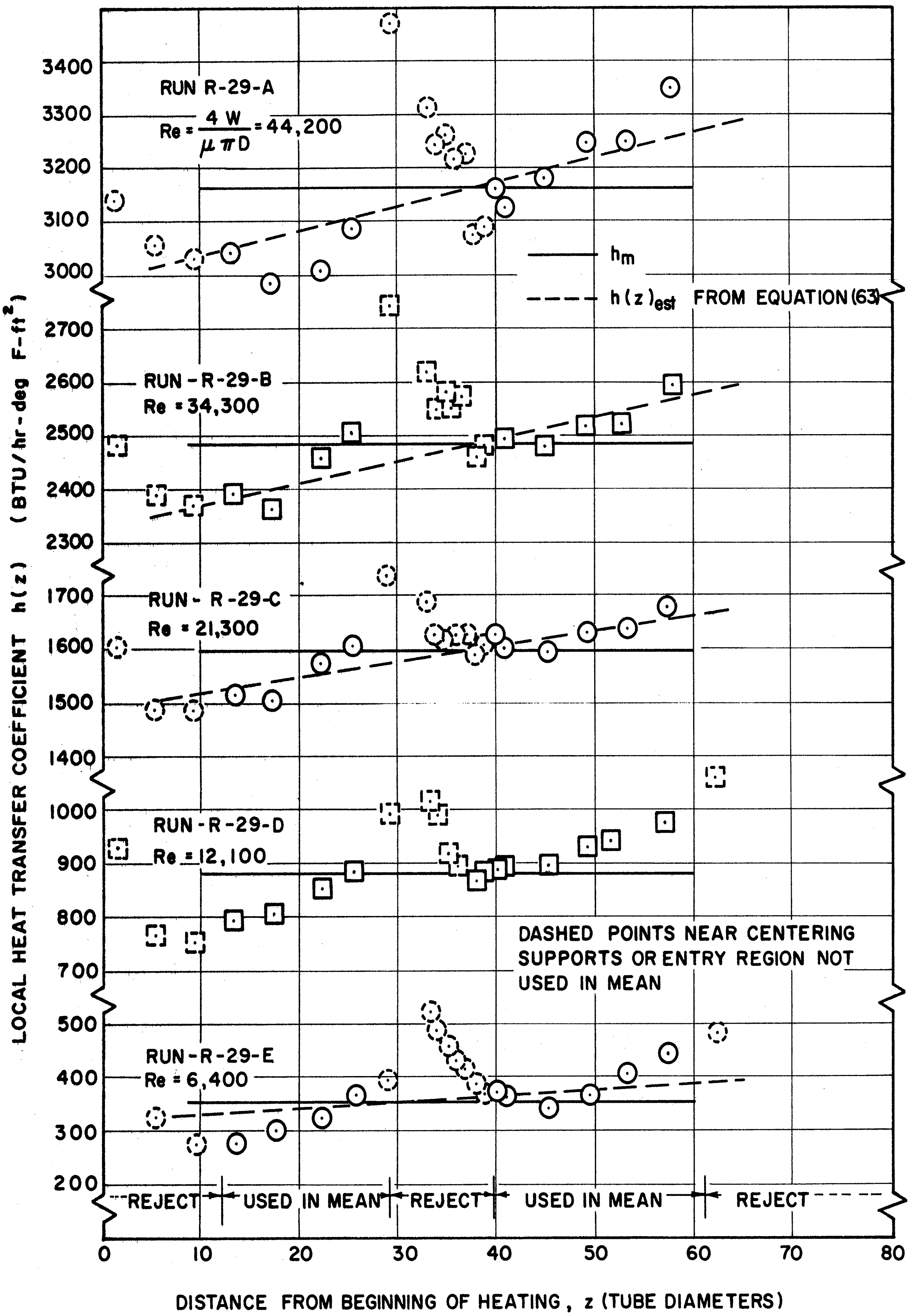

Figure 18. Sample Values of the Local Heat Transfer Coefficient for a Tube with a Solid Rod in the Center as a Function of Longitudinal Position, h(z) vs. z, for d = 0.750.

failure of the dashed lines to explain the increase in heat transfer coefficient as the fluid is heated occurs at the smaller values of Reynolds number. (Note: The transition region of flow, $2,300 < Re^* < 10,000$, corresponds to $5,000 < Re < 21,190$ for $d = 0.750$ and corresponds to $3,000 < Re < 14,700$ for $d = 0.125$.)

The variation in local heat transfer coefficient caused by changes in the physical properties, however, produces effects which are scarcely noticeable when the local coefficients are integrated to obtain mean values.

The dependence of Nusselt number on Reynolds number for the solid rod geometry is indicated in Figure 19 for different values of the diameter ratio d. For the solid rod with $d = 0.125$ the Nusselt number is actually less than (or equal to) that for the empty tube at the same Reynolds number, while for the rod with $d = 0.750$ it is over two times the value for the empty tube at Reynolds numbers greater than 20,000. The effect of the transition region of flow at low Reynolds numbers is quite evident.

A correlation making use of equivalent diameters is shown in Figure 20. In this plot the equivalent Nusselt numbers (divided by $Pr^{1/3} (\mu/\mu_w)^{0.14}$) based on the integrated heat transfer coefficient for a solid rod and the equivalent diameter suggested by Lohrenz and Kurata is plotted versus the equivalent Reynolds number Re*. Several observations may be noted: 1) The data are consistent with the data of Monrad and Pelton. 2) The line which best fits the data is about ten per cent below the line for the Sieder-Tate equation, indicating that a value of

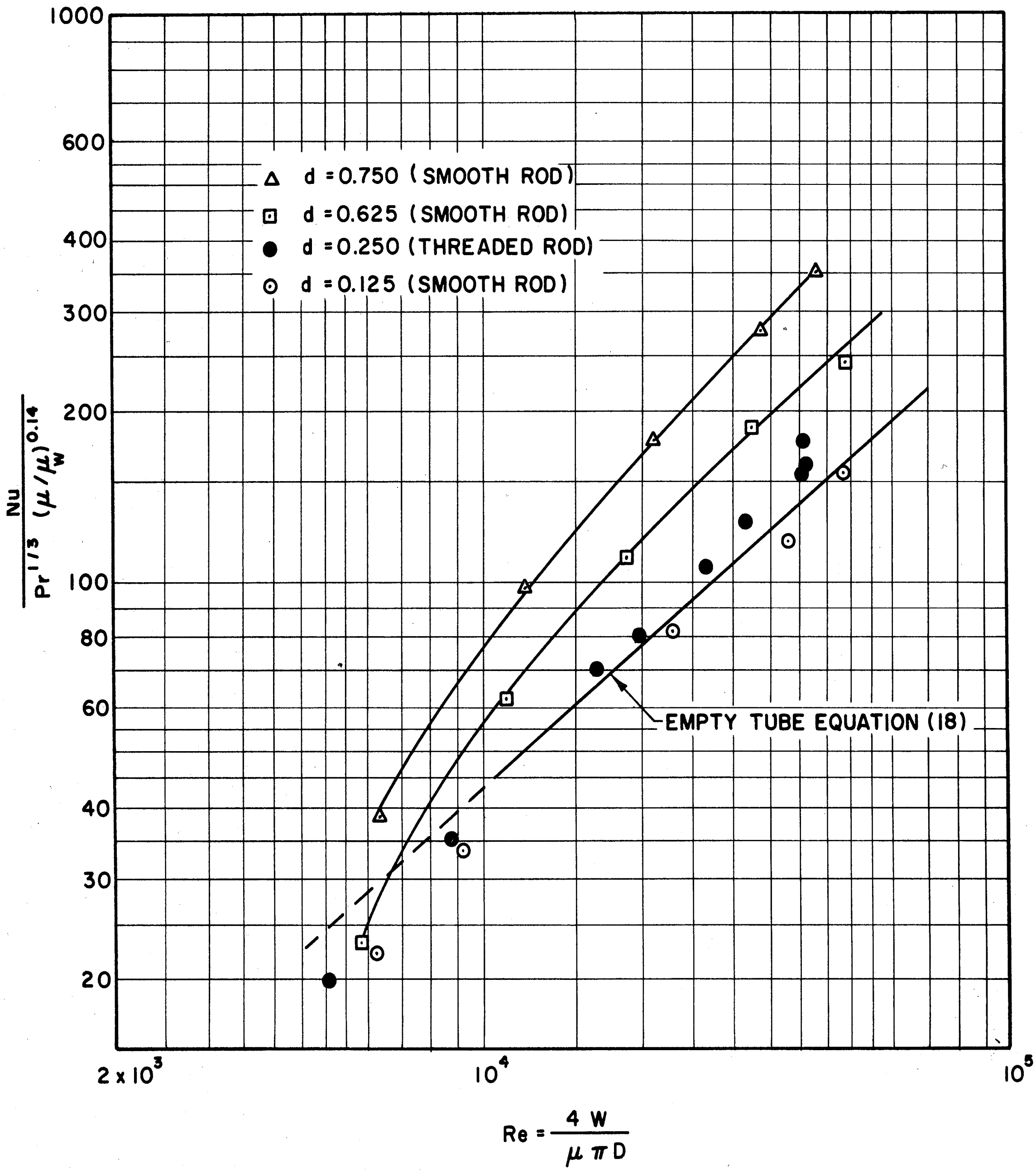

Figure 19. Nusselt Numbers for the Tube with a Solid Rod in the Center as a Function of Reynolds Number, Nu vs. Re, with Parameters of d.

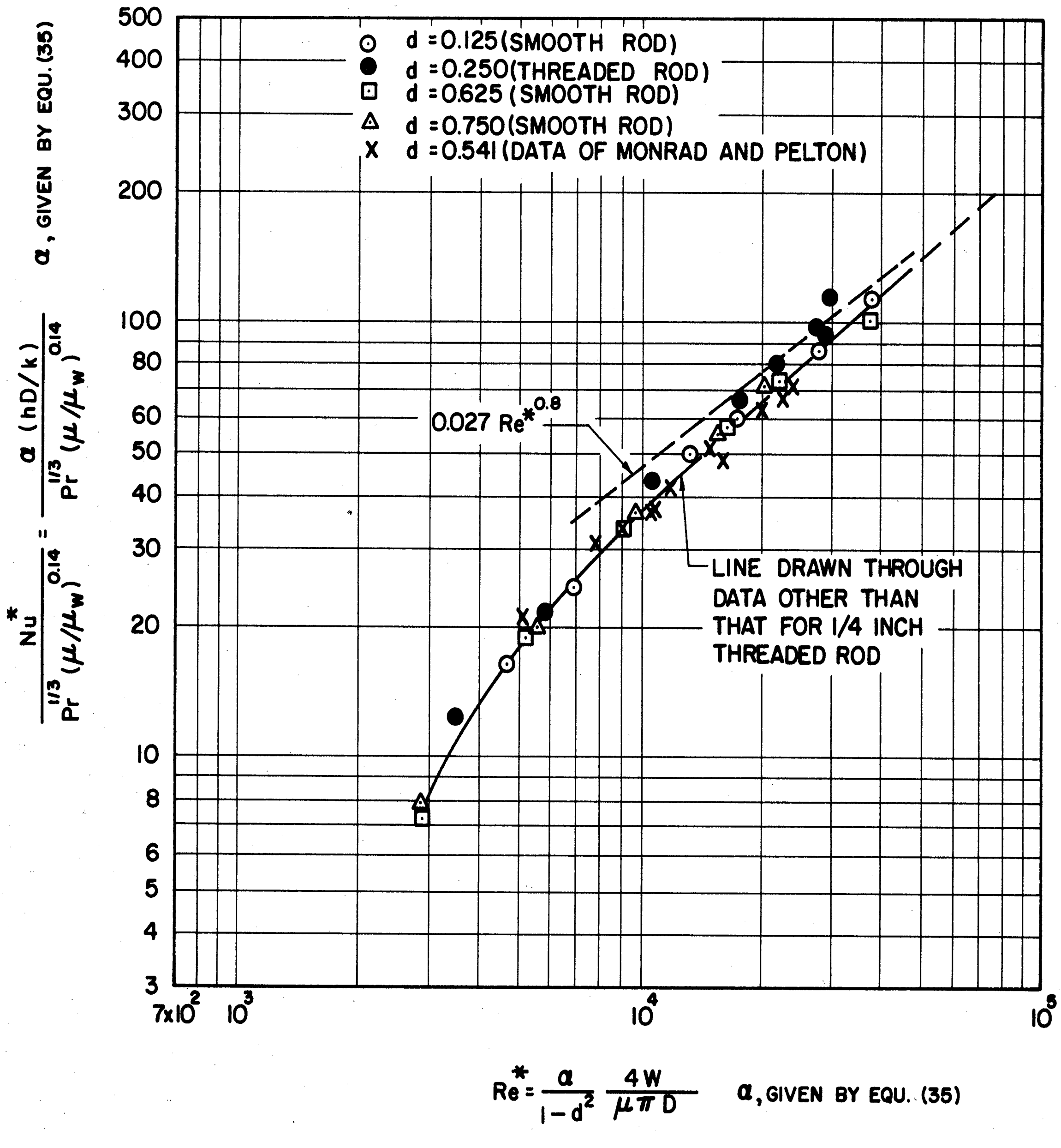

Figure 20. Nusselt Number for the Tube with a Solid Rod in the Center as a Function of Reynolds Number Based on Equivalent Diameters, $Nu^*/(Pr^{1/3}[\mu/\mu_w]^{0.14})$ vs. Re^*.

0.024 should be used for the constant C_2 in the correlation. This trend is suggested by the theoretical analysis of Barrow[2]. 3) The effect of roughness of the rod on the equivalent Nusselt number Nu* is much less than the effect on the equivalent friction factor f* with the points for the threaded rod of diameter ratio d = 0.25 falling only slightly above the line drawn through points for the smooth tube.

Disks Evenly Spaced and Centered in the Tube

Pressure Drop

Friction factors for flow around the disks in the center of the tube are presented in Figures 21, 22, 23, and 24 for s = 2, 4, 8, and 12 with the diameter ratio d as a parameter. Since these friction factors are not based on any equivalent diameter, they indicate directly the effect of the disk geometry on the pressure drop. It is seen that for disks at a spacing of 2 tube diameters with a diameter ratio of 0.875 the pressure drop is over 300 times that for an empty tube. As would be expected, except for small diameter ratios and large spacing, the friction factors are practically independent of Reynolds number.

For a particular geometry (i.e. a given value of d and s) the friction factor can be represented by an equation of the form

$$100 f = C(s,d)\, Re^{n(s,d)} \qquad (64)$$

The constants C(s,d) and n(s,d) evaluated by the method of least squares are listed as a function of s and d in Table VIII in Appendix C. The lines drawn with the data for each geometry in Figures 21, 22, 23, and 24 are the lines given by the above equation.

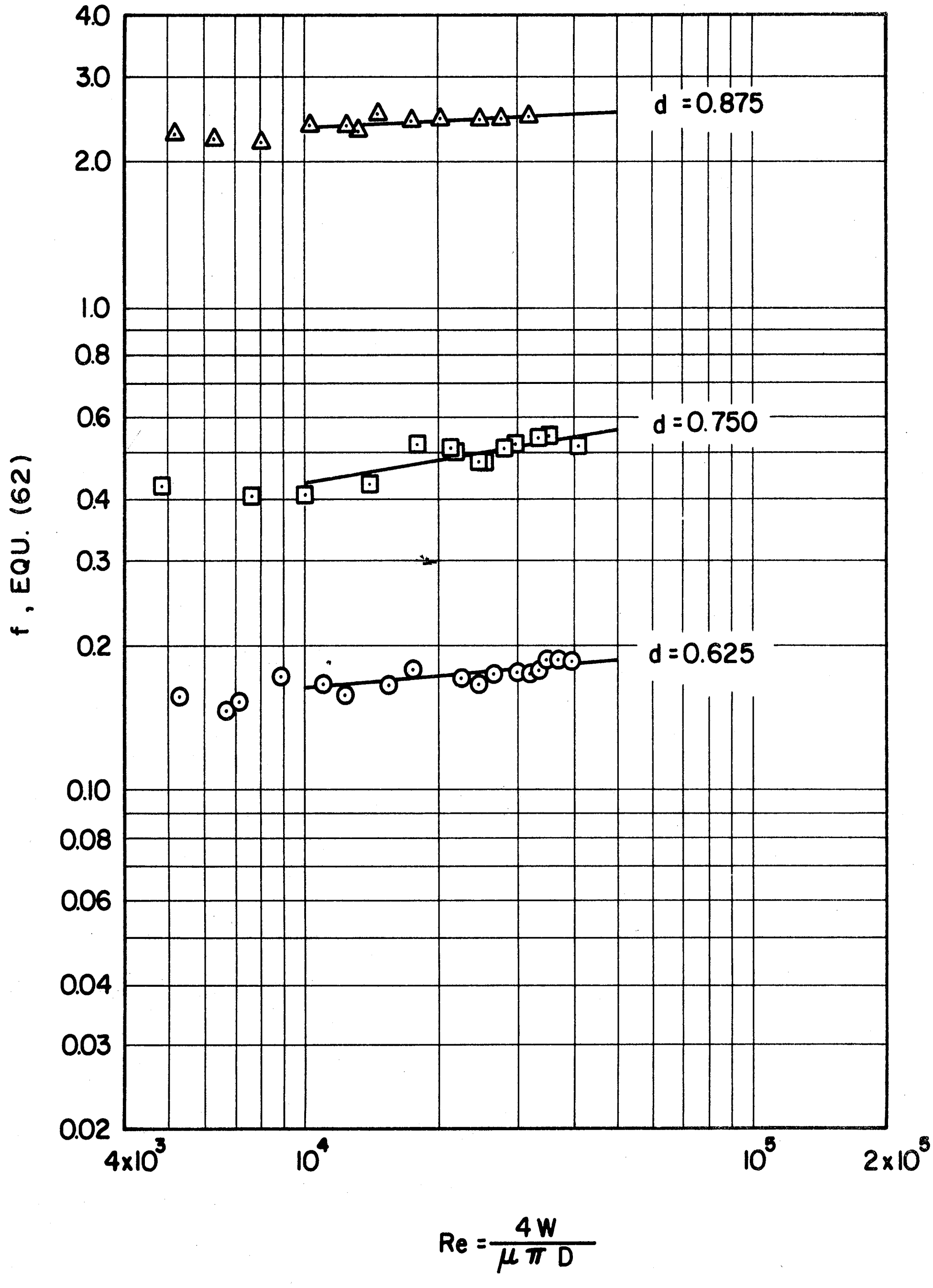

Figure 21. Friction Factor for Disks as a Function of Reynolds Number, f vs. Re, for s = 2 with Parameters of d.

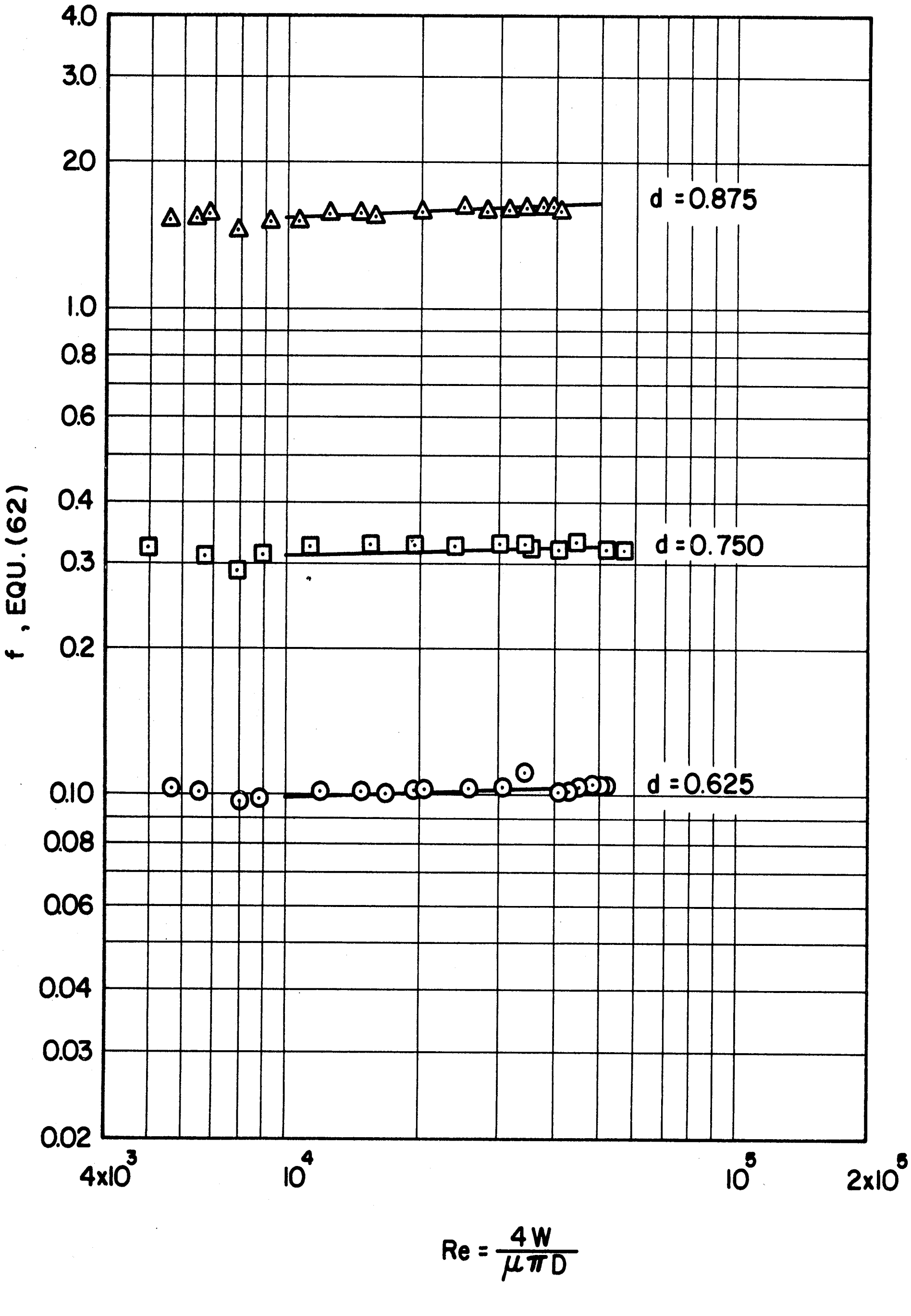

Figure 22. Friction Factor for Disks as a Function of Reynolds Number, f vs. Re, for s = 4 with Parameters of d.

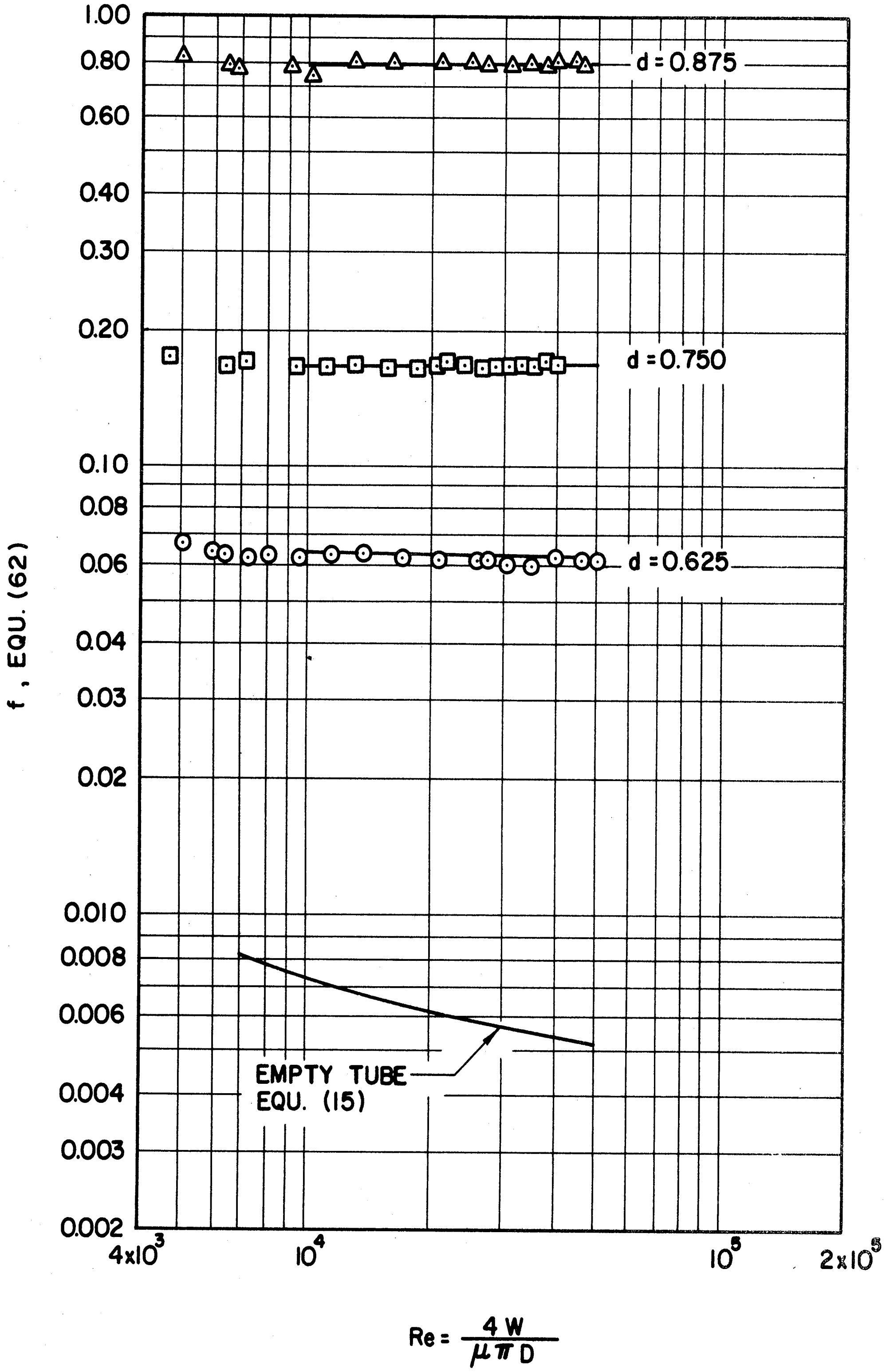

Figure 23. Friction Factor for Disks as a Function of Reynolds Number, f vs. Re, for s = 8 with Parameters of d.

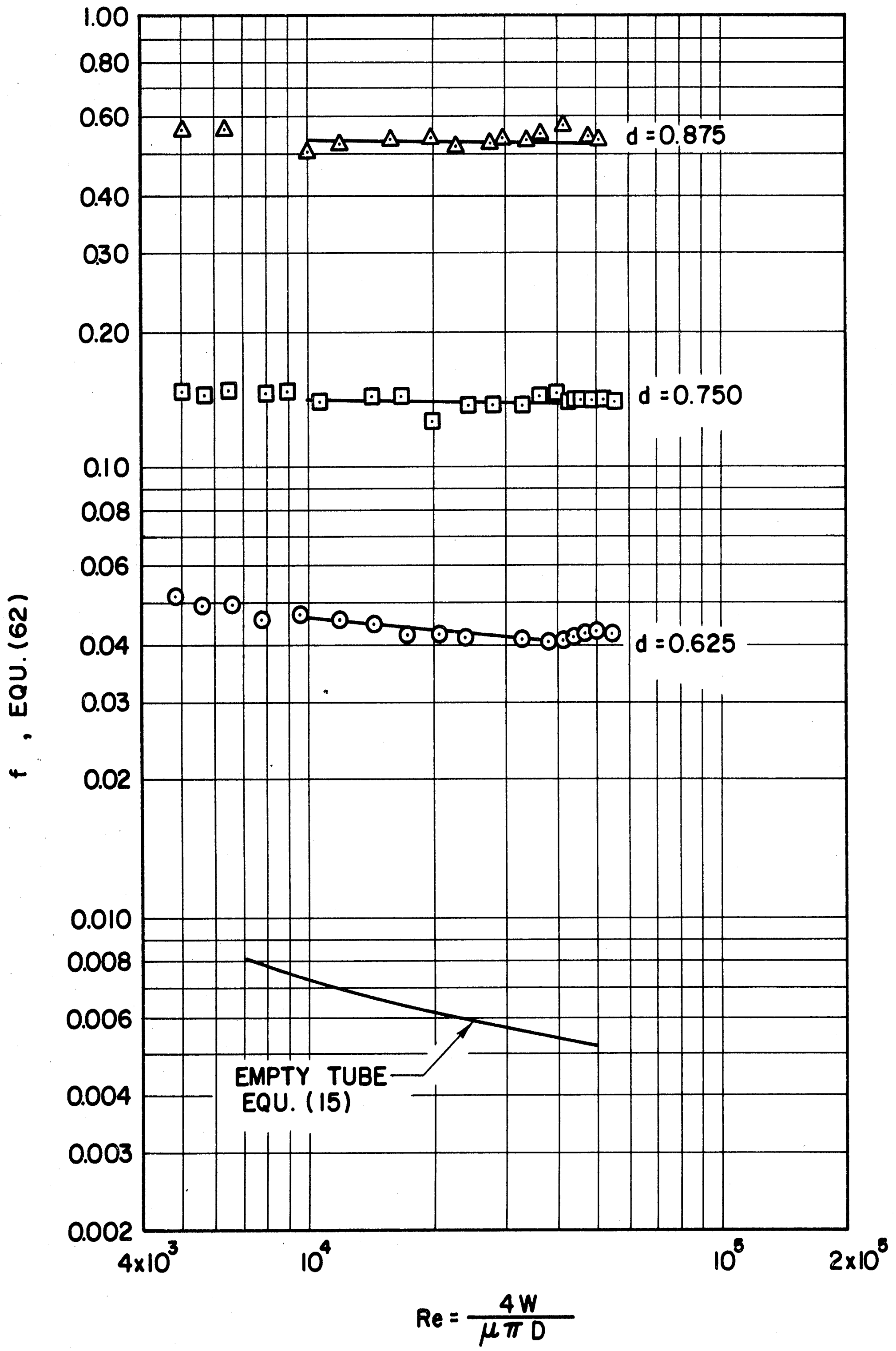

Figure 24. Friction Factor for Disks as a Function of Reynolds Number, f vs. Re, for s = 12 with Parameters of d.

In Figure 25 a trial correlation is attempted, based upon characterizing the pressure drop by an effective drag coefficient (defined by Equation (14)) for a single bluff body rather than by a friction factor of the type used for smooth tubes. The effective drag coefficient f_D is plotted versus Reynolds number for $s = 12, 8, 4$, and 2 with diameter ratio as a parameter. These plots bring the curves for different diameter ratios close together, particularly when it is noted that the ordinates are arithmetic rather than logarithmic.

As with the friction factors, for a particular geometry the effective drag coefficient can be represented by an equation of the form

$$100\, f_D = C(s,d)\ Re^{n(s,d)} \tag{65}$$

The constants $C(s,d)$ and $n(s,d)$ evaluated by the method of least squares are listed as a function of s and d in Table IX in Appendix C. The lines drawn with the data for each geometry in Figure 25 are the lines given by the above equation.

The effective drag coefficients are cross-plotted versus free area in Figure 26 for four different spacings with Reynolds number as a parameter. They are cross-plotted versus spacing in Figure 27 at three different diameter ratios with Reynolds number as a parameter. Again, in both of these plots the ordinate is in arithmetic coordinates. As is expected, the drag coefficient decreases as the disks get closer together (and their wakes start interfering with each other). The slight variation of f_D with free area may well be the result of scatter in the data from which the cross-plots were prepared rather than a real, though second order effect.

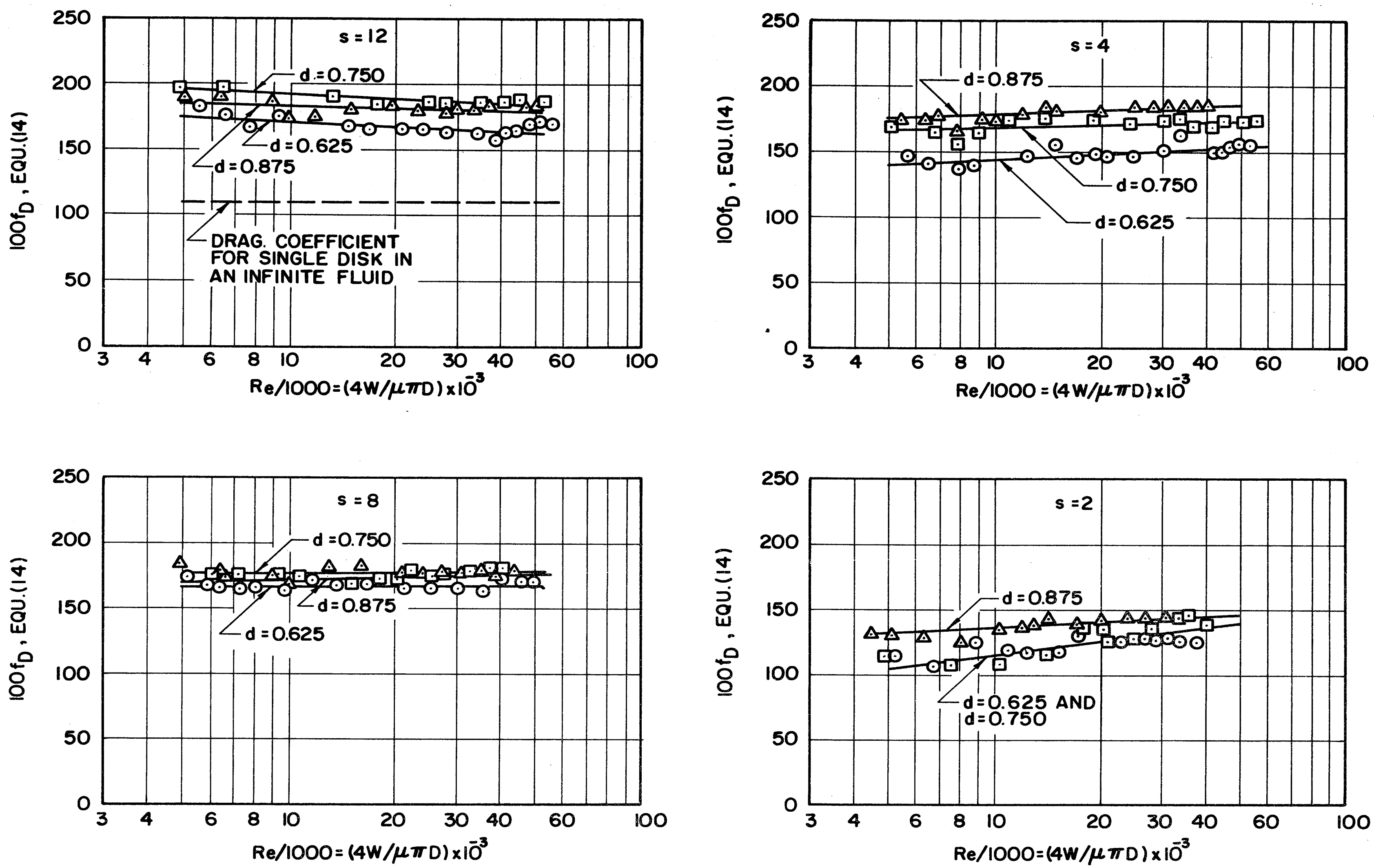

Figure 25. Effective Drag Coefficient for Disks as a Function of Reynolds Number, f_D vs. Re, for s = 12, 8, 4, and 2 with Parameters of d.

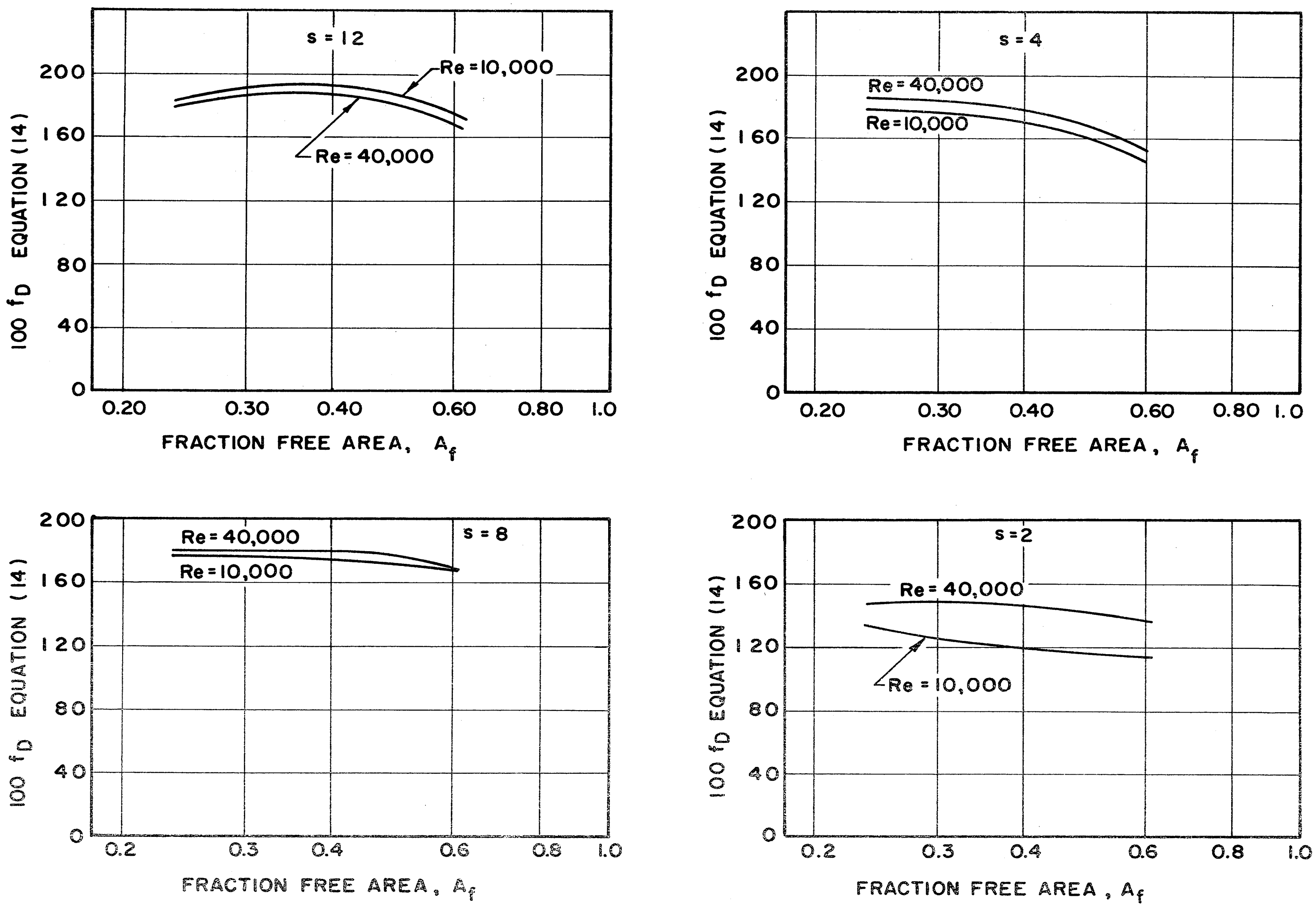

Figure 26. Effective Drag Coefficient for Disks as a Function of Free Area, f_D vs. A_f, for s = 12, 8, 4, and 2 with Parameters of Re.

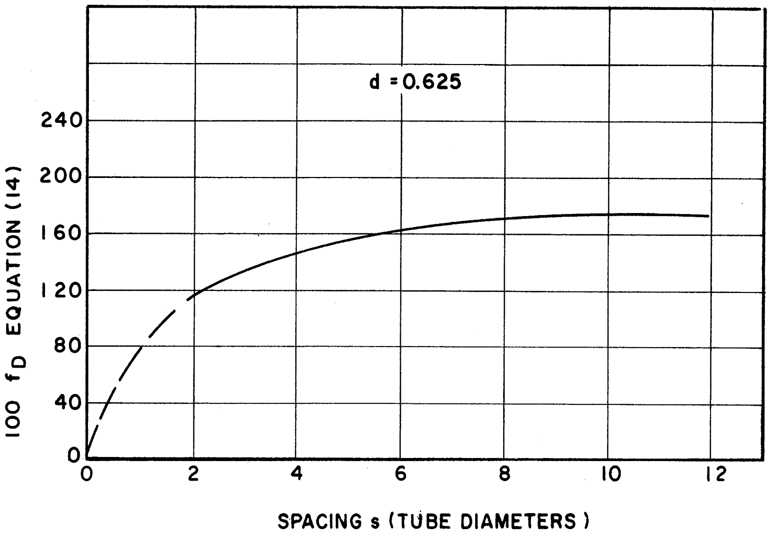

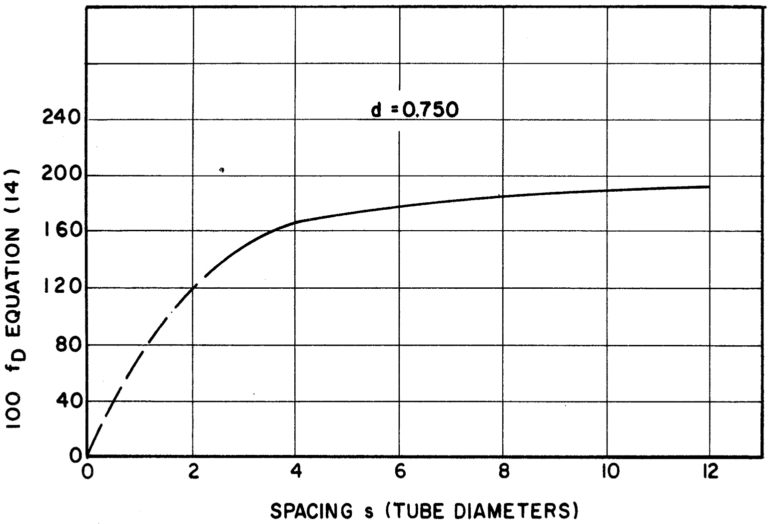

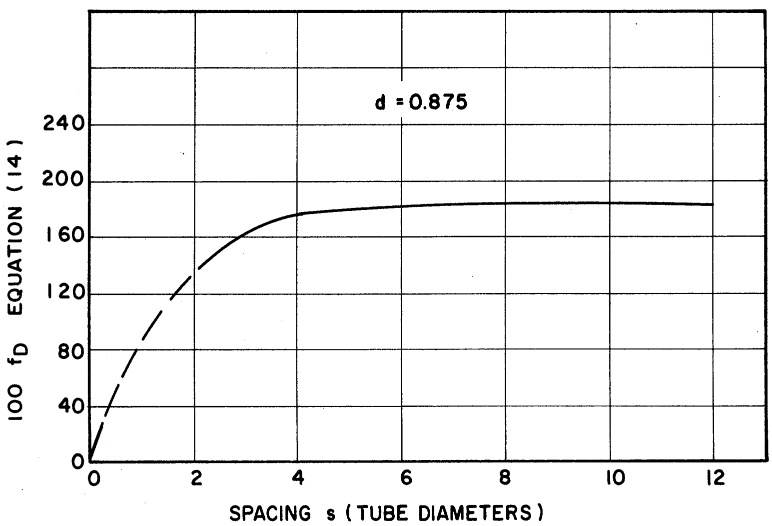

Figure 27. Effective Drag Coefficient for Disks as a Function of Spacing, f_D vs. s, for d = 0.625, 0.750, and 0.875 and any Reynolds Number.

The generally accepted value of the drag coefficient for a disk in an infinite fluid with a uniform flow is independent of Reynolds number when the flow is turbulent and has a value of 1.10. This line is drawn in Figure 25 for s = 12 to indicate that the measured coefficients are at least in the expected range. One might expect the effective drag coefficients for disks in a tube to approach 1.10 as the diameter ratio becomes small and the spacing large. In this case, however, the effect of the solid rod on which the disks are mounted and the effect of the non-uniform flow (i.e., the fluid velocity in a tube is a logarithmic function of radius) would have to be considered.

The cross-plots indicate that the effective drag coefficients for disks are relatively independent of free area and Reynolds number. Therefore, a generalized correlation for disks of the form

$$100\ f_D = \frac{C_1\ s}{C_2 + s} \qquad (66)$$

is suggested. Best values of the constants for the above, generalized correlation were obtained from the data of this investigation and found to be

$$C_1 = 156$$
$$C_2 = 0.78$$

An indication of the validity of the correlation is given in Figure 28 where f_D predicted by Equation (66) is plotted versus the value measured experimentally. All of the data were correlated with an average deviation of 6.6 per cent.

The only similar type data available in the literature for comparison are those taken by Koch[23]. Koch presented plots of

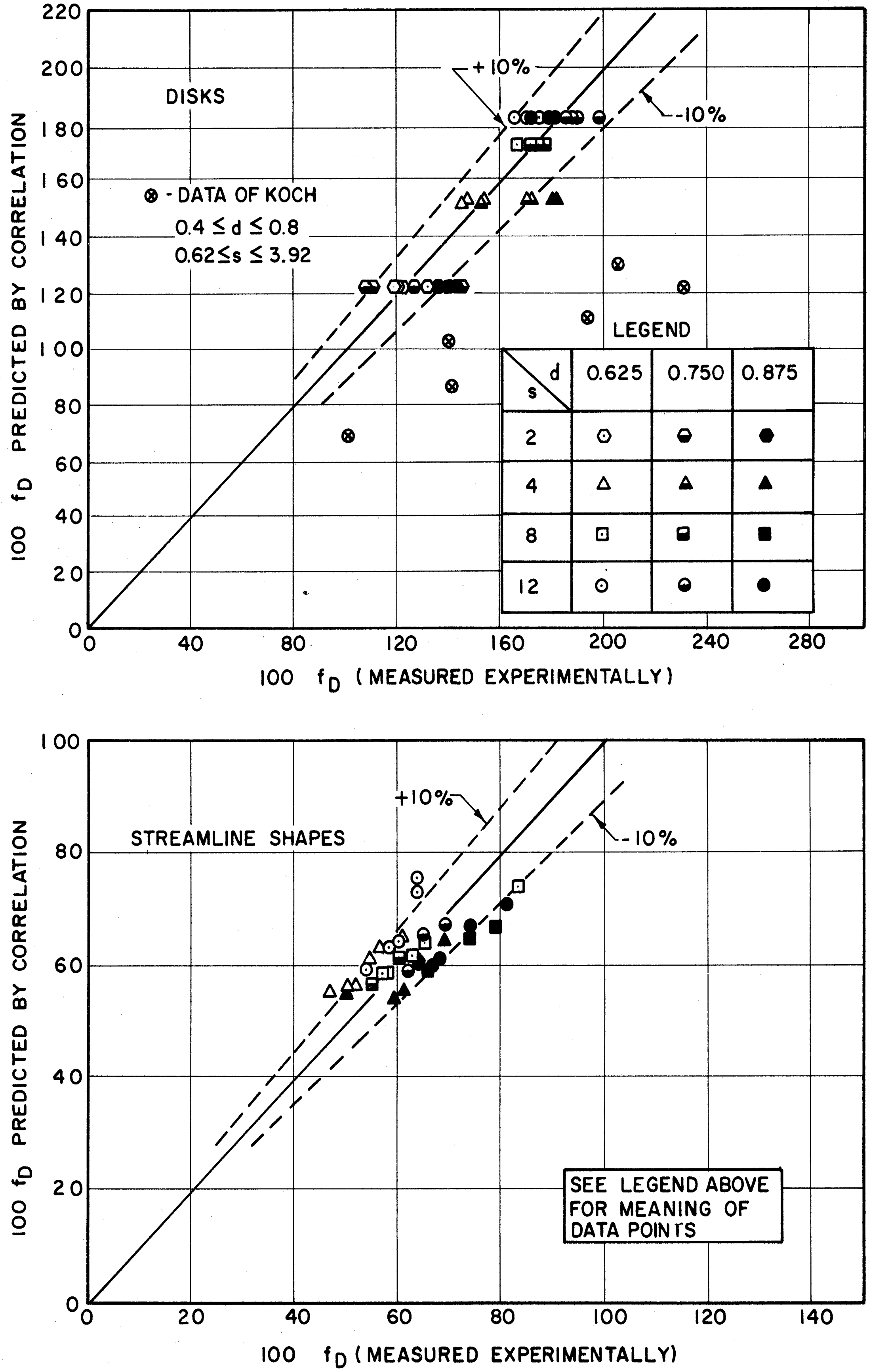

Figure 28. Test of Effective Drag Coefficient Correlation, f_D values Predicted by Correlation vs. Values Measured Experimentally for Disks and Streamline Shapes.

experimentally measured friction factors using air as the fluid as a function of Reynolds number for seven combinations of s and d. The spacing s ranged from 0.62 to 3.92 and the diameter ratio d was between 0.4 and 0.8. For Reynolds numbers between 10,000 and 40,000 the agreement of Koch's data with Equation (66) is indicated in Figure 28. It can be seen that, in general, Koch's experimental results are approximately 50 to 100 per cent greater than would be predicted by Equation (66). Possible explanations for this discrepancy are: 1) Koch's disks were centered in the horizontal tube with various centering supports which probably contributed to the total pressure drop, while the disks used in this experiment were mounted in a vertical tube and only centered at each end of the test section; 2) the size of Koch's centering rod which is not specified may have been such that his rod contributed more drag than the centering rod used in this investigation, and 3) any slight error in the measurement of the flow rate of the fluid or the dimensions of the tube and promoters are greatly magnified in the calculation of effective drag coefficients.

A better test of the correlation would be obtained if data at larger spacings were available for comparison. Unfortunately, however, the largest promoter spacings for which Koch reports pressure drop results is a spacing of 3.92 tube diameters and this corresponds to a diameter ratio of 0.40 where the influence of the centering rod is large.

Heat Transfer

Local values of the heat transfer coefficient ratio h/h_0 are plotted in Figure 29 versus distance from the disk x in tube diameters

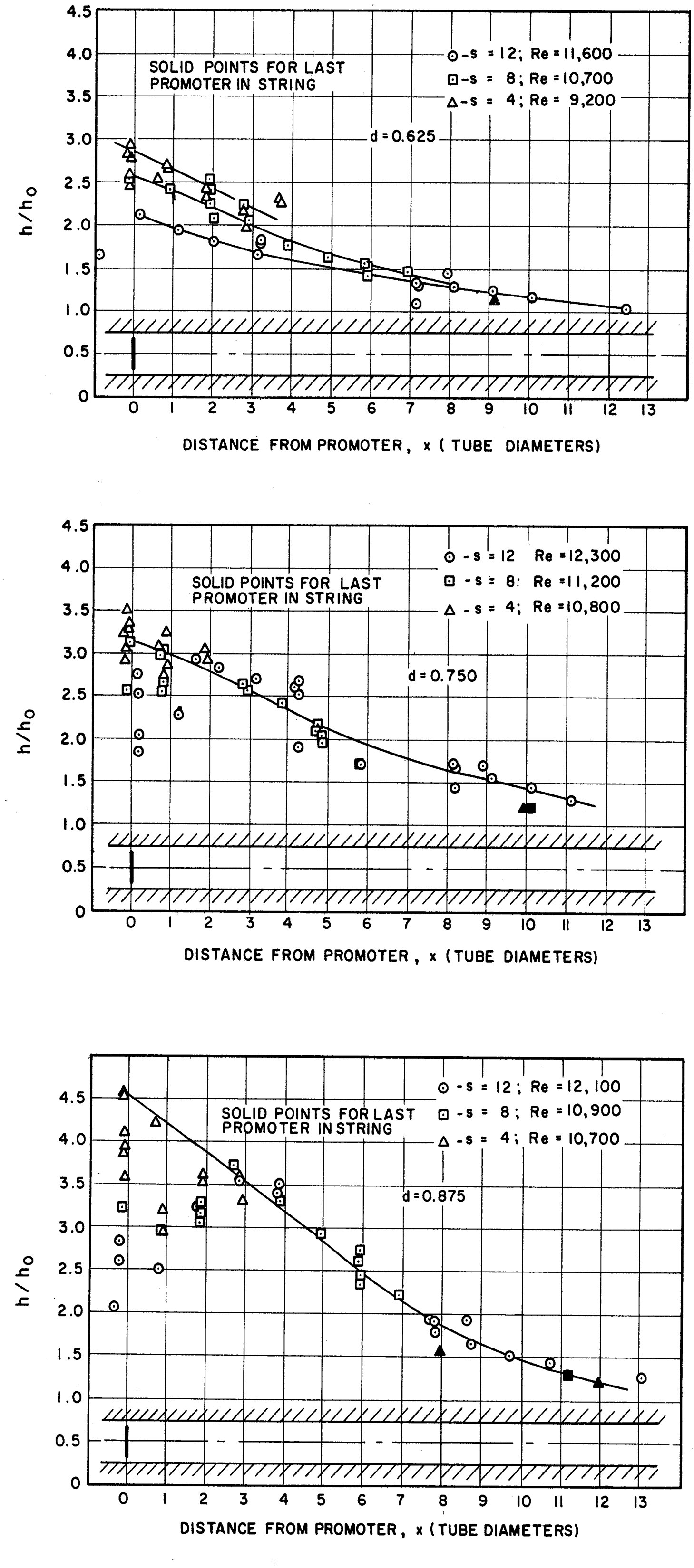

Figure 29. Sample Values of Local Heat Transfer Coefficient Ratio for Disks as a Function of Longitudinal Position from Disk with Reynolds Number Approximately 10,000, h/h_0 vs. x, for d = 0.625, 0.750, and 0.875.

for three different diameter ratios. The coefficient h refers to the local heat transfer coefficient. The quantity h_0 refers to the value calculated for the empty tube using the Sieder-Tate equation and the same mass flow rate. A diagram of the inside of the tube is shown in each plot to indicate the relative dimensions of the disk and the position at which the local heat transfer coefficient is presented.

In some cases for values of x nearly equal to the spacing s the corresponding local value of h/h_0 was influenced more by the presence of the next promoter than by the decaying effect of the previous promoter. In these cases the value h/h_0 was plotted ahead of the promoter instead of behind or, in other words, the distance from the promoter was considered negative and interpreted as the distance to the next promoter.

For each case illustrated in Figure 29 the set of experimental results corresponding to the Reynolds number nearest 10,000 was selected. The following may be noted from the figure:

1. In general, the points fall on the same smooth curve regardless of spacing downstream from the disk. This is expected, since the effect of constricting the flow overpowers the effect of the previous history of the fluid. The biggest separation of curves for different spacings occurs for the diameter ratio 0.625 which is the case in which the fluid flow is least constricted.

2. The point of maximum heat transfer coefficient appears to be shifted downstream about two tube diameters from the disk in the case of the disk with the largest diameter ratio. This may be explained by

two factors: a) the point of maximum velocity of the fluid does not occur at the point of minimum free area, but is shifted downstream due to a "vena-contracta" effect; b) axial conduction along the tube wall causes the step change in heat transfer coefficient which might be expected to be damped, somewhat. (This last effect is considered in more detail in Part 4 of Appendix B.)

3. The heat transfer coefficient approaches the heat transfer coefficient for the empty tube about 12 to 15 diameters downstream from the disk.

The integrated mean heat transfer coefficients were calculated by fitting a first, second, and third order polynomial by the method of least squares to the local coefficients as a function of x, the dimensionless distance in tube diameters from the promoter. The polynomial was then integrated analytically to obtain the mean value. In almost every case the mean results for all three polynomials agreed very well (usually to within one per cent). The values for the first order polynomials were chosen for consistency. Data points in the vicinity of the first and last promoter in a string were not used in calculating the mean value in order to eliminate any entrance or exit effect.

The mean coefficients (in the form h_m/h_0 where h_0 is the heat transfer coefficient for the empty tube as calculated by the Sieder-Tate equation at the same mass flow rate) are presented in Figure 30 versus Reynolds number for each spacing with d as a parameter.

For a particular geometry the heat transfer coefficient ratios fall roughly on a line given by

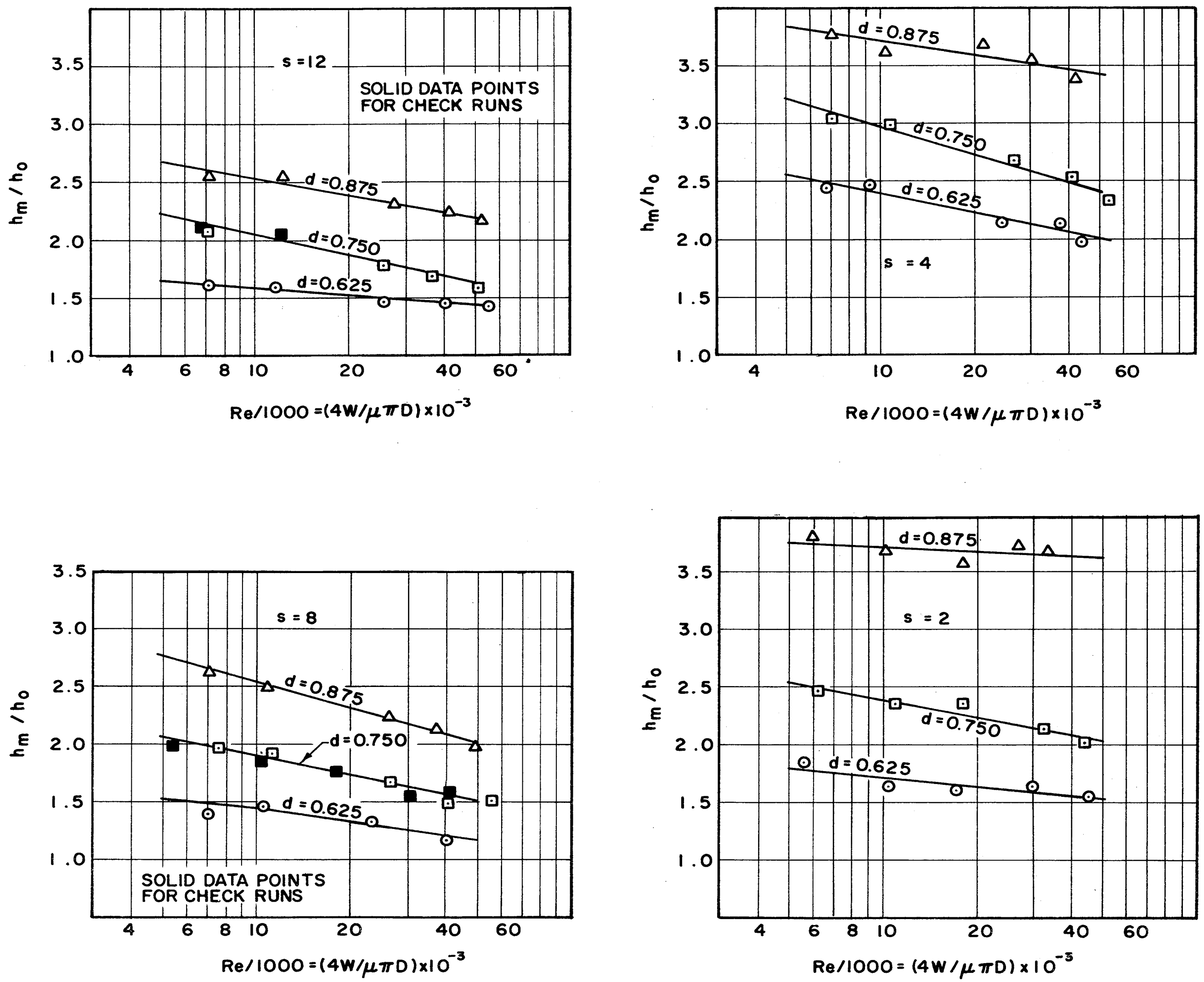

Figure 30. Overall Mean Heat Transfer Coefficient Ratio for Disks as a Function of Reynolds Number, h_m/h_o vs. Re, for s = 12, 8, 4 and 2 with Parameters of d.

$$h_m/h_0 = C(s,d)\ Re^{n(s,d)} \qquad (67)$$

The constants $C(s,d)$ and $n(s,d)$ evaluated by the method of least squares are given as a function of s and d in Table X of Appendix C. The lines drawn with the data for each geometry in Figure 30 are the lines given by the above equation.

It is not surprising that the ratio h_m/h_0 decreases as the Reynolds number increases, since at high Reynolds numbers the flow is extremely turbulent and the added disturbance produced by the disks does not produce as great an effect.

The results are cross-plotted versus logarithm of the free area in Figure 31 for $s = 12$, 8, 4, and 2 with Reynolds number as a parameter. It is seen that the cross-plotted values of the h_m/h_0 ratio produce an almost straight line approaching unity as the free area approaches one. The data are cross-plotted versus spacing in Figure 32 for Reynolds numbers of 10,000, 20,000, and 40,000 with diameter ratio as a parameter. There is a spacing at which the maximum heat transfer coefficient occurs before the coefficient starts decreasing (as the disk spacing is reduced) to the value for a solid rod in the center of the tube.

A generalized correlation of the heat transfer coefficient ratio as a function of diameter ratio d, spacing s, and Reynolds number of the following form was suggested by the appearance of the cross-plots.

$$\frac{h_m}{h_0} = 1 + C_1 \left[\frac{Re}{10{,}000}\right]^{n_1} (-\ln A_f) \left[\frac{1}{1 + C_2 s} - \frac{C_3}{C_4 + s^4}\right] \qquad (68)$$

Best values of the constants for the above, generalized correlation were

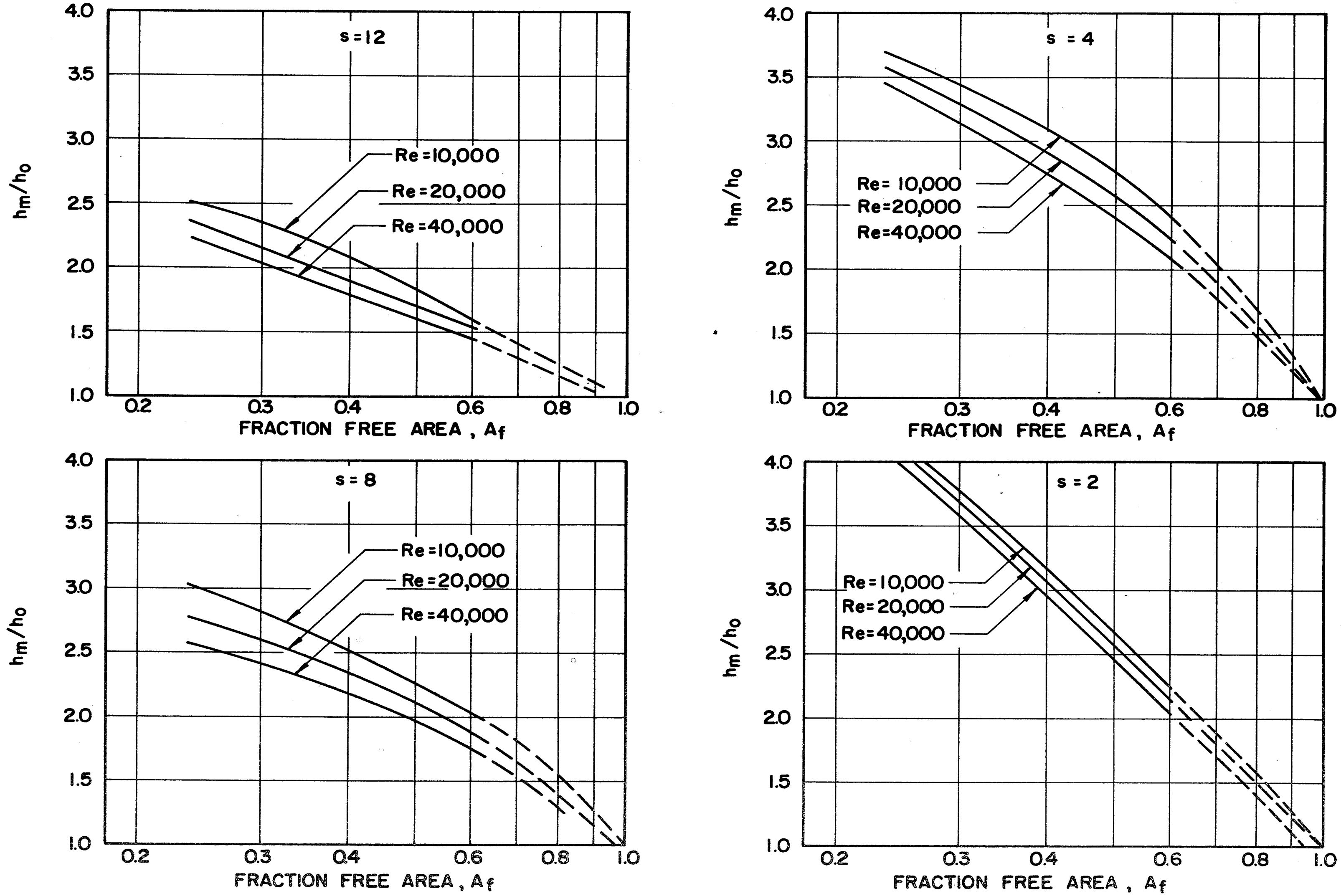

Figure 31. Overall Mean Heat Transfer Coefficient Ratio for Disks as a Function of Free Area, h_m/h_o vs. A_f, for s = 12, 8, 4, and 2 with Parameters of Re.

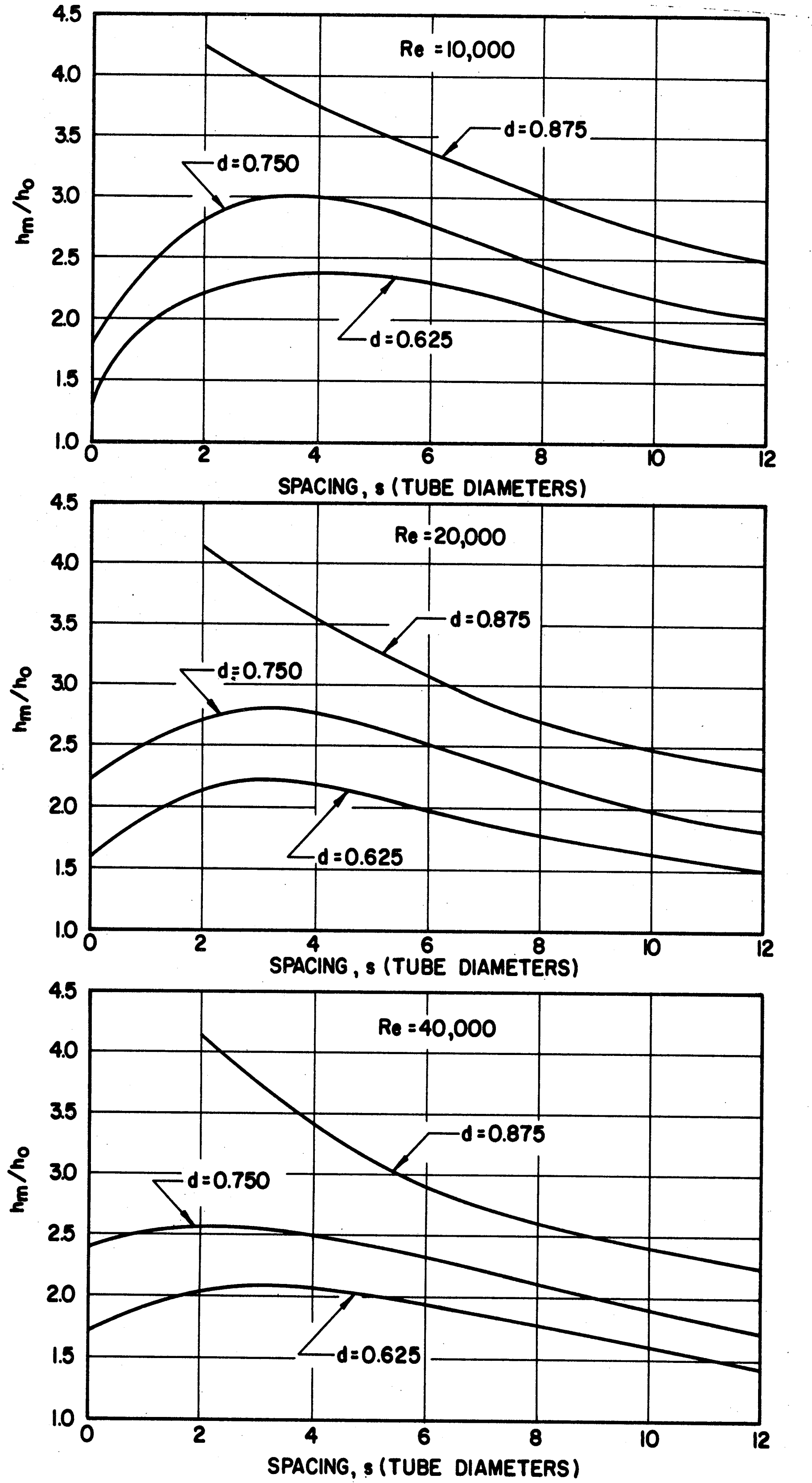

Figure 32. Overall Mean Heat Transfer Coefficient Ratio for Disks as a Function of Spacing, h_m/h_0 vs. s, for Re = 10,000, 20,000, and 40,000 with Parameters of d.

obtained from the experimental data of this investigation and found to be

$$C_1 = 3.28$$

$$C_2 = 0.15$$

$$C_3 = 1.7$$

$$C_4 = 11.9$$

$$n_1 = -0.14$$

As an indication of the validity of the correlation h_m/h_0 predicted by the correlation equation (68) is plotted in Figure 33 versus the value measured experimentally for each combination of d, s, and Re. All of the data are correlated with an average deviation of 5.6 per cent. The type of plot given by Figure 33 tends to emphasize the points which deviate from the correlation, since the many points which are correctly predicted overlap one another.

There are several sources of heat transfer data for disks to use for comparison. First, there is the work by Koch[23] in which experimental values of the Nusselt number are plotted as a function of Reynolds number using air as the fluid, for six different disk combinations of the same type as that used in this investigation. The diameter ratio varied between 0.4 and 0.8 and the spacing was between 0.62 and 2.80. As indicated in Figure 33 the agreement is good with all of Koch's data predicted with an average deviation of 9.8 per cent by Equation (68).

A second source of data is that of Sundstrom and Churchill[40]. The major portion of their experimental work concerned heat transfer from gas flames to a cylindrical tube one inch in inside diameter. As part of their investigation, however, non-burning, local rates of heat

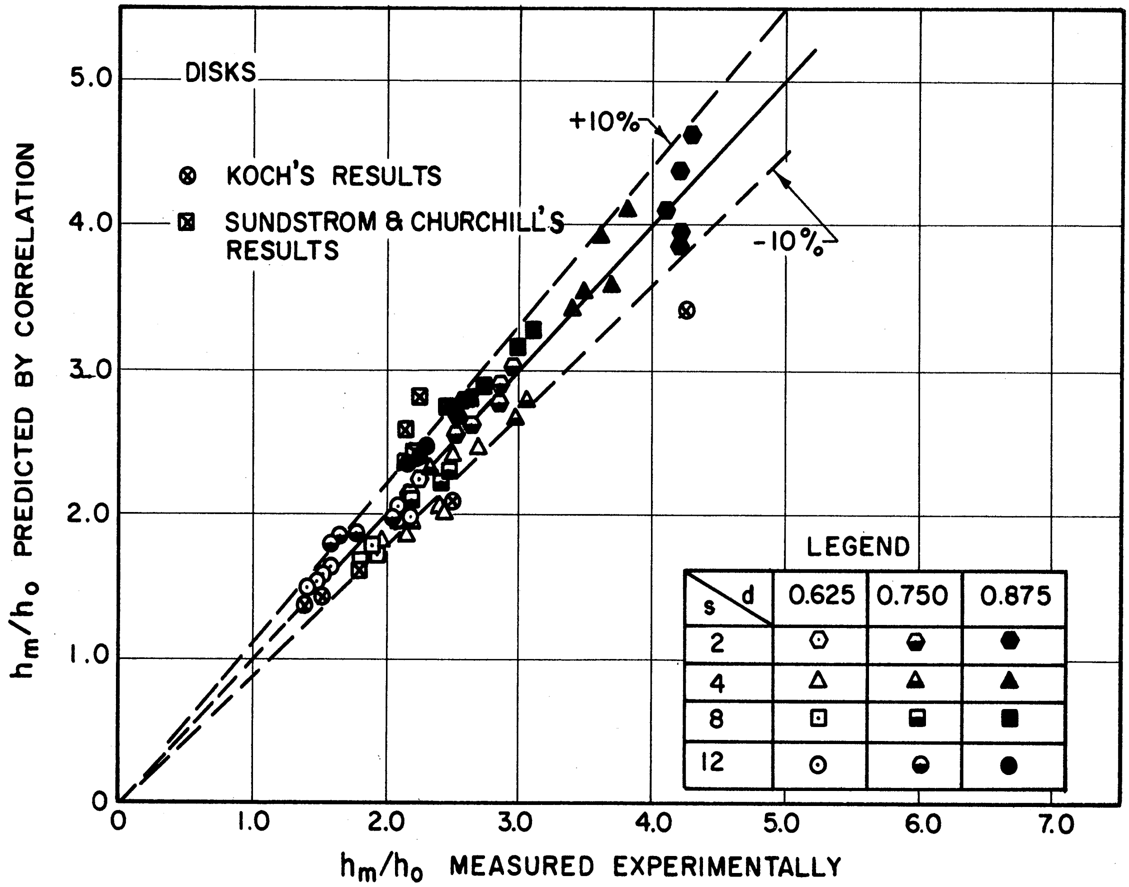

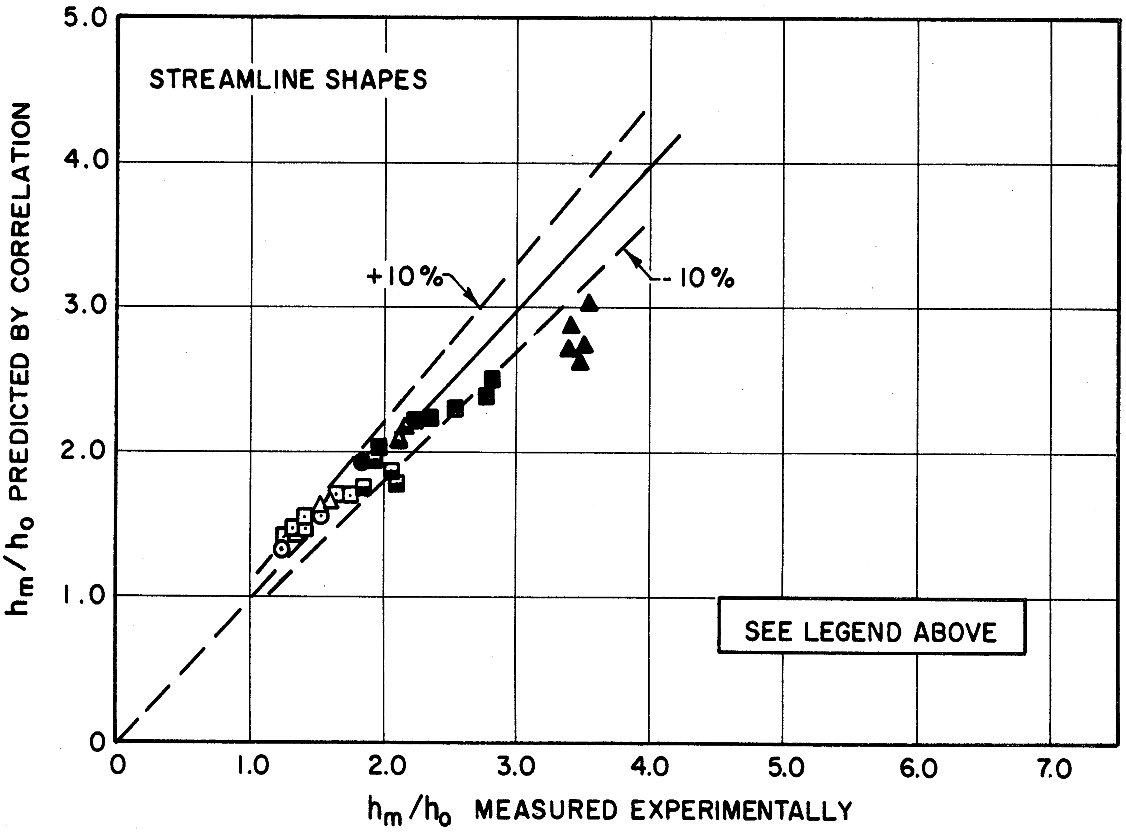

Figure 33. Test of Heat Transfer Correlation, h_m/h_0 Ratios Predicted by Correlation vs. Values Measured Experimentally for Disks and Streamline Shapes.

transfer from hot air to cold water flowing outside the tube were measured. The flow was disturbed by the presence of a single disk-shape, bluff-body flame holder centered in the burner. The flame holder provided 48 per cent free area and the Reynolds number varied from 5,000 to 20,000.

For a Reynolds number of 10,000 Sundstrom and Churchill noted a maximum value of h_m/h_0 of 2.6 occuring about 1-1/2 tube diameters downstream from the flame holder. Strictly speaking, the results of their work are not comparable with the results of this investigation and with Koch's work, since they had only one disk rather than a series of them. The effect of spacing can be simulated, though, by considering the integrated average heat transfer coefficient from the flame holder to a distance s tube diameters downstream as corresponding to the same results that would be obtained if a series of promoters were spaced a distance s tube diameters apart. Using this technique, results of their experiments may be compared with the predictions of Equation (68). It is found that, in general, their measurements were approximately ten per cent below the values predicted.

A third source of data is the work of Zartman and Churchill[43]. Their measurements were made with the same type of apparatus and with practically the same intent as those of Sundstrom and Churchill except that they used a tube of five inch inside diameter, only one Reynolds number (14,000) and disk-shape, bluff-body flame holders which provided free areas of 9 per cent and 5 per cent. A maximum value of h_m/h_0 of 4.5 was found to occur at the flame holder. Values predicted by Equation (68) for these very low values of A_f (which represent quite an extrapolation of the equation) were almost two times the values observed experimentally by Zartman and Churchill. This indicates that the correlation can not be used with confidence for values of A_f much smaller than 0.234 (i.e., the smallest A_f for which data were obtained in this investigation).

Both the results of Koch and of Sundstrom and Churchill in which the Reynolds number was varied confirm the trend of decreasing h_m/h_0 with increasing Reynolds number for any given geometry.

Koch presented a graphical correlation of h_m/h_0 as a function of d and s for use in the Reynolds number range 10,000 to 40,000. His correlation was based upon results for ten combinations of s and d (of which data for only seven are given in his paper) with the diameter ratio ranging from 0.40 to 0.80 and the spacing from 0.62 to 7.82 tube diameters. This correlation seems to be in error for very close spacing, in that the predicted value of h_m/h_0 keeps increasing with closer spacing and there is no spacing which produces a maximum value. For a free area of 0.50 and a spacing of 1.05 a value of h_m/h_0 of 4.2 is predicted by his graph. This does not seem reasonable, since for a free area of 0.48, Sundstrom and Churchill found the maximum value of the local coefficient ratio h/h_0 to be 2.6. It would seem that at close spacings the highest value of the <u>mean</u> heat transfer coefficient would not be greater than the maximum value of the <u>local</u> coefficient for a single disk and, in fact, would probably start to get smaller and approach the value for a solid rod.

The probable explanation for the difficulty with Koch's correlation at close spacings is that it was based on too few combinations of d and s. In any experiment of this nature the high heat transfer coefficients are the most difficult to measure, since they correspond to the smallest temperature differences. Thus, with only one or two sets of data (corresponding to close spacings and high values of h_m/h_0) in error the whole correlation would be easily biased.

Even though Koch's correlation does not agree with Equation (68) at close spacings, the bulk of his data do.

Streamline Shapes Evenly Spaced and Centered in the Tube

Results for the streamline shapes have been plotted in exactly the same manner as the results for the disks. In other words, for every plot of results for the streamline shapes there has already been presented a corresponding plot for the disks. Therefore, attention will be called only to the dissimilarities between the results for streamline shapes and the results for disks.

Pressure Drop

Friction factors are plotted versus Reynolds number in Figures 34, 35, and 36 for $s = 4$, 8, and 12 with d as a parameter. It can be seen that the pressure drop is approximately a fourth that observed for the disks. Unlike the results for the disks, the friction factors for the streamline shapes decrease as they do for a smooth tube with increasing Reynolds number, even for the large diameter shapes.

The lines drawn with the data in Figures 34-36 are given by the equation

$$100\ f = C(s,d)\ Re^{n(s,d)} \qquad (64)$$

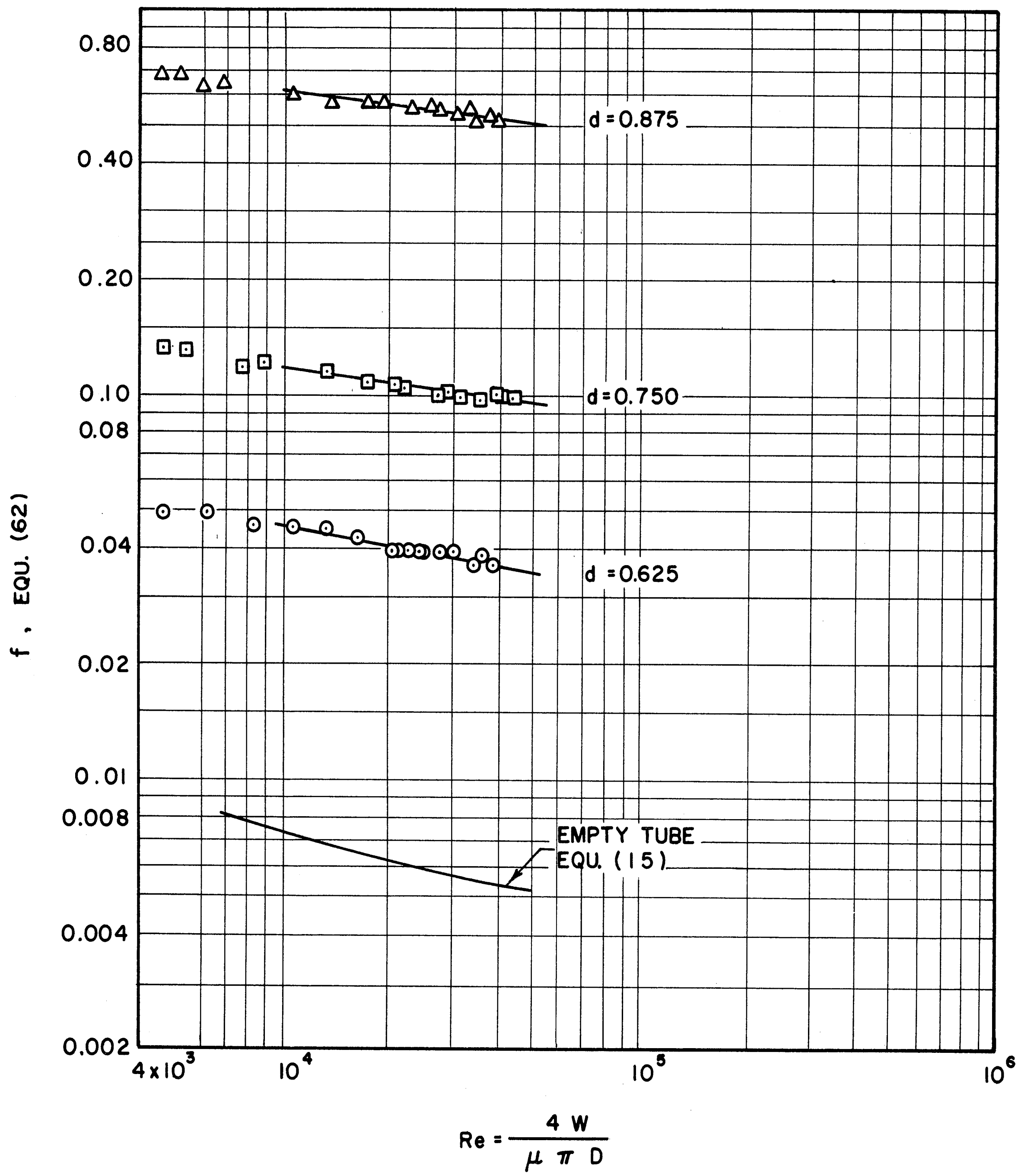

Figure 34. Friction Factor for Streamline Shapes as a Function of Reynolds Number, f vs. Re, for s = 4 with Parameters of d.

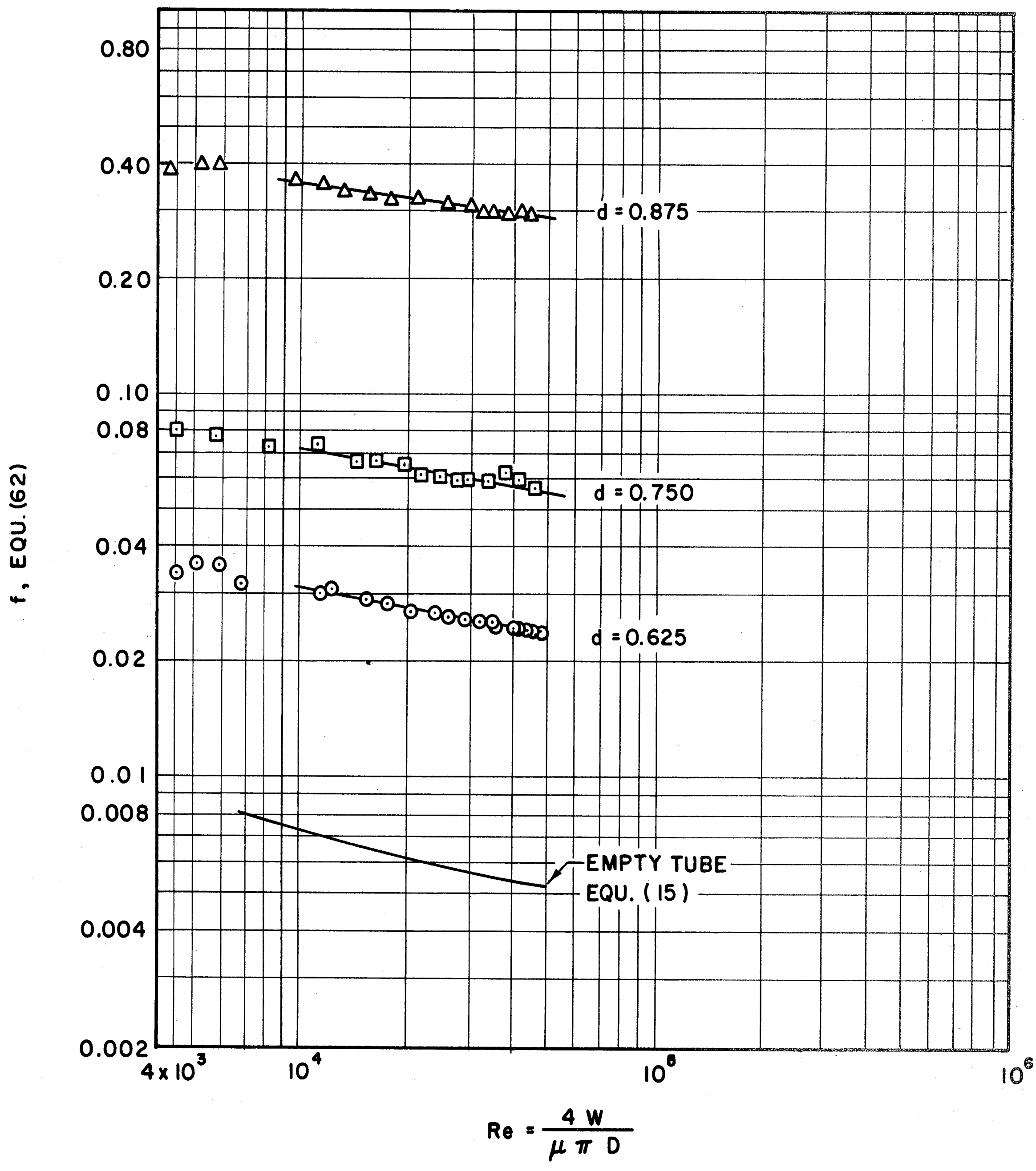

Figure 35. Friction Factor for Streamline Shapes as a Function of Reynolds Number, f vs. Re, for s = 8 with Parameters of d.

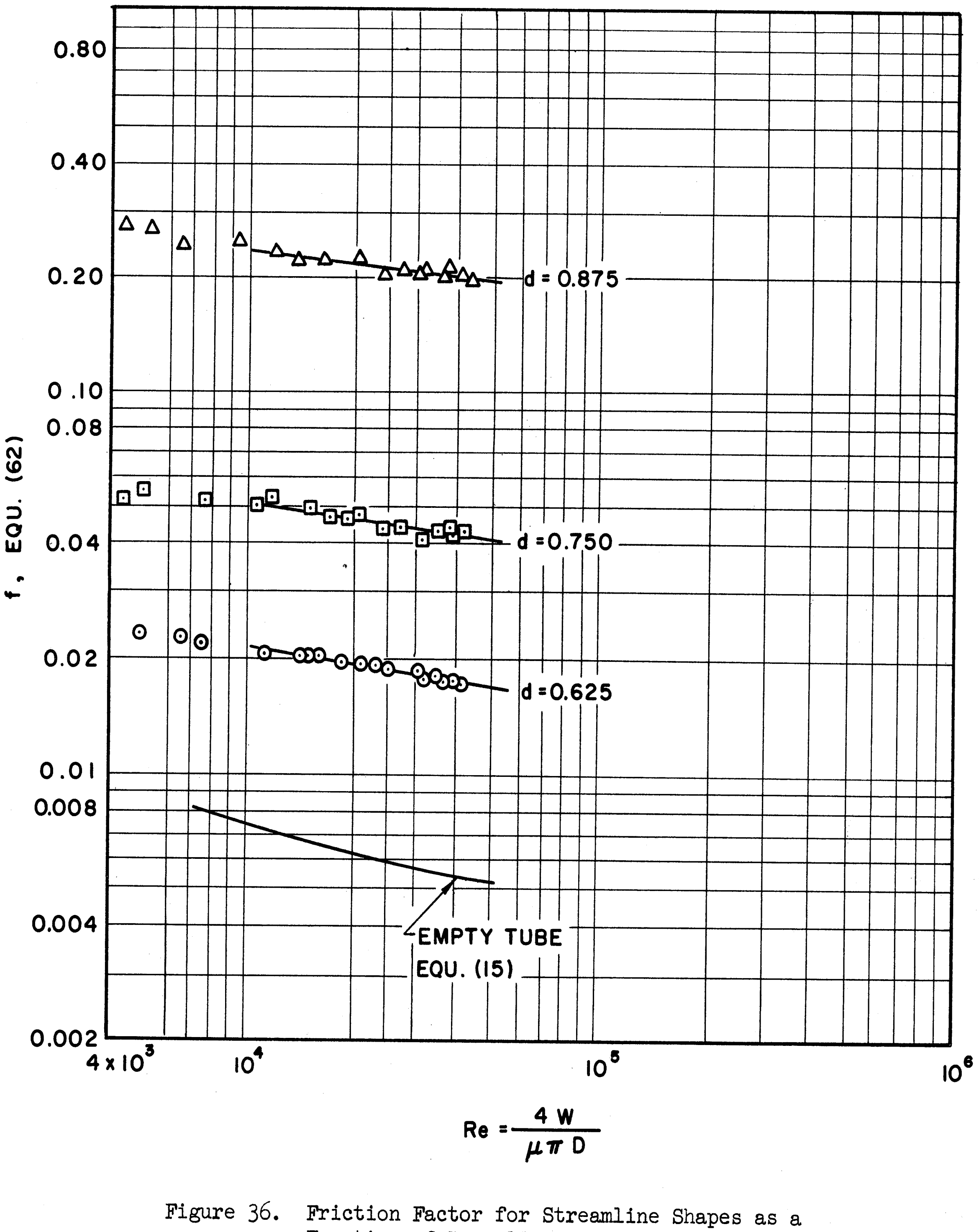

Figure 36. Friction Factor for Streamline Shapes as a Function of Reynolds Number, f vs. Re, for s = 12 with Parameters of d.

The constants $C(s,d)$ and $n(s,d)$ are listed as a function of s and d in Table VIII of Appendix C.

The effective drag coefficients are shown as a function of Reynolds number for $s = 12, 8$, and 4 in Figure 37 with d as a parameter. They are cross-plotted versus free area in Figure 38 and versus spacing in Figure 39. The lines drawn with the data in Figure 37 are given by the equation

$$100\ f_D = C(s,d)\ Re^{n(s,d)} \qquad (65)$$

The constants $C(s,d)$ and $n(s,d)$ are listed in Table IX of Appendix C as a function of s and d.

Figure 37 indicates that the effective drag coefficient for streamline shapes has a slight dependence on Reynolds number. Therefore, a generalized correlation for streamline shapes is suggested of the form

$$100\ f_D = \frac{C_1 s}{1 + C_2\ s} \left[\frac{Re}{10,000}\right]^{n_1} \qquad (69)$$

Best values of the constants were obtained from the data of this investigation and found to be

$$C_1 = 117$$

$$C_2 = 1.6$$

$$n_1 = -0.12$$

An indication of the validity of the correlation is given in Figure 28 where values of f_D predicted by Equation (69) are plotted versus values measured experimentally. All of the data are correlated with an average deviation of 7.95 per cent. There apparently are no similar type data available in the literature for comparison.

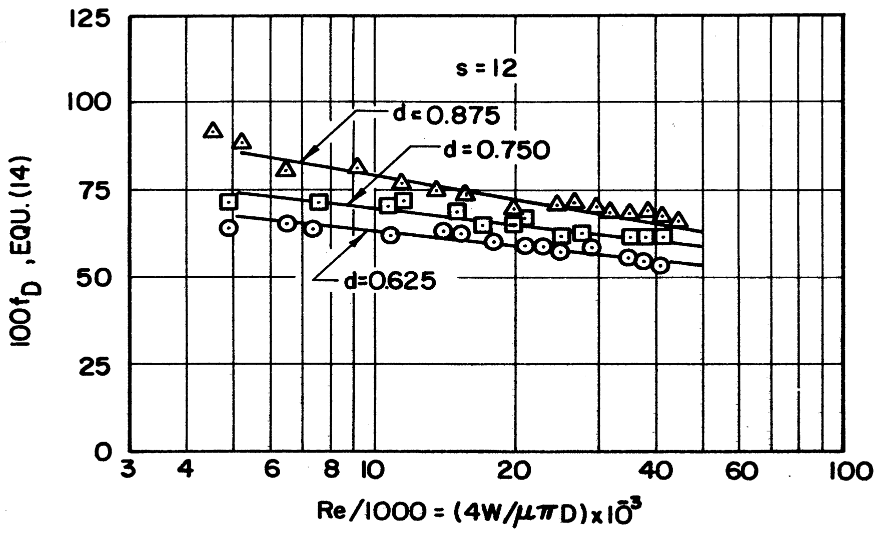

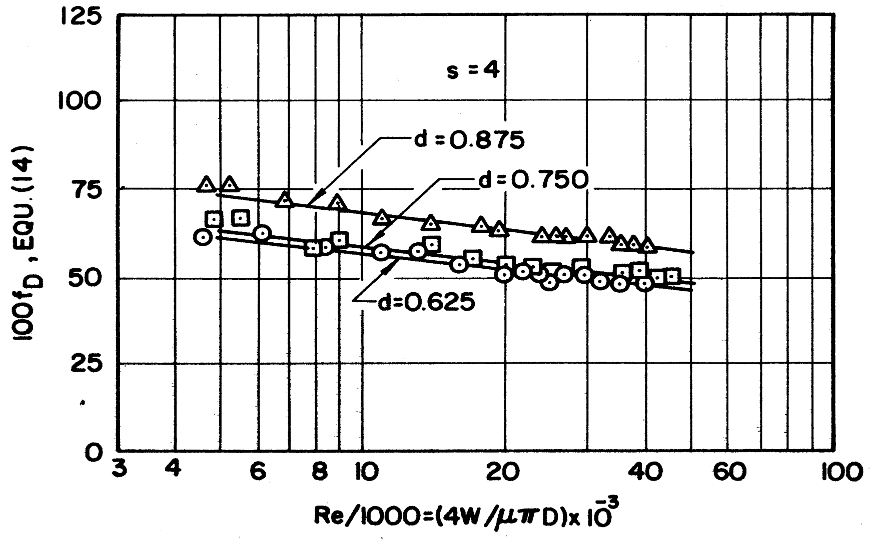

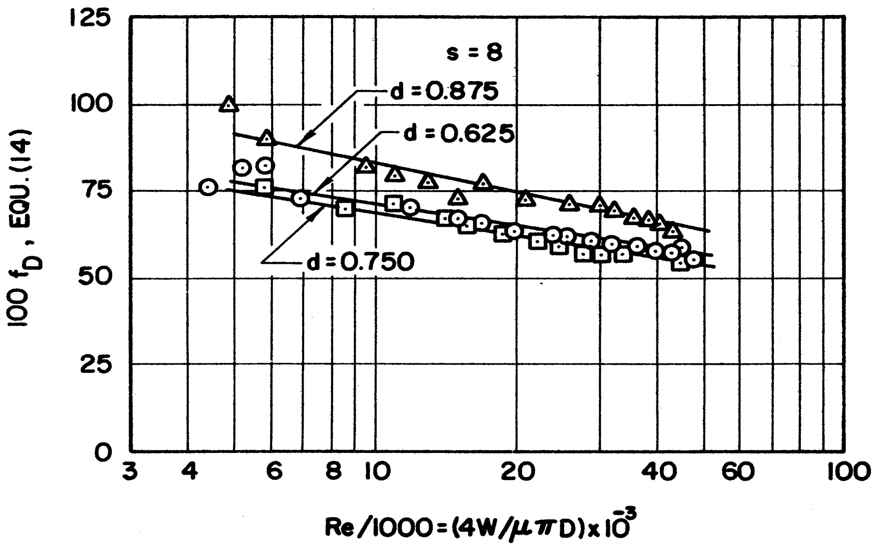

Figure 37. Effective Drag Coefficient for Streamline Shapes as a Function of Reynolds Number, f_D vs. Re, for s = 12, 8, and 4 with Parameters of d.

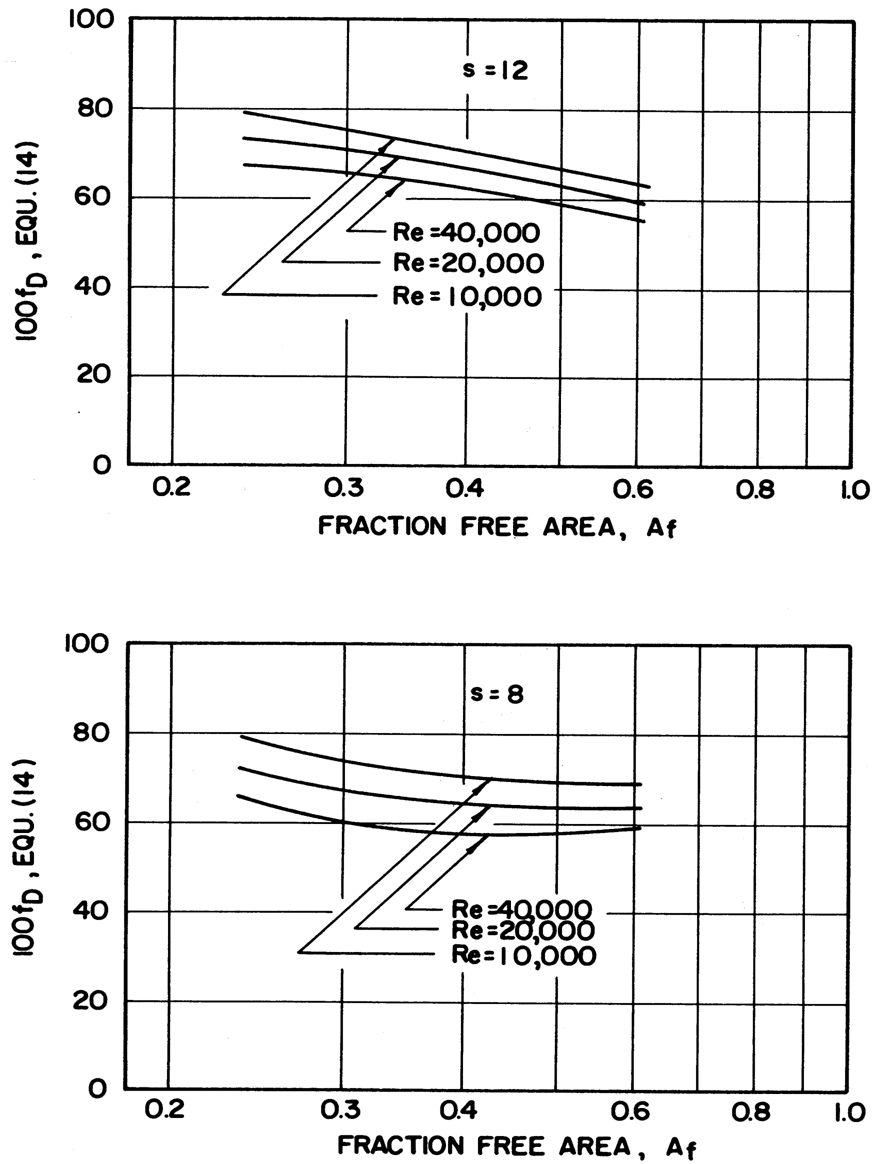

Figure 38. Effective Drag Coefficient for Streamline Shapes as a Function of Free Area, f_D vs. A_f, for s = 12, 8, and 4 with Parameters of Re.

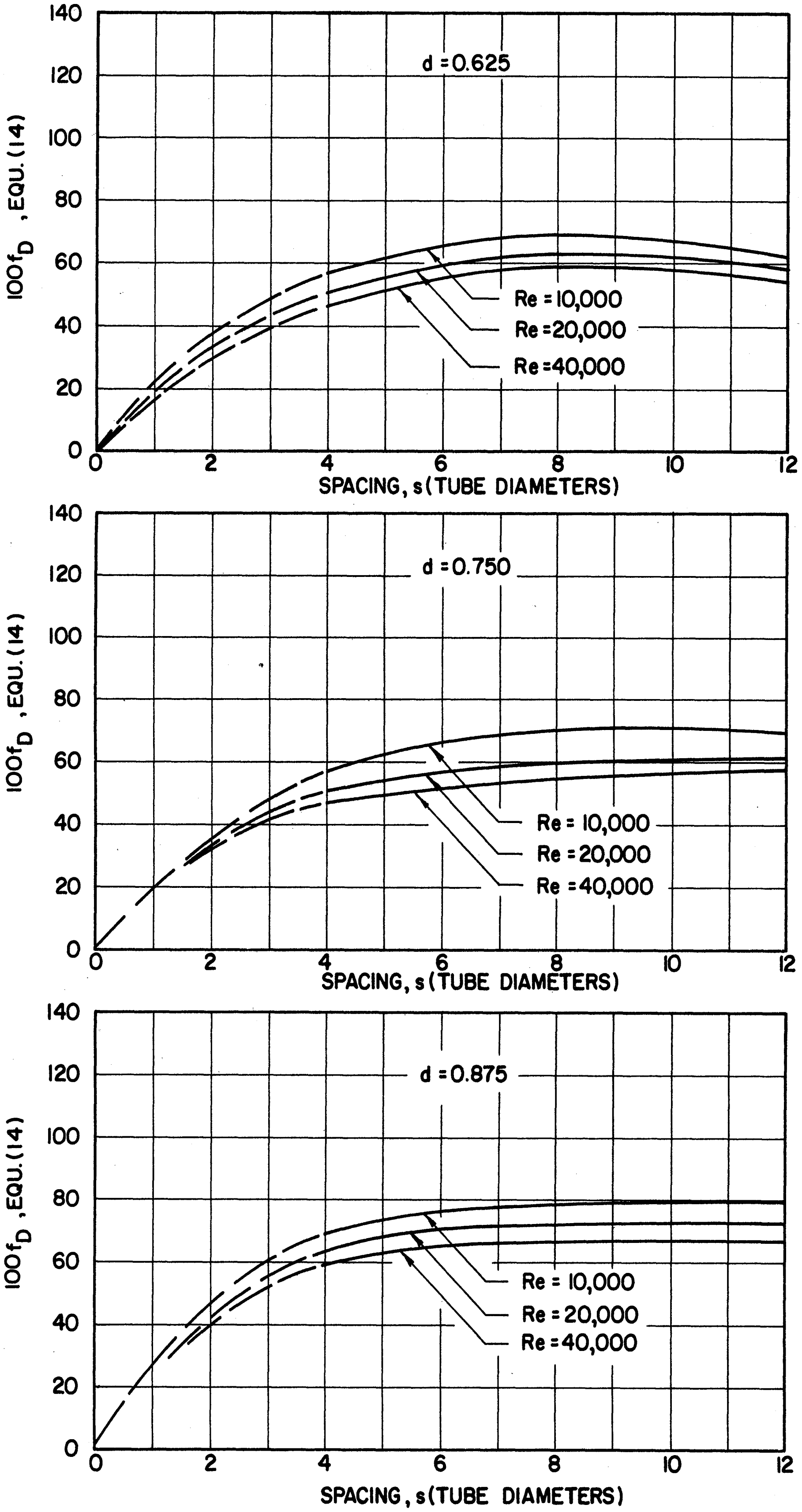

Figure 39. Effective Drag Coefficient for Streamline Shapes as a Function of Spacing, f_D vs. s, for d = 0.625, 0.750, and 0.875 with Parameters of Re.

Heat Transfer

The local heat transfer coefficient for Reynolds numbers of approximately 10,000 are plotted for diameter ratios of 0.625, 0.750, and 0.875 in Figure 40. The shape and position of the streamline bodies are illustrated with a diagram just as for the disks. Some interesting features of these curves are:

1. The points for all three diameters (including even d = 0.625) fall on approximately the same smooth curve. This is to be expected, since the streamline shapes should produce a smaller wake than the disks and, hence, should interfere less with each other.

2. The point of maximum heat transfer is shifted downstream from the point of maximum velocity just as for the disks (although because of the scatter in the data at this point, it is difficult to tell exactly where the maximum occurs). There is reason to believe that some separation occurs in flow around the streamline shape just as it does around the disk, thus producing a vena-contracta. Even though there may be separation in the flow around the streamline shape, one would still expect the pressure drop to be considerably less than for a disk. The reason is that the tail of the streamline shape physically occupies volume where wasted turbulent motion takes place in the wake of a disk.

3. The heat transfer coefficients approach those of an empty tube within a shorter distance for the streamline shapes than for the disks.

Values of h_m/h_0 are plotted versus Reynolds number in Figure 41 for s = 12, 8, 4, and 0 (for the solid rod), with d as a parameter.

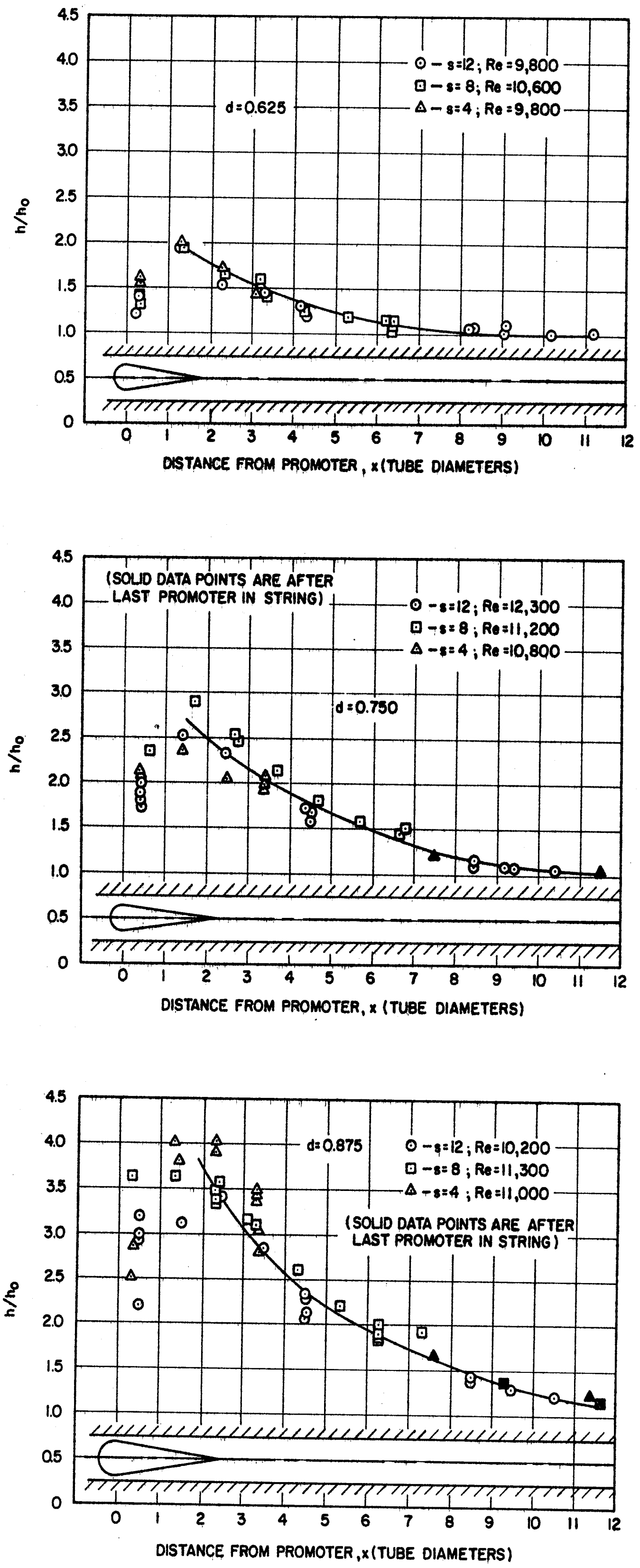

Figure 40. Sample Values of Local Heat Transfer Coefficient Ratio for Streamline Shapes as a Function of Longitudinal Position from Shape with Reynolds Number Approximately 10,000, h/h_0 vs. x, for d = 0.625, 0.750, and 0.875.

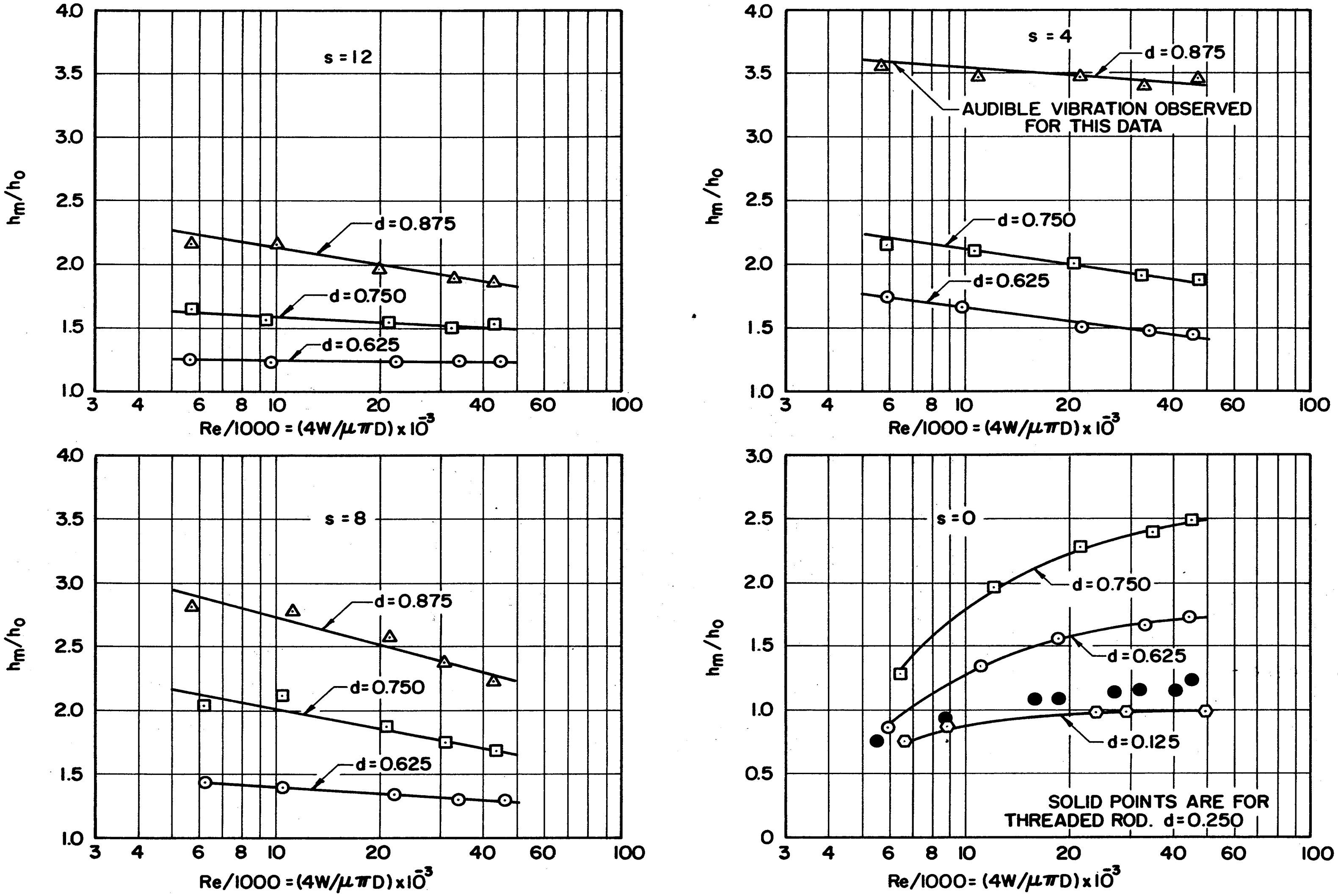

Figure 41. Overall Mean Heat Transfer Coefficient Ratio for Streamline Shapes as a Function of Reynolds Number, h_m/h_0 vs. Re, for s = 12, 8, 4, and 0 with Parameters of d.

The lines drawn with the data are given by the equation

$$h_m/h_0 = C(s,d)\ Re^{n(s,d)} \qquad (67)$$

with the constants $C(s,d)$ and $n(s,d)$ given in Table X of Appendix C as a function of s and d.

The data are cross-plotted versus free area in Figure 42 for $s = 12, 8, 4$, and 0 with Reynolds number as a parameter. They are cross-plotted versus s in Figure 43 for Reynolds numbers of 10,000, 20,000, and 40,000 with diameter ratio as a parameter.

The following observations should be noted: As the data for the largest diameter ratio ($d = 0.875$) and the closest spacing ($s = 4$) were taken, noticeable vibration of the shapes against the tube wall was observed from the sound produced. At the completion of the run, when the string of promoters was removed, it was found that the centering pins had been badly damaged. The only other run for which audible vibration was heard was that for $d = 0.875$ and $s = 8$, but in this instance no damage to the centering pins took place.

The vibration phenomenon was probably caused by pressure disturbances created by the periodic shedding of vortices from the streamline shape and very likely depends in addition upon the natural frequency of the centering rod.

Approximately the same behavior is shown as for the disks with the heat transfer coefficients about 20 to 50 per cent lower for the streamline shapes than for the disks. A much smoother transition to the case of a solid rod in the center of the tube occurs for the streamline shapes as the spacing is decreased than for the disks.

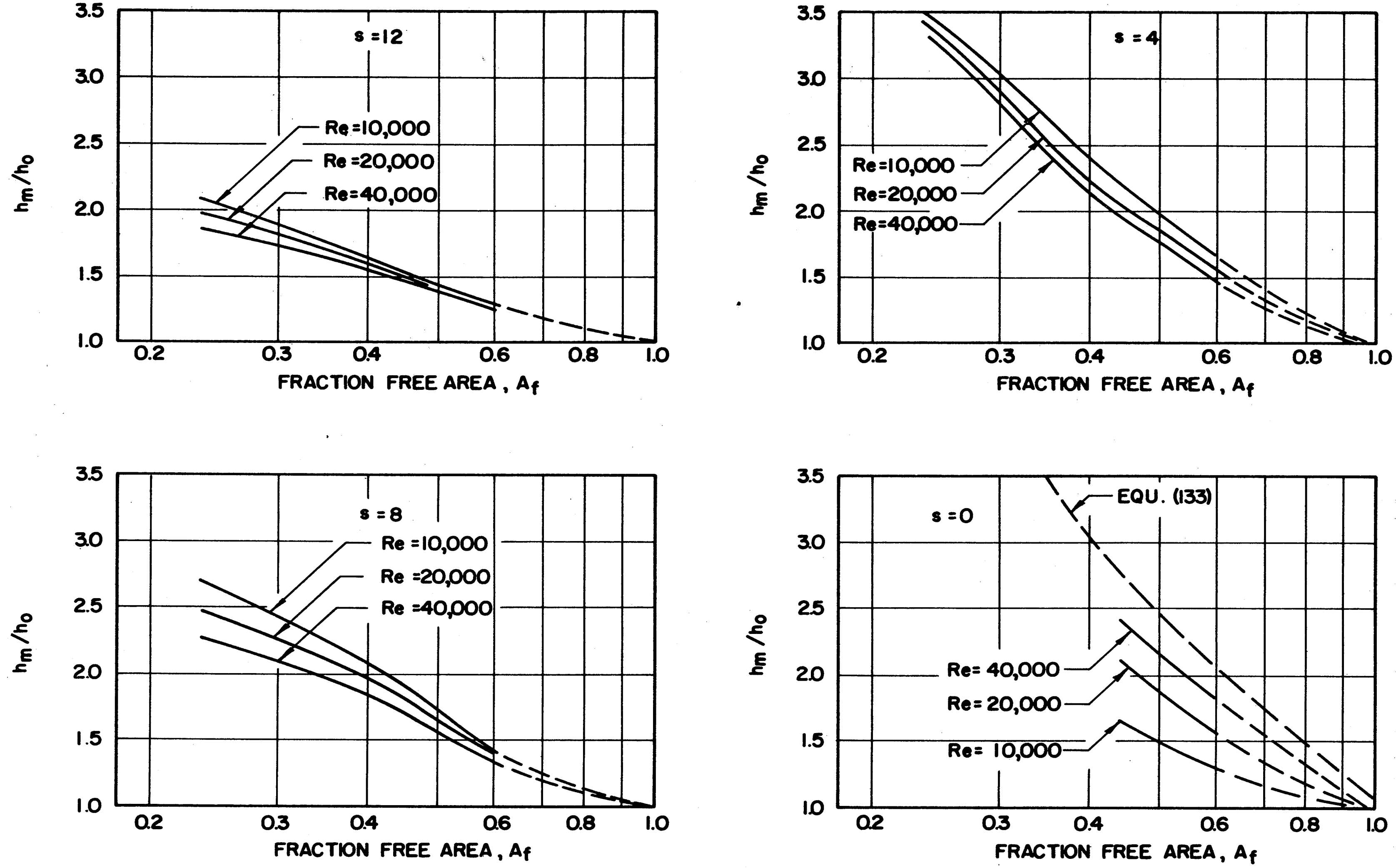

Figure 42. Overall Mean Heat Transfer Coefficient Ratio for Streamline Shapes as a Function of Free Area, h_m/h_o vs. A_f, for s = 12, 8, 4, and 0 with Parameters of Re.

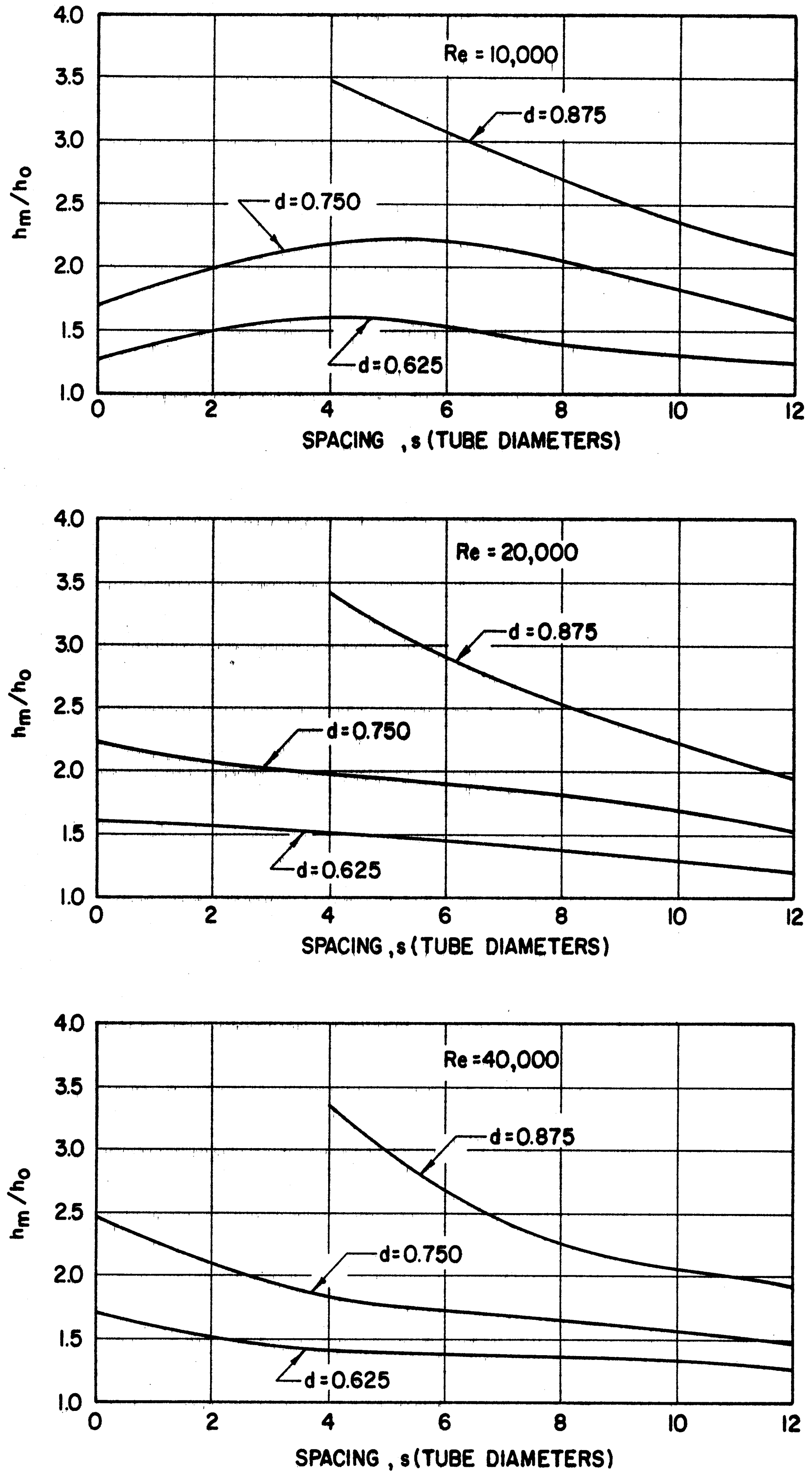

Figure 43. Overall Mean Heat Transfer Coefficient Ratio for Streamline Shapes as a Function of Spacing, h_m/h_0 vs. s, for Re = 10,000, 20,000, and 40,000 with Parameters of d.

A generalized correlation of the heat transfer coefficient ratio for streamline shapes as a function of diameter ratio d, spacing s, and Reynolds number was obtained of the following form

$$\frac{h_m}{h_0} = 1 + C_1 \; (-\ln A_f) \left[\frac{Re}{10{,}000}\right]^{n_1} \frac{1}{1 + C_2 \; s} \qquad (70)$$

Best values of the constants were obtained from the data of this investigation and found to be

$$C_1 = 2.04$$

$$C_2 = 0.14$$

$$n_1 = -0.11$$

As an indication of the validity of the correlation, values of h_m/h_0 predicted by the correlation are plotted versus values measured experimentally in Figure 33. All of the data are correlated with an average deviation of 7.3 per cent. The biggest deviation from the correlation occurs at close spacing and large diameter ratio, particularly for $d = 0.875$ and $s = 4$. Since this is the set of results for which noticeable vibration of the shapes occurred, the high experimental values are probably due to this cause. Thus, the correlation given by Equation (70) is probably best applicable only to streamline shapes in which there is no vibration.

There are apparently no data available in the literature for comparison.

Reliability of the Data for All Geometries

In order to effectively utilize the experimental results just presented, some judgment concerning the reliability of the data must be made by the user. For this purpose a critical discussion of the errors, reproducibilities, etc. of the data will be given.

Pressure Drop

The relative error (i.e. the precision) of the friction factors may be estimated from the form of the defining equation used in this investigation.

$$f = \frac{g_c \ \pi^2 \ \rho \ D^5}{32 \ W^2} \left[\frac{-\Delta P}{L_p}\right] \left[\frac{L_p}{n_p \ S}\right] - f_0 \left[\frac{L_p}{n_p \ S} \quad -1\right] \qquad (62)$$

It should be noted that when the product n_pS is equal to L_p (i.e., the string of promoters occupies the complete distance between pressure taps) Equation (62) reduces to Equation (22). Equation (22) was used for the empty tube and solid rod geometries.

The density of the water and the dimensions of the experimental equipment were known quite accurately. The last term in brackets in the expression above contributes from ten per cent to less than 0.3 per cent of the value of the friction factor. Thus, almost all of the uncertainty in the experimental friction factor arises from errors in measuring the pressure drop and the mass flow rate.

The pressure drop could be measured to within about 0.10 inches of indicating fluid, so that the relative error depends upon the magnitude of the pressure drop. At a Reynolds number of 10,000 the pressure drop for the empty tube was about 2 inches of indicating fluid; at a Reynolds number of 50,000 the pressure drop was about 20 inches; and, for some turbulence promoting geometries the pressure drop was 100 inches of indicating fluid. Thus, the error in measuring the pressure drop contributed an error ranging from 0.1 to 5 per cent, but usually less than 2 per cent.

The mass flow rate, determined from the rotameter readings, may be considered as accurate to within $\pm$ one per cent, which when added to the error just discussed (doubled since W^2 is required) produces an estimate of 2 to 7 per cent for the precision of the friction factor results. The excellent agreement of the experimental friction factors with accepted correlations for empty tubes and annuli confirms the estimate of the precision of the data.

The reproducibility of the data, however, requires a separate consideration and depends almost entirely upon the ability to reproduce the exact geometry. In particular, for the types of systems studied in this investigation, reproducing the geometry involves centering the devices (or measuring the degree of eccentricity). It is estimated that the variation in the per cent eccentricity of the solid rods and streamline shapes (which had centering supports) was within about 20 per cent, while the per cent eccentricity of the disks (which had no centering supports) was probably within about 40 per cent. The per cent eccentricity is defined as the per cent of annulus width by which the inner element (at its maximum diameter) is eccentric.

A theoretical analysis by Deisler and Taylor[13] for a solid rod in the center of a tube with d = 0.286 indicates that the friction factor for an eccentric annulus is about ten per cent lower than the friction factor for a concentric annulus when the per cent eccentricity is 60 per cent and is about 25 per cent lower when the eccentricity is 100 per cent. This effect of eccentricity (difficult to control experimentally) probably accounts for part of the difficulty encountered in the past by various investigators in obtaining a good, generalized friction factor correlation for annuli.

It is difficult to estimate the effect of eccentricity on the pressure drop results for bluff bodies. It is likely, however, that part of the dependence of the effective drag coefficient on free area observed in the cross-plots of Figures 26 and 38 is due to slightly different eccentricities.

A check on the reproducibility of the results was obtained for two strings of disks with $d = 0.750$ and $s = 12$ and 8 in which the strings were prepared and inserted completely independently in runs made a month and a year respectively from the original measurements. In both cases the check results differed by about ten per cent from the original results.

Therefore, in summary, the following may be stated:

1. The precision of the pressure drop data probably varies from about 2 to 7 per cent with most of the results corresponding to the lower figure.

2. The reproducibility of the pressure drop data is probably within about 15 per cent with most of the problems of reproducibility consisting of difficulty in controlling the exact degree of eccentricity. The irreproducibility appears as scatter in the overall correlations.

Heat Transfer

The precision of the local heat transfer coefficients may be estimated from the form of the defining equation

$$h(z) = \frac{q(z)}{T_{wall}(z) - T_f(z)} \tag{45}$$

Errors may be introduced from two sources: 1) errors in measuring the experimental variables: $T_b(z)$, T_{inlet}, T_{outlet}, and I; 2) errors propagated in the calculation of $q(z)$ and $\Delta T_{generation}$ due to uncertainties in the parameters of the experimental apparatus: a, b, $\bar{\rho}_0$, K_0, γ, and β. A statistical analysis of the propagation of errors given in Appendix B indicates that $q(z)$ is accurate to within $\pm$ 5 per cent and the temperature difference between fluid and inside wall is accurate to within about $\pm$ 2 deg. F.

The percentage error in the local heat transfer coefficient, however, depends upon the magnitude of the total difference between fluid and inside wall. This temperature difference ranged from 12 to 100 deg. F with the large majority of the runs at a mean temperature difference of about 25 deg. F. The estimated precision of the heat transfer coefficients, therefore, may be taken as being about 8 per cent.

There are two important tests of the precision of the data which confirm the preceding analysis: 1) the agreement of the overall Nusselt numbers measured for an empty tube with those predicted by the generally accepted correlations; and 2) the agreement of the heat balances.

The first (agreement with accepted correlations) has already been demonstrated in Figure 13.

The percentage error in the heat balances is shown in the frequency plot of Figure 44 where the per cent error is defined as follows.

$$Q_{in} = 2\pi \int_0^L q(Z)dZ \tag{70}$$

$$Q_{out} = W\, c(T_{outlet} - T_{inlet}) \tag{71}$$

$$\text{Per Cent Error} = \frac{(Q_{in} - Q_{out}) \times 100}{0.5(Q_{in} + Q_{out})} \tag{72}$$

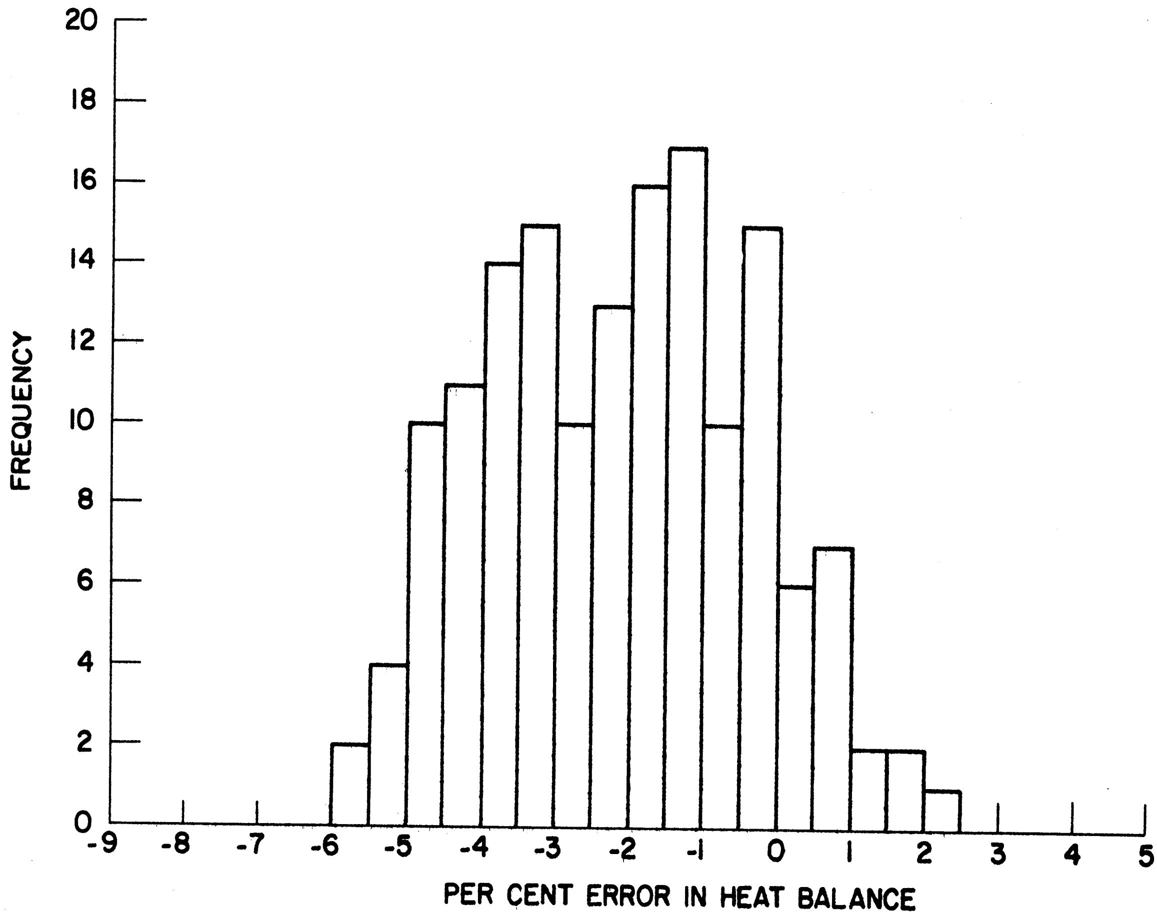

Figure 44. Frequency Distribution of Heat Balance Errors.

It is seen that this percentage error generally falls between plus one per cent and minus five per cent. Since the temperature rise of the water was usually between 5 deg. F and 20 deg. F, an error of one per cent in the heat balance corresponds to an error in measuring the difference between inlet and outlet water temperature of 0.05 to 0.20 deg. F. Thus, the heat balance error seems to be within acceptable limits.

The reproducibility of the local heat transfer coefficients is subject to the same difficulty in centering the devices as was the reproducibility of the friction factors. For the heat transfer results, however, a better estimate is available, since measurements were made at three different angular positions for three different axial positions for each run. The angular variation is indicated in Figures 45 and 46 where the frequency of the difference between the local angular ΔT and the average ΔT for all three angular positions is plotted versus the difference. It is seen that the difference was generally less than $\pm$ 2 deg. F which means that any irreproducibility in the local heat transfer coefficient caused by inexact axial symmetry was less than 10 to 15 per cent.

A test of the reproducibility of the local heat transfer coefficients for disks and streamline shapes is given by the plots of Figures 29 and 40 since the data for different values of s were taken as part of completely separate runs. In fact, the local data near each of the 4 to 12 bluff bodies used in each run may be thought of as data from a different experiment since any eccentricity of the bodies probably varied somewhat from promoter to promoter along the tube. The

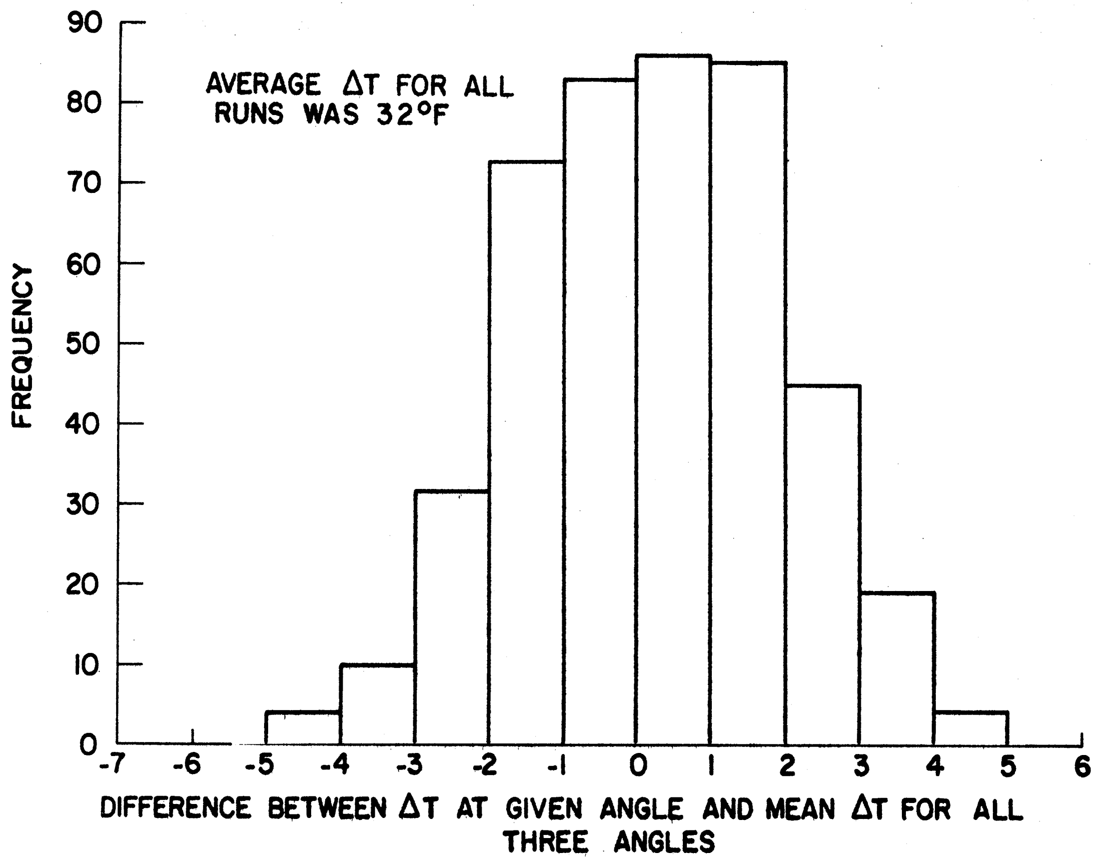

Figure 45. Frequency Distribution of Difference Between Local Angular ΔT and Mean ΔT for All Three Angles for Streamline Shapes.

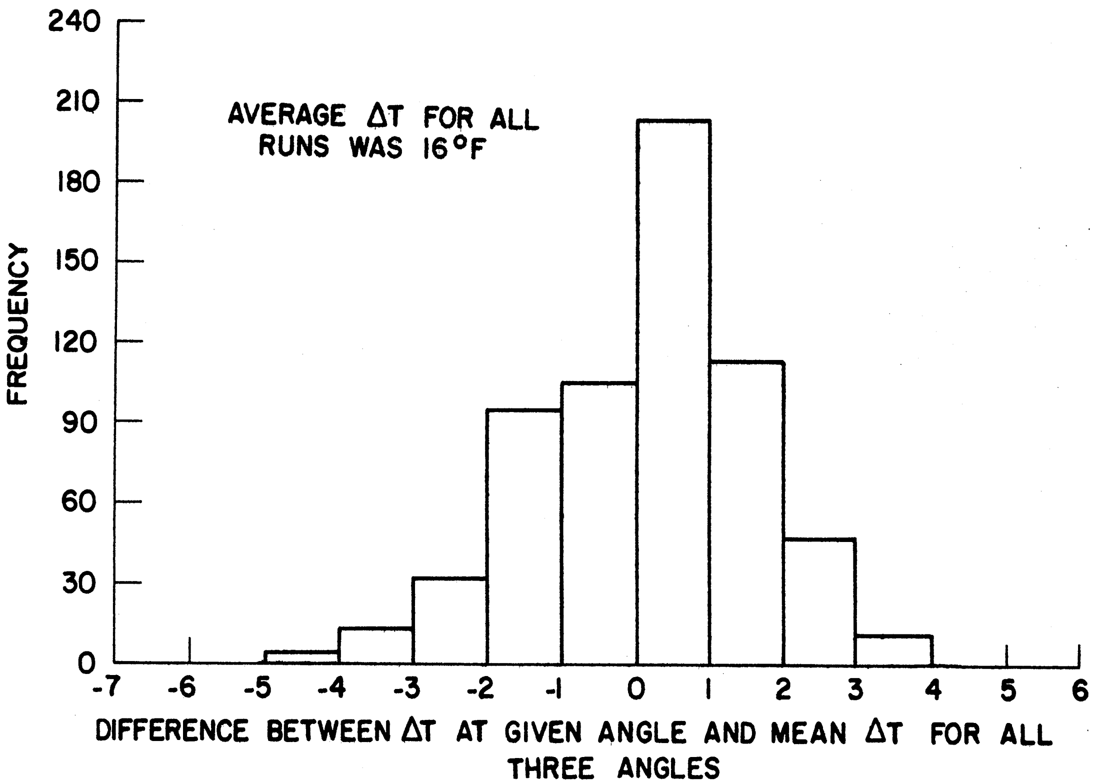

Figure 46. Frequency Distribution of Difference Between Local Angular ΔT and Mean ΔT for All Three Angles for Disks.

effect of inexact axial symmetry probably accounts for some of the scatter of the local heat transfer data, but the fact that all the data fall roughly on the same curve indicates that the local data are reproducible.

The reproducibility of the mean heat transfer coefficients should be considerably better than that for the local heat transfer coefficients, since the data are subjected to an averaging process. This is indicated by the results of check runs made for disks at d = 0.750 and s = 12 and 8 just as for the friction factors. As shown in Figure 30 the mean heat transfer coefficients for the check runs (which were taken one month and one year respectively from the original runs) fall on the same smooth curves as the results for the original runs. This confirms the good reproducibility of the mean transfer coefficients.

In summary the following may be stated:

1. The precision of the heat transfer coefficients is probably within 8 per cent.

2. The reproducibility of the local heat transfer coefficients is within about 10 to 15 per cent and the reproducibility of the mean heat transfer coefficients is considerably better than that.

ECONOMICS

One of the primary goals of this investigation is to determine whether turbulence promoters can be used economically to improve the rate of heat transfer to a fluid flowing in a tube and whether there exists an optimum type of promoter. Any general economic study of this nature, however, is difficult because of the many different types of equipment in which the transfer of heat and momentum to a fluid flowing in a tube is an important part.

Mathematical Model of a Heat Exchanger

Throughout the consideration of the economics of turbulence promoters it will be assumed, for convenience in explanation, that heat is being transferred to a cool fluid inside the tube and, thus, the temperature of the fluid is being increased. The conclusions reached are equally applicable to the situation where heat is transferred from the fluid and the temperature of the fluid is lowered.

A schematic diagram of a piece of equipment for transferring heat to a fluid flowing in a tube is shown below

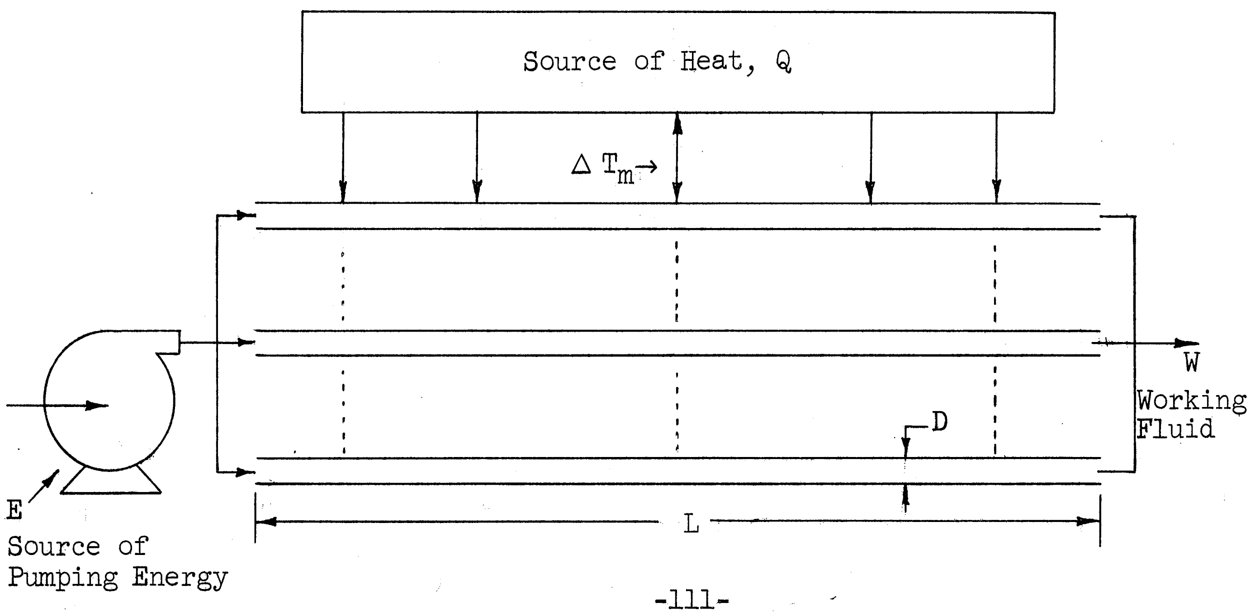

The essential characteristics of the apparatus with typical examples are:

1. Source of heat, Q
   a. hot fluid flowing outside the tube
   b. condensing vapor
   c. electrical generation of heat
   d. chemical reaction
   e. nuclear reaction

2. A single tube or group of tubes in parallel of specified inside geometry, length L, and inside diameter D. The number of tubes is denoted by N_{tube}.

3. A working fluid (with physical properties μ, k, c, ρ) which flows through the tube at mass flow rate, W
   a. water
   b. air
   c. liquid metal

4. A source of pumping energy, E
   a. pump
   b. head due to height of reservoir

5. A temperature driving force to cause heat to flow to the tube(s), ΔT_m

The equations which relate the variables (with typical units) are

Q = total rate of heat transfer (BTU/hr)

$$= U_{oa} \, A \, \Delta T_m \tag{73}$$

where U_{oa} = overall heat transfer coefficient (BTU/hr-deg F-ft^2)

$$= \frac{1}{1/h + 1/h'} \tag{74}$$

$$= \frac{Nu \, (k/D)}{1 + h/h'} \tag{75}$$

$$= \frac{Nu \, (k/D)}{1 + \dfrac{Nu}{h'D/k}} \tag{76}$$

A = total heat transfer surface based on inside tube diameter (ft^2)

$$= N_{tube} \pi\ D\ L \tag{77}$$

E = pumping energy required (BTU/hr)

$$= \frac{W\ \Delta P}{J_c\ \rho} \tag{78}$$

ΔP = overall pressure drop (lb_f/ft^2)

$$= \frac{2\ f\ L\ \rho\ U^2}{g_c\ D} \tag{79}$$

The Nusselt number Nu and friction factor f are generally empirical functions of the inside diameter D, mass flow rate W, physical properties of the fluid (c, k, μ, ρ) and the geometry of the inside of the tube

$$Nu = \text{function of } (D,\ W,\ \mu,\ \rho,\ c,\ k,\ \text{geometry}) \tag{80a}$$

$$f = \text{function of } (D,\ W,\ \mu,\ \rho,\ \text{geometry}) \tag{81a}$$

In some cases, of course, Nu and f may depend on still other factors such as ΔT_m, L, pressure, etc. For many geometries (including that of the empty tube) the forms of the above functions are

$$Nu = C_2\ Re^{n_2}\ Pr^{1/3} \tag{80}$$

$$f = C_1\ Re^{-n_1} \tag{81}$$

where

$$Re = \frac{4\ W}{\mu\ \pi\ D\ N_{tube}} \tag{82}$$

$$Pr = \frac{c\ \mu}{k} \tag{83}$$

The term h is the mean, inside, convective heat transfer coefficient, while the term h' is an effective coefficient which takes into account the resistance of the rest of the heat exchanger to the transfer of heat.

When h' is very large compared to h, then almost all of the resistance to heat transfer is provided by the flow inside the tube and

$$U_{oa} \cong h \tag{84}$$

or, in other words, the value of the mean inside heat transfer coefficient is controlling.

On the other hand, when h' is very small compared with h, then

$$U_{oa} \cong h' \tag{85}$$

and the rate of heat transfer will be independent of conditions inside the tube.

Factors Which Affect the Economics

In order to determine the economic desirability of using various turbulence promoting devices it is necessary to consider in some detail the factors which affect the economics of heat exchangers in general. Thus, a large part of the discussion which follows will be equally applicable to the design of conventional heat transfer equipment.

In order to design the optimum heat exchanger the designer must strike a proper balance between fixed and operating costs. This immediately introduces complications, since there will be both fixed and operating costs associated with the part of the exchanger outside the tube. In order to avoid these complications the term "cost" will be interpreted to mean "the cost which is influenced by the selection of the geometry of the inside of the tube."

In addition the following assumptions will be made:

1. Q is specified

2. W is specified

3. ΔT_m is specified

4. h' is specified

The problem, then, is to make the best selection of D, L, N_{tube}, and inside tube geometry. Throughout this presentation the term L will mean the effective length. Thus, if multiple tube passes are used, the effective length L is the actual tube length times the number of tube passes.

The fixed costs for a given unit of time are usually expressed as a percentage of the initial investment and include such items as depreciation and maintenance. The amount of the initial investment depends upon the size of the exchanger, the type, materials of construction, etc. As a first approximation, however, the fixed cost is given by

$$\text{Fixed Cost} = C_F\, A^m \tag{86}$$

where the coefficient C_F (in typical units of dollars/ft^{2m}-hr) depends upon the materials of construction and type of exchanger; the exponent m of the area is often taken as 0.60.

The operating costs consist mainly of the cost of pumping energy and the actual cost of the fluid. If the fluid is some product, its cost is probably considered negligible, but if it is a utility (for example cooling water), its cost may be significant.

The cost of pumping is given by

$$\text{Pumping Cost} = C_E\, E \tag{87}$$

where C_E is the cost of pumping energy (in typical units of dollars/BTU). The cost of the fluid is given by

$$\text{Fluid Cost} = C_W\, W \tag{88}$$

where C_W is the cost of the fluid (in typical units of dollars/lb_m).

The total operating cost is given by

$$\text{Operating Cost} = C_E\ E + C_W\ W \tag{89}$$

and the total cost is given by

$$\text{Total Cost} = C_F\ A^m + C_E\ E + C_W\ W \tag{90}$$

Each of the above costs per unit heat transfer is given by

$$\text{Fixed Cost/BTU} = C_F\ A^m/Q \tag{91}$$

$$\text{Pumping Cost/BTU} = C_E\ E/Q \tag{92}$$

$$\text{Fluid Cost/BTU} = C_W\ W/Q \tag{93}$$

$$\text{Operating Cost/BTU} = C_E\ E/Q + C_W\ W/Q \tag{94}$$

$$\text{Total Cost/BTU} = C_F\ A^m/Q + C_E\ E/Q + C_W\ W/Q \tag{95}$$

The fluid cost is being carried throughout this analysis, even though both W and Q are assumed to be specified and, hence, the fluid cost is independent of the variables remaining to be selected. This is done to simplify a consideration later of removing the restrictions requiring that both W and Q be known. On the basis of the assumptions made thus far, the relevant cost is given by

$$\text{Relevant Cost} = C_F\ A^m + C_E\ E \tag{96}$$

and

$$\text{Relevant Cost/BTU} = C_F\ A^m/Q + C_E\ E/Q \tag{97}$$

Procedure for Designing the Optimum Heat Exchanger

One procedure for minimizing the relevant cost/BTU is as follows:

1. Obtain an expression for A^m/Q and E/Q for any particular geometry in terms of the variables D, L, and N_{tube}.

2. Select the particular set of variables which produces the minimum relevant cost/BTU as calculated by Equation (97).

As a starting point it will be assumed that the inside tube geometry is specified, for example as an empty tube. This establishes the specific form of the functional relationships (80a) and (81a).

Next, a reasonable value of the inside tube diameter is selected on a fairly arbitrary basis.

The remaining variables to be selected are N_{tube} and L. Only one of these, however, may be chosen independently. Once N_{tube} is specified the fluid velocity and Reynolds number in the tube are also determined. This enables the Nusselt number to be calculated from the empirical correlation for the given geometry which, in turn, sets the value of U_{oa}, required area, and hence the length L.

For purposes of comparing different geometries it will be more useful to select a desired (or optimum) Nusselt number and calculate the required number of tubes (and the length) rather than specify the number of tubes and calculate the resulting Nusselt number. The derivation of A^m/Q and E/Q in terms of D, Nu, and the specified data is given below.

$$\frac{A^m}{Q} = \left[\frac{A}{Q}\right]^m \frac{1}{Q^{1-m}} \tag{98}$$

since

$$\frac{A}{Q} = \frac{1}{U_{oa}\Delta T_m} \tag{99}$$

then

$$\frac{A^m}{Q} = \frac{(D/k\ \Delta T_m)^m\ [1 + Nu/(h'D/k)]^m}{Nu^m\ Q^{1-m}} \tag{100}$$

It can be seen that A^m/Q and, thus, the fixed cost depend only on Nu, D, and the parameters which were assumed specified. The fixed cost is independent of the empirical correlation for friction factor and Nusselt number inside the tube and, thus, does not depend upon the choice of inside geometry.

When Nu is small compared with $h'D/k$, then A^m/Q produces a straight line with slope $-m$ when plotted versus Nu on logarithmic coordinates. This is the case when the value of the inside heat transfer coefficient is the limiting factor in the rate of heat transfer. On the other hand, when Nu is large compared with $h'D/k$ then A^m/Q is independent of the Nusselt number inside the tube and is given by

$$\frac{A^m}{Q} \doteq \frac{(D/k\,\Delta T_m)^m}{(h'D/k)^m\,Q^{1-m}} \tag{101}$$

$$= \left[\frac{1}{h'\,\Delta T_m}\right]^m \frac{1}{Q^{1-m}} \tag{102}$$

An expression for E/Q will now be derived.

$$E = \frac{W\,\Delta P}{J_c\,\rho} \tag{78}$$

since $$\Delta P = \frac{32\,f\,L\,W^2}{g_c\,\pi^2\,\rho\,D^5\,N_{tube}^2} \tag{103}$$

and $$W = \frac{\mu\,\pi\,D\,N_{tube}\,Re}{4} \tag{104}$$

then $$E = \frac{f\,Re^3\,L\,\mu^3\,\pi\,N_{tube}}{2\,J_c\,g_c\,\rho^2\,D^5} \tag{105}$$

and $$\frac{E}{Q} = \frac{f\,Re^3}{2\,Nu}\left[1 + \frac{Nu}{h'D/k}\right] Pr \quad \frac{\mu^2}{J_c\,g_c\,\rho^2\,D^2\,c\,\Delta T_m} \tag{106}$$

Since, for any given tube geometry

Nu = function of Re

f = function of Re

then expressions for the friction factor and Reynolds number in terms of the Nusselt number may be substituted into Equation (106). For example, for the empty tube geometry (or any other geometry for which Equations (80) and (81) are valid)

$$f = C_1 \, Re^{-n_1} \tag{81}$$

$$Nu = C_2 \, Re^{n_2} Pr^{1/3} \tag{80}$$

Thus,

$$Re = \left[\frac{Nu}{C_2 \, Pr^{1/3}}\right]^{1/n_2} \tag{107}$$

and

$$f = C_1 \left[\frac{Nu}{C_2 \, Pr^{1/3}}\right]^{-n_1/n_2} \tag{108}$$

and

$$\frac{E}{Q} = \frac{C_1}{2 \, Nu} \left[\frac{Nu}{C_2 \, Pr^{1/3}}\right]^{\frac{3-n_1}{n_2}} \left[1 + \frac{Nu}{h'D/k}\right] Pr \left[\frac{\mu^2}{J_c \, g_c \, \rho^2 \, D^2 \, c \, \Delta T_m}\right] \tag{109}$$

The expression for E/Q is of the general form

$$\frac{E}{Q} = B_1 \frac{Nu^{p-1}}{Pr^{p/3}} \, [1 + B_2 \, Nu] \; B_3 \, Pr \tag{110}$$

where

$$p = \frac{3 - n_1}{n_2} \tag{111}$$

$$B_1 = \frac{C_1}{2C_2^p} \tag{112}$$

Dependent only on empirical correlation for particular geometry. Independent of working fluid, tube diameter, etc.

$$B_2 = \left[\frac{h'D}{k}\right]^{-1} \tag{113}$$

$$B_3 = \frac{\mu^2}{J_c \, g_c \, \rho^2 \, D^2 \, c \, \Delta T_m} \tag{114}$$

Independent of inside tube geometry. Dependent mainly on tube diameter, physical properties of the fluid, ΔT_m, etc.

When B_2Nu is much smaller than unity (i.e. inside heat transfer coefficient controlling) then E/Q vs. Nu on logarithmic coordinates yields a straight line with slope p-1. Likewise, when B_2Nu is much larger than one (rate of heat transfer independent of Nu inside the tube) then E/Q also plots as a straight line with a slope of p.

Substitution of Equations (100) and (110) into the cost equation (97) gives the cost per BTU in terms of Q, ΔT_m, D, Nu, and the physical properties of the fluid. The first three of these items (total rate of heat transfer Q, mean temperature difference ΔT_m, and equivalent outside heat transfer coefficient h') were assumed specified. Thus, a relation for the cost per BTU has been obtained as a function of the inside tube diameter D, the Nusselt number Nu in the tube, and the specified constant parameters.

Since the fixed cost decreases with Nusselt number and the pumping cost increases, it is evident that there will be an optimum value of Nu at which the total cost is a minimum. The various costs are illustrated in Figure 47. The case where the inside heat transfer is limiting (i.e. $h' = \infty$ and, therefore, $B_2 = 0$) is of particular interest.

In this case

$$\frac{\text{Total Cost}}{\text{BTU}} = \frac{C_F\ (D/k\Delta T_m)^m}{Nu^m\ Q^{1-m}} + \frac{C_E\ B_1\ B_3\ Nu^{p-1}}{Pr^{p/3-1}} \tag{115}$$

The optimum Nusselt number can be found by setting the derivative of this expression to zero and solving for Nu to obtain

$$Nu_{optimum} = \left[\frac{m\ C_F\ (D/k\Delta T_m)^m}{(p-1)\ C_E\ B_1\ B_3\ Pr^{(1-p/3)}\ Q^{1-m}}\right]^{\frac{1}{p+m-1}} \tag{116}$$

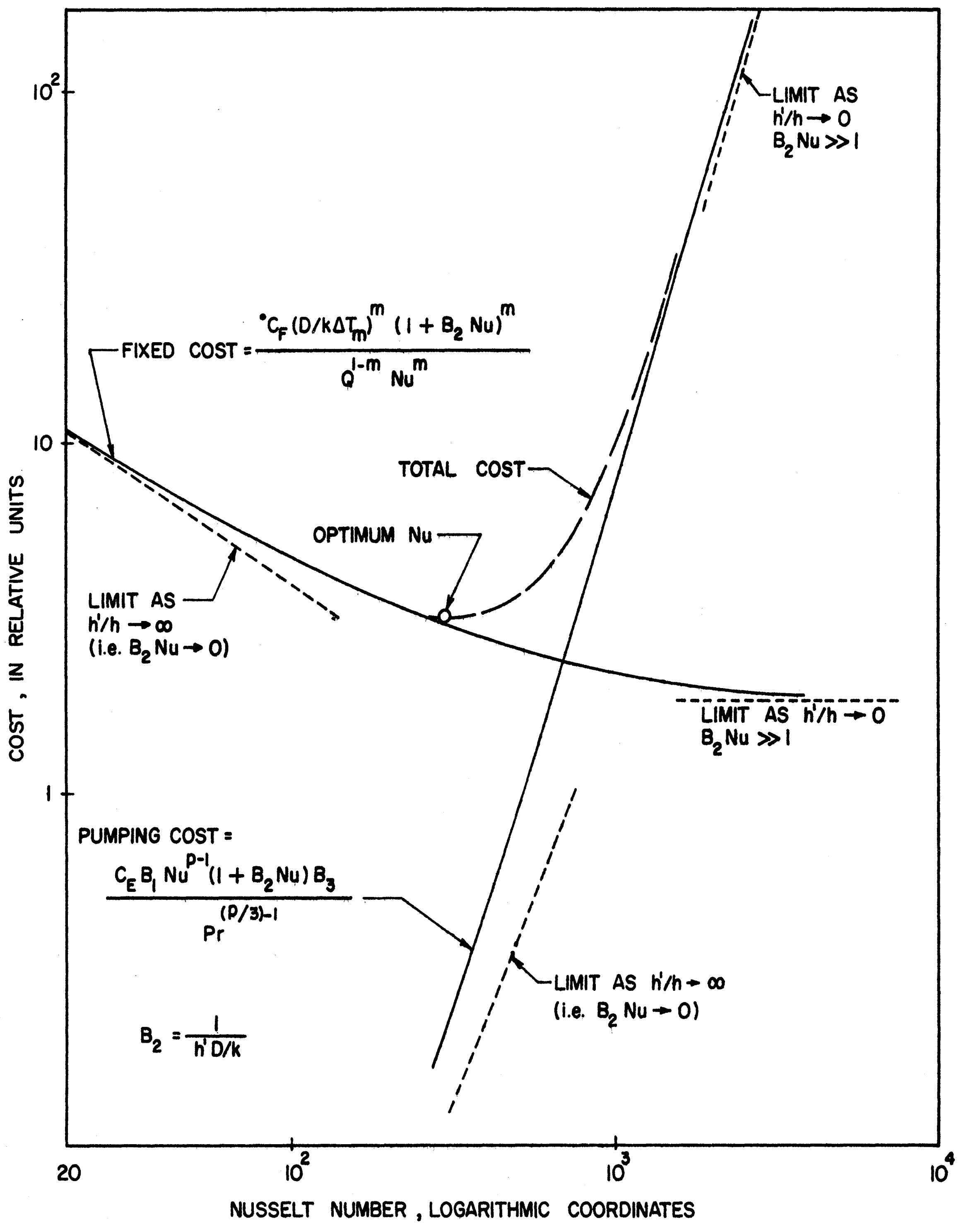

Figure 47. Illustration of Heat Exchanger Costs for a Given Geometry and Tube Diameter as a Function of Nusselt Number.

This is not valid, of course, for non-zero values of B_2 As the effective outside heat transfer coefficient becomes more important, the optimum Nusselt number will be less than the value given by Equation (116).

From an examination of Equation (116) and the definition of B_3 it can be seen that

$$Nu_{optimum} \ \alpha \ [D]^{\frac{2 + m}{p + m - 1}} \qquad (117a)$$

$$\alpha \ [\Delta T_m]^{\frac{1 - m}{p + m - 1}} \qquad (117b)$$

$$\alpha \ [Q]^{\frac{1 - m}{p + m - 1}} \qquad (117c)$$

For common values of p and m (i.e. p = 3.5, m = 0.6)

$$Nu_{optimum} \ \alpha \ D^{0.838} \qquad (118a)$$

$$\alpha \ \Delta T_m^{0.129} \qquad (118b)$$

$$\alpha \ Q^{0.129} \qquad (118c)$$

Thus, for example, a change of diameter by a factor of two changes the optimum Nusselt number by a factor of approximately 1.8. On the other hand, a change in ΔT_m or Q by a factor of 10 changes the optimum Nusselt number by only about $\pm$ 35 per cent. The same proportionality is true, but to a lesser extent, for non-zero values of B_2.

Once the desired (or optimum) Nusselt number is selected, the remaining design parameters N_{tube} and L may be calculated as follows. From Equation (82), valid for any geometry, the number of tubes is given by

$$N_{tube} = \frac{4 \ W}{\mu \ \pi \ D \ Re} \qquad (119)$$

and, specifically for a geometry for which Equations (80) and (81) are valid

$$N_{tube} = \frac{4\ W}{\mu\ \pi\ D} \left[\frac{C_2\ Pr^{1/3}}{Nu}\right]^{1/n_2} \tag{120}$$

The tube length can be obtained by substituting Equations (77) and (76) into Equation (73) and rearranging

$$L = \frac{Q\ [1 + Nu/(h'D/k)]}{\pi\ Nu\ N_{tube}\ k\ \Delta T_m} \tag{121}$$

and, specifically for a geometry for which Equations (80) and (81) are valid

$$L = \frac{Q\ \mu\ D}{4\ W\ k\ \Delta T_m} \quad \frac{[1 + Nu/(h'D/k)]Nu^{(1/n_2-1)}}{(C_2\ Pr^{1/3})^{1/n_2}} \tag{122}$$

Example Design of a Typical Heat Exchanger

The relative importance of the variables on the design of the optimum heat exchanger can best be shown by an example problem. This problem is to design an optimum heat exchanger for a particular application in which actual numerical values of the parameters are specified.

The quantitative results of the solution of the problem will, naturally, be applicable to some other arbitrary heat exchanger design only insofar as the costs and specified variables are the same as for this example. Throughout this presentation, however, the qualitative effect of assuming different costs and different values of the specified variables will be considered in some detail.

The statement of the problem is as follows: A condenser is to be designed in which some vapor condenses on the outside of the tube and water flows inside the tube. The amount of vapor to be condensed is such that the required rate of heat transfer by the condenser is 10,000,000 BTU/hr. The equivalent outside heat transfer coefficient (including the effect of any extended surface) is 3000 BTU/hr-deg. F - ft^2.

The mass flow rate of the water is 250,000 lb_m/hr and the mean temperature difference is 100 deg. F. The specified variables, then, are

$$W = 250{,}000 \ lb_m/hr$$

$$Q = 10{,}000{,}000 \ BTU/hr$$

$$\Delta T_m = 100 \ deg.\ F$$

$$h' = 3000 \ BTU/hr\text{-}deg.\ F - ft^2$$

Values of the physical properties of water will be assumed constant as specified below

$$c = 1 \ BTU/lb_m\text{-}deg.\ F$$

$$\rho = 62.4 \ lb_m/ft^3$$

$$k = 0.353 \ BTU/hr\text{-}deg.\ F - ft$$

$$\mu = 2.42 \ lb_m/ft - hr$$

$$Pr = 6.855$$

The following costs will be assumed

1. The initial investment in dollars is given by

$$\text{Initial investment} = 100 \ A^{0.6} \tag{123}$$

where the area A is measured in ft^2. It will be assumed that the depreciation per year is ten per cent of the initial investment, the maintenance cost per year is also ten per cent of the initial investment and the number of operating hours per year is 8760. Thus,

$$\text{Fixed Cost} = \frac{(0.20)(100)}{8760} A^{0.6} \tag{124}$$

and $$C_F = 2.28 \times 10^{-3} \text{ (dollars/ft}^{1.2}\text{ hr)} \tag{125}$$

with $$m = 0.6 \tag{126}$$

2. The cost of electric power will be taken as \$0.01 per kilowatt hour. Based on a mechanical efficiency of 60 per cent for the pump

$$C_E = \frac{0.01}{(0.60)(3412.76)} \tag{127}$$

$$= 4.88 \times 10^{-7} \text{ dollars/BTU}$$

Design calculations are presented in detail in Appendix D with only the results summarized here.

For purposes of comparison and illustration of the problems involved, designs will be considered initially using an empty tube with three different values of the inside diameter: 0.25, 0.50, and 1.0 inch. Since the purpose of this example problem is to illustrate the relationship between the variables, rather than to build a specific heat exchanger, no attempt will be made to choose values of the tube diameter, number of tubes, tube length, etc. corresponding to dimensions of heat exchanger components available commercially.

The fixed cost, pumping cost, and total cost for each diameter tube are plotted as a function of Nusselt number in Figure 48.

It can be seen that for each tube diameter there is a particular Nusselt number for which the total cost is a minimum. The "flattness" of the minimum appears exaggerated because the costs are plotted on logarithmic coordinates. Nonetheless, any value of the Nusselt number within ± 25 per cent of the optimum value would probably be acceptable. It can also be seen that the cost of designing for a Nusselt number considerably

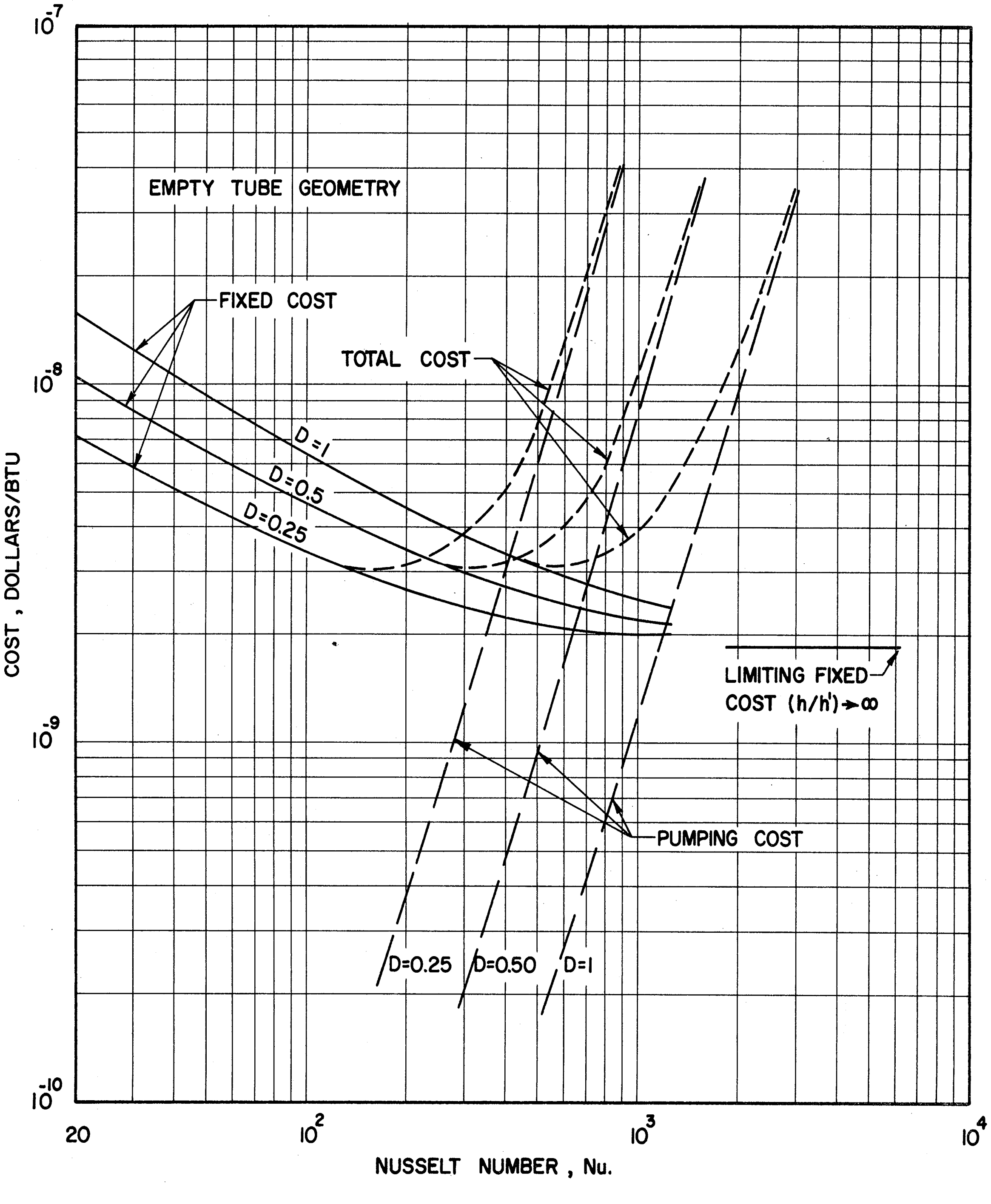

Figure 48. Fixed Cost, Pumping Cost, and Total Cost Per BTU as a Function of Nusselt Number for Example Heat Exchanger Design Using an Empty Tube Geometry. Parameters of d.

greater than the optimum is much higher than the cost of designing for one that is too small.

As the tube diameter is increased the curve of fixed cost vs. Nu is raised, while the curve of pumping cost vs. Nu is lowered which results in a shift of the optimum Nusselt number toward higher values of Nu for larger tube diameters.

Despite the fact that the optimum Nusselt number is quite different for different diameters, the total cost at the optimum is almost identical.

The optimum exchanger designs are summarized below.

Diameter	0.25 inch	0.50 inch	1.00 inch
Optimum Nu	175	330	600
Total Cost (dollars/BTU)	0.031×10^{-7}	0.0315×10^{-7}	0.0321×10^{-7}
Number of Tubes	241	55	13
Length (ft)	4.2	9.6	21.4

Next, two designs will be considered using two types of turbulence promoters in a tube of diameter 0.50 inch for comparison with the design for the empty tube. The two geometries (selected arbitrarily for purposes of illustration) are

Geometry I Disks; d = 0.625; s = 4

Geometry II Disks; d = 0.875; s = 8

It should be noted that for any of the geometries studied in the experimental portion of this investigation

$$100\ f = C(s,d)\ Re^{n(s,d)} \qquad (65)$$

$$h_m/h_0 = C(s,d)\ Re^{n(s,d)} \qquad (67)$$

with the appropriate functions $C(s,d)$ and $n(s,d)$ -- different for each geometry and not the same for calculating f as for calculating h_m/h_0 -- tabulated in Tables VIII and X of Appendix C. Since

$$h_0 = (0.027)\ \frac{k}{D}\ Re^{0.8}\ Pr^{1/3} \qquad (128)$$

The constants C_1, C_2, n_1 and n_2 may be readily obtained.

The fixed cost, pumping cost, and total cost for each geometry are plotted as a function of Nusselt number in Figure 49. For comparison, the curve for the empty tube is also included. It can be seen that for the same tube diameter the fixed cost is the same for all three geometries. The curve of pumping cost vs. Nusselt number, however, is higher for both turbulence promoters than for the empty tube. The curve for geometry II is higher than the curve for geometry I.

The optimum exchanger designs are summarized below.

	Empty Tube	Geometry I disks s = 4 d = 0.625	Geometry II disks s = 8 d = 0.875
Optimum Nu	330	300	245
Total Cost (dollars/BTU)	0.0315×10^{-7}	0.032×10^{-7}	0.035×10^{-7}
Number of Tubes	55	143	159
Length (ft)	9.6	3.96	3.86

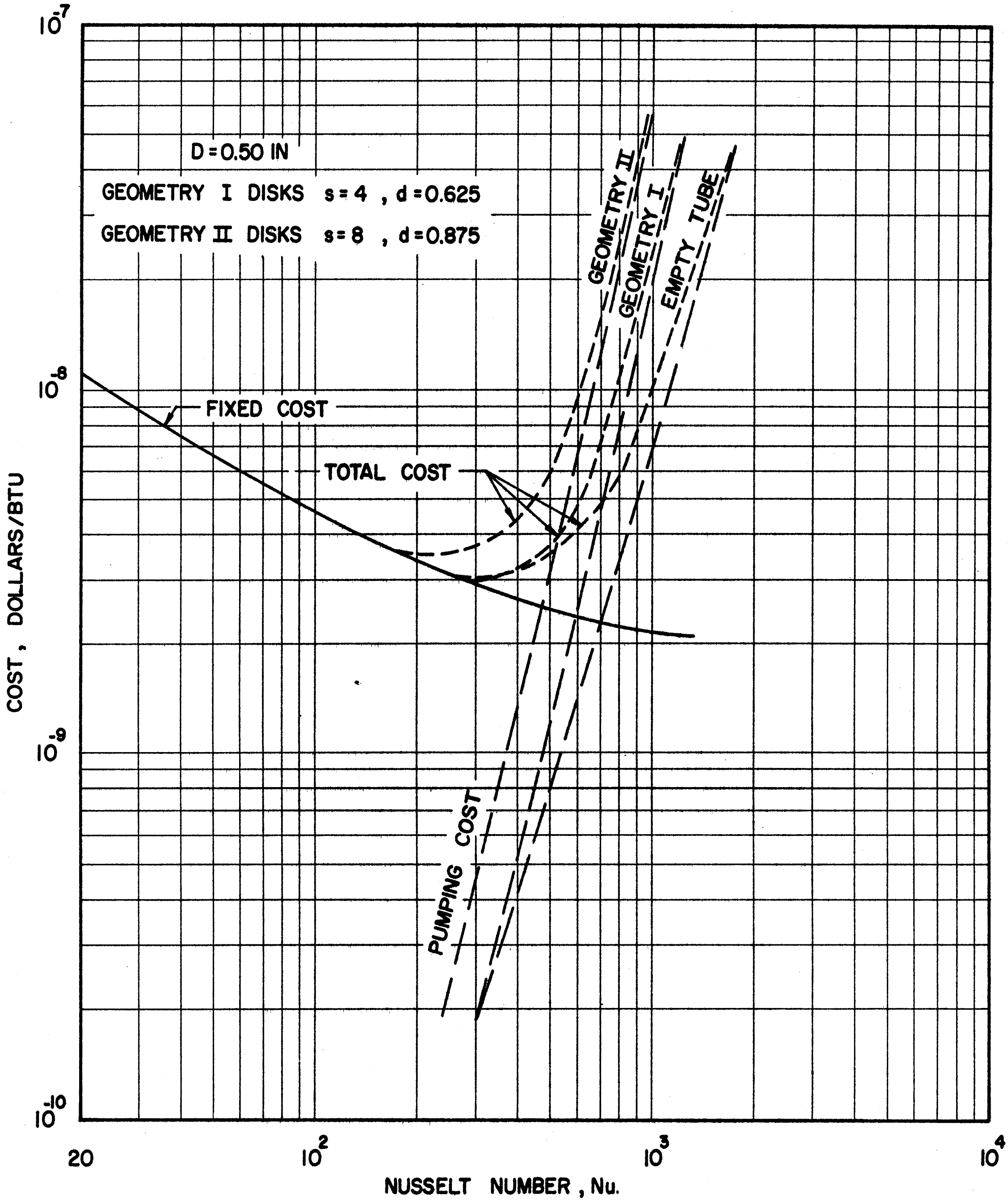

Figure 49. Fixed Cost, Pumping Cost, and Total Cost Per BTU as a Function of Nusselt Number for Example Heat Exchanger Design Using Turbulence Promoters with D = 0.50 inch.

It can be seen that in each case the turbulence promoting geometry produces a higher total cost than the empty tube, but for all geometries the costs are within ten per cent. This example illustrates an important conclusion: The only way a turbulence promoting geometry can produce a lower total cost is for its curve of E/Q vs. Nusselt number to be below that for an empty tube.

Even though the E/Q curve for the turbulence promoter does lie considerably above that for the empty tube, if an exchanger is properly designed (in the optimum manner) for the promoter, its total cost may be only slightly greater than that for the optimum exchanger designed using empty tubes. This is well illustrated by the example problem. The effect of geometries with high E/Q vs. Nu curves is to lower the optimum Nusselt number.

Conclusions Regarding the Economics of Using Turbulence Promoters

It was illustrated in the solution of the example problem that the total cost of a heat exchanger designed in an optimum manner to use turbulence promoters may be only slightly greater than the total cost of an exchanger designed in an optimum manner using an empty tube. Nonetheless, it was shown that the only way one inside tube geometry can produce a lower total cost than another is for its curve of E/Q vs. Nu to be lower. This suggests that a valuable measure of any proposed turbulence promoting scheme for improving the rate of heat transfer in a tube is the ratio of E/Q for the turbulence promoter to $(E/Q)_{ET}$ for the empty tube as a function of Nusselt number. This ratio is plotted as a function of Nu in Figure 50 for disks and in Figure 51 for streamline shapes and the solid rod.

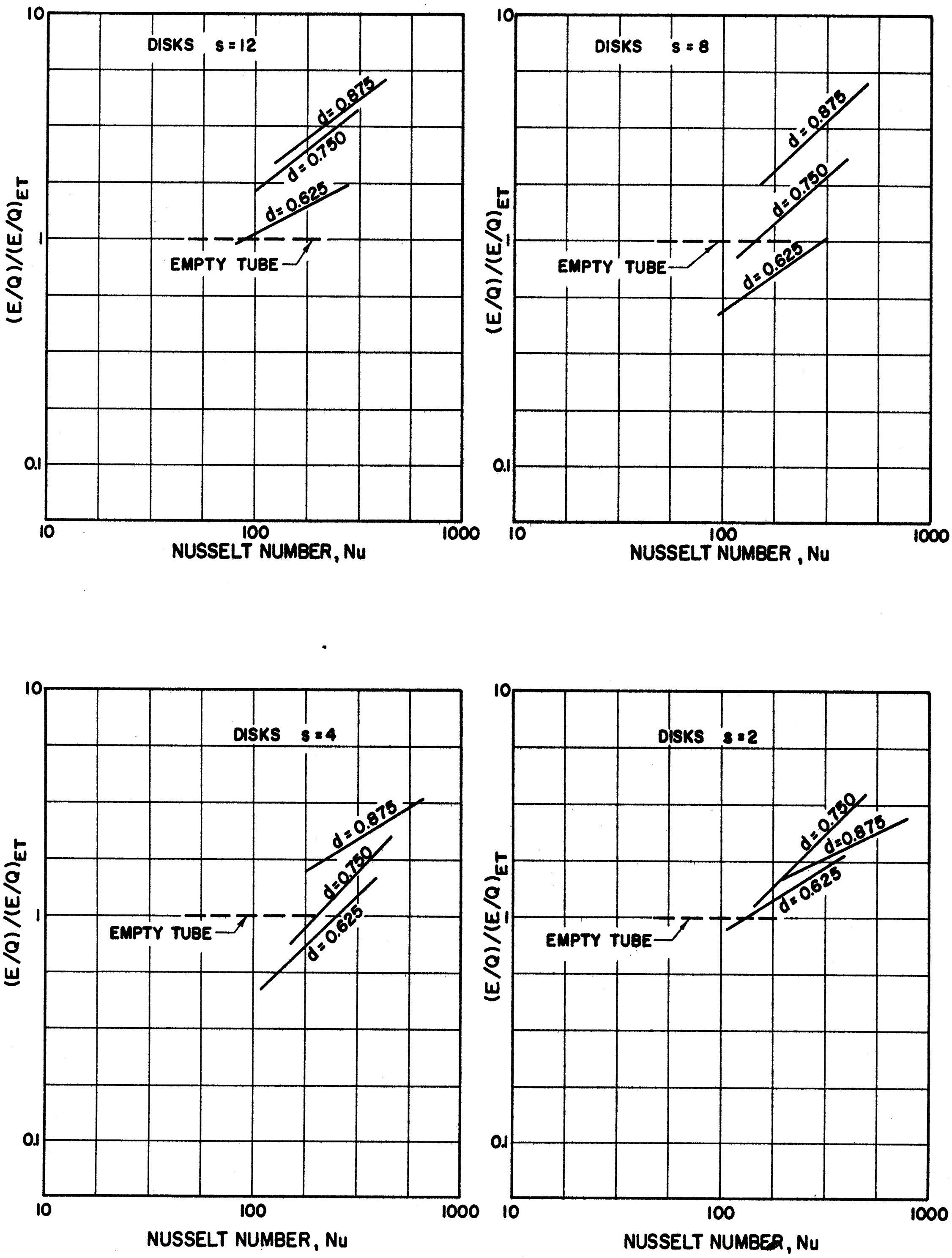

Figure 50. Ratio of Pumping Cost for Disks to Pumping Cost for Empty Tube as a Function of Nusselt Number, $(E/Q)/(E/Q)_{ET}$ vs. Nu for s = 12, 8, 4, and 2 with Parameters of d.

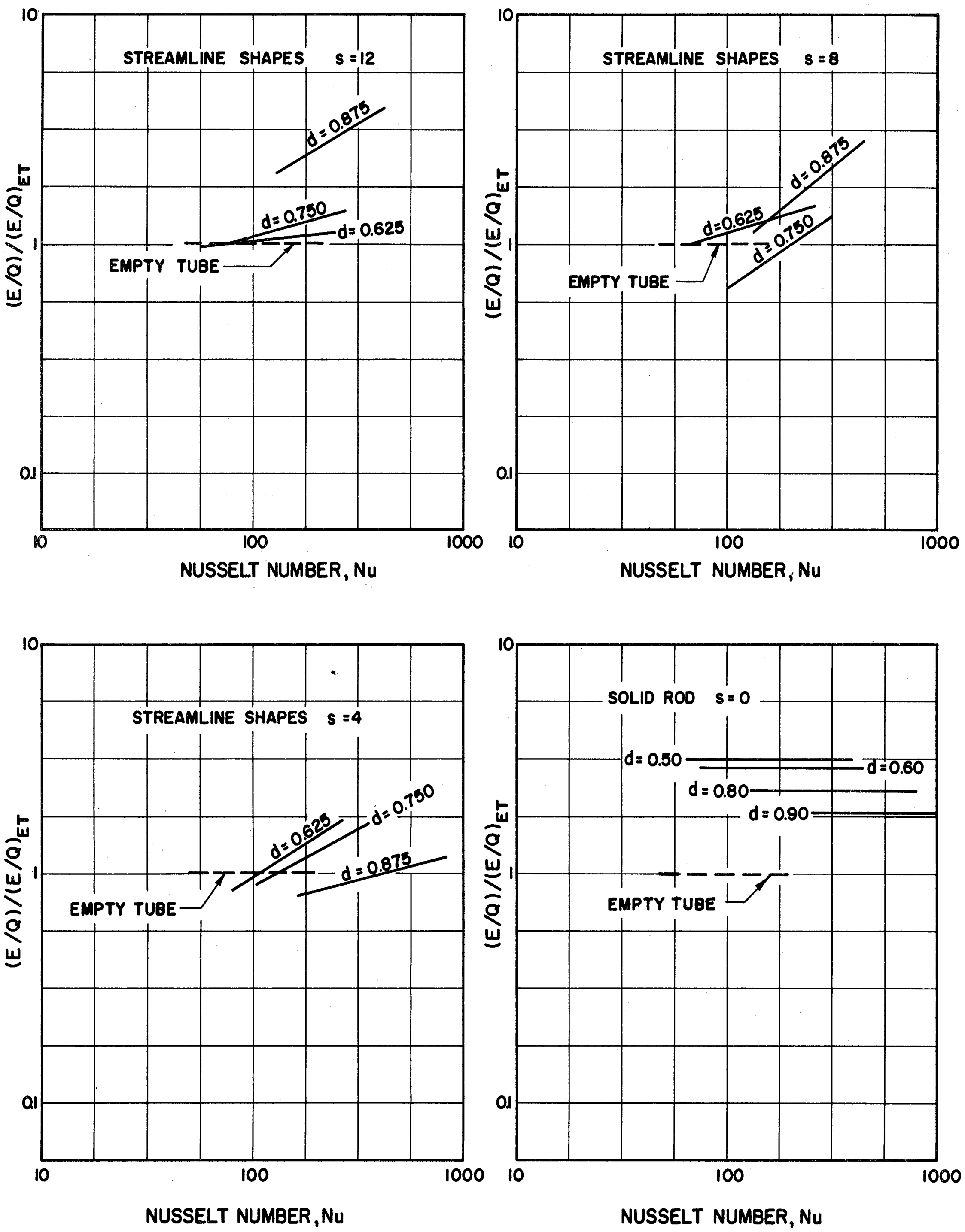

Figure 51. Ratio of Pumping Cost for Streamline Shapes and Solid Rod to Pumping Cost for Empty Tube as a Function of Nusselt Number, $(E/Q)/(E/Q)_{ET}$ vs. Nu for s = 12, 8, 4, and 0 with Parameters of d.

It can be seen that all of the promoter combinations except the solid rods become less efficient at higher Nusselt numbers. For the disks at spacings greater than 8 tube diameters and streamline shapes at spacings of 12 tube diameters, the most economical design is the one with the smallest diameter and the least economical is the one with the greatest diameter. At closer spacings, particularly for the streamline shapes, the trend is reversed and the most economical promoter is the one with the largest diameter. This is also true for the solid rod in the center. In other words, it appears that systems which behave similar to a solid rod are best with large diameter ratios, while systems which behave like individual bluff bodies are best with small diameter ratios. It is also noticed that both the disks and streamline shapes tend to become more efficient at closer spacings, but in the case of the disks a spacing of 4 diameters is more efficient than either 2 or 8 diameters, indicating an optimum spacing of about 4 tube diameters for disks.

One important observation to be made from the example problem is that even though the total cost is almost the same for the two exchangers using the turbulence promoters and the one using empty tubes, the "shape" of the exchangers is quite different. Both of the optimally designed exchangers using turbulence promoters were much shorter and required more tubes than the optimally designed exchanger using empty tubes. This is a general characteristic of well-designed exchangers employing turbulence promoters.

Effect of Variables Assumed Specified

In the economic study it was assumed that four variables were specified by the process: W, Q, ΔT_m, and h'. The following comments are intended for the cases where these variables are not specified, but are subject to optimization.

As was shown earlier, changing ΔT_m has little effect on the value of the optimum Nusselt number for any type geometry. The total cost, however, (excluding the cost of fluid) per unit of heat transfer is less for higher values of ΔT_m. This is obvious, since increasing ΔT_m increases the rate of heat transfer without any increase in area or pumping power required. Of course, in order to obtain high values of ΔT_m it is usually necessary to provide large mass flow rates W of the fluid, so that the optimum value of ΔT_m is obtained by balancing the increased cost of the fluid against the decreased fixed and pumping costs per unit of heat transfer. If the Nusselt number in the tube is known (and, hence, the value of U_{oa}) charts prepared by Colburn and presented by Perry(35) are available for quickly obtaining the optimum value of ΔT_m based on the relative cost of fluid and fixed cost per unit area. Thus, an approximate estimate of the best ΔT_m should be adequate for selecting the optimum Nusselt number for any geometry. On the basis of this optimum Nusselt number, Colburn's charts can be used to obtain a more exact estimate of the optimum value of ΔT_m. This may be continued, if necessary, until an optimum set of conditions is obtained, but usually the first assumption will be adequate.

Changing the mass flow rate W has no effect on the optimum geometry or Nusselt number if it does not affect ΔT_m. For a constant temperature difference, increasing the mass flow rate simply reduces the length and increases the number of tubes (keeping the Nusselt number and required area the same). If changing W also changes ΔT_m then the comments in the preceding paragraph are applicable.

The outside heat transfer coefficient h' is dependent upon conditions external to the geometry of the inside of the tube, and hence, must be assumed specified. Also the rate of heat transfer Q will almost always be specified.

It should be noted that anything which tends to result in a large heat exchanger reduces the fixed cost relative to the pumping cost per unit heat transfer. This, in turn, favors operating at lower Nusselt numbers where turbulence promoters are most effective. Thus, high values of Q, low values of h', and low values of ΔT_m all tend to favor the use of turbulence promoters.

Use of Turbulence Promoters in Design of New Exchangers

On the basis of the preceding economic study, including the results of the example problem, some recommendations will be made concerning the applicability of including turbulence promoters in the design of new heat transfer equipment.

From Figures 50 and 51 it can be seen that the pumping power required per unit heat transfer for the types of turbulence promoters considered in this investigation ranges from about 80 to 500 per cent of that required using an empty tube. Since the promoters are almost always most effective at low Nusselt numbers, it would appear that their greatest promise is in designs where pumping cost is very high compared with the fixed cost, since in these cases the optimum Nusselt number is usually low.

What is probably more important than the savings in cost by using promoters is the added flexibility in design which may be afforded, usually with only a slight increase in the total cost of operation. Their use adds one more independent variable that the designer may have in specifying the exchanger. Even after the fluid velocity in the tubes has been set, it is still possible to independently raise the heat transfer coefficient by a factor from less than 10 per cent to almost 400 per cent. It has been shown that, properly designed, this may impose only a slight additional cost.

The use of turbulence promoters is essentially equivalent to designing a longer exchanger with fewer tubes (or, in other words, to adding more tube passes). This suggests that whenever a study indicates that the best designed exchanger would require more tube passes than it is feasible to build, then turbulence promoters should certainly be considered.

In certain cases a design may be encountered where one tube pass will not produce a high enough heat transfer coefficient, but two tube passes causes an excessive pressure drop, produces a heat transfer coefficient greater than that required, and reduces the effective value of ΔT_m. In this situation a better solution might be to install promoters for at least part of the length of the exchanger.

The use of turbulence promoters also has the advantage that the local heat transfer coefficient can be controlled. This may be useful when the local rate of heat transfer varies considerably along the length of the tube as, for example, in a chemical reactor.

Use of Turbulence Promoters in Improving Existing Exchangers

The considerations involved in improving the performance of an existing exchanger are simpler in some respects and more complicated in others. The problem is simpler in that, since the exchanger is already built, the number of tubes, diameter, length, etc. are set and there are a minimum of variables which are free to be changed and, hence, fewer which need to be considered. On the other hand, the problem is more complicated, since when one variable imbedded within a process is changed, often all the others are affected in a manner which is hard to predict and for which the economics are not known.

The rate of heat transfer by an exchanger is given by

$$Q = U_{oa} \, A \, \Delta T_m \tag{73}$$

In an existing exchanger the area A is fixed, so there are only two means for improving the rate of heat transfer: increase the overall coefficient U_{oa} or increase the temperature difference ΔT_m. Now, increasing ΔT_m involves changing the process external to the heat exchanger, for example by increasing the mass flow rate of the fluid through the exchanger or changing certain process temperatures. Since the advisability of this approach depends strongly upon the specific situation it will not be considered further.

If it is desired to increase U_{oa} without changing the mass flow rate, there are essentially two alternatives: 1) increase the fluid velocity by increasing the number of tube passes, or 2) install some sort of turbulence promoting devices. In many cases increasing the number of tube passes will not be feasible, particularly when the exchanger is a multiple pass exchanger to begin with.

It is in this case that the use of turbulence promoters provides a quick, simple method of improving the performance of an existing heat exchanger. The data and correlations of the experimental phase of this investigation provide a guide to the selection of the best type of promoter for a given application. The use of promoters has the big advantage that changes to the process in which the exchanger operates are localized as much as possible.

Streamlined *vs*. Non-streamlined Promoters

There appears to be little advantage (or disadvantage) in using streamline shapes in preference to disks. Since the cost of fabricating streamline shapes is greater than the cost of fabricating disks and since possible problems with vibration may occur with their use, the use of disks is recommended over the use of streamline shapes for most applications.

SUMMARY AND CONCLUSIONS

The main objectives of this investigation were twofold: 1) to obtain generalized correlations for predicting the rate of heat transfer and the pressure drop for a fluid flowing in a tube in which bluff-body turbulence promoters were mounted axially, and 2) to determine whether bluff-body turbulence promoters can be used economically in equipment for transferring heat.

The variables chosen for investigation were the shape of the bluff-body turbulence promoter, the ratio of the diameter of the promoter to the inside diameter of the tube, the spacing between promoters, flow rate of the fluid, and physical properties of the fluid.

Two different shapes were investigated which represent extremes in the degree of streamlining. The first was a disk, the second was a combination of a hemisphere and cone to form a teardrop-like shape. In addition, data were obtained for a solid rod centered in the tube which corresponds to a string of bluff-bodies at zero spacing.

A variety of diameter ratios, spacings and flow rates were tested with one fluid: water. All results are presented in the form of dimensionless ratios to extend the applicability of the results.

Two different techniques were employed to characterize the pressure drop. The first was to define a friction factor similar to that used for smooth tubes as given by Equation (22). The second was to define an effective drag coefficient for each bluff-body similar to that used for immersed objects in an infinite fluid with uniform flow. The effective drag coefficient is defined by Equation (14).

The rate of heat transfer was characterized by a ratio h_m/h_0 where h_m is the mean overall heat transfer coefficient for a tube with turbulence promoters and h_0 is the mean overall heat transfer coefficient (given by the Sieder-Tate equation) for an empty tube and the same mass flow rate. When presented in this form, it is presumed that the results of this investigation using water are applicable to any other fluid for which the Sieder-Tate equation is valid.

Separate correlations for the friction factor, effective drag coefficient, and heat transfer coefficient ratio in terms of Reynolds number were obtained for each combination of shape, spacing, and promoter diameter. In addition, generalized correlations were obtained for each shape to predict the effective drag coefficient and heat transfer coefficient ratio in terms of spacing, promoter diameter, and Reynolds number. The generalized correlations correlate the data of this investigation with an average deviation of less than 10 per cent.

A comparison was made of existing correlations for the friction factor based upon the use of an equivalent diameter for the annuli, and it was found that recent correlations of Lohrenz and Kurata(26), Meter and Bird(29), and Walker, Whan, and Rothfus(42) give comparable results. Accordingly, a correlation for predicting the rate of heat transfer to the <u>outside</u> wall of an annulus was developed using the equivalent diameter suggested by Lohrenz and Kurata.

A comprehensive study of the economics of using turbulence promoters in heat transfer equipment was made and a general procedure was outlined for evaluating the effectiveness of any turbulence promoting scheme. This procedure was illustrated with an example problem.

The main conclusions resulting from this study may be summarized as follows.

1. The pressure drop caused by a fluid flowing in a tube in which axial bluff-body turbulence promoters have been inserted can be better described by an effective drag coefficient based on the drag of a single bluff body than by a friction factor of the type normally used for smooth tubes.

2. For diameter ratios between 0.625 and 0.875 the effective drag coefficients for disks axially centered in the tube are correlated by

$$100\ f_D = \frac{156\ s}{1 + 0.78\ s} \tag{129}$$

3. For diameter ratios between 0.625 and 0.875 the effective drag coefficients for streamline shapes of the shape shown in Figure 8, axially centered in the tube, are correlated by

$$100\ f_D = \frac{117\ s}{1 + 1.6\ s} \left[\frac{Re}{10,000}\right]^{-0.12} \tag{130}$$

4. The mean heat transfer coefficient ratios for disks axially centered in the tube with diameter ratio between 0.625 and 0.875 are correlated as follows.

$$\frac{h_m}{h_0} = 1 + 3.28\ (-\ln A_f) \left[\frac{Re}{10,000}\right]^{-0.14} \times \left[\frac{1}{1 + 0.15\ s} - \frac{1.7}{11.9 + s^4}\right] \tag{131}$$

5. The mean heat transfer coefficient ratios for streamline shapes of the shape shown in Figure 8, axially centered in the tube with diameter ratio between 0.625 and 0.875 are correlated as

$$\frac{h_m}{h_0} = 1 + 2.04\ (-\ln A_f) \left[\frac{Re}{10,000}\right]^{-0.11} \left[\frac{1}{1 + 0.14\ s}\right] \qquad (132)$$

6. The rate of heat transfer to the <u>outside</u> wall of an annulus is best correlated in terms of an "equivalent Nusselt number" which is a function of the "equivalent Reynolds number." The recommended correlation is

$$Nu^* = 0.024\ Re^{*0.8}\ Pr^{1/3}\ (\mu/\mu_w)^{0.14} \qquad (133)$$

where Nu^* and Re^* are based on the equivalent diameter recommended by Lohrenz and Kurata[26] and defined by Equation (35).

7. The most important parameter required for an economic evaluation of turbulence promoters in a given heat transfer application is the dimensionless ratio of pumping energy required to total rate of heat transfer, E/Q, as a function of the Nusselt number produced. This parameter may be obtained from experimental measurements by use of Equation (106).

8. When designed for use at low Nusselt numbers, the use of certain types of turbulence promoters as indicated by Figures 50 and 51 can produce a more economical heat exchanger than the use of empty tubes.

9. By careful design the use of an inefficient turbulence promoter can be used to advantage in giving additional flexibility in designing a new heat exchanger or in improving an old one. Although the total cost of using an inefficient turbulence promoter will always be higher than that for an empty tube, it may be only slightly higher.

BIBLIOGRAPHY

1. Allegheny Ludlum Steel Corporation, Brackenbridge, Pennsylvania, Allegheny Ludlum Blue Sheet, "Allegheny Metal 18-8 A.I.S.I. Types 301, 302, 304, and 308".

2. Barrow, H., "Convection Heat Transfer Coefficients for Turbulent Flow Between Parallel Plates with Unequal Heat Fluxes," Intern. J. Heat Mass Transfer, 1, 306-11 (January, 1961).

3. Bingham, E. C., "Fluidity and Plasticity," McGraw-Hill, New York (1922).

4. Bird, R. B., Stewart, W. B., and Lightfoot, E. N., "Transport Phenomena," John Wiley and Sons, New York (1960).

5. Blasius, H., Forschungsarbeiten des Ver. deutsch. Ing., No. 131, 1-40 (1913).

6. Boelter, L. M. K., Young, G., and Iverson, H. W., "An Investigation of Aircraft Heaters-XXVII -- Distribution of Heat Transfer Rate in the Entrance Section of a Circular Tube," Nat. Advisory Comm. Aeronaut. Tech. Note 1451 (1948).

7. Carslaw, H. S. and Jaeger, J. C., "Conduction of Heat in Solids," Oxford University Press, London (1959).

8. Clark, J. A., Discussion of Paper by Leppert, G., Costello, C. P. and Hoglund, B. M., "Boiling Heat Transfer to Water Containing a Volatile Additive," Trans. Am. Soc. Mech. Engrs., 80, 1395-1404 (1958).

9. Colburn, A. P. and King, W. J., "Relationship Between Heat Transfer and Pressure Drop," Ind. Eng. Chem., 23, 919-23 (1931) and Trans. Am. Inst. Chem. Engrs., 26, 296-307 (1931).

10. Colburn, A. P., Trans. Am. Inst. Chem. Engrs., 29, 174 (1933).

11. Colburn, A. P., "Heat Transfer by Convection," Purdue Univ. Eng. Bull. Research Ser. No. 84, 52-3 (1942).

12. Davis, E. S., Trans. Am. Soc. Mech. Engrs., 65, 755 (1943).

13. Deisler, R. G. and Taylor, M. F., "Analysis of Fully Developed Turbulent Flow in an Annulus with Various Eccentricities," Nat. Advisory Comm. Aeronaut. Tech. Note 3451 (May, 1955).

14. Drexel, R. E. and McAdams, W. H., Nat. Advisory Comm. Aeronaut. Wartime Rept. 108 (1945).

15. Evans, S. I. and Sarjant, R. J., "Heat Transfer and Turbulence in Gases Flowing Inside Tubes," J. Inst. Fuel, 24, 216-27 (September, 1951).

16. Faruqui, A. A. and Knudsen, J. G., "Rates of Heat Transfer from Short Sections of an Isothermal Pipe," Chem. Engr. Progr. Symposium Ser. No. 32, 57, 96-103 (1961).

17. Gambill, W. R., Bundy, R. D., and Wansbrough, R. W., "Heat Transfer, Burnout, and Pressure Drop for Water in Swirl Flow through Tubes with Internal Twisted Tapes," Oak Ridge National Laboratory Report ORNL-2911 (March 28, 1960).

18. Gambill, W. R., Bundy, R. D., and Wansbrough, R. W., "Heat Transfer, Burnout, and Pressure Drop for Water in Swirl Flow through Tubes with Internal Twisted Tapes," Chem. Engr. Progr. Symposium Ser. No. 32, 57, 127-37 (1961).

19. Gambill, W. R. and Bundy, R. D., "High-Flux Heat Transfer Characteristics of Pure Ethylene Glycol," Preprint of Paper Presented at the 46th National Meeting of the American Institute of Chemical Engineers, Los Angeles, California (February 4-7, 1962).

20. Hartnett, J. P., "Experimental Determination of Thermal Entrance Length for Flow of Water and Oil in Circular Pipes," Am. Soc. Mech. Engrs. Paper No. 54-A-184 (1954).

21. Kemeny, G. A. and Cyphers, J. A., "Heat Transfer and Pressure Drop in an Annulur Gap with Surface Spoilers," Am. Soc. Mech. Engrs. Paper No. 60-HT-15 (1960).

22. Knudsen, J. G. and Katz, D. L., "Fluid Dynamics and Heat Transfer," McGraw-Hill, New York (1958).

23. Koch, R., "Pressure Loss and Heat Transfer in Turbulent Flow," VDI--Forschungsheft 469 Supplement to Forsch. Gebite Ingenieurw. 22B (1958).

24. Kreith, F. and Margolis, D., "Heat Transfer and Friction in Swirling Turbulent Flow," Heat Transfer and Fluid Mechanics Institute, Preprints of Papers, 126-42 (June, 1958).

25. Kreith, F. and Margolis, D., "Heat Transfer and Friction in Turbulent Vortex Flow," Appl. Sci. Research A, 8, 457-73 (1959).

26. Lohrenz, J. and Kurata, F., "A Friction Factor Plot for Smooth, Circular Conduits, Concentric Annuli, and Parallel Plates," Ind. Eng. Chem., 52, 703-06 (1960).

27. Margolis, D., "The Effect of Turbulence Promoters on the Rate of Heat Transfer and the Pressure Drop in Straight Tubes," M.S. Thesis, Lehigh Univ., Bethlehem, Pennsylvania (June, 1957).

28. McAdams, W. H., "Heat Transmission--Third Edition," McGraw-Hill, New York (1954).

29. Meter, D. M. and Bird, R. B., "Turbulent Newtonian Flow in Annuli," A.I.Ch.E. Journal, 7, 41-45 (March, 1961).

30. Monrad, C. C. and Pelton, J. F., "Heat Transfer by Convection in Annular Spaces," Trans. Am. Inst. Chem. Engrs., 38, 593-611 (1942).

31. Nagaoka, J. and Watanabe, A., "Maximum Rate of Heat Transfer with Minimum Loss of Energy," Proc. 7th Intern. Congr. Refrig., The Hauge--Amsterdam (1936).

32. National Research Council of the United States of America, "International Critical Tables," Volume I (1928).

33. Nikuradse, J., VDI-Forschungsheft 356 Supplement to Forsch. Gebite Ingenieurw. (1932).

34. Nunner, W., "Heat Transfer and Pressure Drop in Rough Pipes," VDI-Forschungsheft 455 Supplement to Forsch. Gebite Ingenieurw., 22B (1956).

35. Perry, J. H., "Chemical Engineers Handbook--Third Edition," McGraw-Hill, New York (1949).

36. Royds, R., "Heat Transmission by Radiation, Conduction, and Convection," Constable and Company Ltd., London (1921).

37. Shelton, A. M., "Thermal Conductivity of Some Irons and Steels over the Temperature Range 100-500 C," Bur. Standards J. Research, 12, 441-50 (1934).

38. Sieder, E. N. and Tate, G. E., Ind. Eng. Chem., 28, 1429 (1936).

39. Siegel, L. G., Heating Piping Air Conditioning, 18, 111-14 (June, 1946).

40. Sundstrom, D. W. and Churchill, S.W., "Heat Transfer from Pre-Mixed Gas Flames in a Cooled Tube," Chem. Engr. Progr. Symposium Ser. No. 30, 56, 65-73 (1960).

41. Timrot and Vargaftik, J. Tech. Phys. (U.S.S.R.), 10, 1063 (1940).

42. Walker, J. E., Whan, G. A. and Rothfus, R. R., "Fluid Friction in Non-Circular Ducts," A.I.Ch.E. Journal, 3, 484-89 (1957).

43. Zartman, W. N. and Churchill, S. W., "Heat Transfer from Acoustically Resonating Gas Flames in a Cylindrical Burner," A.I.Ch.E. Journal, 7, 588-92 (December, 1961).

APPENDIX A

DESCRIPTION OF COMPUTER TECHNIQUES FOR PROCESSING DATA

In this section the method of processing pressure drop and heat transfer data will be discussed. Some of the problems of converting the raw measurements into usable engineering units and evaluating the physical properties of water were common to both types of data, so they will be explained first.

Because of the tremendous amount of data generated by the experiments, all data processing was performed on the IBM 704 computer. Most of the procedures for converting the raw data and evaluating physical properties were actually incorporated into general-purpose computer subroutines and used by the main data processing program.

Conversion of Raw Measurements into Engineering Units and Evaluation of Physical Properties

Thermocouple Readings

The copper-constantan thermocouples used were calibrated against precision thermometers certified by the National Bureau of Standards in a constant temperature oil bath over the range 50 deg F to 220 deg F and found to agree with tabulated values in the International Critical Tables.(32) The range of values which is of interest is reproduced in Table IV. All thermocouple emfs were converted to deg F using linear interpolation on the table and converting from deg C to deg F with

$$\text{Deg F} = 1.8 \text{ Deg C} + 32 \qquad \text{(A-1)}$$

TABLE IV

THERMOCOUPLE EMF VS. DEGREES CENTIGRADE FOR COPPER-CONSTANTAN THERMOCOUPLES

EMF (mv)	TEMP (Deg C)	EMF (mv)	TEMP (Deg C)	EMF (mv)	TEMP (Deg C)
0.00	0.00	1.50	37.38	3.00	72.08
0.10	2.59	1.60	39.77	3.10	74.31
0.20	5.16	1.70	42.15	3.20	76.54
0.30	7.72	1.80	44.51	3.30	78.76
0.40	10.27	1.90	46.86	3.40	80.97
0.50	12.80	2.00	49.20	3.50	83.17
0.60	15.32	2.10	51.53	3.60	85.37
0.70	17.83	2.20	53.85	3.70	87.56
0.80	20.32	2.30	56.16	3.80	89.74
0.90	22.80	2.40	58.46	3.90	91.91
1.00	25.27	2.50	60.76	4.00	94.07
1.10	27.72	2.60	63.04	4.10	96.23
1.20	30.15	2.70	65.31	4.20	98.38
1.30	32.57	2.80	67.58	4.30	100.52
1.40	34.98	2.90	69.83	4.40	102.66

Rotameter Readings

Four rotameters (numbered 1 to 4) were available covering different flow rates. These rotameters had assorted scales, depending upon their original use. Each, however, was calibrated prior to use by measuring the time required for a given weight of water to fill a tank while the water was flowing at a constant rate. Each of the rotameters was found to have a linear scale; the calibration curves are presented in Figure 52. The rotameter number, range in gpm, range in Reynolds number for water flowing in the test section at 60 deg F and equations for calculating the flow rate in gpm from the rotameter reading are given below.

Rotameter Number	Range of GPM	Range of Re at 60 deg F	Equation for Calculating Flow Rate
1	0.1 to 0.7	340 to 2000	+ 0.02 + 0.454 x Reading
2	0.5 to 2.3	1400 to 6200	-0.395 + 0.1095xReading
3	0.8 to 3.8	2300 to 11,000	-0.075 + 0.3265xReading
4	2.1 to 18	6000 to 50,000	-0.100 + 0.299 x Reading

About 80 per cent of the data were taken using rotameter 4, 20 per cent using rotameter 2, and less than one per cent using rotameters 1 and 3.

Pressure Drop

All pressure drops were measured using the single-tube King manometers with either mercury or purple indicating fluid of specific gravity 1.750. The equations for converting the pressure drop to lb_f/in^2 (psi) are

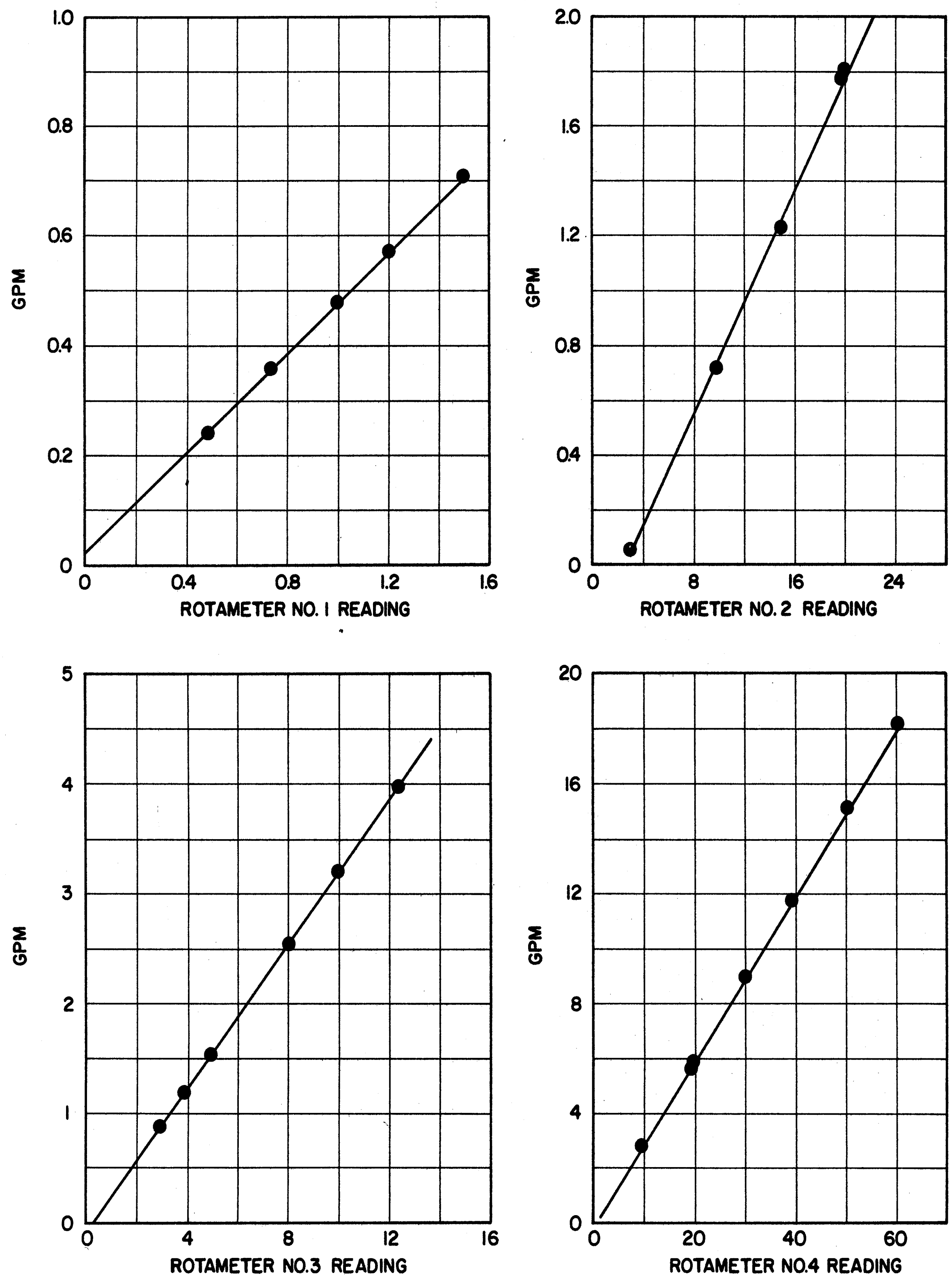

Figure 52. Flow Rate as a Function of Rotameter Reading, GPM vs. Reading, for Rotameters 1, 2, 3, and 4.

$$\Delta P_{psi} = \frac{\Delta P_{\text{inches mercury}}}{2.20392} \qquad \text{(A-2a)}$$

$$\Delta P_{psi} = \frac{\Delta P_{\text{inches purple fluid}}}{36.90533} \qquad \text{(A-2b)}$$

Viscosity of Water

The viscosity of water at any temperature T was calculated using Bingham's[3] formula as given by Perry[35]. This formula is

$$\mu = \frac{1}{2.1482\ [T - 8.435 + \sqrt{8078.4 + (T - 8.435)^2}] - 120} \qquad \text{(A-3)}$$

where the viscosity μ is given in centipoises.

Thermal Conductivity of Water

The thermal conductivity of water as a function of the temperature T was obtained by fitting a second order polynomial to tabulated values obtained by Timrot and Vargaftik[41] and presented by Perry.[35] These values are

Temperature (Deg F)	k (BTU/hr-deg F-ft)
32	0.343
100	0.363
200	0.393

The polynomial is

$$k = 0.343 + 2.941 \times 10^{-4}\ (T - 32) + 3.5014 \times 10^{-8}\ (T-32)(T-100) \qquad \text{(A-4)}$$

Density and Heat Capacity of Water

The density of water over the range of fluid temperatures encountered was taken as

$$\rho = 62.43 \ lb_m/ft^3$$

The heat capacity was taken as

$$c = 1.0 \ BTU/lb_m\text{-deg F}$$

Processing of Pressure Drop Data

The method of processing data on the IBM 704 can best be described by considering a sample set of data. Thus, we will examine the pressure drop data from run A-18 taken for streamline shapes with d = 0.750 and s = 8.

The raw data sheet is shown in Figure 53. Each line on the data sheet corresponds to one IBM card. The computer program was written so that items not repeated on a line were assumed to be the same as on the preceding line. The term labeled PSCALE signifies which indicating fluid was being used. If it was 0.0 then the purple fluid was used; if it was 1.0 then mercury was used. The term labeled RATIO is (μ/μ_w); for all isothermal runs this was 1.000. A listing (i.e., printed copy) of the punched cards for this set of data is shown in Figure 54. An "L" in column 71 of the cards signified the end of the set of remarks or the end of the set of data. A blank card also signified the end of the set of data if the "L" was not punched in column 71.

DATA SHEET FOR PRESSURE DROP MEASUREMENTS

RUN NUMBER	DATE	NP	S	
A-18	1-9-61	6.	8.	
1	15	29	36	43

REMARKS

3/4 INCH TEARDROPS AT 8 INCH

SPACING L

1	8	15	22	29	36	43	50	57	64	71
OBS. NO.	TEMP.	NROTA	ROTA	P-IN	P-OUT	P-SCALE	RATIO			
	0.462	2.	14.4	0.95	0.	0.	1.000			
			19.8	2.1						
			21.0	3.0						
			24.6	3.45						
		4.	11.4	6.55						
			15.0	11.6						
			19.4	18.15						
			22.5	24.2						
			26.0	31.4						
			30.0	40.1						
			33.5	49.0						
			37.6	59.8						
			40.6	70.5						
			45.4	87.8						
			51.0	6.8		1.				
			54.6	7.7						
			61.5	9.2						L
1	8	15	22	29	36	43	50	57	64	71

Figure 53. Sample Raw Data Sheet for Pressure Drop Measurements.

The data processing will be illustrated with the fourth from the last data value on the sheet. The raw measurements were:

1. Thermocouple reading of inlet water temperature: 0.462 millivolts.

2. Rotameter number 4 reading: 45.4

3. Pressure drop: 87.8 inches purple fluid (sp. gr. 1.750).

Converting these to engineering units as previously described,

1. Inlet water temperature: 53.3 deg F

2. Flow Rate: 13.47 gpm

3. Pressure drop: 2.379 psi

The Reynolds number was calculated using

$$Re = \frac{4\ W}{\mu\ \pi\ D} \tag{21}$$

$$= \frac{4 \times (62.43/7.481) \times 60 \times gpm}{2.42 \times \mu \times 3.14159 \times (1.005/12)}$$

$$= \frac{3145.5\ gpm}{\mu} \tag{A-5}$$

For the specific example, Re = 34,131.

The friction factor was calculated using

$$f = \frac{g\ \pi^2 \rho\ \ D^5}{32\ W^2} \left[\frac{-\Delta P}{L_p}\right] \left[\frac{L_p}{n_p S}\right] - f_o \left[\frac{L_p}{n_p S} - 1\right] \tag{62}$$

$$f = \frac{2.9075\ (-\Delta P_{psi})}{(gpm)^2} \left[\frac{78.41}{n_p S}\right] - f_0 \left[\frac{78.41}{n_p S} - 1\right] \tag{A-6}$$

For this set of data, the friction factor for the empty tube was calculated using Nikuradse's equation

```
A-18          1-9-61          6.    8.
3/4 INCH DEARDROPS AT  8  INCH SPACING                              L
      .462    2.      14.4    0.95   0.001    0.001    1.0
                      19.8    2.1
                      21.0    3.0
                      24.6    3.45
              4.      11.4    6.55
                      15.0   11.6
                      19.4   18.15
                      22.5   24.2
                      26.0   31.4
                      30.0   40.1
                      33.5   49.0
                      37.6   59.8
                      40.6   70.5
                      45.4   87.8
                      51.0    6.8             1.
                      54.6    7.7
                      61.5    9.2                                   L
```

Figure 54. Listing of Data Cards for Pressure Drop Measurements of Sample Problem.

$$f_0 = \frac{1}{(1.73718 \ln(\sqrt{f_0}\, Re) - 0.40)^2} \qquad \text{(A-7)}$$

for Re = 34,131, f_0 = 0.00570 and the experimental friction factor for the above set of data is 0.05862. (Note: In the above formula f_0 was obtained by iterating until $(f_0)_{assumed}$ agreed with $(f_0)_{calculated}$ to three significant figures.)

The printed output from the computer containing the analysis of the pressure drop data just illustrated is shown in Figure 55. The particular data point which was illustrated is the point numbered 14 under the column headed OBSV. In addition to the Reynolds number and experimental friction factor, empirical estimates for the empty tube were calculated using various other approximations in addition to

ANALYSIS OF PRESSURE DROP DATA

RUN NUMBER A-18
DATA TAKEN 1-9-61
DATA PROCESSED 3-14-61

REMARKS

3/4 INCH TEARDROPS AT 8 INCH SPACING

PARTIALLY PROCESSED DATA

OBSV	TEMP (DEG F)	NROTA	ROTA	GPM	INLET P	OUTLET P	PRESSURE SCALE	DELTA P (PSIA*100)	VR
1	53.3	2	14.40	1.18	0.95	0.00	INCHES PURPLE	2.57	1.000
2	53.3	2	19.80	1.77	2.10	0.00	INCHES PURPLE	5.69	1.000
3	53.3	2	21.00	1.90	3.00	0.00	INCHES PURPLE	8.13	1.000
4	53.3	2	24.60	2.30	3.45	0.00	INCHES PURPLE	9.35	1.000
5	53.3	4	11.40	3.31	6.55	0.00	INCHES PURPLE	17.75	1.000
6	53.3	4	15.00	4.38	11.60	0.00	INCHES PURPLE	31.43	1.000
7	53.3	4	19.40	5.70	18.15	0.00	INCHES PURPLE	49.18	1.000
8	53.3	4	22.50	6.63	24.20	0.00	INCHES PURPLE	65.57	1.000
9	53.3	4	26.00	7.67	31.40	0.00	INCHES PURPLE	85.08	1.000
10	53.3	4	30.00	8.87	40.10	0.00	INCHES PURPLE	108.65	1.000
11	53.3	4	33.50	9.92	49.00	0.00	INCHES PURPLE	132.77	1.000
12	53.3	4	37.60	11.14	59.80	0.00	INCHES PURPLE	162.03	1.000
13	53.3	4	40.60	12.04	70.50	0.00	INCHES PURPLE	191.03	1.000
14	53.3	4	45.40	13.47	87.80	0.00	INCHES PURPLE	237.90	1.000
15	53.3	4	51.00	15.15	6.80	0.00	INCHES MERCURY	308.50	1.000
16	53.3	4	54.60	16.23	7.70	0.00	INCHES MERCURY	349.33	1.000
17	53.3	4	61.50	18.29	9.20	0.00	INCHES MERCURY	417.39	1.000

FRICTION FACTORS

OBSV	RE X 1000	F-EXPT X 100	F-BLAS X 100	F-DREW X 100	F-J X 100	F-MOODY X 100	F-NIK X 100	R-BLAS	R-DREW	R-J	R-MOODY	R-NIK
1	2.994	8.034	1.068	1.105	0.928	1.075	1.122	7.522	7.270	8.658	7.470	7.159
2	4.491	7.968	0.965	0.988	0.856	0.951	0.985	8.257	8.069	9.313	8.380	8.087
3	4.824	10.030	0.948	0.968	0.843	0.918	0.964	10.581	10.358	11.892	10.931	10.407
4	5.823	7.823	0.904	0.920	0.812	0.863	0.911	8.651	8.504	9.631	9.062	8.592
5	8.381	7.180	0.826	0.834	0.755	0.789	0.819	8.696	8.608	9.507	9.099	8.766
6	11.107	7.283	0.770	0.774	0.714	0.738	0.757	9.465	9.406	10.202	9.871	9.615
7	14.440	6.740	0.721	0.723	0.677	0.671	0.706	9.353	9.319	9.950	10.042	9.545
8	16.788	6.660	0.694	0.696	0.657	0.662	0.679	9.596	9.572	10.133	10.067	9.808
9	19.438	6.447	0.669	0.670	0.638	0.623	0.654	9.637	9.618	10.101	10.347	9.857
10	22.468	6.160	0.645	0.646	0.620	0.624	0.631	9.546	9.531	9.934	9.871	9.765
11	25.119	6.024	0.628	0.629	0.606	0.609	0.614	9.599	9.584	9.934	9.889	9.816
12	28.224	5.821	0.609	0.611	0.592	0.587	0.597	9.550	9.532	9.825	9.909	9.758
13	30.496	5.889	0.598	0.599	0.583	0.585	0.586	9.850	9.828	10.095	10.061	10.057
14	34.131	5.862	0.581	0.583	0.570	0.569	0.570	10.086	10.057	10.279	10.304	10.284
15	38.373	6.033	0.564	0.567	0.557	0.546	0.555	10.689	10.648	10.829	11.057	10.879
16	41.099	5.957	0.555	0.557	0.550	0.547	0.546	10.736	10.688	10.839	10.884	10.913
17	46.325	5.591	0.538	0.542	0.537	0.526	0.531	10.382	10.322	10.420	10.591	10.528

Figure 55. Computer Analysis of Pressure Drop Data for Sample Problem.

Nikuradse's. The friction factor calculated using the Blasius equation is labeled F-BLAS; the friction factor calculated using Colburn's j-factor equation is labeled F-J; the friction factor calculated using Nikuradse's equation is labeled F-NIK. Other estimates of the empty-tube friction factor are labeled F-DREW and F-MOODY.

The ratio of the friction factor obtained experimentally for each turbulence promoter combination to the friction factor for the empty tube using each of the empirical approximations was calculated and printed for each run.

Processing of Heat Transfer Data

The method of processing heat transfer data will be illustrated using a set of data for the same turbulence promoter combination (streamline shapes with d = 0.750 and s = 8) as was used to illustrate the method of processing the pressure drop data. The particular run, R-19-B, corresponds to only one flow rate.

The raw data sheet is shown in Figure 56. As in the case of the pressure drop data, each line on the data sheet corresponds to one IBM card. The first line contains the run number and date. The next few lines are for remarks; the last data card containing remarks has an "L" punched in column 71 to indicate that it is the last card containing remarks. The next set of cards (the last of which also has an "L" in column 71) are readings of rotameter number, rotameter reading, voltmeter scale, voltage, millivolts across 5000 amp shunt, ambient thermocouple reading, inlet water thermocouple

DATA SHEET FOR HEAT TRANSFER MEASUREMENTS

RUN NUMBER	DATE		
R-19-B	1-9-61		
1	15	29	

REMARKS	
3/4 INCH TEAR DROPS AT 8 INCH	
SPACING. PSCALE = PURPLE	L

NROTA	ROTA	VM	VOLTS	AMPSMV	EAMB	EIN	EOUT	PIN	POUT	
4.	42.4	2.	9.2	21.83	1.050	0.300	0.552	73.5	0.	
	42.4		9.23	21.81		0.300	0.556	73.6		L
1	8	15	22	29	36	43	50	57	64	71

REF TC 19.	20.	12.								
REF EMF 1.40	2.20	1.675								L
1	8	15	22	29	36	43	50	57	64	71

1R 0.559	2R 0.691	3R 0.717	4R 0.111	5R 0.567	6R 0.192	7R 0.609	8R 0.242	9R 0.658	10R 0.250	
11R 0.661	12R 0.319	13R 0.710	14R 0.360	15R 0.718	16R 0.815	17R 0.390	18R 0.154	19R 0.020	20R 0.860	
9L 0.424	10L 0.260	11L 0.626	12L 0.305	13L 0.165	14L 0.578	15L 0.605	16L 0.528	17L 0.394	18L 0.158	
19L 0.245	20L 0.638									
1R 0.558	2R 0.689	3R 0.718	4R 0.118	5R 0.568	6R 0.195	7R 0.611	8R 0.240	9R 0.655	10R 0.250	
11R 0.661	12R 0.318	13R 0.708	14R 0.360	15R 0.720	16R 0.815	17R 0.395	18R 0.155	19R 0.014	20R 0.861	
9L 0.422	10L 0.259	11L 0.630	12L 0.308	13L 0.170	14L 0.579	15L 0.605	16L 0.527	17L 0.395	18L 0.155	
19L 0.248	20L 0.640									
1R 0.560	2R 0.690	3R 0.720	4R 0.118	5R 0.561	6R 0.200	7R 0.612	8R 0.241	9R 0.660	10R 0.248	
11R 0.660	12R 0.321	13R 0.710	14R 0.361	15R 0.715	16R 0.815	17R 0.397	18R 0.155	19R 0.015	20R 0.861	
9L 0.425	10L 0.261	11L 0.627	12L 0.309	13L 0.169	14L 0.578	15L 0.609	16L 0.526	17L 0.395	18L 0.156	
19L 0.249	20L 0.641									
1R 0.561	2R 0.690	3R 0.720	4R 0.114	5R 0.565	6R 0.190	7R 0.608	8R 0.245	9R 0.659	10R 0.250	
11R 0.664	12R 0.308	13R 0.710	14R 0.360	15R 0.719	16R 0.815	17R 0.392	18R 0.155	19R 0.021	20R 0.861	
9L 0.425	10L 0.260	11L 0.629	12L 0.306	13L 0.170	14L 0.579	15L 0.606	16L 0.526	17L 0.396	18L 0.158	
19L 0.249	20L 0.642									L
1	8	15	22	29	36	43	50	57	64	71

Figure 56. Raw Data Sheet for Heat Transfer Measurements.

reading, outlet water thermocouple reading, inlet water pressure, and outlet water pressure. The next line contains the identification numbers of reference thermocouples (used in converting AZAR readings to emfs as will be described) followed on the following line by reference thermocouple emfs.

The remaining 16 lines (or cards) on the data sheet are for readings taken from the chart of the AZAR recorder. Four complete sets of 32 AZAR readings are used for each experimental run. A listing of the punched cards of this run is shown in Figure 57. The printed computer output (requiring four pages) which is the complete analysis of this set of data is shown in Figure 58 for pages I, II, III, and IV.

The first step by the computer program consists of reading the data. Where there are more than one set of values for one item of data, the average and standard deviation of each were calculated. Values of the input data corresponding to all of the raw observations were printed on page I of the computer analysis along with the mean values and standard deviation for each particular item. A quick visual check of the standard deviations of each item served to eliminate errors in punching cards. Each of the AZAR readings was converted to thermocouple emf and identified with its longitudinal and angular position on the tube. The conversion to emf was made using the following formulas.

$$\text{RANGE} = \frac{\text{EMF2} - \text{EMF1}}{\text{AZAR2} - \text{AZAR1}} \tag{A-8}$$

$$\text{ZERO} = \text{AZAR1} - \text{EMF1}/\text{RANGE} \tag{A-9}$$

$$\text{emf}_i = \text{RANGE}\ (\text{azar}_i - \text{ZERO}) \tag{A-10}$$

```
R-19-B          1-9-61
3/4 INCH TEARDROPS AT  8 INCH SPACING.  PACALE = PURPLE                     L
4.       42.4    2.      9.2     21.83   1.05     .300    .552    73.5    0.
         42.4            9.23    21.81            .300    .556    73.6          L
19.      20.     12.
1.40     2.20    1.675                                                          L
 0.559   0.691   0.717   0.111   0.567   0.192   0.609   0.242   0.658   0.250
 0.661   0.319   0.710   0.360   0.718   0.815   0.390   0.154   0.020   0.860
 0.424   0.260   0.626   0.305   0.165   0.578   0.605   0.528   0.394   0.158
 0.245   0.638
 0.558   0.689   0.718   0.118   0.568   0.195   0.611   0.240   0.655   0.250
 0.661   0.318   0.708   0.360   0.720   0.815   0.395   0.155   0.014   0.861
 0.422   0.259   0.630   0.308   0.170   0.579   0.605   0.527   0.395   0.155
 0.248   0.640
 0.560   0.690   0.720   0.118   0.561   0.200   0.612   0.241   0.660   0.248
 0.660   0.321   0.710   0.361   0.715   0.815   0.397   0.155   0.015   0.861
 0.425   0.261   0.627   0.309   0.169   0.578   0.609   0.526   0.395   0.156
 0.249   0.641
 0.561   0.690   0.720   0.114   0.565   0.190   0.608   0.245   0.659   0.250
 0.664   0.308   0.710   0.360   0.719   0.815   0.392   0.155   0.021   0.861
 0.425   0.260   0.629   0.306   0.170   0.579   0.606   0.526   0.396   0.158
 0.249   0.642                                                                  L
```

Figure 57. Listing of Data Cards for Heat Transfer Measurements of Sample Problem.

ANALYSIS OF HEAT TRANSFER DATA

PAGE I

RUN NUMBER R-19-B
DATA TAKEN 1-9-61
DATA PROCCESSED 1-20-61

REMARKS

3/4 INCH TEARDROPS AT 8 INCH SPACING. PACALE = PURPLE

DATA OTHER THAN RECORDER THERMOCOUPLE READINGS

	NROTA	ROTA	VM	VOLTS	AMPS/100	EAMB	EIN	EOUT	INLET P	OUTLET P
	4.	42.400	2.	9.200	21.830	1.050	0.300	0.552	73.500	0.000
	0.	42.400	0.	9.230	21.810	0.000	0.300	0.556	73.600	0.000
MEAN VALUE	4.	42.400	2.	9.215	21.820	1.050	0.300	0.554	73.550	0.000
STANDARD DEVIATION	0.	0.000	0.	0.015	0.010	0.000	0.000	0.002	0.051	0.000

CALIBRATION READINGS FOR RECORDER THERMOCOUPLES

TC NUMBER	19	20	12
	1.400	2.200	1.675
MEAN VALUE	1.400	2.200	1.675
STD. DEV.	0.000	0.000	0.000

THERMOCOUPLE READINGS, MEAN VALUES, AND STANDARD DEVIATIONS

1R	2R	3R	4R	5R	6R	7R	8R	9R	20L	19L	18L	10R	17L	16L	15L	11R	12R	13R	14R
0.559	0.691	0.717	0.111	0.567	0.192	0.609	0.242	0.658	0.638	0.245	0.158	0.250	0.394	0.528	0.605	0.661	0.319	0.710	0.360
0.558	0.689	0.716	0.118	0.568	0.195	0.611	0.240	0.655	0.640	0.248	0.155	0.250	0.395	0.527	0.605	0.661	0.318	0.708	0.360
0.560	0.690	0.720	0.118	0.561	0.200	0.612	0.241	0.660	0.641	0.249	0.156	0.248	0.395	0.526	0.609	0.660	0.321	0.710	0.361
0.561	0.690	0.720	0.114	0.565	0.190	0.608	0.245	0.659	0.642	0.249	0.158	0.250	0.396	0.526	0.606	0.664	0.308	0.710	0.360
0.559	0.690	0.719	0.115	0.565	0.194	0.610	0.242	0.658	0.640	0.248	0.157	0.249	0.395	0.527	0.606	0.661	0.316	0.709	0.360
0.001	0.001	0.001	0.003	0.003	0.004	0.002	0.002	0.002	0.001	0.002	0.001	0.001	0.001	0.001	0.002	0.002	0.005	0.001	0.000

THERMOCOUPLE READINGS, MEAN VALUES, AND STANDARD DEVIATIONS (CONTINUED)

15R	16R	14L	13L	12L	11L	10L	9L	17R	18R	19R	20R
0.718	0.815	0.578	0.165	0.305	0.626	0.260	0.424	0.390	0.154	0.020	0.860
0.720	0.815	0.579	0.170	0.308	0.630	0.259	0.422	0.395	0.155	0.014	0.861
0.715	0.815	0.578	0.169	0.309	0.627	0.261	0.425	0.397	0.155	0.015	0.861
0.719	0.815	0.579	0.170	0.306	0.629	0.260	0.425	0.392	0.155	0.021	0.861
0.718	0.815	0.578	0.168	0.307	0.628	0.260	0.424	0.393	0.155	0.017	0.861
0.002	0.000	0.000	0.002	0.002	0.002	0.001	0.001	0.003	0.000	0.003	0.000

RAW DATA FOR RUN R-19-B

PAGE II

ROTAMETER 4 READING = 42.40
VOLTMETER READING = 9.21 (METER SCALE = 2)
INLET WATER THERMOCOUPLE = 0.300 MILLIVOLTS
OUTLET WATER THERMOCOUPLE = 0.554 MILLIVOLTS
AMBIENT AIR THERMOCOUPLE = 1.050 MILLIVOLTS
MILLIVOLTS ACROSS 5000 AMP SHUNT = 21.820

THERMOCOUPLE NUMBER	POSITION (DIAMETERS)	EMF (MILLIVOLTS)	WEIGHT FACTOR
1R	1.49	1.914	0.0539
2R	5.41	2.038	0.0619
3R	9.42	2.065	0.0624
4R	13.40	1.493	0.0624
5R	17.41	1.920	0.0685
6R	22.17	1.568	0.0619
7R	25.34	1.962	0.0558
8R	29.32	1.613	0.0622
9R	33.30	2.008	0.0389
20L	34.30	1.991	0.0156
19L	35.30	1.618	0.0155
18L	36.29	1.532	0.0155
10R	37.28	1.620	0.0155
17L	38.28	1.758	0.0156
16L	39.28	1.883	0.0156
15L	40.28	1.959	0.0150
11R	41.20	2.011	0.0390
12R	45.27	1.684	0.0626
13R	49.22	2.057	0.0624
14R	53.26	1.725	0.0629
15R	57.28	2.065	0.0719
16R	62.47	2.157	0.0647
14L	34.30	1.932	0.0000
13L	36.29	1.543	0.0000
12L	38.28	1.675	0.0000
11L	34.30	1.979	0.0000
10L	36.29	1.630	0.0000
9L	38.28	1.786	0.0000
17R	0.00	1.757	0.0000
18R	0.00	1.530	0.0000
19R	0.00	1.400	0.0000
20R	0.00	2.200	0.0000

INLET PRESSURE = 73.550 INCHES OF KING PURPLE FLUID
OUTLET PRESSURE = 0.000 INCHES OF KING PURPLE FLUID

Figure 58. Computer Analysis of Heat Transfer Data for Sample Problem, Pages I, II, III, and IV.

SUMMARY OF PROCESSED DATA FOR RUN R-19-B

PAGE III

FLOW RATE = 12.58 GPM
INLET WATER TEMPERATURE = 45.89 DEGREES F.
OUTLET WATER TEMPERATURE = 57.49 DEGREES F.
AMBIENT AIR TEMPERATURE = 79.69 DEGREES F.
ELECTRIC CURRENT = 2182.0 AMPS
OVERALL VOLTAGE DROP = 9.31 VOLTS

CHANNEL	POSITION (DIAMETERS)	ANGULAR POSITION (DEGREES)	DISTANCE TO PROMOTER	DISTANCE FROM PROMOTER	DELTA T (DEG. F)	H (BTU/HR-DEG-SQ FT)	RE/1000	THEORETICAL H (SAME AS H)	H/HTH
1R	1.49	0.0	9.20	0.00	43.5	1155.3	28.433	948.5	1.184
2R	5.41	0.0	5.28	0.00	48.0	1050.4	28.767	960.4	1.076
3R	9.42	0.0	1.27	0.00	48.4	1042.1	29.110	966.2	1.068
4R	13.40	0.0	5.25	2.71	24.2	2053.0	29.452	932.9	2.103
5R	17.41	0.0	1.24	6.72	40.8	1230.5	29.798	965.1	1.261
6R	22.17	0.0	4.44	3.52	25.3	1967.8	30.211	946.1	2.016
7R	25.34	0.0	1.27	6.69	41.2	1221.4	30.487	975.9	1.251
8R	29.32	0.0	5.25	2.71	25.7	1942.4	30.835	956.0	1.990
9R	33.30	0.0	1.27	6.69	41.7	1208.9	31.184	986.9	1.239
20L	34.30	0.0	0.27	7.69	40.8	1234.7	31.273	986.8	1.265
19L	35.30	0.0	7.23	0.73	24.8	2009.1	31.361	962.2	2.058
18L	36.29	0.0	6.24	1.72	21.6	2309.9	31.448	957.9	2.367
10R	37.28	0.0	5.25	2.71	24.5	2032.7	31.536	964.3	2.083
17L	38.28	0.0	4.25	3.71	30.2	1655.3	31.624	975.1	1.696
16L	39.28	0.0	3.25	4.71	35.3	1420.7	31.712	984.7	1.456
15L	40.28	0.0	2.25	5.71	38.3	1312.2	31.801	990.7	1.344
11R	41.20	0.0	1.33	6.63	40.4	1247.7	31.883	995.1	1.278
12R	45.27	0.0	5.22	2.74	25.8	1935.8	32.245	976.7	1.983
13R	49.22	0.0	1.27	6.69	40.8	1235.2	32.598	1006.1	1.265
14R	53.26	0.0	0.00	2.77	26.1	1914.2	32.960	987.5	1.961
15R	57.28	0.0	0.00	6.79	39.7	1270.3	33.322	1014.7	1.302
16R	62.47	0.0	0.00	11.98	42.6	1186.5	33.792	1025.8	1.216
14L	34.30	120.0	0.27	7.69	38.3	1312.2	31.273	982.9	1.344
13L	36.29	120.0	6.24	1.72	21.9	2270.6	31.448	958.6	2.326
12L	38.28	120.0	4.25	3.71	26.7	1871.5	31.624	969.2	1.917
11L	34.30	240.0	0.27	7.69	40.3	1249.3	31.273	986.0	1.280
10L	36.29	240.0	6.24	1.72	25.1	1984.3	31.448	964.0	2.033
9L	38.28	240.0	4.25	3.71	31.4	1594.9	31.624	977.0	1.634
MEAN VALUES						1483.8	31.087	976.1	

INTEGRATED LOCAL HEAT INPUT = 70.796 MM BTU/HR
OVERALL HEAT INPUT = 69.328 MM BTU/HR
HEAT REMOVED BY WATER = 73.012 MM BTU/HR

HEAT LOSS ON BASIS OF INTEGRATED LOCAL INPUT = -2.216 MM BTU/HR
PER CENT LOSS = -3.04

HEAT LOSS ON BASIS OF OVERALL INPUT = -3.684 MM BTU/HR
PER CENT LOSS = -5.05

MEAN VR TO THE .14 = 1.0699 MEAN PR TO THE 1/3 = 2.0683 MEAN PHYSICAL PROPERTIES FACTOR = 9.2154

PAGE IV

ADDITIONAL PROCESSED DATA FOR RUN R-19-B

CHANNEL	Q/F (MMBTU/HR)	T(A) (DEG. F)	T(B) (DEG. F	WATER TEMP. (DEG. F)
1R	50.240	89.7	116.9	46.2
2R	50.392	94.8	122.2	46.9
3R	50.425	96.0	123.3	47.6
4R	49.743	72.6	99.8	48.3
5R	50.247	89.9	117.2	49.0
6R	49.820	75.2	102.5	49.9
7R	50.299	91.7	119.0	50.5
8R	49.869	76.9	104.1	51.2
9R	50.355	93.6	120.9	51.9
20L	50.334	92.9	120.2	52.1
19L	49.875	77.1	104.4	52.3
18L	49.785	74.0	101.3	52.5
10R	49.877	77.2	104.4	52.6
17L	50.049	83.1	110.3	52.8
16L	50.202	88.3	115.6	53.0
15L	50.295	91.5	118.8	53.2
11R	50.359	93.7	121.0	53.4
12R	49.957	79.9	107.2	54.1
13R	50.414	95.6	122.9	54.8
14R	50.008	81.7	108.9	55.5
15R	50.424	96.0	123.3	56.3
16R	50.536	99.8	127.1	57.2
14L	50.262	90.4	117.7	52.1
13L	49.796	74.4	101.7	52.5
12L	49.945	79.5	106.8	52.8
11L	50.320	92.4	119.7	52.1
10L	49.890	77.6	104.9	52.5
9L	50.083	84.2	111.5	52.8
MEAN VALUES	50.185	87.7	115.0	51.7

Figure 58. (Continued)

where $EMF2$ = upper reference emf

$AZAR2$ = AZAR reading for channel recording upper reference emf

$EMF1$ = lower reference emf

$AZAR1$ = AZAR reading for channel recording lower reference emf

$azar_i$ = arbitary AZAR reading to be converted to emf

emf_i = emf corresponding to $azar_i$

For example, in the data of Run R-19-B

$$RANGE = \frac{2.200 - 1.400}{0.861 - 0.017} = 0.9478 \text{ millivolts}$$

$$ZERO = 0.017 - 1.400/0.9478 = -1.460$$

Thus, for channel 9R, for example, where the mean value of the four AZAR readings is 0.658 the emf is given by

$$emf = 0.9478 \cdot (0.658 + 1.460)$$

$$= 2.008 \text{ millivolts}$$

All of the mean values of each item of raw data were printed on Page II of the computer analysis. The raw data were converted into engineering units and presented on Pages III and IV. At each axial and angular position on the tube the following items are presented on Page III of the analysis.

III-1. Channel number

III-2. Distance from beginning of heating

III-3. Angular position on the tube

III-4. Distance to downstream promoter (tube diameters)

III-5. Distance from upstream promoter (tube diameters)

III-6. Wall temperature - fluid temperature (deg F)

III-7. $h(z)$, local experimental heat transfer coefficient (BTU/hr-deg F-ft^2)

III-8. Re_z, local Reynolds number calculated using local fluid temperature

III-9. Empirical estimate of h calculated using Sieder-Tate equation based on local values of the physical properties (BTU/hr-deg F-ft^2)

III-10. $h(z)/h_0$ where $h(z)$ is given by item III-7 and h_0 is the overall integrated value of III-8.

On Page IV of the computer analysis the following items are presented.

IV-1. Channel number

IV-2. Local rate of heat flux (BTU/hr-ft^2), i.e., $q(z)$

IV-3. Inside wall temperature (deg F)

IV-4. Outside wall temperature (deg F)

IV-5. Water temperature (deg F)

Mean values of III- , III-8, III-9, IV-2, IV-3, IV-4, and IV-5 were obtained by multiplying each local value by the fraction of the total tube length it represents (listed on Page II of the computer analysis as WEIGHT FACTOR) and summing. In addition, local values of (μ/μ_w) and Pr were integrated in this manner to obtain mean values.

The overall heat input is obtained by

$$Q_{in} = 2\pi \int_0^L q(Z)\, dZ \tag{70}$$

The heat removed by the water was obtained by

$$Q_{out} = W\, c\, (T_{outlet} - T_{inlet}) \tag{71}$$

and, thus, the heat losses were calculated.

The application of Equations (54), (56), (58), and (45) to calculate $T_{wall}(z)$, $q(z)$, $T_f(z)$, and $h(z)$ can best be illustrated by an example. Consider the data for channel 9R. This thermocouple is located 33.30 tube diameters from the beginning of heating; it is at the 0 degree angular position (i.e., where the large majority of the thermocouples were located). This thermocouple is located 1.27 diameters upstream from one promoter and 6.69 diameters downstream from another promoter. The outside tube temperature which was measured was 120.9 deg F.

According to Equation (54) the inside tube temperature is given by an equation of the form

$$T_{wall}(z) = T_b(z) - A_2(\phi\ I^2) - \frac{A_3(\phi\ I^2)^2}{(1 + \gamma T_b)(1 + \beta T_b)} \qquad \text{(A-11)}$$

And, according to Equation (56) the local rate of heat flux is given by an equation of the form

$$q(z) = A_4(1 + \gamma T_b)\ I^2 \qquad \text{(A-12)}$$

where

$$A_2 = \frac{3.41276\ \bar{\rho}_0}{2\pi^2\ (b^2 - a^2)^2\ K_0} \left[b^2 \ln \frac{b}{a} - \frac{(b^2 - a^2)}{2}\right] \qquad \text{(A-13)}$$

$$A_3 = \left[\frac{3.41276\ \bar{\rho}_0}{2\pi^2\ (b^2 - a^2)^2\ K_0}\right]^2 \frac{(3\beta + \gamma)}{6}\ (b - a)^4 \qquad \text{(A-14)}$$

$$A_4 = \frac{3.41276\ \bar{\rho}_0}{2\pi^2\ (b^2 - a^2)\ a} \qquad \text{(A-15)}$$

and

$$\phi = \frac{1 + \gamma T_b}{1 + \beta T_b} \qquad \text{(A-16)}$$

The electrical resistivity data $\bar{\rho}_o$ and γ for type 304 stainless steel were obtained from the Allegheny Ludlum Steel Corporation[1]. Thermal conductivity data K_0 and β were obtained from Shelton[37].

The values of the parameters in the above constants are

$$a = 0.5025 \text{ inches}$$

$$b = 0.624 \text{ inches}$$

$$\bar{\rho}_o = 2.265 \times 10^{-6} \text{ ohm-ft}$$

$$K_0 = 8.5 \text{ BTU/hr-deg F-ft}$$

$$\gamma = 0.00062 \text{ (deg F)}^{-1}$$

$$\beta = 0.000517 \text{ (deg F)}^{-1}$$

From which the numerical values of the constants are

$$A_2 = 5.6259 \times 10^{-6} \text{ (deg F)/amps}^2$$

$$A_3 = 9.8891 \times 10^{-15} \text{ (deg F)/amps}^4$$

$$A_4 = 9.8389 \times 10^{-4} \text{ BTU/hr-ft}^2\text{-amps}^2$$

For the inside wall temperature of 120.9 deg F

$$\phi = \frac{1 + 0.00062 \times 120.9}{1 + 0.000517 \times 120.9}$$

$$= 1.0117$$

Since the electric current was 2182 amps, then

$$\phi I^2 = 4.8176 \times 10^6 \text{ amps}^2 .$$

and

$$T_{wall} = 120.9 - (5.6259)(4.8178) - \frac{(9.8891 \times 10^{-15})(4.8178 \times 10^{6})^2}{(1.0625)(1.0749)}$$

$$= 120.9 - 27.10 - 0.20$$

$$= 93.6 \text{ deg F}$$

$$q(z) = (9.8398 \times 10^{-3})(2.0749)(2.182 \times 10^{3})^2$$

$$= 50{,}355 \text{ BTU/hr-ft}^2$$

$$T_f = 45.89 + \frac{33.30}{64.02}(57.49 - 45.89)$$

$$= 51.9 \text{ deg F}$$

$$h(z) = \frac{50{,}3555}{93.6 - 51.9}$$

$$= 1208.9 \text{ BTU/hr-deg F-ft}^2$$

The mean value h_m/h_0 of the ratio of the local heat transfer coefficient to the overall value for the empty tube $h(z)/h_0$ was obtained by fitting a polynomial to the local values as a function of the distance (in tube diameters) downstream from the nearest promoter. For this purpose, values downstream from the first and last promoter were not considered. The following are those which were used for the data of run R-19-B.

Diameter from Beginning of heating, z	Distance from Nearest Promoter, x	$h(z)/h_0$
22.17	3.52	2.016
25.34	6.69	1.251
29.32	2.71	1.999
33.30	6.69	1.239
34.30	7.69	1.265
35.30	0.73	2.058
36.29	1.72	2.367
37.28	2.71	2.083
38.38	3.71	1.696
39.28	4.71	1.456
40.28	5.71	1.344
41.20	6.63	1.278
45.27	2.74	1.983
49.22	6.69	1.265

The polynomials which were fitted were of the form

$$h(x)/h_0 = a_0 + a_1 x + a_2 x^2 + a_3 x^3 \qquad \text{(A-17)}$$

where the coefficients were obtained by the method of least squares. Values of the coefficients for a first, second, and third order polynomial and the above data are shown below with the integrated mean heat transfer coefficient for each case.

Order	a_0	a_1	a_2	a_3	h_m/h_0
1	2.433	-0.1719			1.745
2	2.414	-0.1605	-0.001311		1.744
3	1.935	0.3824	-0.1594	0.1292	1.718

The value $h_m/h_0 = 1.745$ is the value which was used.

APPENDIX B

DERIVATIONS

Derivation of the Conduction Equation

The solution of the conduction equation subject to the correct boundary conditions is essential to the successful measurement of local heat transfer coefficients by the experimental technique used in this investigation. Because of the importance of this equation, it will be derived in this section; the effect of the various simplifying assumptions made in the solution will be shown to be negligible.

A diagram of the longitudinal cross-section of the tube wall, insulated at the outside, is shown below to illustrate the nomenclature. Heat generation is in the shaded area. In this analysis the longitudinal distance from the center of the heated section will be denoted by the symbol y. Thus, the heating section begins at $y = -L/2$ and extends to $y = +L/2$. The inside radius is a; the outside radius is b.

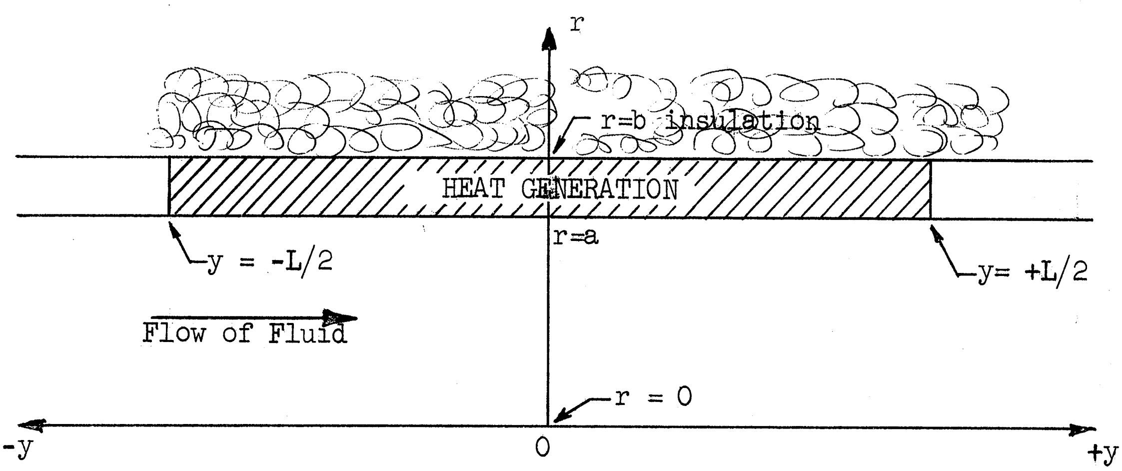

When an electric current passes through the tube wall, heat is generated. This causes a temperature gradient to be developed so that the heat will flow to the inside wall.

The differential equation (i.e., the conduction equation) which describes this process is well known and can be derived as follows. An annular element of the tube bounded by cylindrical surfaces at radius r and $r + dr$ and bounded by planes perpendicular to the axis at y and $y + dy$ is considered as shown below.

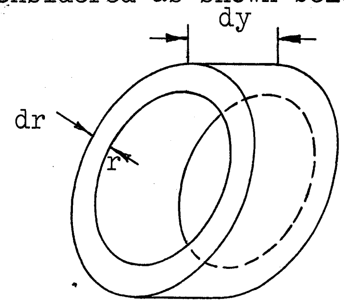

Expressions for the heat entering and leaving the element across each plane can be written as

<u>Input at r</u> $\quad -K(2\pi\ r\ dy)\ \frac{\partial T}{\partial r}$ (B-1a)

<u>Output at r + dr</u> $\quad -K(2\pi\ r\ dy)\ \frac{\partial T}{\partial r} - \frac{\partial}{\partial r}\ [K\ (2\pi\ r\ dy)\ \frac{\partial T}{\partial r}]\ dr$ (B-1b)

<u>Input at y</u> $\quad -K(2\pi\ r\ dr)\ \frac{\partial T}{\partial y}$ (B-1c)

<u>Output at y + dy</u> $\quad -K(2\pi\ r\ dr)\ \frac{\partial T}{\partial y} - \frac{\partial}{\partial y}\ [K\ (2\pi\ r\ dr)\ \frac{\partial T}{\partial y}]\ dy$ (B-1d)

These expressions are then substituted into the formula

$$\text{Input} + \text{Generation} - \text{Output} = 0 \qquad \text{(B-2)}$$

which is simply the first law of thermodynamics for a steady-state system. The resulting differential equation is

$$\frac{1}{r}\frac{\partial}{\partial r}\left[r\,K\frac{\partial T}{\partial r}\right] + \frac{\partial}{\partial y}\left[K\frac{\partial T}{\partial y}\right] + A = 0 \qquad (46)$$

where T = temperature (deg F)

r = radius (ft)

y = longitudinal distance from center of heated section (ft)

A = rate of heat generation per unit volume of tube wall (BTU/hr-ft^3)

K = thermal conductivity of the tube wall (BTU/hr-deg F-ft).

The next step is to derive an expression for the rate of heat generation A in terms of the electric current and the physical properties of the tube. The rate of heat generation per unit volume dV of the tube wall is given by

$$A = \frac{3.41276\,(dI)^2\,R}{dV} \qquad (B\text{-}3)$$

where dI = electric current passing through the infinitesimal volume dV (amps)

R = electrical resistance of the volume (ohms).

However, the volume of any annular segment of the tube of length dy is

$$dV = 2\pi\, r\, dr\, dy \qquad (B\text{-}4)$$

The current flowing through the element is

$$dI = 2\pi\, r\, J(r)\, dr \qquad (B\text{-}5)$$

where $J(r)$ = current density at r (amps/ft^2).

The electrical resistance of the element is

$$R = \frac{\bar{\rho}\, dy}{2\pi\, r\, dr} \tag{B-6}$$

where $\bar{\rho}$ = electrical resistivity (ohm-ft). The resistivity can usually be expressed as a linear function of temperature so that

$$\bar{\rho} = \bar{\rho}_o(1 + \gamma T) \tag{48}$$

with $\gamma \ll 1$.

Substituting the above expressions into Equation (B-3) the following is obtained.

$$A = 3.41276\, J^2(r)\, \bar{\rho}_o\, (1 + \gamma T) \tag{B-7}$$

By assuming that the voltage gradient dE/dy is independent of radius, then

$$J(r) = \frac{dE/dy}{\bar{\rho}_o\, (1 + \gamma T)} \tag{B-8}$$

$$= \frac{I\, \bar{\rho}_m}{\bar{\rho}_o\, (1 + \gamma T)\, \pi\, (b^2 - a^2)} \tag{B-9}$$

where $\bar{\rho}_m$ is an average value of the resistivity determined using the condition

$$I = 2\pi \int_a^b r\, J(r)\, dr \tag{B-10}$$

$$I = \int_a^b \frac{I\, \bar{\rho}_m\, 2\pi\, r\, dr}{\bar{\rho}_o\, (1 + \gamma T)\, \pi\, (b^2 - a^2)} \tag{B-11}$$

Thus, $$I = \frac{2\,I\,\bar{\rho}_m}{\bar{\rho}_o\,(b^2 - a^2)} \int_a^b \frac{r\,dr}{1 + \gamma T(r)} \qquad \text{(B-12)}$$

or $$\bar{\rho}_m = \frac{\bar{\rho}_o\,(b^2 - a^2)}{2\int_a^b \frac{r\,dr}{1 + \gamma T(r)}} \qquad (49)$$

and $$A = \frac{3.41276\,I^2\,\bar{\rho}_m^{\,2}}{\bar{\rho}_o\,(1 + \gamma T)\,\pi^2\,(b^2 - a^2)^2} \qquad (47)$$

Equation (46) and the expressions defined by (47) and (49) represent a complete derivation of the conduction equation for heat generation in an infinite hollow cylinder. This is a non-linear partial differential equation. The boundary condition at the two cylindrical surfaces $r = a$ and $r = b$ are

$\frac{\partial T}{\partial r}(b,y) = 0$	insulated surface	(B-13)
$T\,(a,y) = g(y)$	arbitrary function of y depending upon the inside heat transfer coefficient	(B-14)

The boundary conditions at any given pair of planes perpendicular to the axis of the tube (which are necessary in order to completely specify the problem) are more complicated since, in reality, the hollow cylinder is not infinite, but is composed of a finite length section in which heat is generated. This section is bounded on each end by a section in which no heat is generated and into which there will be some conduction of heat. However, the problem may be treated in the following manner:

1. Assume that axial conduction may be neglected except within a certain, short distance from each end of the section of the tube in which heat is generated. (This implies that $\partial T/\partial y$ is constant.)

2. Show that with the assumption of step 1 the problem is reduced to that of solving a non-linear, ordinary differential equation. Solve this equation and show that the effect of variation of physical properties of the tube wall with temperature is small, although computable. (This is done in Part 2 of this appendix.)

3. Since the non-linear nature of the differential equation can be shown to be of second-order importance, solve the linear form of the partial differential equation which allows for heat conduction into the non-heat-generating portion of the tube and show that, indeed, axial conduction into this portion of the tube can be neglected within one tube diameter from each end of the heated section. (This is done in Part 3 of this appendix.)

4. Solve the linear form of the differential equation for an infinite hollow cylinder with an arbitrary temperature distribution at the inside wall. Thus, determine the effect of axial conduction caused by a fluctuating inside wall temperature distribution and show that this effect is negligible. (This is done in Part 4 of this appendix.)

Effect of Temperature Dependence of Physical Properties of the Tube

Assume that the thermal conductivity and electrical resistivity of the stainless steel tube are linear functions of temperature so that

$$K = K_0\,(1 + \beta T) \tag{50}$$

and $$\bar{\rho} = \bar{\rho}_o (1 + \gamma T) \tag{48}$$

In order to make Equation (46) solvable, neglect axial conduction ($\partial T/\partial y$ = constant) so that the equation becomes an ordinary, but non-linear differential equation.

$$\frac{d^2T}{dr^2} + \frac{1}{r}\frac{dT}{dr} + \frac{\beta}{(1 + \beta T)}\left[\frac{dT}{dr}\right]^2 + \frac{3.41276\, I^2\, \bar{\rho}_m^2}{K_0\bar{\rho}_o\,(1 + \gamma T)(1 + \beta T)\pi^2(b^2 - a^2)^2} = 0 \tag{51}$$

with the boundary conditions

$$\frac{dT}{dr}(b) = 0 \tag{52a}$$

$$T(a) = T(a) \tag{52b}$$

simplify by letting

$$A_0 = \frac{3.41276\, I^2\, \bar{\rho}_m^2}{\bar{\rho}_o\, \pi^2(b^2 - a^2)^2} \tag{53}$$

and the solution as suggested by Clark[8] is

$$T(b) - T(a) = \frac{A_0}{2\,K_b}\left[b^2 \ln\left(\frac{b}{a}\right) - \frac{(b^2 - a^2)}{2}\right] + \left[\frac{A_0}{2\,K_b}\right]^2\left[\frac{3\beta + \gamma + 4\gamma\beta\, T_b}{6\,(1 + \gamma T_b)(1 + \beta T_b)}\right](b-a)^4 \tag{54}$$

where the subscript b indicates that the quantity is evaluated at a temperature T(b). Notice that the first part of the solution is simply the solution to the linear form of the differential equation, while the last part is a "correction" to take care of the effect of the temperature dependence of K and $\bar{\rho}$.

The temperature difference T(b) - T(a) caused by the generation of heat in the tube wall is referred to as $\Delta T_{generation}$.

As was shown in Appendix A for the particular dimensions and physical properties of the tube used in the experimental portion of this investigation, Equation (54) is of the following form.

$$T(b) - T(a) = 5.6259\left[\frac{\phi\ I}{1000}\right]^2 + 9.8891 \times 10^{-3}\left[\frac{\phi\ I}{1000}\right]^4 (1 + \gamma T_b)(1 + \beta T_b) \qquad \text{(B-15)}$$

where

$$\phi = \frac{1 + \gamma T_b}{1 + \beta T_b} \qquad \text{(A-16)}$$

Since, for $T_b < 250$ deg F

$$1.0 \leq (1 + \gamma T_b) < 1.20$$

$$1.0 \leq (1 + \beta T_b) < 1.20$$

$$1.0 \leq \phi \leq 1.03$$

The ratio of the "correction term" to the non-corrected temperature difference is approximately

$$\frac{\text{Temperature Dependence Correction}}{\text{Total Temperature Difference}} \cong \frac{9.8891}{5.6259} \times 10^{-3} \left[\frac{I}{1000}\right]^2$$

$$\cong 1.75 \times 10^{-3} \left[\frac{I}{1000}\right]^2$$

Thus, at the maximum value of electric current (I = 3000 amps) the correction is approximately 1.5 per cent. This correction was made in calculation of all inside wall temperatures from the measurements of the outside wall temperatures. However, the effect seems small enough so that any conclusions (for example, on the importance of axial conduction) made on the basis of solutions to the linear partial differential equations should be valid.

Effect of Axial Conduction into the Non-Heat-Generating Portion of the Tube

Axial conduction can arise in one of two ways: 1) through conduction into the non-heat-generating portion of the tube; and 2) through presence of a nonconstant axial temperature gradient at the inside wall. In this section of the appendix the first way will be considered; in Part 3 of this appendix the second way will be considered.

For this analysis consider the linear form of Equation (46).

$$\frac{\partial^2 T}{\partial r^2} + \frac{1}{r}\frac{\partial T}{\partial r} + \frac{\partial^2 T}{\partial y^2} + \frac{A}{K} = 0 \qquad \text{(B-16)}$$

A solution to this equation is required for a hollow cylinder of inside radius a and outside radius b, where (A/K) is independent of temperature and heat is generated in a finite section of the tube between $y = -L/2$ and $y = +L/2$.

Thus, for

$$-L/2 \leq y \leq +L/2 \qquad A = A_0$$

$$\left.\begin{array}{l} -\infty \leq y \leq -L/2 \\ +L/2 \leq y \leq +\infty \end{array}\right\} \qquad A = 0 \qquad \text{(B-17)}$$

The boundary conditions are

$$T\,(a,y) = 0 \qquad \text{(B-18a)}$$

$$\frac{\partial T}{\partial r}\,(b,y) = 0 \qquad \text{(B-18b)}$$

$$\frac{\partial T}{\partial y}\,(0,r) = 0 \qquad \text{(B-18c)}$$

$$\frac{\partial T}{\partial y}\,(\pm\infty,r) = 0 \qquad \text{(B-18d)}$$

It is obvious that the solution will be symmetric about the center of the heated section (y = 0) so that it is only necessary to obtain a solution for $0 \leq y \leq \infty$.

Equation (B-16) may be placed in dimensionless form by defining the following dimensionless variables.

$$\tilde{y} = 2y/L \qquad \text{(B-19)}$$

$$\tilde{r} = 2r/L \qquad \text{(B-20)}$$

$$\tilde{a} = 2a/L \qquad \text{(B-21)}$$

$$\tilde{b} = 2b/L \qquad \text{(B-22)}$$

$$\tilde{T} = 4KT/(L^2 A_0) \qquad \text{(B-23)}$$

The resulting dimensionless equation is

$$\frac{\partial^2 \tilde{T}}{\partial \tilde{r}^2} + \frac{1}{\tilde{r}} \frac{\partial \tilde{T}}{\partial \tilde{r}} + \frac{\partial^2 \tilde{T}}{\partial \tilde{y}^2} + \tilde{A} = 0 \qquad \text{(B-24)}$$

where for

$$\begin{aligned} 0 &\leq \tilde{y} \leq 1 & \tilde{A} &= 1 \\ 1 &< \tilde{y} < \infty & \tilde{A} &= 0 \end{aligned} \qquad \text{(B-25)}$$

with the boundary conditions

$$\tilde{T}(\tilde{a},\tilde{y}) = 0 \qquad \text{(B-26a)}$$

$$\frac{\partial \tilde{T}}{\partial \tilde{r}}(\tilde{b},\tilde{y}) = 0 \qquad \text{(B-26b)}$$

$$\frac{\partial \tilde{T}}{\partial \tilde{y}}(0,\tilde{r}) = 0 \qquad \text{(B-26c)}$$

$$\frac{\partial \tilde{T}}{\partial \tilde{y}}(\infty,\tilde{r}) = 0 \qquad \text{(B-26d)}$$

Henceforth, the notation $\tilde{T}_{\tilde{y}}$ and $\tilde{T}_{\tilde{r}}$ will denote $\partial\tilde{T}/\partial\tilde{y}$ and $\partial\tilde{T}/\partial\tilde{r}$, respectively.

Divide the cylinder into two regions, I and II (the heat-generating and non-heat generating regions), as shown in Figure 59. Then set $\tilde{T}_{\tilde{y}}(\tilde{r},1) = g(\tilde{r})$ at the boundary between I and II, where $g(\tilde{r})$ is some unknown, arbitrary function.

In Region I

$$\frac{\partial^2 \tilde{T}}{\partial \tilde{r}^2} + \frac{1}{\tilde{r}}\frac{\partial \tilde{T}}{\partial \tilde{r}} + \frac{\partial^2 \tilde{T}}{\partial \tilde{y}^2} + 1 = 0 \tag{B-27}$$

with the boundary conditions

$$\tilde{T}_{\tilde{r}}\,(\tilde{b},\tilde{y}) = 0 \tag{B-28a}$$

$$\tilde{T}\,(\tilde{a},\tilde{y}) = 0 \tag{B-28b}$$

$$\tilde{T}_{\tilde{y}}\,(\tilde{r},0) = 0 \tag{B-28c}$$

$$\tilde{T}_{\tilde{y}}\,(\tilde{r},1) = g(\tilde{r}) \tag{B-28d}$$

In Region II

$$\frac{\partial^2 \tilde{T}}{\partial \tilde{r}^2} + \frac{1}{\tilde{r}}\frac{\partial \tilde{T}}{\partial \tilde{r}} + \frac{\partial^2 \tilde{T}}{\partial \tilde{y}^2} = 0 \tag{B-29}$$

with the boundary conditions

$$\tilde{T}_{\tilde{r}}\,(\tilde{b},\tilde{y}) = 0 \tag{B-30a}$$

$$\tilde{T}\,(\tilde{a},\tilde{y}) = 0 \tag{B-30b}$$

$$\tilde{T}_{\tilde{y}}\,(\tilde{r},\infty) = 0 \tag{B-30c}$$

$$\tilde{T}_{\tilde{y}}\,(\tilde{r},1) = g(\tilde{r}) \tag{B-30d}$$

Consider, first, only the solution for region I.

Let

$$\tilde{T}_I = \tilde{V} - (\tilde{r}^2 - \tilde{a}^2)/4 \tag{B-31}$$

Then

$$\frac{\partial^2 \tilde{V}}{\partial \tilde{r}^2} + \frac{1}{\tilde{r}}\frac{\partial \tilde{V}}{\partial \tilde{r}} + \frac{\partial^2 \tilde{V}}{\partial \tilde{y}^2} = 0 \tag{B-32}$$

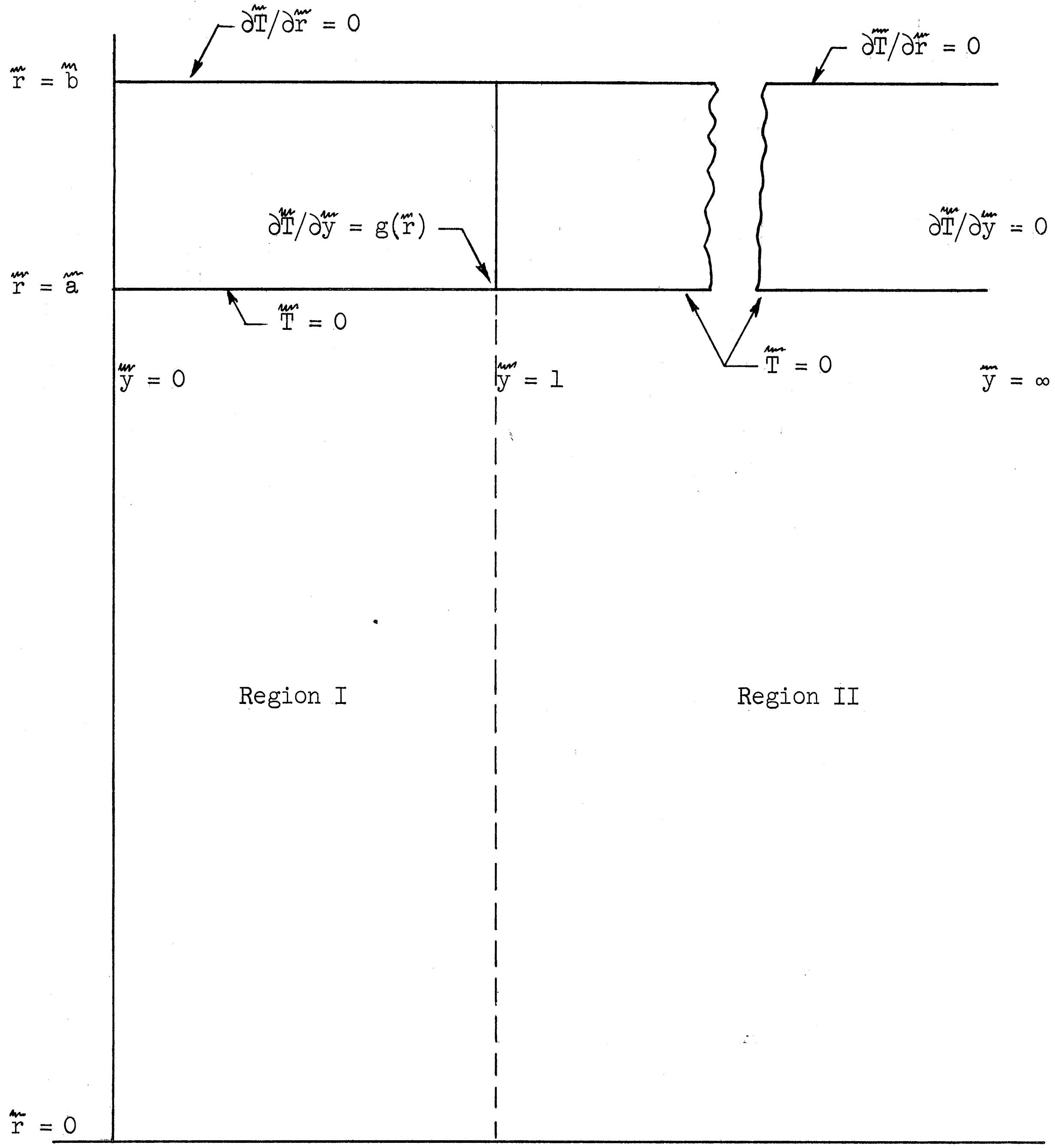

Figure 59. Boundary Conditions for Solution of Conduction Equation Considering Axial Conduction into the Non-Heat-Generating Portion of the Tube.

subject to the boundary conditions

$$\hat{V}_{\hat{r}}\ (\hat{b},\hat{y}) = \hat{b}/2 \tag{B-33a}$$

$$\hat{V}\ (\hat{a},\hat{y}) = 0 \tag{B-33b}$$

$$\hat{V}_{\hat{y}}\ (\hat{r},0) = 0 \tag{B-33c}$$

$$\hat{V}_{\hat{y}}\ (\hat{r},1) = g(\hat{r}) \tag{B-33d}$$

This can be solved by the method of separation of variables.

Assume
$$\hat{V} = \mathcal{R}(\hat{r})\,\mathcal{Y}(\hat{y}) \tag{B-34}$$

Then
$$\hat{r}^2 \frac{d^2\mathcal{R}}{d\hat{r}^2} + \hat{r}\frac{d\mathcal{R}}{d\hat{r}} - \hat{\lambda}^2\hat{r}^2 = 0 \tag{B-35}$$

$$\frac{d^2\mathcal{Y}}{d\hat{y}^2} + \hat{\lambda}^2\hat{y} = 0 \tag{B-36}$$

For $\hat{\lambda}^2$ positive

$$\mathcal{R}_+ = a_1\, I_0\,(\hat{\lambda}\hat{r}) + a_2\, K_0(\hat{\lambda}\hat{r}) \tag{B-37}$$

$$\mathcal{Y}_+ = b_1 \sin\,(\hat{\lambda}\hat{y}) + b_2 \cos\,(\hat{\lambda}\hat{y}) \tag{B-38}$$

For $\hat{\lambda}^2$ negative

$$\mathcal{R}_- = a_1\, J_0\,(\hat{\lambda}\hat{r}) - a_2\, Y_0(\hat{\lambda}\hat{r}) \tag{B-39}$$

$$\mathcal{Y}_- = b_1 \sinh\,(\hat{\lambda}\hat{y}) + b_2 \cosh\,(\hat{\lambda}\hat{y}) \tag{B-40}$$

For $\hat{\lambda}^2$ zero

$$\mathcal{R}_o = a_1 \ln \hat{r} + a_2 \tag{B-41}$$

$$\mathcal{Y}_o = b_1\,\hat{y} + b_2 \tag{B-42}$$

Attempt to find two solutions, $\hat{V}_1$ and $\hat{V}_2$ such that

$$\hat{V} = \hat{V}_1 + \hat{V}_2 \tag{B-43}$$

with $\tilde{V}_1$ satisfying the conditions

$$\hat{V}_{\hat{r}}(\hat{b},\hat{y}) = \hat{b}/2 \qquad \hat{V}_{\hat{y}}(\hat{r},0) = 0 \qquad \text{(B-44a) to}$$

$$\hat{V}(\hat{a},\hat{y}) = 0 \qquad \hat{V}_{\hat{y}}(\hat{r},1) = 1 \qquad \text{(B-44d)}$$

and with $\hat{V}_2$ satifying

$$\hat{V}_{\hat{r}}(\hat{b},\hat{y}) = 0 \qquad \hat{V}_{\hat{y}}(\hat{r},0) = 0 \qquad \text{(B-45a) to}$$

$$\hat{V}(\hat{a},\hat{y}) = 0 \qquad \hat{V}_{\hat{y}}(\hat{r},1) = g(\hat{r}) \qquad \text{(B-45d)}$$

The solutions for $\hat{\lambda}^2 = 0$ will satisfy the requirements for $\hat{V}_1$ if

$$b_1 = 1 \qquad a_1 = \hat{b}^2/2$$

$$b_2 = 0 \qquad a_2 = \ln \hat{a} \qquad \text{(B-46)}$$

or, in other words

$$\hat{V}_1 = (\hat{b}^2/2) \ln (\hat{r}/\hat{a}) \qquad \text{(B-47)}$$

The solutions for $\hat{\lambda}^2$ negative will satisfy the requirements for $\hat{V}_2$ if

$$b_1 = 0 \qquad a_1 = Y_0(\hat{\lambda}_n\hat{a})$$

$$b_2 = \hat{\lambda}_n \sinh \hat{\lambda}_n \qquad a_2 = J_0(\hat{\lambda}_n\hat{a}) \qquad \text{(B-48)}$$

In order to satisfy the remaining boundary condition, $\hat{\lambda}_n$ will be chosen such that

$$Y_0(\hat{\lambda}_n\hat{a}) \, J_1(\hat{\lambda}_n\hat{b}) - J_0(\hat{\lambda}_n\hat{a}) \, Y_1(\hat{\lambda}_n\hat{b}) = 0 \qquad \text{(B-49)}$$

For convenience it will be useful to define a new parameter

$$\lambda_n = \hat{\lambda}_n\hat{a} \qquad \text{(B-50)}$$

so that the relation above is replaced by

$$Y_0(\lambda_n)\, J_1\,(\lambda_n \hat{\tilde{b}}/\hat{\tilde{a}}) - J_0\,(\lambda_n)\, Y_1\,(\lambda_n \hat{\tilde{b}}/\hat{\tilde{a}}) \;=\; 0 \qquad \text{(B-51)}$$

Thus,

$$\hat{\tilde{V}}_2 = Y_0(\lambda_n)\, J_0\,(\lambda_n \hat{\tilde{r}}/\hat{\tilde{a}}) - J_0\,(\lambda_n)\, Y_0\,(\lambda_n \hat{\tilde{r}}/\hat{\tilde{a}})\, \frac{\cosh \lambda_n \hat{\tilde{y}}/\hat{\tilde{a}}}{\lambda_n \sinh \lambda_n/\hat{\tilde{a}}} \qquad \text{(B-52)}$$

At this point it will be useful to define the function

$$\Lambda(\lambda_n, \hat{\tilde{r}}/\hat{\tilde{a}}) \;=\; Y_0(\lambda_n)\, J_0\,(\lambda_n \hat{\tilde{r}}/\hat{\tilde{a}}) - J_0(\lambda_n)\, Y_0\,(\lambda_n \hat{\tilde{r}}/\hat{\tilde{a}}) \qquad \text{(B-53)}$$

It can be shown that the $\Lambda(\lambda_n, \hat{\tilde{r}}/\hat{\tilde{a}})$ form an orthogonal set of functions so that the arbitrary function $g(\hat{\tilde{r}})$ may be expanded in the following manner

$$g(\hat{\tilde{r}}) \;=\; \sum_{n=1}^{\infty} \hat{\tilde{A}}_n\, \Lambda(\lambda_n, \hat{\tilde{r}}/\hat{\tilde{a}}) \qquad \text{(B-54)}$$

Therefore, let

$$\hat{\tilde{V}}_2 \;=\; \sum_{n=1}^{\infty} \hat{\tilde{A}}_n\, \Lambda(\lambda_n, \hat{\tilde{r}}/\hat{\tilde{a}})\, \frac{\cosh \lambda_n \hat{\tilde{y}}/\hat{\tilde{a}}}{\frac{\lambda}{\hat{\tilde{a}}} n \sinh \lambda_n/\hat{\tilde{a}}} \qquad \text{(B-55)}$$

and

$$\hat{\tilde{V}} \;=\; (\hat{\tilde{b}}^2/2) \ln\,(\hat{\tilde{r}}/\hat{\tilde{a}}) \;+\; \sum_{n=1}^{\infty} \hat{\tilde{A}}_n\, \Lambda(\lambda_n, \hat{\tilde{r}}/\hat{\tilde{a}})\, \frac{\cosh \lambda_n\, \hat{\tilde{y}}/\hat{\tilde{a}}}{(\lambda_n/\hat{\tilde{a}}) \sinh \lambda_n/\hat{\tilde{a}}} \qquad \text{(B-56)}$$

Thus,

$$\hat{\tilde{T}}_I = \frac{\hat{\tilde{b}}^2}{2} \ln \frac{\hat{\tilde{r}}}{\hat{\tilde{a}}} - \frac{(\hat{\tilde{r}}^2 - \hat{\tilde{a}}^2)}{4} \;+\; \sum_{n=1}^{\infty} \hat{\tilde{A}}_n \Lambda(\lambda_n, \hat{\tilde{r}}/\hat{\tilde{a}})\, \frac{\cosh \lambda_n \hat{\tilde{r}}/\hat{\tilde{a}}}{(\lambda_n/\hat{\tilde{a}}) \sinh \lambda_n/\hat{\tilde{a}}} \qquad \text{(B-57)}$$

The only remaining problem is the selection of the $\hat{\tilde{A}}_n$.

The solution in Region II may be written by inspection as

$$\hat{\tilde{T}}_{II} = \sum_{n=1}^{\infty} \hat{\tilde{A}}_n \Lambda(\lambda_n, \hat{r}/\hat{a}) \frac{\exp(-\lambda_n [\hat{y} - 1] /\hat{a})}{-\lambda_n/\hat{a}} \tag{B-58}$$

Now, equate the temperatures at $\hat{y} = 1$.

$$\hat{\tilde{T}}_I(1) = \hat{\tilde{T}}_{II}(1) \tag{B-59}$$

and

$$\hat{b}^2 \ln \frac{\hat{r}}{\hat{a}} - \frac{1}{4}(\hat{r}^2 - \hat{a}^2) + \sum_{n=1}^{\infty} \hat{\tilde{A}}_n \Lambda(\lambda_n, \hat{r}/\hat{a}) \frac{\cosh \lambda_n/\hat{a}}{(\lambda_n/\hat{a}) \sinh \lambda_n/\hat{a}}$$

$$= - \sum_{n=1}^{\infty} \hat{\tilde{A}}_n \frac{\Lambda(\lambda_n, \hat{r}/\hat{a})}{\lambda_n/\hat{a}} \tag{B-60}$$

Let

$$\hat{b}^2/2 \ln(\hat{r}/\hat{a}) - (\hat{r}^2 - \hat{a}^2)/4 = \sum_{n=1}^{\infty} \hat{\tilde{D}}_n \Lambda(\lambda_n, \hat{r}/\hat{a}) \tag{B-61}$$

where the $\hat{\tilde{D}}_n$ are to be determined from Sturm-Liouiville theory.

Then

$$\hat{\tilde{D}}_n + \frac{\hat{\tilde{A}}_n \cosh \lambda_n/\hat{a}}{\lambda_n/\hat{a} \sinh \lambda_n/\hat{a}} = \frac{-\hat{\tilde{A}}_n}{\lambda_n/\hat{a}} \tag{B-62}$$

The solution for $\hat{\tilde{A}}_n$ becomes

$$\hat{\tilde{A}}_n = -(\lambda_n/\hat{a}) \sinh \lambda_n/\hat{a} \exp(-\lambda_n/\hat{a}) \hat{\tilde{D}}_n \tag{B-63}$$

The expansion for $\hat{\tilde{D}}_n$ which satisfies Equation (B-61) is

$$\hat{\tilde{D}}_n = -\frac{2\pi \hat{a}^2}{\lambda_n^2 (\xi_n^2 - 1)} \tag{B-62}$$

where

$$\xi_n = Y_0(\lambda_n)/Y_1(\lambda_n \tilde{b}/\tilde{a}) = J_0(\lambda_n)/J_1(\lambda_n \hat{b}/\hat{a}) \qquad \text{(B-63)}$$

Thus

$$\tilde{A}_n = \frac{(\sinh \lambda_n/\hat{a}) \exp(-\lambda_n/\hat{a})\, 2\pi\, \hat{a}}{\lambda_n(\xi_n^2 - 1)} \qquad \text{(B-64)}$$

Substituting into Equations (B-57) and (B-58)

$$\hat{T}_I = \frac{\tilde{b}^2}{2} \ln \frac{\hat{r}}{\hat{a}} - \frac{1}{4}(\hat{r}^2 - \hat{a}^2)$$

$$+ \frac{\pi}{2} \sum_{n=1}^{\infty} \frac{\hat{a}^2}{\lambda_n^2 (\xi_n^2 - 1)} \left[\exp[\frac{\lambda_n}{\hat{a}}(\hat{y} - 1)] + \exp[-\frac{\lambda_n}{\hat{a}}(\hat{y} + 1)] \right] \Lambda(\lambda_n, \frac{\hat{r}}{\hat{a}}) \qquad \text{(B-67)}$$

and

$$\hat{T}_{II} = -\frac{\pi\hat{a}}{2} \sum_{n=1}^{\infty} \frac{[1 - \exp(-2\lambda_n/\hat{a})]}{\lambda_n^2 [\xi_n^2 - 1]} \exp[-(\lambda_n/\hat{a})(\hat{y} - 1)] \Lambda(\lambda_n, \hat{r}/\hat{a}) \qquad \text{(B-68)}$$

Replacing the dimensionless variables by the physical variables, the following solution is obtained. It may be observed that the solution (B-67) is valid for $\hat{y} < 0$ and is symmetric about $\hat{y} = 0$.

For $|y| \leq L/2$

$$T(r,y) = \frac{A_0 a^2}{2K} \left\{ (\frac{b}{a})^2 \ln (\frac{r}{a}) - \frac{1}{2}\left[(\frac{r}{a})^2 - 1 \right] \right.$$

$$\left. + \sum_{n=1}^{\infty} \frac{\pi}{\lambda_n^2(\xi_n^2 - 1)} \left[\exp[\frac{\lambda_n}{a}(y - L/2)] + \exp[\frac{\lambda_n}{a}(y + L/2)] \right] \Lambda(\lambda_n, r/a) \right\} \qquad \text{(B-69)}$$

for $y > L/2$

$$T(r,y) = -\frac{A_0 a^2}{2K} \sum_{n=1}^{\infty} \frac{\pi}{\lambda_n^2 (\xi_n^2 - 1)} \left[1 - \exp(-\lambda_n L/a)\right]\left[\exp[-\frac{\lambda_n}{a}(y - L/2)]\right]$$

$$\times \Lambda(\lambda_n, r/a) \qquad \text{(B-70)}$$

where $\Lambda(\lambda_n, r/a) = Y_0(\lambda_n)\, J_0(\lambda_n r/a) - J_0(\lambda_n)\, Y_0(\lambda_n r/a)$ (B-71)

with the λ_n satisfying

$$Y_0(\lambda_n)\, J_1(\lambda_n b/a) = J_0(\lambda_n)\, Y_1(\lambda_n b/a) \qquad \text{(B-72)}$$

and

$$\xi_n = \frac{J_0(\lambda_n)}{J_1(\lambda_n b/a)} = \frac{Y_0(\lambda_n)}{Y_1(\lambda_n b/a)} \qquad \text{(B-73)}$$

The first three roots of Equation (B-72) were determined for values of b/a equal to 1.100, 1.2418, and 1.5000. The results are presented in Table V. In Table VI the corresponding values of the function $\Lambda(\lambda_n, r/a)$ are tabulated.

It should be noted that the first part of the solution (B-69) outside the summation is simply the solution to the linear, ordinary differential equation. The part inside the summation accounts for axial conduction into the portion of the tube where there is no heat generation.

The dimensionless form of the solution (at r = b) is plotted in Figure 60. It is apparent that the "end effect" extends for a distance of less than one or two diameters from the beginning or end of

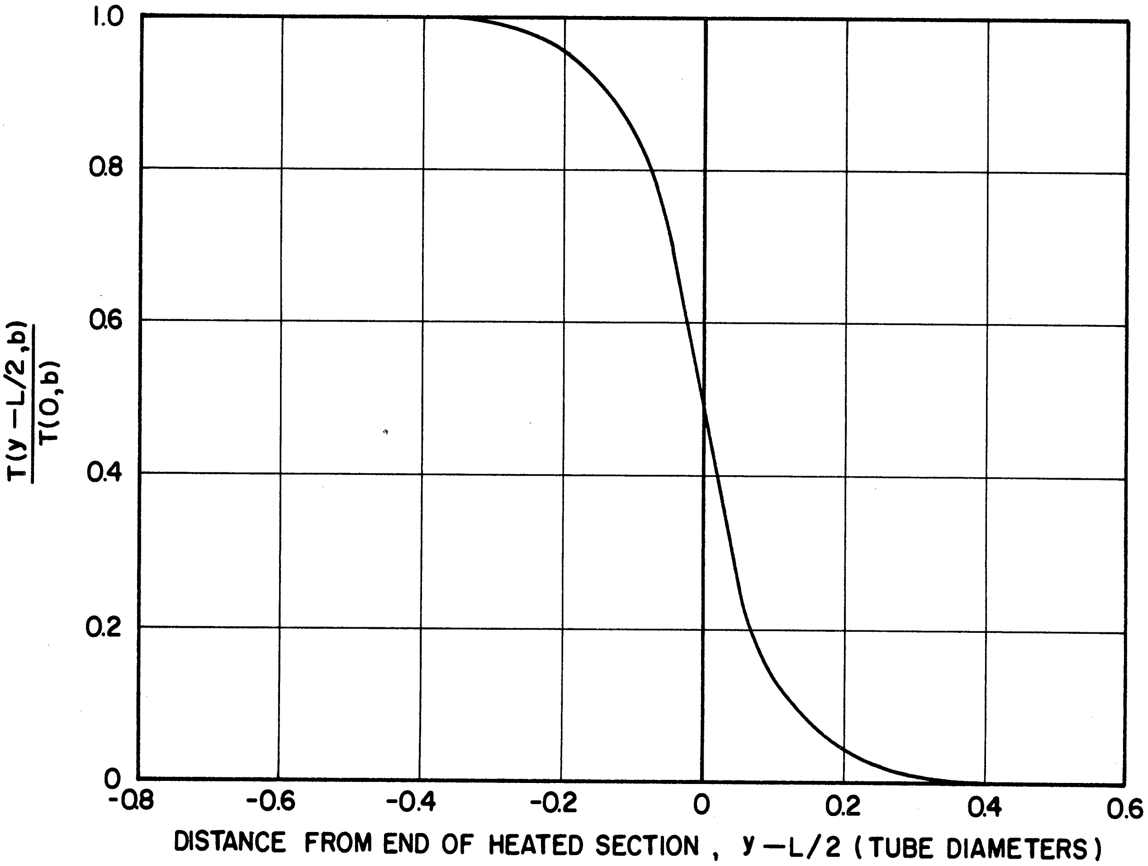

Figure 60. Dimensionless Form of Solution for Axial Conduction into the Non-Heat-Generating Portion of the Tube, Showing that the End Effect is Negligible.

the heating section and outside this region axial conduction into the non-heat-generating portion of the tube is negligible.

TABLE V

FIRST THREE ROOTS λ_i OF EQUATION (B-72) AND ASSOCIATED VALUES OF ξ_i FOR b/a = 1.100, 1.2418, AND 1.5000.

	b/a = 1.1000	b/a = 1.2418	b/a = 1.5000
λ_1	15.4061	6.2146	2.8899
λ_2	47.024	19.3979	9.3448
λ_3	78.4804	32.4268	15.6602
ξ_1	1.0479	1.1092	1.2054
ξ_2	-1.0487	-1.1138	-1.2228
ξ_3	1.0488	1.1142	1.2240

Effect of Axial Variation of Inside Wall Temperature Gradient

It was shown in Part 2 of this appendix that longitudinal conduction into the non-heat-generating portion of the tube can be neglected except for a short distance within one diameter of each end of the heated section. In this part of the appendix, it will be shown that the effect of longitudinal conduction caused by any axial variation in the inside wall temperature gradient is also negligible.

For this analysis a solution will be developed for the general case where T(a,y) is not zero, but some arbitrary function g(y). This solution will then be interpreted in terms of the parameters of the experimental apparatus used in this investigation.

TABLE VI

THE FUNCTION $\Lambda(\lambda_n, r/a)$ FOR b/a = 1.100, 1.2418, AND 1.500 AS A FUNCTION OF $(r-a)/(b-a)$

$\frac{r-a}{b-a}$	b/a = 1.1000			b/a = 1.2418		
	Λ_1	Λ_2	Λ_3	Λ_1	Λ_2	Λ_3
0.000	0.0000	0.00000	0.00000	0.00000	0.00000	0.00000
0.100	-0.0063	-0.00610	-0.00570	-0.01515	-0.91466	-0.01370
0.200	-0.0124	-0.01083	-0.00803	-0.02962	-0.02585	-0.01917
0.300	-0.0182	-0.01317	-0.00566	-0.04309	-0.03126	-0.01345
0.400	-0.0234	-0.01264	-0.00002	-0.05530	-0.02987	-0.00009
0.500	-0.0281	-0.00939	0.00558	-0.06601	-0.02214	0.01303
0.600	-0.0320	-0.00414	0.00788	-0.07502	-0.00983	0.01834
0.700	-0.0352	0.00196	0.00557	-0.08217	0.00431	0.01295
0.800	-0.0375	0.00757	0.00004	-0.08734	0.01725	0.00018
0.900	-0.0389	0.01150	-0.00547	-0.09046	0.02624	-0.01244
1.000	-0.0394	0.01291	-0.00773	-0.09150	0.02944	-0.01761

$\frac{r-a}{b-a}$	b/a = 1.5000		
	Λ_1	Λ_2	Λ_3
0.000	0.00000	0.00000	0.00000
0.100	-0.03095	-0.02994	-0.02798
0.200	-0.05984	-0.05222	-0.03874
0.300	-0.08621	-0.06256	-0.02696
0.400	-0.10971	-0.05936	-0.00031
0.500	-0.13001	-0.04378	0.02543
0.600	-0.14685	-0.01963	0.03564
0.700	-0.16006	0.00774	0.02509
0.800	-0.16951	0.03248	0.00058
0.900	-0.17515	0.04951	-0.02340
1.000	-0.17702	0.05553	-0.03317

If a solution can be obtained to

$$\frac{\partial^2 T}{\partial r^2} + \frac{1}{r}\frac{\partial T}{\partial r} + \frac{\partial^2 T}{\partial y^2} = 0 \qquad \text{(B-74)}$$

(i.e., the linear equation for no heat generation in the tube wall) subject to the boundary conditions

$$\frac{\partial T}{\partial r}(b,y) = 0 \qquad \text{(B-75a)}$$

$$T(a,y) = g(y) \qquad \text{(B-75b)}$$

and if the solution is added to the solution to (B-16) which accounts for the effect of heat generation, then (because the partial differential equations are linear) one will still have a solution to (B-16) but with the boundary condition

$$T(a,y) = 0 \qquad \text{(B-18a)}$$

replaced by

$$T(a,y) = g(y) \qquad \text{(B-76)}$$

Represent g(y) by the sum of a linear term plus a Fourier series expansion between the points y_1 and y_2.

$$g(y) = T(a,y_1) + m(y-y_1) + \sum_{n=1}^{\infty} B_n \cos\left[n\pi \frac{(y - y_1)}{(y_2 - y_1)}\right] \qquad \text{(B-77)}$$

Then simplify the writing of g(y) by replacing $y_2 - y_1$ with S and from Carslaw and Jaeger(7) the solution is

$$T(r,y) = T(a,y_1) + m(y - y_1) + \sum_{n=1}^{\infty} B_n \cos\left[n\pi \frac{(y-y_1)}{S}\right] \frac{I_0(n\pi r/S)K_1(n\pi b/S) + K_0(n\pi r/S)I_1(n\pi b/S)}{I_0(n\pi a/S)K_1(n\pi b/S) + K_0(n\pi a/S)I_1(n\pi b/S)}$$

(B-78)

In particular

$$T(b,y) = T(a,y_1) + m(y-y_1) + \sum_{n=1}^{\infty} \delta(na/S,b/a) \cos\left[n\pi (y-y_1)/S\right]$$

(B-79)

where $\delta(na/S,b/a)$ is a "damping function" equal to

$$\delta(na/S,b/a) = \frac{I_0(n\pi r/S)K_1(n\pi b/S) + K_0(n\pi r/S)I_1(n\pi b/S)}{I_0(n\pi a/S)K_1(n\pi b/S) + K_0(n\pi a/S)I_1(n\pi b/S)} \qquad \text{(B-80)}$$

This function is plotted in Figure 61 for b/a = 1.24.

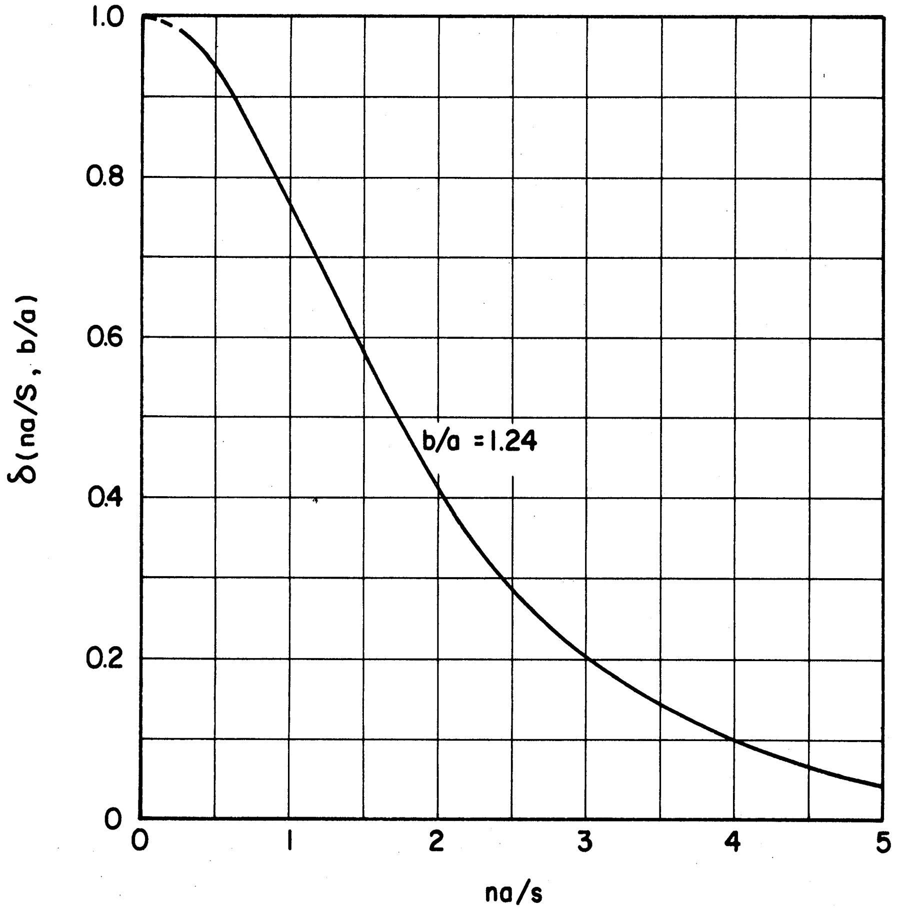

Figure 61. Damping Function Defined by Equation (B-80) as a Function of the Parameter na/S, δ(na/S, b/a) vs. na/S, for b/a = 1.24.

Of course, $\Delta T_{generation}$ must be added to the above in order to account for the temperature difference between inside and outside tube wall due to internal generation of heat. The general solution will now be interpreted in light of the specific experimental conditions encountered in this investigation.

For water being heated at a constant rate as it flows in an empty tube with constant heat transfer coefficient the inside wall temperature distribution is linear, showing only the steady rise in temperature caused by heating of the water. From Equation (B-79) it is seen that this linear temperature change is transmitted through the tube with only the magnitude of the temperature changed by a constant amount $\Delta T_{generation}$ along the length of the tube as would be given by Equation (54). This is also true for a tube with a solid rod in the center, or for any other geometry for which h(z) is constant.

However, when turbulence promoters are inserted at uniform spacing, causing the inside heat transfer coefficient to vary periodically, then the inside temperature will also vary periodically and this variation will be superimposed on the linear increase in the temperature caused by the heating of the water. Thus, a typical (although extreme) example of an inside wall temperature distribution is shown in Figure 62.

The equation describing the inside wall temperature as a function of y is

$$T_a(y) = T_f(-L/2) + m(y - L/2) + \Delta T_{mean} + \Delta T_{periodic} \qquad \text{(B-81)}$$

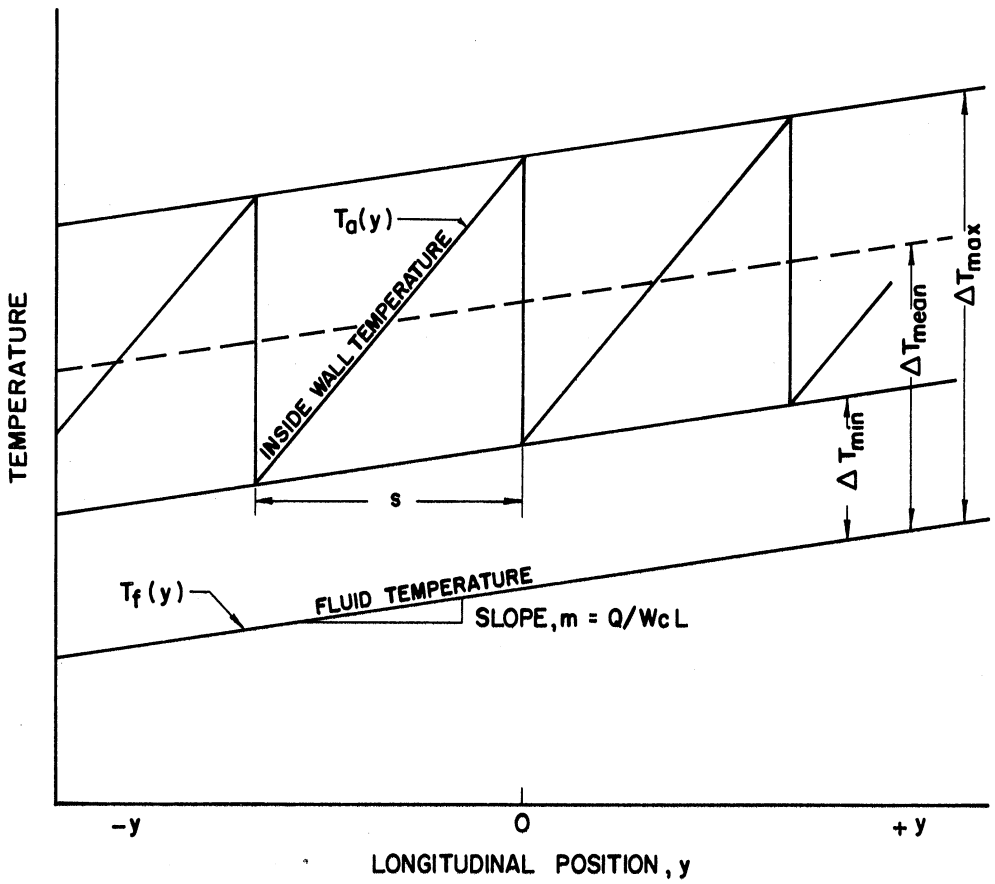

Figure 62. Sample Hypothetical Values of Fluid Temperature and Inside Wall Temperature as a Function of Longitudinal Position, $T_f(y)$ and $T_a(y)$ vs. y, for Rapidly Varying Inside Wall Temperature.

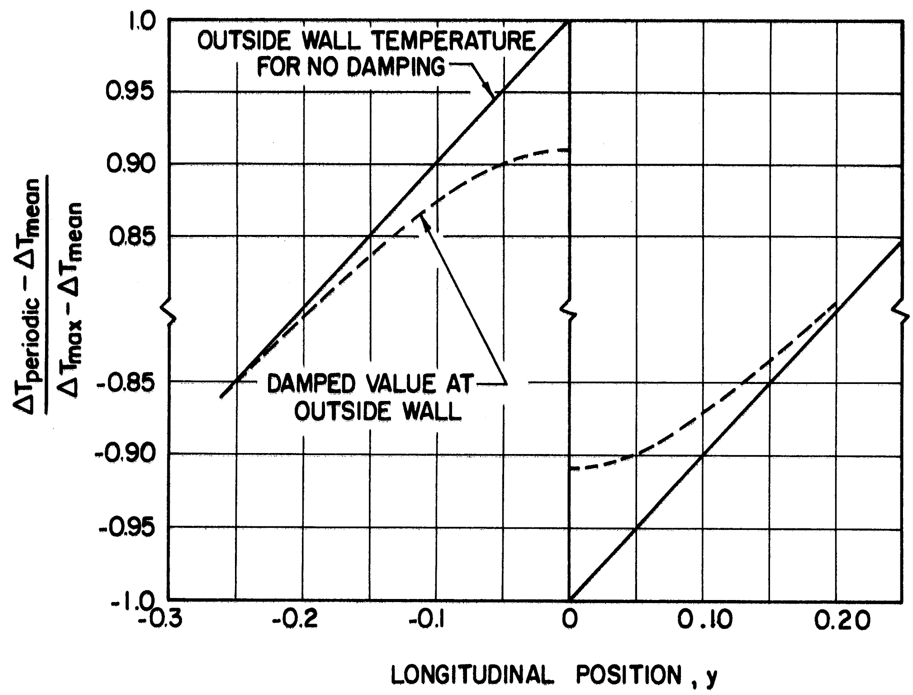

Figure 63. Effect of Neglecting Damping of Outside Wall Temperature When Inside Wall Temperature is Rapidly Varying with Longitudinal Position.

The fluctuating component of the temperature difference $\Delta T_{periodic}$ in this example is defined for $0 \leq y \leq S$ by

$$\Delta T_{periodic} - \Delta T_{mean} = [\Delta T_{max} - \Delta T_{mean}][\frac{2y}{S} - 1] \qquad \text{(B-82)}$$

The Fourier series expansion of the last term is

$$\frac{\Delta T_{periodic} - \Delta T_{mean}}{\Delta T_{max} - \Delta T_{mean}} = \sum_{k=0}^{\infty} A_k \cos\left[\frac{(2k+1)\pi y}{S}\right] \qquad \text{(B-83)}$$

$$= \frac{8}{\pi^2} \sum_{k=0}^{\infty} \frac{1}{(2k+1)^2} \cos\left[\frac{(2k+1)\pi y}{S}\right] \qquad \text{(B-84)}$$

The temperature distribution at the outside wall according to Equation (B-79) is given by

$$T_b(y) = T_f(-L/2) + m(y + L/2) + \Delta T_{mean} + \Delta T'_{periodic} + \Delta T_{generation} \qquad \text{(B-85)}$$

where $\Delta T_{generation}$ is the temperature increase from $r = a$ to $r = b$ caused by heat generation alone. If the solution of the linear ordinary differential equation is used, this term is

$$\Delta T_{generation} \cong \frac{A_0}{2 K_b}\left[b^2 \ln\left(\frac{b}{a}\right) - \frac{(b^2 - a^2)}{2}\right] \qquad \text{(B-86)}$$

The term $\Delta T'_{periodic}$ is the "damped" fluctuating component of the temperature difference

$$\Delta T'_{periodic} = \Delta T_{periodic} \, \delta(na/S, b/a) \qquad \text{(B-87)}$$

For the example chosen ($S = s = 2$ tube diameters, $S/a = 4$, $b/a = 1.24$) the first 11 coefficients of the Fourier series expansion are listed below, with the argument of the damping function, and with the value of the damping function to be used in Equation (B-80).

k	A_k	$(2k + 1)/4$	$\delta[(2k+1)/4, 1.24]$
0	8.106×10^{-1}	0.25	0.9822
1	9.006×10^{-2}	0.75	0.8568
2	3.242×10^{-2}	1.25	0.6731
3	1.654×10^{-2}	1.75	0.4956
4	1.001×10^{-2}	2.25	0.3425
5	6.696×10^{-3}	2.75	0.2465
6	4.796×10^{-3}	3.25	0.1711
7	3.603×10^{-3}	3.75	0.1184
8	2.805×10^{-3}	4.25	0.0818
9	2.245×10^{-3}	4.75	0.0565
10	1.838×10^{-3}	5.25	0.0391

Values of the term $(\Delta T_{periodic} - \Delta T_{mean})/(\Delta T_{max} - \Delta T_{mean})$ are listed below. In the first column the values are for the true function given by Equation (B-82). In the second column the values are for the Fourier series expansion valid at the inside wall (or at the outside wall if there is no damping). In the third column are values for the damped Fourier series valid at the outside wall. The "true values" (which would be predicted neglecting damping) and the damped value predicted are plotted in Figure 63.

y	True Value	Approximation by Fourier Series	Damped Value at Outside Wall
0.00	-1.0000	-0.9816	-0.9102
0.20	-0.8000	-0.8009	-0.7926
0.40	-0.6000	-0.6013	-0.5995
0.60	-0.4000	-0.4010	-0.4000
0.80	-0.2000	-0.2005	-0.2000
1.00	0.0000	0.0000	0.0000
1.20	0.2000	0.2005	0.2000
1.40	0.4000	0.4010	0.4000
1.60	0.6000	0.6013	0.5995
1.80	0.8000	0.8009	0.7926
2.00	1.0000	0.9816	0.9102

It can be seen that the damping causes an error of approximately 7 per cent of $[\Delta T_{max} - \Delta T_{mean}]$ at the acute "peak" of the fluctuating temperature distribution. At all the other points tabulated above, however, there is a negligible difference between the damped and undamped temperature distribution. Since, 1) this is a very extreme example emphasizing damping; 2) the error at the worst point is only 7 per cent of $[\Delta T_{max} - \Delta T_{mean}]$ and $[\Delta T_{max} - \Delta T_{mean}]$ is usually only a small part of the total temperature difference between fluid and wall; 3) the error is compensated for in obtaining the integrated mean heat transfer coefficient, because it reduces the temperature difference at one point, but increases it at another. The conclusion is that axial conduction caused by variation in the inside wall temperature may be neglected in processing the experimental data of this investigation.

Estimate of Accuracy

In the preceding section it was shown that, in theory, if the outside tube temperature were known exactly as a function of longitudinal position and if the physical properties of the tube were known exactly, then the inside temperature of the tube (and, in turn, the heat transfer coefficient) could be determined exactly. In this section a discussion is given of the errors introduced by the practical limitation that the outside wall temperature and the physical properties of the tube are not known exactly.

Accuracy of the AZAR Recorder

The emf produced by the thermocouples on the outside tube wall were measured by a Leeds and Northrup Speedomax AZAR recorder.

An average of four readings (each recorded at intervals of about 30 seconds) was taken to reduce any random errors by the recorder. For each run in addition to the two known reference emfs introduced into the AZAR recorder for use in calibration, at least one of the tube wall thermocouple emfs was measured separately using the 8662 portable precision potentiometer. The particular thermocouple to be used was selected randomly for each run and was used as a check on the accuracy of the AZAR recorder.

A frequency distribution of the difference between the emf obtained from the AZAR recorder and the check value obtained by the 8662 potentiometer is shown in Figure 64. It can be seen that the error is roughly normally distributed with a mean of zero and was usually less than $\pm$ 15 microvolts. This corresponds to an error of about $\pm$ 0.70 deg F.

Effect of Temperature Difference Across Mica Insulation

A second source of error in measuring the outside wall temperature is the fact that the thermocouples were separated from the outside tube wall by a thin (0.002 inch) sheet of mica to provide electrical insulation. An exaggerated diagram of the outside wall thermocouple is shown below.

The following nomenclature will be used to estimate the temperature difference across the sheet of mica.

let b = outside radius of tube (0.612 inches)

r_{ins} = outside radius of insulation (1.5 inches)

t_{mica} = thickness of mica (0.002 inches)

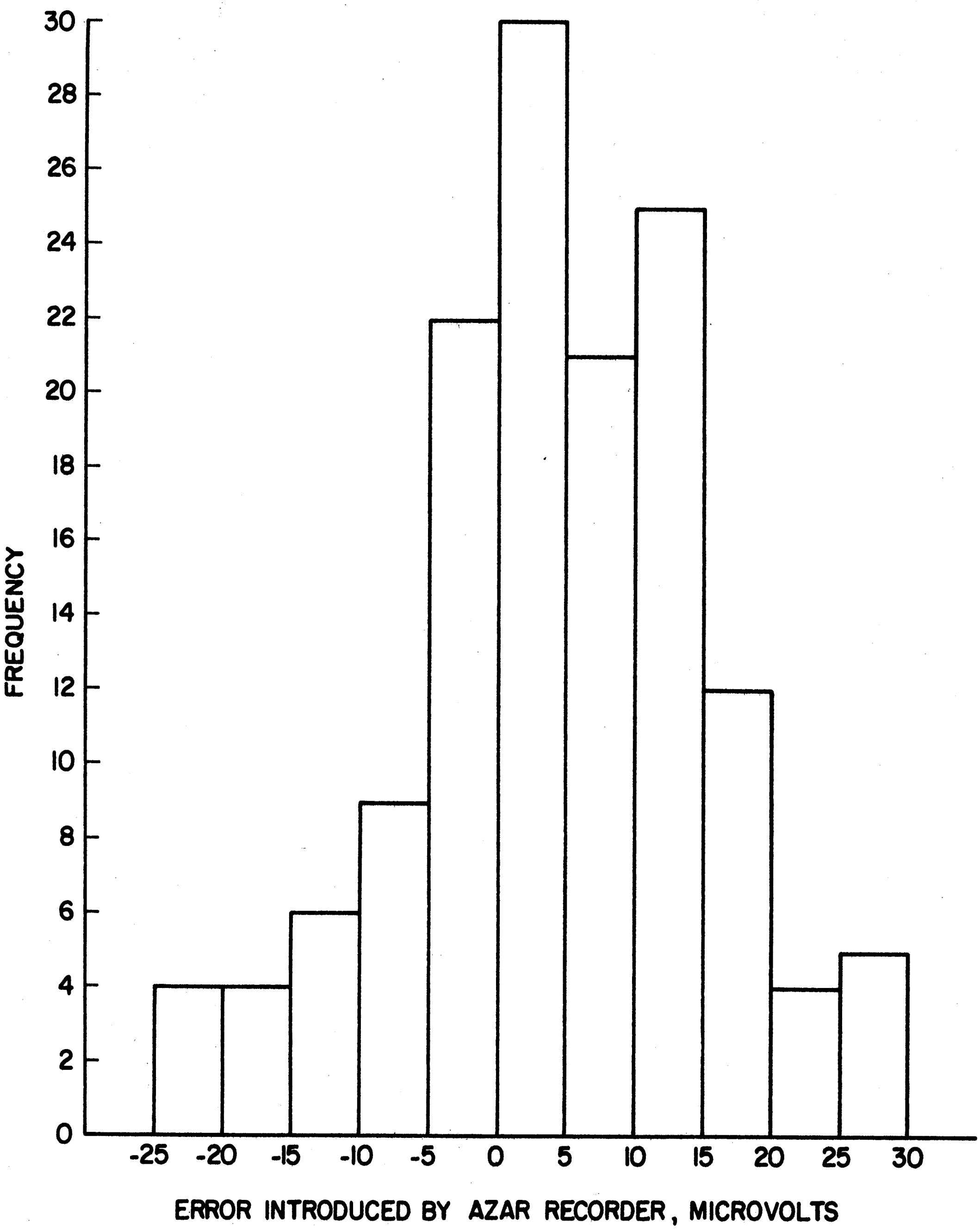

Figure 64. Frequency Distribution of Error Introduced by AZAR Recorder.

T_b = temperature at outside radius of tube

T_{ins} = temperature at r_{ins}

T_{amb} = ambient air temperature

T_{tc} = temperature measured by thermocouple at outside edge of mica sheet

q_L = heat loss per unit area measured at the outside radius of the tube

K_{mica} = thermal conductivity of mica (0.25 BTU/hr-deg F-ft)

K_{fg} = thermal conductivity of Fiberglas (0.05 BTU/hr-deg F-ft)

h_c = convection coefficient for heat transfer by natural convection from Fiberglas to air.

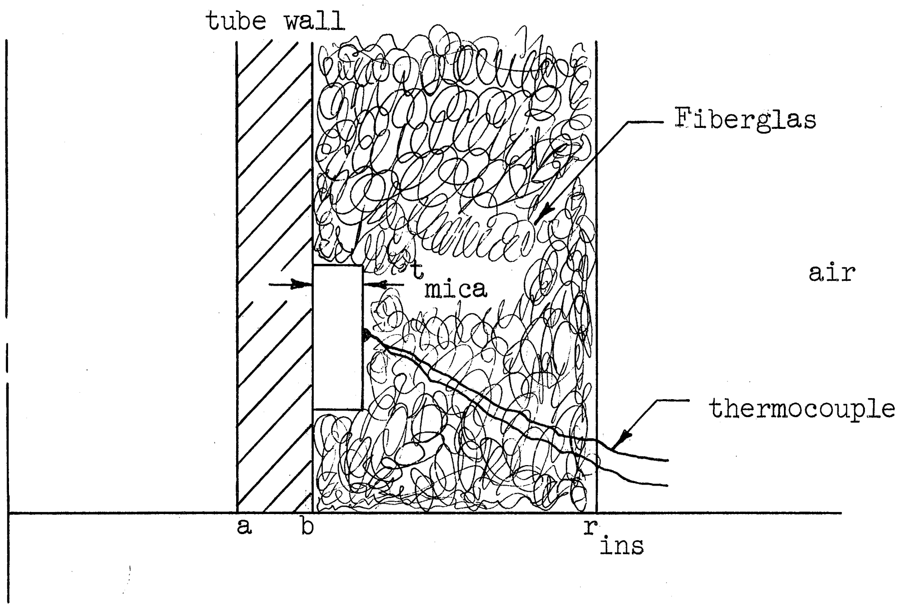

Using simplified correlations recommended by McAdams[28] for the convection coefficient from vertical cylinders to air, the largest value obtainable for temperature differences less than 140 deg F at distances greater than 1 foot from the bottom of the tube is 1 BTU/hr-deg F-ft^2. The following equations may be written

$$\frac{T_b - T_{amb}}{q_L} = \left[\frac{t_{mica}}{K_{mica}} + \frac{b \ln r_{ins}/b}{K_{fg}} + \frac{1}{h_c\, r_{ins}/b}\right] \qquad \text{(B-88)}$$

$$= \left[\frac{0.002}{12 \times 0.25} + \frac{0.612 \ln 2.52}{12 \times 0.05} + \frac{1}{1 \times 2.52}\right] \qquad \text{(B-89)}$$

$$= 0.667 \times 10^{-3} + 0.945 + 0.397$$

$$= 1.34$$

The ratio

$$\frac{T_b - T_{tc}}{T_b - T_{amb}} = \frac{0.667 \times 10^{-3}}{1.34}$$

$$= 4.98 \times 10^{-4} \qquad \text{(B-90)}$$

or, in other words, the error due to reading T_{tc} instead of T_b is approximately 0.05 per cent of the difference between T_b and T_{amb}. Since the outside wall temperature was always less than 100 deg F greater than the ambient air temperature, the error caused by the temperature difference across the mica insulation was less than 0.05 deg F.

Propagation of Errors in Calculating Local Heat Transfer Coefficients

The two important calculated quantities (i.e., dependent variables) which must be evaluated from the physical properties of the tube and the experimental measurements (i.e., the independent variables) in order to obtain the local heat transfer coefficient are q(z) and $\Delta T_{generation}$. The error in these calculated quantites which is propagated by the defining Equations (56) and (54) will be estimated in this section.

In symbolic form

$$q(z) = \text{function of } (a, b, \bar{\rho}_o, K_0, \gamma, \beta, T_b, I) \qquad \text{(B-91)}$$

$$\Delta T_{generation} = \text{function of } (a, b, \bar{\rho}_o, K_0, \gamma, \beta, T_b, I) \qquad \text{(B-92)}$$

A propagation constant for each of the independent variables (a,b,...etc.) applicable to each of the above relations will be defined. The propagation constant is the percentage change in dependent variable caused by a change of one per cent in the value of the independent variable (with the other independent variables held constant). These constants were evaluated by numerical partial differentiation of the defining expressions. They are listed below.

Independent Variable	Propagation Constant for q(z)	Propagation Constant for $\Delta T_{generation}$
a	-1.2	+2.8
b	-0.8	-6.1
γ	+0.09	+0.09
β	-0.06	0
$\bar{\rho}_o$	+1.0	+1.0
K_0	+1.0	0
T_b	+0.01	+0.09
I	+2.0	+2.0

The estimated maximum error associated with each independent variable is listed below.

Independent Variable	Absolute Error	Per Cent Error
a	0.002 in.	0.4%
b	0.002 in.	0.4%
γ	Error is Relative	5.0%
β	Error is Relative	5.0%
$\bar{\rho}_o$	Error is Relative	5.0%
K_0	Error is Relative	5.0%
I	5 amps	0.5%
T_b	1 deg F	0.67%

The maximum percentage error associated with q(z) and $\Delta T_{generation}$ is the sum of the absolute values of the products of the relative error of each of the independent variables and its propagation constant. This is the error that would occur if each error were in the proper direction so that it exerted its maximum effect. In practice, these errors tend to compensate and a better, statistical estimate of the relative error of the dependent variable is given by the square root of the sum of the squares of the products of the relative errors and propagation constants. On the basis of the statistical procedure, q(z) is accurate to within $\pm$ 5 per cent and $\Delta T_{generation}$ is accurate to within $\pm$ 7 per cent.

The temperature difference between inside wall and fluid $(T_a - T_f)$ is actually required in the calculation of the heat transfer coefficient. The error associated in this term is given by the sum of the errors (or statistically by the square root of the sum of the squares of the errors) in T_b, $\Delta T_{generation}$, and T_f.

The error in determining T_b (caused by error introduced by the temperature difference across the mica insulation and by the AZAR recorder) is less than 1 deg F.

The error in determining T_f is less than 0.05 deg F.

The error in calculating $\Delta T_{generation}$ was shown to be less than 7 per cent. Since $\Delta T_{generation}$ was almost always less than 25 deg F, the absolute error in it was less than 1.75 deg F.

Thus the error in $(T_a - T_f)$ on a statistical basis may be considered less than $\pm$ 2.08 deg F.

APPENDIX C

ORIGINAL AND PROCESSED DATA

In the course of this investigation over 15,000 local heat transfer coefficients and over 750 values of the overall pressure drop were measured. In order to present all of the original data a volume almost as large as this dissertation would be required. An attempt will be made, however, to present the data in a semi-processed form with enough information so that the values of the original measured variables can be "back-calculated."

Table VII is a summary of the experimental conditions used. It lists the geometry, diameter ratio, spacing, number of promoters (for bluff-body promoters), heat transfer run number, number of flow rates for which heat transfer data were obtained, and the pressure drop run number. This table serves as a guide to the location of the data. In order to find the original data corresponding to any particular geometry, the first step is to locate the appropriate run number from Table VII.

Tables VIII, IX, and X present the constants $C(s,d)$ and $n(s,d)$ for use in the Equations (64), (65), and (67) to predict the friction factor f, the effective drag coefficient f_D, or the heat transfer coefficient ratio h_m/h_0 as a function of Reynolds number for a given geometry. In addition, values of the respective variables calculated by the appropriate equation are tabulated at various values of the Reynolds number. These are the values used in preparing the cross-plots of Figures 26, 27, 31, 32, 38, 39, 42, and 43.

Table XI presents the isothermal friction factor and effective drag coefficient (where applicable) as a function of Reynolds number for each pressure drop run. The water temperature for each run was always greater than 40 deg. F and less than 70 deg. F, depending upon the particular time of year when the run was made. The exact value of the fluid temperature for each run is listed (as the inlet temperature) with the heat transfer data in Table XII.

Thus, the mass flow rate can be "back-calculated" using Equation (21). Since the number of promoters n_p is given in Table III, the pressure drop may be calculated using Equation (62) or (22). The inches of purple indicating fluid or mercury may then be calculated using Equation (A-2a) or (A-2b). Most of the pressure drops were measured with the purple fluid, unless this was greater than 100 inches in which case mercury was used.

Table XII presents the integrated results of the heat transfer measurements. For each geometry, diameter ratio, and spacing, the overall (i.e. mean) value of Reynolds number Re_m, heat flux q, heat transfer coefficient h_0 for the empty tube calculated using the Sieder-Tate Equation (18), heat transfer coefficient ratio h_m/h_0, the factor $(\mu/\mu_w)^{0.14}$ x $Pr^{1/3}$ (k/D), and the inlet water temperature are listed.

Table XIII presents the local heat transfer coefficient ratios h/h_0 at each longitudinal position on the tube. In addition, the distance from the nearest promoter x (where appropriate) is given. For longitudinal stations upstream from the first promoter, the distance from the promoter is listed arbitrarily as zero.

From Table XII the heat flux q and inlet water temperature T_{inlet} may be obtained. The fluid temperature at any longitudinal distance z in tube diameters from the beginning of heating may be calculated from

$$T_f(z) = T_{inlet} + \frac{2 \pi D^2 z q}{W c} \qquad \text{(C-1)}$$

From Table XII the mean value of the heat transfer coefficient h_0 for the empty tube is listed. Thus, using the value h/h_0 at each longitudinal position, the actual value of the heat transfer coefficient may be obtained at each longitudinal position. Since h and q are known, the inside wall temperature may be determined from

$$T_{wall}(z) = T_f(z) + q/h \qquad \text{(C-2)}$$

In a similar fashion, almost all of the measured experimental variables can be recovered from the data presented in this appendix.

For longitudinal positions marked with an asterisk (*) the data were for an angular position of 120 degrees and for the longitudinal positions marked with a plus (+) the data were for an angular position of 240 degrees.

All of the information in Tables VIII to XIII was obtained from punched cards used and prepared by the computer at various stages in the data processing. Thus, the number of significant figures does not indicate the estimated precision of the quantity printed. A detailed discussion of the precision of the data is given on pages 103-110.

TABLE VII

SUMMARY OF EXPERIMENTAL CONDITIONS

Geometry	d	s	n_p	Heat Transfer Run Numbers	F*	Pressure Drop Run Number
EMPTY TUBE	0.000	—	—	P-1 TO P-14	14	P-1
EMPTY TUBE	0.000	—	—	R-1-A TO R-1-I	9	P-2
SOLID ROD IN CENTER OF TUBE	0.125	0.0	—	R-3-A TO R-3-E	5	A-2
THREADED SOLID ROD IN CENTER OF TUBE	0.250	0.0	—	R-2-A TO R-2-I	9	A-1
SOLID ROD IN CENTER OF TUBE	0.625	0.0	—	R-28-A TO R-28-E	5	A-27
SOLID ROD IN CENTER OF TUBE	0.750	0.0	—	R-29-A TO R-29-E	5	A-28
DISKS	0.625	12.0	4	R-13-A TO R-13-E	5	A-11
DISKS	0.625	8.0	6	R-12-B TO R-12-E	4	A-12
DISKS	0.625	4.0	12	R-14-A TO R-14-E	5	A-13
DISKS	0.625	2.0	11	R-24-A TO R-24-E	5	A-23
DISKS	0.750	12.0	4	R-5-A,B,C,AND E	4	A-4
DISKS	0.750	12.0	4	R-6-D TO R-6-E	2	A-5
DISKS	0.750	8.0	6	R-7-A TO R-7-E	5	A-6
DISKS	0.750	8.0	6	R-27-A TO R-27-E	5	A-26
DISKS	0.750	4.0	12	R-8-A TO R-8-E	5	A-7
DISKS	0.750	2.0	11	R-26-A TO R-26-E	5	A-25
DISKS	0.875	12.0	4	R-9-A TO R-9-E	5	A-8
DISKS	0.875	8.0	6	R-10-A TO R-10-E	5	A-9
DISKS	0.875	4.0	8	R-11-A TO R-11-E	5	A-10
DISKS	0.875	2.0	8	R-25-A TO R-25-E	5	A-24
STREAMLINE SHAPES	0.625	12.0	4	R-15-A TO R-15-E	5	A-14
STREAMLINE SHAPES	0.625	8.0	6	R-16-A TO R-16-E	5	A-15
STREAMLINE SHAPES	0.625	4.0	6	R-17-A TO R-17-E	5	A-16
STREAMLINE SHAPES	0.750	12.0	4	R-18-A T R-18-E	5	A-17
STREAMLINE SHAPES	0.750	8.0	6	R-19-A TO R-19-E	5	A-18
STREAMLINE SHAPES	0.750	4.0	6	R-20-A TO R-20-E	5	A-19
STREAMLINE SHAPES	0.875	12.0	4	R-21-A TO R-21-E	5	A-20
STREAMLINE SHAPES	0.875	8.0	6	R-22-A TO R-22-E	5	A-21
STREAMLINE SHAPES	0.875	4.0	6	R-23-A TO R-23-E	5	A-22

* Number of flow rates for which heat transfer data were obtained

TABLE VIII

CONSTANT C(s,d) AND n(s,d) USED IN FRICTION FACTOR CORRELATION EQUATION (64) FOR INDIVIDUAL PROMOTER COMBINATIONS

Geometry	ΔP Run	s	d	C(s,d)	n(s,d)	100xf at various values of Re/1000					
						Re/1000					
						5	10	20	30	40	50
SOLID ROD	A-1	0.0	0.250	6.6240	-0.1255	2.274	2.085	1.911	1.816	1.752	1.704
SOLID ROD	A-2	0.0	0.125	7.5207	-0.2307	1.053	0.898	0.765	0.697	0.652	0.619
SOLID ROD	A-27	0.0	0.625	19.190	-0.1271	6.738	6.169	5.649	5.365	5.172	5.028
SOLID ROD	A-28	0.0	0.750	51.594	-0.1217	18.34	16.85	15.49	14.74	14.23	13.86
DISK	A-11	12.0	0.625	8.1420	-0.0620	4.910	4.600	4.180	4.110	4.070	3.999
DISK	A-12	8.0	0.625	7.4316	-0.0173	6.417	6.341	6.265	6.221	6.190	6.167
DISK	A-13	4.0	0.625	6.7241	0.0425	9.657	9.945	10.24	10.42	10.55	10.65
DISK	A-23	2.0	0.625	8.3359	0.0731	15.52	16.33	17.18	17.70	18.07	18.37
DISK	A-4	12.0	0.750	64.253	-0.1612	16.27	14.55	13.01	12.09	11.64	11.22
DISK	A-5	12.0	0.750	15.320	-0.0100	14.08	13.98	13.89	13.83	13.79	13.76
DISK	A-6	8.0	0.750	17.833	0.0092	19.30	19.42	19.55	19.62	19.67	19.71
DISK	A-26	8.0	0.750	14.255	0.0162	16.37	16.55	16.74	16.85	16.93	16.99
DISK	A-7	4.0	0.750	25.298	0.0220	30.53	30.99	31.48	31.76	31.96	32.11
DISK	A-25	2.0	0.750	8.5280	0.1740	37.53	42.35	47.80	51.30	53.94	56.08
DISK	A-8	12.0	0.875	56.884	-0.0084	52.97	52.67	52.36	52.18	52.06	51.96
DISK	A-9	8.0	0.875	72.954	0.0066	77.20	77.55	77.91	78.11	78.26	78.38
DISK	A-10	4.0	0.875	101.94	0.0435	147.7	152.2	156.8	159.6	161.7	163.2
DISK	A-24	2.0	0.875	126.48	0.0670	223.9	234.5	245.7	252.5	257.4	261.3
STREAMLINE	A-14	12.0	0.625	9.2961	-0.1579	2.423	2.172	1.947	1.826	1.745	1.685
STREAMLINE	A-15	8.0	0.625	15.734	-0.1754	3.533	3.128	2.770	2.580	2.453	2.359
STREAMLINE	A-16	4.0	0.625	20.934	-0.1657	5.105	4.551	4.057	3.793	3.616	3.486
STREAMLINE	A-17	12.0	0.750	17.041	-0.1310	5.583	5.099	4.657	4.417	4.254	4.131
STREAMLINE	A-18	8.0	0.750	28.835	-0.1520	7.902	7.111	0.400	6.017	5.759	5.567
STREAMLINE	A-19	4.0	0.750	37.155	-0.1264	12.66	11.60	10.63	10.09	9.736	9.465
STREAMLINE	A-20	12.0	0.875	70.880	-0.1190	25.73	23.69	21.81	20.78	20.08	19.56
STREAMLINE	A-21	8.0	0.875	123.05	-0.1355	38.81	35.33	32.16	30.44	29.28	28.41
STREAMLINE	A-22	4.0	0.875	190.68	-0.1230	66.87	61.41	56.39	53.64	51.78	0=38

TABLE IX

CONSTANTS C(s,d) AND n(s,d) USED IN CORRELATION EQUATION (65)
OF EFFECTIVE DRAG COEFFICIENT FOR INDIVIDUAL PROMOTER COMBINATIONS

						$100 \times f_D$ at various values of Re/1000					
						Re/1000					
Geometry	ΔP Run	s	d	C(s,d)	n(s,d)	5	10	20	30	40	50
DISK	A-11	12.0	0.625	222.07	-0.0280	174.9	171.5	168.2	166.3	165.0	164.0
DISK	A-12	8.0	0.625	170.60	-0.0020	167.8	167.6	167.3	167.2	167.1	167.0
DISK	A-13	4.0	0.625	103.49	0.0357	140.3	143.8	147.4	149.6	151.1	152.3
DISK	A-23	2.0	0.625	38.280	0.1192	105.7	114.8	124.7	130.9	135.4	139.1
DISK	A-4	12.0	0.750	244.42	-0.0265	195.0	191.5	188.0	186.0	184.6	183.5
DISK	A-5	12.0	0.750	241.49	-0.0100	221.8	220.2	218.7	217.8	217.2	216.2
DISK	A-6	8.0	0.750	203.13	0.0017	206.0	206.3	206.5	206.6	206.7	206.8
DISK	A-26	8.0	0.750	132.00	0.0288	168.8	172.2	175.7	177.8	179.3	180.4
DISK	A-7	4.0	0.750	132.58	0.0248	163.8	166.6	169.5	171.2	172.4	173.4
DISK	A-25	2.0	0.750	30.520	0.1458	105.7	116.9	129.3	137.2	143.1	147.8
DISK	A-8	12.0	0.875	204.09	-0.0121	184.0	182.5	180.9	180.0	179.4	179.0
DISK	A-9	8.0	0.875	161.70	0.0095	175.4	176.5	177.7	178.4	178.9	179.2
DISK	A-10	4.0	0.875	137.02	0.0277	173.6	176.9	180.4	182.4	183.9	185.0
DISK	A-24	2.0	0.875	87.250	0.0478	131.2	135.6	140.2	142.9	144.9	146.9
STREAMLINE	A-14	12.0	0.625	150.67	-0.0949	67.15	62.88	58.87	56.66	55.13	53.98
STREAMLINE	A-15	8.0	0.625	199.67	-0.1153	74.80	69.05	63.75	60.84	58.85	57.36
STREAMLINE	A-16	4.0	0.625	199.04	-0.1361	62.42	56.80	51.69	48.91	47.03	45.62
STREAMLINE	A-17	12.0	0.750	173.02	-0.0985	74.75	69.81	65.20	62.65	60.90	59.58
STREAMLINE	A-18	8.0	0.750	263.32	-0.1449	76.60	69.28	62.66	59.08	56.67	54.86
STREAMLINE	A-19	4.0	0.750	160.71	-0.1096	63.20	58.58	54.30	51.94	50.33	49.11
STREAMLINE	A-20	12.0	0.875	248.56	-0.1236	86.72	79.60	73.07	69.49	67.07	65.24
STREAMLINE	A-21	8.0	0.875	262.70	-0.1302	86.62	79.15	72.31	68.59	66.07	64.18
STREAMLINE	A-22	4.0	0.875	198.72	-0.1145	74.93	69.21	63.93	61.04	59.06	57.57

TABLE X

CONSTANT C(s,d) AND n(s,d) USED IN CORRELATION EQUATION (67) OF MEAN HEAT TRANSFER COEFFICIENTS FOR INDIVIDUAL PROMOTER COMBINATIONS

Geometry	HT Run	s	d	C(s,d)	n(s,d)	h_m/h_0 at various values of Re/1000					
						Re/1000					
						5	10	20	30	40	50
DISK	R-13	12.0	0.625	2.7532	-0.0605	1.645	1.577	1.512	1.476	1.456	1.431
DISK	R-12	8.0	0.625	3.9618	-0.0792	2.017	1.909	1.808	1.750	1.711	1.681
DISK	R-14	4.0	0.625	6.3460	-0.1059	2.575	2.392	2.223	2.130	2.066	2.018
DISK	R-24	2.0	0.625	3.6284	-0.0534	2.302	2.218	2.137	2.092	2.060	2.035
DISK	R-5+6	12.0	0.750	7.0341	-0.1355	2.218	2.019	1.838	1.740	1.673	1.624
DISK	R-7+27	8.0	0.750	6.0226	-0.1008	2.553	2.380	2.219	2.131	2.070	2.023
DISK	R-8	4.0	0.750	9.5482	-0.1267	3.246	2.973	2.723	2.587	2.494	2.424
DISK	R-26	2.0	0.750	6.0535	-0.0803	3.054	2.889	2.732	2.645	2.584	2.538
DISK	R-9	12.0	0.875	5.5118	-0.0849	2.675	2.522	2.378	2.298	2.242	2.200
DISK	R-10	8.0	0.875	8.4104	-0.1112	3.262	3.020	2.796	2.672	2.588	2.524
DISK	R-11	4.0	0.875	5.7542	-0.0479	3.825	3.700	3.598	3.510	3.462	3.426
DISK	R-25	2.0	0.875	4.8231	-0.0144	4.265	4.223	4.181	4.156	4.139	4.126
STREAMLINE	R-15	12.0	0.625	1.2934	-0.0053	1.237	1.232	1.228	1.225	1.223	1.222
STREAMLINE	R-16	8.0	0.625	2.1630	-0.0487	1.429	1.382	1.336	1.310	1.292	1.278
STREAMLINE	R-17	4.0	0.625	4.0624	-0.0983	1.759	1.643	1.535	1.475	1.434	1.403
STREAMLINE	R-18	12.0	0.750	2.1214	-0.0328	1.604	1.568	1.533	1.513	1.499	1.488
STREAMLINE	R-19	8.0	0.750	5.4733	-0.1094	2.156	1.998	1.853	1.773	1.718	1.676
STREAMLINE	R-20	4.0	0.750	4.3002	-0.0781	2.211	2.099	1.983	1.922	1.879	1.847
STREAMLINE	R-21	12.0	0.875	4.6661	-0.0873	2.218	2.088	1.965	1.896	1.849	1.814
STREAMLINE	R-22	8.0	0.875	8.2288	-0.1208	2.940	2.704	2.486	2.367	2.287	2.226
STREAMLINE	R-23	4.0	0.875	3.8897	-0.0122	3.506	3.477	3.448	3.431	3.419	3.409

TABLE XI

PRESSURE DROP RESULTS

Run P-1
Empty Tube

Re/1000	100xf
3.765	0.697
3.645	0.697
5.545	0.662
5.639	0.582
6.495	0.673
9.751	0.675
8.106	0.723
13.194	0.681
17.295	0.648
21.563	0.615
25.663	0.604
32.777	0.578
40.309	0.540
45.330	0.530
49.933	0.513

Run P-2
Empty Tube

Re/1000	100xf
2.349	0.778
2.099	0.979
3.495	0.881
4.831	0.838
5.233	0.790
5.446	0.848
6.918	0.761
8.953	0.789
12.001	0.708
16.157	0.659
21.961	0.621
28.336	0.569
32.705	0.568
35.899	0.555
38.479	0.545
41.650	0.538

Run A-1
Threaded Rod
d = 0.250

Re/1000	100xf
2.895	1.711
1.919	2.007
3.829	2.078
4.997	2.182
7.307	2.137
11.731	2.075
15.152	1.996
20.624	1.899
25.785	1.855
32.750	1.792
37.724	1.755

Run A-2
Plain Rod
d = 0.125

Re/1000	100xf
3.133	1.007
4.646	0.919
5.829	0.876
8.599	0.904
10.624	0.922
14.748	0.809
18.498	0.782
22.998	0.740
28.248	0.708
33.872	0.672
39.872	0.653
43.622	0.639
44.747	0.636

Run A-4
Disks
d = 0.750 s = 12.0

Re/1000	100xf	100xf$_D$
2.635	12.675	188.509
3.906	12.562	188.753
4.930	13.003	197.036
6.605	12.828	195.400
7.764	17.983	280.214
13.270	12.392	190.680
18.098	11.752	181.109
23.858	12.065	186.929
28.941	11.809	183.203
35.294	12.000	186.761
41.647	11.821	184.181
45.882	12.069	188.425
52.658	11.774	183.870

Run A-5
Disks
d = 0.750 s = 12.0

Re/1000	100xf	100xf$_D$
2.812	14.534	219.240
3.817	14.244	216.113
4.990	14.893	227.959
5.660	14.097	215.501
6.465	14.733	226.430
7.001	14.461	222.298
9.007	14.597	225.441
10.871	13.908	214.819
14.133	14.199	220.382
16.928	14.143	219.980
20.003	12.274	189.899
24.383	13.718	213.981
25.315	13.540	211.164
28.483	13.337	208.124
33.090	13.457	210.420
36.750	14.063	220.543
40.867	14.031	220.240
43.612	13.769	216.091
44.984	13.721	215.368
45.899	13.646	214.183
47.272	13.932	218.912
48.644	13.908	218.575
50.016	14.349	225.831
51.846	13.935	219.137
53.219	13.994	220.150
55.049	13.859	218.008

Run A-6
Disks
d = 0.750 s = 8.0

Re/1000	100xf	100xf$_D$
0.978	37.469	212.909
2.500	20.872	214.724
3.988	19.819	204.923
5.442	19.315	200.375
6.189	19.666	204.552
7.187	19.874	207.207
8.233	18.594	193.605
9.548	20.818	218.168
10.487	18.453	192.624
11.802	18.769	196.318
12.835	20.123	211.235
15.653	20.296	213.507
17.626	19.321	203.110
19.504	19.184	201.798
21.383	19.123	201.292
25.140	19.204	202.439
27.957	20.027	211.568
34.626	19.505	206.201
38.195	19.618	207.570
43.831	19.916	211.001
47.118	19.875	210.650
49.936	20.307	215.428
53.693	19.000	201.287
55.196	19.989	212.091
56.511	19.655	208.483

Run A-7
Disks
d = 0.750 s = 8.0

Re/1000	100xf	100xf$_D$
2.109	32.057	167.910
3.825	30.906	162.756
5.145	32.080	169.605
6.695	30.993	164.049
7.890	28.809	152.366
9.073	30.807	163.410
11.531	32.731	174.150
15.629	32.687	174.214
19.544	32.411	172.914
24.161	32.000	170.855
30.163	32.159	171.893
33.395	32.258	172.508
34.780	28.696	153.144
36.627	31.819	170.183
41.706	31.679	169.510
44.015	32.337	173.129
50.940	31.988	171.323
53.249	32.439	173.806
56.019	32.623	174.839

Run A-8
Disks
d = 0.875 s = 12.0

Re/1000	100xf	100xf$_D$
2.232	64.759	218.908
3.689	55.585	187.905
5.146	55.931	189.423
6.409	56.162	190.412
9.045	54.661	185.513
10.380	50.608	171.653
12.248	52.106	176.923
16.164	52.893	179.806
20.613	53.495	182.017
23.282	51.010	173.523
28.176	52.511	178.788
30.845	52.989	180.478
34.404	52.848	180.042
37.252	53.559	182.527
41.345	46.435	158.038
48.196	53.893	183.786
49.976	53.159	181.273

Run A-9
Disks
d = 0.875 s = 8.0

Re/1000	100xf	100xf$_D$
1.878	72.063	162.551
3.627	81.954	185.799
5.046	80.643	183.007
6.563	77.839	176.723
6.761	76.132	172.820
9.244	77.231	175.505
10.153	74.336	168.903
13.063	80.140	182.340
16.064	79.900	181.874
21.520	78.362	178.452
24.521	78.509	178.835
27.431	77.503	176.563
31.250	77.602	176.832
34.705	78.745	179.488
37.252	77.500	176.651
39.343	78.847	179.760
44.435	78.402	178.772
46.891	77.175	175.970

Run A-10
Disks
d = 0.875 s = 4.0

Re/1000	100xf	100xf$_D$
1.369	199.451	227.350
2.316	164.706	187.720
3.164	152.679	174.039
3.948	161.492	184.235
5.384	151.972	173.406
6.331	152.421	173.969
6.788	156.280	178.418
7.814	144.377	164.791
9.240	150.990	172.425
10.578	152.266	173.921
12.271	157.316	179.752
14.233	159.271	182.027
15.748	157.738	180.288
20.384	156.746	179.198
25.554	161.048	184.176
28.764	159.254	182.136
31.081	160.076	183.092
34.469	160.494	183.588
37.054	159.712	182.701
38.926	159.254	182.182
37.054	159.712	182.701

Run A-11
Disks
d = 0.625 s = 12.0

Re/1000	100xf	100xf$_D$
3.616	4.677	166.453
4.768	5.020	185.776
5.656	4.874	181.185
6.643	4.718	175.887
7.874	4.536	169.383
9.671	4.599	174.282
14.701	4.394	168.594
17.126	4.326	166.693
21.259	4.274	165.914
24.672	4.228	164.844
28.894	4.151	162.313
34.553	4.106	161.419
38.326	4.006	157.468
42.369	4.089	161.828
44.255	4.132	164.033
47.309	4.271	170.741
50.812	4.266	170.895
55.843	4.230	169.745

TABLE XI (CONT'D)

Run A-12 — Disks — d = 0.625, s = 8.0

Re/1000	100xf	$100xf_D$
3.706	6.692	172.495
5.116	6.729	176.416
5.944	6.428	168.446
6.403	6.332	166.085
7.336	6.212	163.416
8.256	6.288	166.538
9.763	6.172	164.098
11.771	6.298	169.066
13.696	6.267	168.985
16.207	7.629	211.322
21.312	6.078	165.499
26.082	6.003	164.138
26.919	6.088	166.862
30.852	5.986	164.340
35.706	5.929	163.199
40.309	6.198	171.853
43.405	6.648	185.820
47.422	6.121	170.113
50.686	6.110	170.016

Run A-13 — Disks — d = 0.625, s = 4.0

Re/1000	100xf	$100xf_D$
3.278	10.259	139.916
4.666	10.676	147.863
5.738	10.456	145.353
6.558	10.126	140.837
7.980	9.708	135.173
8.841	9.876	138.069
12.372	10.279	145.228
14.956	10.109	143.169
17.367	10.054	142.723
19.521	10.263	146.193
20.382	10.181	145.050
25.980	10.230	146.353
30.286	10.501	150.805
34.851	11.270	162.788
41.568	10.209	146.992
43.205	10.386	149.756
46.047	10.710	154.802
48.114	10.711	154.896
50.525	10.526	152.170
52.937	10.584	153.134

Run A-14 — Streamline Shapes — d = 0.625, s = 12.0

Re/1000	100xf	$100xf_D$
1.163	3.685	100.379
2.692	1.895	35.086
3.857	2.331	60.301
4.973	2.343	64.146
6.471	2.316	65.995
7.399	2.239	63.926
11.044	2.114	62.116
14.026	2.090	63.079
15.020	2.039	61.308
15.550	2.047	61.950
18.599	1.976	60.085
21.316	1.947	59.752
23.237	1.911	58.711
25.623	1.876	57.775
29.864	1.874	58.675
31.919	1.793	55.395
34.238	1.783	55.366
36.226	1.759	54.608
38.877	1.720	53.241
40.865	1.728	53.891

Run A-15 — Streamline Shapes — d = 0.625, s = 8.0

Re/1000	100xf	$100xf_D$
2.503	3.328	66.194
4.586	3.432	75.221
5.205	3.648	82.837
5.880	3.612	82.700
6.890	3.218	71.892
11.271	3.106	71.709
12.424	3.035	70.118
15.498	2.872	66.379
17.804	2.810	65.209
20.759	2.708	62.858
24.104	2.688	62.944
26.413	2.613	61.070
29.599	2.586	60.738
32.386	2.533	59.500
34.377	2.529	59.620
36.767	2.516	59.491
40.350	2.428	57.173
41.545	2.453	58.044
43.536	2.438	57.763
46.323	2.408	57.078
48.713	2.353	55.587

Run A-16 — Streamline Shapes — d = 0.625, s = 4.0

Re/1000	100xf	$100xf_D$
2.986	4.073	45.360
3.943	4.489	53.024
4.713	4.944	60.721
6.160	4.932	61.604
8.391	4.640	58.257
10.941	4.493	56.862
13.299	4.457	56.881
16.677	4.225	53.960
20.310	3.953	50.313
21.776	3.964	50.646
23.050	3.909	49.941
24.644	3.823	48.785
27.703	3.931	50.685
30.061	3.884	50.144
32.611	3.786	48.822
34.523	3.647	46.823
38.347	3.641	46.939

Run A-17 — Streamline Shapes — d = 0.750, s = 12.0

Re/1000	100xf	$100xf_D$
3.003	4.441	54.752
4.393	5.210	69.230
4.940	5.370	72.373
7.571	5.187	71.119
10.622	5.061	70.243
11.300	5.227	73.154
15.029	4.921	69.020
17.063	4.665	65.195
19.368	4.649	65.274
20.996	4.744	67.034
24.861	4.376	61.442
27.573	4.425	62.487
31.302	4.137	58.071
34.353	4.350	61.753
37.404	4.398	62.718
39.777	4.343	61.947
40.794	4.314	61.525

Run A-18 — Streamline Shapes — d = 0.750, s = 8.0

Re/1000	100xf	$100xf_D$
2.994	8.054	75.832
4.491	7.981	76.394
4.824	10.042	99.051
5.823	7.833	75.538
8.381	7.186	69.427
11.107	7.287	71.163
14.440	6.743	65.776
16.788	6.662	65.179
19.438	6.449	63.122
22.468	6.160	60.222
25.119	6.024	58.923
28.224	5.821	56.895
30.496	5.889	57.752
34.131	5.862	57.623
38.373	6.033	59.651
41.099	5.956	58.906
46.325	5.590	55.080

Run A-19 — Streamline Shapes — d = 0.750, s = 4.0

Re/1000	100xf	$100xf_D$
2.700	12.477	61.805
4.754	13.100	66.153
5.456	13.194	66.866
7.869	11.797	59.742
8.902	12.035	61.185
13.330	11.430	58.327
17.609	10.869	55.538
20.856	10.475	53.541
22.995	10.200	52.126
27.349	9.850	50.359
29.636	10.104	51.803
32.440	9.848	50.476
35.760	9.753	50.029
39.228	10.004	51.460
42.179	9.832	50.573
44.762	9.788	50.373

Run A-20 — Streamline Shapes — d = 0.875, s = 12.0

Re/1000	100xf	$100xf_D$
2.356	28.457	93.959
4.457	27.414	91.079
5.225	27.029	89.903
6.343	24.142	80.130
9.212	24.414	81.359
11.801	23.064	76.882
13.620	22.343	74.491
16.559	22.060	73.635
20.533	22.131	74.001
24.489	21.272	71.135
27.880	20.978	70.187
30.565	21.005	70.324
32.614	20.558	68.815
35.439	20.044	67.083
37.629	20.377	68.256
39.466	20.195	67.650
41.444	19.966	66.883

Run A-21 — Streamline Shapes — d = 0.875, s = 8.0

Re/1000	100xf	$100xf_D$
4.164	37.967	84.904
5.178	38.803	86.962
5.808	39.340	88.263
9.628	36.380	81.734
11.499	35.440	79.657
13.071	30.925	69.347
15.615	32.793	73.709
17.711	34.436	77.530
21.827	32.185	72.439
26.093	31.342	70.565
30.283	31.131	70.128
32.529	29.873	67.262
35.298	29.440	66.293
37.168	29.647	66.784
39.189	29.362	66.145
40.536	29.313	66.042
44.203	28.334	63.819

Run A-22 — Streamline Shapes — d = 0.875, s = 4.0

Re/1000	100xf	$100xf_D$
2.729	68.001	76.775
3.857	69.731	78.890
4.634	66.875	75.672
5.135	67.409	76.317
6.887	63.987	72.473
8.803	64.283	72.877
10.718	59.871	67.859
13.797	57.436	65.118
17.834	57.380	65.105
19.681	56.493	64.105
23.581	55.000	62.424
26.113	54.556	61.931
27.481	54.670	62.070
30.560	53.770	61.054
33.297	53.865	61.177
34.870	51.981	59.021
38.428	52.231	59.322
40.823	51.439	58.422

Run A-23 — Disks — d = 0.625, s = 2.0

Re/1000	100xf	$100xf_D$
3.129	13.473	94.285
4.024	14.405	101.969
5.291	15.713	112.496
6.830	14.695	105.240
8.866	17.087	123.879
11.308	16.514	119.900
12.326	15.732	114.079
15.515	16.313	118.815
17.687	17.889	130.970
22.504	17.089	125.177
24.336	16.729	122.529
26.286	17.496	128.447
29.334	17.540	128.900
31.919	17.103	125.665
33.244	17.963	132.247
35.298	18.383	135.501
36.557	18.607	137.239
39.208	18.265	134.706

TABLE XI (CONT'D)

Run A-24 Disks d = 0.875 s = 2.0 Re/1000	100xf	$100xf_D$	Run A-25 Disks d = 0.750 s = 2.0 Re/1000	100xf	$100xf_D$	Run A-26 Disks d = 0.750 s = 8.0 Re/1000	100xf	$100xf_D$
2.866	232.988	133.096	1.360	60.395	160.579	2.375	14.917	149.676
3.798	225.507	128.854	2.813	41.244	109.251	3.684	17.018	174.164
4.515	229.885	131.396	3.713	40.778	108.227	4.727	17.474	179.917
5.112	228.556	130.653	4.383	42.296	112.493	6.400	16.550	170.712
6.307	224.014	128.077	4.798	42.254	112.447	7.195	17.022	176.155
8.134	220.539	126.116	7.602	40.870	108.993	9.380	16.862	175.051
10.548	239.141	136.825	10.055	41.037	109.612	11.102	16.629	172.887
12.049	236.767	135.477	14.033	42.705	114.326	15.340	16.273	169.663
13.158	244.368	139.849	18.209	51.979	139.694	18.121	16.399	171.342
14.790	250.647	143.466	21.325	50.720	136.336	20.703	16.852	176.508
17.400	244.516	139.963	21.948	47.098	126.488	21.630	16.990	178.085
20.010	245.860	140.747	24.491	48.357	129.960	23.749	16.658	174.625
24.577	248.895	142.507	25.860	48.244	129.674	26.266	16.621	174.383
27.187	247.591	141.767	28.142	50.688	136.360	28.583	16.958	178.183
31.429	248.666	142.396	29.511	52.389	141.009	30.239	16.967	178.367
			33.357	53.776	144.830	32.887	16.932	178.110
			35.639	53.991	145.439	35.536	16.967	178.602
			40.529	50.990	137.314	38.847	17.089	180.055
						39.906	16.841	177.392

Run A-27 Plain Solid Rod d = 0.625 Re/1000	100xf	Run A-28 Plain Solid Rod d = 0.750 Re/1000	100xf
1.383	15.119	3.275	22.734
3.590	7.302	4.342	19.496
4.717	6.102	4.755	18.399
6.195	6.413	5.119	18.459
8.311	6.447	9.321	15.100
10.362	6.205	11.375	17.226
14.977	5.908	13.430	16.543
16.259	5.780	16.014	16.549
18.182	5.608	18.665	16.182
20.746	5.519	20.852	15.648
22.412	5.384	22.641	15.548
24.720	5.333	23.966	15.568
27.668	5.503	25.292	15.297
29.271	5.448	26.948	15.258
31.194	5.389	29.997	14.907
33.437	5.260	32.846	14.415
35.040	5.234	34.238	14.096
38.565	5.421	38.877	13.206

TABLE XII

INTEGRATED RESULTS FROM HEAT TRANSFER MEASUREMENTS

Run	Geometry	d	s	$\frac{Re}{1000}$	$\frac{q}{1000}$	h_0	h_m/h_0	(*)	T_{in}
P-1	EMPTY TUBE	0.000	--	49.854	9.276	1302.0	1.008	8.416	59.2
P-2	EMPTY TUBE	0.000	--	56.618	103.713	1518.1	1.038	8.876	59.7
P-3	EMPTY TUBE	0.000	--	51.059	37.575	1362.8	0.998	8.644	58.9
P-4	EMPTY TUBE	0.000	--	10.235	35.520	381.5	0.967	8.803	60.0
P-5	EMPTY TUBE	0.000	--	49.938	39.494	1355.1	0.980	8.749	56.9
P-6	EMPTY TUBE	0.000	--	23.886	39.432	760.3	0.962	8.863	57.8
P-7	EMPTY TUBE	0.000	--	37.604	39.337	1082.4	0.975	8.770	57.8
P-8	EMPTY TUBE	0.000	--	7.052	10.912	280.6	0.914	8.679	59.2
P-9	EMPTY TUBE	0.000	--	2.819	9.517	131.0	1.245	8.485	59.9
P-10	EMPTY TUBE	0.000	--	6.763	8.396	268.0	0.888	8.570	60.8
P-11	EMPTY TUBE	0.000	--	14.857	30.903	547.3	0.935	9.332	48.2
P-12	EMPTY TUBE	0.000	--	30.951	50.187	984.2	0.951	9.324	48.5
P-13	EMPTY TUBE	0.000	--	43.707	49.907	1305.1	0.947	9.378	45.8
P-14	EMPTY TUBE	0.000	--	43.689	52.765	1303.3	1.060	9.367	45.0
R-1-A	EMPTY TUBE	0.000	--	21.829	8.334	725.3	0.964	9.078	44.8
R-1-B	EMPTY TUBE	0.000	--	24.085	41.402	818.0	0.974	9.472	45.0
R-1-C	EMPTY TUBE	0.000	--	27.085	93.400	918.7	0.964	9.722	45.1
R-1-D	EMPTY TUBE	0.000	--	43.983	8.701	1227.7	0.952	8.772	50.4
R-1-E	EMPTY TUBE	0.000	--	45.532	47.221	1316.5	1.008	9.153	49.1
R-1-F	EMPTY TUBE	0.000	--	46.075	95.956	1386.4	1.017	9.560	46.0
R-1-G	EMPTY TUBE	0.000	--	10.179	42.003	413.0	0.903	9.588	45.4
R-1-H	EMPTY TUBE	0.000	--	8.501	10.685	346.6	0.887	9.228	46.3
R-1-I	EMPTY TUBE	0.000	--	5.622	7.593	245.3	0.848	9.091	49.2
R-2-A	SOLID ROD	0.250	0.0	40.907	10.502	1185.7	1.152	8.978	45.6
R-2-B	SOLID ROD	0.250	0.0	42.370	42.079	1257.9	1.120	9.264	45.2
R-2-C	SOLID ROD	0.250	0.0	45.245	94.776	1353.8	1.214	9.472	44.9
R-2-D	SOLID ROD	0.250	0.0	27.027	9.364	853.8	1.113	9.007	44.5
R-2-E	SOLID ROD	0.250	0.0	32.239	94.536	1032.9	1.162	9.495	45.9
R-2-F	SOLID ROD	0.250	0.0	16.477	9.217	574.2	1.074	9.000	46.8
R-2-G	SOLID ROD	0.250	0.0	19.966	66.561	696.8	1.068	9.411	47.4
R-2-H	SOLID ROD	0.250	0.0	8.765	13.330	352.2	0.911	9.154	48.2
R-2-I	SOLID ROD	0.250	0.0	5.270	7.702	232.5	0.778	9.080	49.8
R-3-A	SOLID ROD	0.125	0.0	49.745	36.026	1355.4	0.996	8.778	55.5
R-3-B	SOLID ROD	0.125	0.0	36.556	29.280	1068.7	0.963	8.856	54.0
R-3-C	SOLID ROD	0.125	0.0	23.372	23.848	747.4	0.967	8.859	54.5
R-3-D	SOLID ROD	0.125	0.0	9.202	8.956	349.2	0.832	8.725	56.8
R-3-E	SOLID ROD	0.125	0.0	6.326	6.753	258.1	0.754	8.702	58.2
R-5-A	DISKS	0.750	12.0	50.518	28.866	1337.7	1.598	8.556	57.4
R-5-B	DISKS	0.750	12.0	36.797	27.442	1045.9	1.683	8.622	56.0
R-5-C	DISKS	0.750	12.0	25.889	27.853	772.0	1.790	8.434	61.3
R-5-E	DISKS	0.750	12.0	7.007	7.774	267.6	2.072	8.319	62.5
R-6-D	DISKS	0.750	12.0	12.317	15.853	415.1	2.058	8.216	66.2
R-6-E	DISKS	0.750	12.0	6.910	11.342	260.3	2.095	8.188	66.6
R-7-A	DISKS	0.750	8.0	55.763	35.447	1382.6	2.020	8.172	67.5
R-7-B	DISKS	0.750	8.0	42.072	28.819	1106.8	2.008	8.197	66.8
R-7-C	DISKS	0.750	8.0	26.609	23.501	766.2	2.186	8.187	67.0
R-7-D	DISKS	0.750	8.0	11.170	12.067	379.9	2.428	8.131	67.5
R-7-E	DISKS	0.750	8.0	7.681	8.668	280.0	2.461	8.086	68.7
R-8-A	DISKS	0.750	4.0	54.345	38.632	1375.9	2.326	8.302	63.5
R-8-B	DISKS	0.750	4.0	42.285	31.139	1123.3	2.518	8.285	63.5
R-8-C	DISKS	0.750	4.0	26.744	24.177	776.9	2.681	8.268	63.7
R-8-D	DISKS	0.750	4.0	10.750	13.061	371.6	2.984	8.201	64.5
R-8-E	DISKS	0.750	4.0	7.089	8.877	265.0	3.045	8.163	64.9
R-9-A	DISKS	0.875	12.0	52.216	35.269	1321.0	2.170	8.230	65.7
R-9-B	DISKS	0.875	12.0	40.626	28.177	1078.9	2.253	8.217	66.0
R-9-C	DISKS	0.875	12.0	27.195	25.230	783.0	2.311	8.223	66.0
R-9-D	DISKS	0.875	12.0	12.068	13.536	406.7	2.545	8.183	66.2
R-9-E	DISKS	0.875	12.0	7.181	9.000	267.6	2.547	8.156	66.3
R-10-A	DISKS	0.875	8.0	48.655	35.721	1249.0	2.485	8.234	65.2
R-10-B	DISKS	0.875	8.0	37.349	30.612	1007.9	2.630	8.211	65.6
R-10-C	DISKS	0.875	8.0	26.487	25.011	766.2	2.755	8.217	65.3
R-10-D	DISKS	0.875	8.0	10.944	13.391	375.1	2.994	8.162	65.8
R-10-E	DISKS	0.875	8.0	7.087	9.084	264.3	3.114	8.143	65.8
R-11-A	DISKS	0.875	4.0	42.300	31.636	1130.0	3.404	8.332	62.5
R-11-B	DISKS	0.875	4.0	30.804	27.522	877.3	3.505	8.338	62.3
R-11-C	DISKS	0.875	4.0	21.200	22.149	651.0	3.686	8.344	61.9
R-11-D	DISKS	0.875	4.0	10.707	13.140	375.8	3.607	8.323	65.2
R-11-E	DISKS	0.875	4.0	7.035	9.100	267.3	3.781	8.282	62.8
R-12-B	DISKS	0.625	8.0	40.145	34.037	1095.0	1.677	8.420	62.1
R-12-C	DISKS	0.625	8.0	23.812	23.890	719.5	1.814	8.403	62.2
R-12-D	DISKS	0.625	8.0	10.678	13.666	374.5	1.962	8.310	64.0
R-12-E	DISKS	0.625	8.0	7.110	9.272	269.4	1.904	8.278	64.6
R-13-A	DISKS	0.625	12.0	55.363	36.550	1401.5	1.425	8.332	64.6
R-13-B	DISKS	0.625	12.0	40.521	30.052	1095.8	1.450	8.362	63.8
R-13-C	DISKS	0.625	12.0	25.811	23.622	765.4	1.478	8.380	63.6
R-13-D	DISKS	0.625	12.0	11.593	13.021	401.0	1.577	8.331	64.1
R-13-E	DISKS	0.625	12.0	7.144	8.815	271.1	1.603	8.298	64.5
R-14-A	DISKS	0.625	4.0	53.538	40.735	1387.9	1.979	8.476	59.9
R-14-B	DISKS	0.625	4.0	37.688	32.553	1045.5	2.130	8.456	59.9
R-14-C	DISKS	0.625	4.0	24.775	26.210	747.1	2.131	8.453	60.1
R-14-D	DISKS	0.625	4.0	9.242	13.465	337.1	2.491	8.397	60.6
R-14-E	DISKS	0.625	4.0	6.826	10.136	263.0	2.433	8.350	61.2
R-15-A	STREAMLINE	0.625	12.0	45.253	83.617	1351.9	1.224	9.454	45.3
R-15-B	STREAMLINE	0.625	12.0	34.088	80.290	1082.4	1.224	9.504	45.1
R-15-C	STREAMLINE	0.625	12.0	22.419	60.199	770.3	1.226	9.464	45.4
R-15-D	STREAMLINE	0.625	12.0	9.844	38.361	390.6	1.230	9.313	46.8
R-15-E	STREAMLINE	0.625	12.0	5.685	15.731	248.7	1.238	9.163	48.0
R-16-A	STREAMLINE	0.625	8.0	46.186	80.803	1342.9	1.297	9.238	48.7
R-16-B	STREAMLINE	0.625	8.0	33.811	58.650	1048.2	1.290	9.255	47.6
R-16-C	STREAMLINE	0.625	8.0	22.363	51.222	750.6	1.319	9.234	48.5
R-16-D	STREAMLINE	0.625	8.0	10.565	30.066	406.3	1.386	9.118	49.6
R-16-E	STREAMLINE	0.625	8.0	6.304	13.434	263.0	1.413	8.910	51.7
R-17-A	STREAMLINE	0.625	4.0	45.709	70.169	1336.0	1.440	9.265	47.7
R-17-B	STREAMLINE	0.625	4.0	33.758	57.388	1046.5	1.451	9.251	48.1
R-17-C	STREAMLINE	0.625	4.0	21.688	41.707	729.9	1.490	9.196	49.2
R-17-D	STREAMLINE	0.625	4.0	9.758	24.701	381.7	1.650	9.126	50.1
R-17-E	STREAMLINE	0.625	4.0	5.869	11.355	253.6	1.744	9.093	49.2
R-18-A	STREAMLINE	0.750	12.0	43.232	59.314	1276.1	1.516	9.251	45.6
R-18-B	STREAMLINE	0.750	12.0	32.102	45.603	1001.3	1.494	9.211	46.2
R-18-C	STREAMLINE	0.750	12.0	21.221	36.093	716.5	1.524	9.182	46.7
R-18-D	STREAMLINE	0.750	12.0	9.338	23.259	368.6	1.557	9.126	47.6
R-18-E	STREAMLINE	0.750	12.0	5.725	12.963	245.7	1.614	8.991	49.0
R-19-A	STREAMLINE	0.750	8.0	43.892	53.706	1284.7	1.680	9.200	45.5
R-19-B	STREAMLINE	0.750	8.0	31.087	50.185	976.1	1.745	9.215	45.9
R-19-C	STREAMLINE	0.750	8.0	21.470	45.695	721.8	1.859	9.171	46.9
R-19-D	STREAMLINE	0.750	8.0	10.424	26.618	397.6	2.102	9.015	48.0
R-19-E	STREAMLINE	0.750	8.0	6.154	13.198	258.4	2.021	8.925	49.1
R-20-A	STREAMLINE	0.750	4.0	47.222	68.788	1353.7	1.845	9.147	49.2
R-20-B	STREAMLINE	0.750	4.0	32.559	50.606	1005.1	1.899	9.145	48.9
R-20-C	STREAMLINE	0.750	4.0	20.862	45.749	706.9	2.001	9.195	48.6
R-20-D	STREAMLINE	0.750	4.0	10.683	26.098	410.4	2.105	9.123	49.2
R-20-E	STREAMLINE	0.750	4.0	5.981	12.576	255.3	2.156	9.023	50.1
R-21-A	STREAMLINE	0.875	12.0	43.288	63.426	1269.8	1.837	9.197	45.8
R-21-B	STREAMLINE	0.875	12.0	32.777	48.950	1012.3	1.880	9.160	45.9
R-21-C	STREAMLINE	0.875	12.0	20.209	31.325	681.6	1.948	9.082	46.7
R-21-D	STREAMLINE	0.875	12.0	10.223	23.464	390.8	2.129	8.995	48.2
R-21-E	STREAMLINE	0.875	12.0	5.718	13.436	242.1	2.166	8.874	49.4
R-22-A	STREAMLINE	0.875	8.0	42.932	56.576	1252.3	2.203	9.129	45.9
R-22-B	STREAMLINE	0.875	8.0	30.639	49.393	952.6	2.358	9.099	46.4
R-22-C	STREAMLINE	0.875	8.0	21.574	45.161	714.2	2.530	9.041	47.3
R-22-D	STREAMLINE	0.875	8.0	11.329	25.823	420.6	2.768	8.918	48.4
R-22-E	STREAMLINE	0.875	8.0	5.776	12.925	241.9	2.792	8.790	50.1
R-23-A	STREAMLINE	0.875	4.0	46.995	67.522	1319.8	3.453	8.954	51.3
R-23-B	STREAMLINE	0.875	4.0	32.127	47.401	987.3	3.390	9.080	48.2
R-23-C	STREAMLINE	0.875	4.0	21.488	46.467	719.5	3.454	9.141	47.7
R-23-D	STREAMLINE	0.875	4.0	11.019	28.048	419.0	3.426	9.093	48.2
R-23-E	STREAMLINE	0.875	4.0	5.677	13.612	242.3	3.538	8.941	49.9
R-24-A	DISKS	0.625	2.0	45.003	69.438	1343.8	2.052	9.438	42.7
R-24-B	DISKS	0.625	2.0	29.534	47.125	952.3	2.139	9.368	43.3
R-24-C	DISKS	0.625	2.0	17.632	36.518	629.1	2.106	9.359	44.1
R-24-D	DISKS	0.625	2.0	10.302	26.808	405.5	2.159	9.286	45.5
R-24-E	DISKS	0.625	2.0	5.725	13.481	250.1	2.341	9.157	47.1
R-25-A	DISKS	0.875	2.0	33.612	66.924	1073.1	4.177	9.526	41.5
R-25-B	DISKS	0.875	2.0	26.854	47.103	886.2	4.215	9.410	42.7
R-25-C	DISKS	0.875	2.0	18.163	40.272	641.4	4.087	9.324	44.6
R-25-D	DISKS	0.875	2.0	10.107	25.924	395.3	4.199	9.193	47.2
R-25-E	DISKS	0.875	2.0	6.019	13.221	257.7	4.301	9.065	48.9
R-26-A	DISKS	0.750	2.0	43.890	62.657	1290.2	2.520	9.244	45.5
R-26-B	DISKS	0.750	2.0	32.324	51.167	1002.0	2.629	9.172	46.8
R-26-C	DISKS	0.750	2.0	18.592	47.713	643.0	2.846	9.182	47.8
R-26-D	DISKS	0.750	2.0	11.048	27.998	420.0	2.850	9.096	48.6
R-26-E	DISKS	0.750	2.0	6.158	13.397	259.8	2.970	8.972	50.1
R-27-A	DISKS	0.750	8.0	41.630	55.134	1234.5	2.093	9.223	44.1
R-27-B	DISKS	0.750	8.0	31.151	60.673	987.5	2.060	9.312	43.5
R-27-C	DISKS	0.750	8.0	18.330	43.113	645.3	2.270	9.307	42.8
R-27-D	DISKS	0.750	8.0	10.275	26.823	402.0	2.337	9.218	43.1
R-27-E	DISKS	0.750	8.0	5.408	13.028	236.9	2.488	9.078	44.5
R-28-A	SOLID ROD	0.625	0.0	43.995	80.223	1291.2	1.718	9.235	44.6
R-28-B	SOLID ROD	0.625	0.0	32.903	69.404	1022.5	1.664	9.231	44.8
R-28-C	SOLID ROD	0.625	0.0	18.813	52.291	654.0	1.539	9.246	45.1
R-28-D	SOLID ROD	0.625	0.0	11.100	37.947	432.0	1.321	9.333	44.1
R-28-E	SOLID ROD	0.625	0.0	5.918	15.391	265.3	0.825	9.462	44.9
R-29-A	SOLID ROD	0.750	0.0	44.201	85.710	1271.4	2.470	9.061	45.2
R-29-B	SOLID ROD	0.750	0.0	34.287	75.702	1036.2	2.379	9.052	45.4
R-29-C	SOLID ROD	0.750	0.0	21.335	54.031	703.7	2.248	8.992	46.4
R-29-D	SOLID ROD	0.7[illegible]	0.0	12.098	39.175	444.4	1.963	8.958	47.2
R-29-E	SOLID ROD	0.750	0.0	6.415	22.352	269.2	1.287	9.025	48.8

(*) Integrated mean value of $(\mu/\mu_w)^{0.14}\ Pr^{1/3}\ (k/D)$

q is in units of (BTU/hr-ft^2)

T_{in} is the inlet water temperature in deg F

TABLE XIII

LOCAL HEAT TRANSFER MEASUREMENTS

RUN	EMPTY TUBE P-1	P-2	P-3	P-4	P-5	P-6	P-7	P-8	P-9	P-10	P-11	P-12
Z	H/HO	H/HO	H/HO	H/HO	H/HO	H/HO	H/HO	H/HO	H/HO	H/HO	H/HO	H/HO
1.49	1.105	1.103	1.074	1.160	1.071	1.099	1.083	1.178	0.851	1.155	1.118	1.061
5.41	1.061	1.044	1.029	0.950	1.015	0.977	0.994	0.972	1.076	0.911	0.957	0.972
9.42	1.034	1.040	1.021	0.909	1.004	0.962	0.991	0.924	1.267	0.889	0.932	0.962
13.40	1.021	1.030	1.007	0.908	0.990	0.953	0.980	0.909	1.254	0.881	0.922	0.952
17.41	1.021	1.030	0.999	0.912	0.984	0.952	0.978	0.904	1.152	0.878	0.919	0.952
22.17	1.031	1.040	1.005	0.932	0.985	0.958	0.978	0.901	1.162	0.877	0.926	0.957
25.34	1.035	1.015	1.007	0.944	0.990	0.959	0.982	0.901	1.179	0.881	0.930	0.959
29.32	1.028	1.052	1.008	0.957	0.988	0.964	0.985	0.909	1.217	0.891	0.938	0.959
33.30	1.022	1.053	1.013	0.976	0.993	0.972	0.990	0.921	1.244	0.896	0.942	0.965
37.28	1.009	1.047	0.997	0.987	0.982	0.971	0.979	0.922	1.258	0.892	0.943	0.953
41.20	0.991	1.063	1.006	1.005	0.991	0.980	0.986	0.932	1.285	0.898	0.952	0.961
45.27	0.973	1.036	0.985	1.004	0.966	0.964	0.964	0.929	1.294	0.892	0.945	0.943
49.22	0.985	1.052	0.995	1.026	0.978	0.976	0.971	0.941	1.337	0.904	0.956	0.957
53.26	0.985	1.049	0.985	1.032	0.967	0.967	0.966	0.924	1.330	0.902	0.955	0.949
57.28	0.998	1.071	0.999	1.053	0.978	0.986	0.980	0.942	1.367	0.915	0.971	0.962
62.47	0.971	1.108	1.023	1.098	1.000	1.014	1.003	0.981	1.447	0.951	1.001	0.994

RUN	EMPTY TUBE P-13	P-14	R-1-A	R-1-B	R-1-C	R-1-D	R-1-E	R-1-F	R-1-G	R-1-H	R-1-I
Z	H/HO	H/HO	H/HO	H/HO	H/HO	H/HO	H/HO	H/HO	H/HO	H/HO	H/HO
1.49	1.035	1.135	1.072	1.129	1.116	1.065	1.107	1.115	1.142	1.092	1.131
5.41	0.984	1.076	1.009	0.998	0.959	1.013	1.044	1.031	0.922	0.943	0.932
9.42	0.974	1.066	0.988	0.977	0.937	0.994	1.025	1.021	0.866	0.901	0.876
13.40	0.962	1.055	0.988	0.970	0.936	0.994	1.019	1.013	0.847	0.886	0.850
17.41	0.957	1.054	0.974	0.974	0.941	0.971	1.015	1.013	0.855	0.883	0.843
22.17	0.955	1.060	0.969	0.975	0.953	0.953	1.014	1.021	0.866	0.879	0.841
25.34	0.956	1.066	0.974	0.978	0.958	0.963	1.015	1.023	0.878	0.885	0.845
29.32	0.959	1.066	0.984	0.981	0.965	0.976	1.018	1.023	0.891	0.888	0.850
33.30	0.959	1.070	0.974	0.993	0.984	0.954	1.027	1.041	0.915	0.892	0.850
37.28	0.951	1.065	0.964	0.979	0.978	0.956	1.011	1.025	0.921	0.890	0.857
41.20	0.950	1.066	0.955	0.990	0.996	0.937	1.019	1.040	0.945	0.896	0.856
45.27	0.929	1.057	0.936	0.965	0.972	0.913	0.984	1.002	0.939	0.885	0.848
49.22	0.944	1.071	0.945	0.976	0.987	0.924	0.995	1.014	0.960	0.900	0.860
53.26	0.936	1.067	0.960	0.982	1.000	0.942	1.003	1.026	0.973	0.901	0.858
57.28	0.947	1.074	0.954	0.994	1.016	0.941	1.014	1.038	0.992	0.910	0.864
62.47	0.975	1.106	0.909	1.019	1.055	0.911	1.042	1.077	1.034	0.907	0.876

THREADED ROD IN CENTER D = 0.250

RUN	R-2-A	R-2-B	R-2-C	R-2-D	R-2-E	R-2-F	R-2-G	R-2-H	R-2-I
Z	H/HO	H/HO	H/HO	H/HO	H/HO	H/HO	H/HO	H/HO	H/HO
1.49	1.265	1.226	1.277	1.175	1.264	1.146	1.234	1.163	1.180
5.41	1.201	1.141	1.191	1.136	1.113	1.078	1.021	0.939	0.861
9.42	1.153	1.119	1.183	1.130	1.109	1.054	0.995	0.866	0.764
13.40	1.187	1.111	1.190	1.119	1.120	1.080	1.007	0.870	0.733
17.41	1.168	1.110	1.200	1.123	1.138	1.080	1.033	0.884	0.736
22.17	1.162	1.117	1.222	1.121	1.164	1.086	1.064	0.901	0.753
25.34	1.165	1.123	1.221	1.143	1.172	1.097	1.076	0.911	0.768
29.32	1.219	1.142	1.249	1.173	1.199	1.135	1.107	0.937	0.799
33.30	1.358	1.418	1.531	1.400	1.542	1.444	1.531	1.518	1.487
37.28	1.176	1.164	1.274	1.197	1.259	1.162	1.209	1.149	1.101
41.20	1.130	1.136	1.243	1.141	1.201	1.073	1.121	0.985	0.907
45.27	1.138	1.123	1.231	1.093	1.189	1.071	1.103	0.950	0.829
49.22	1.140	1.135	1.245	1.103	1.207	1.071	1.128	0.950	0.819
53.26	1.127	1.127	1.227	1.102	1.193	1.061	1.122	0.945	0.815
57.28	1.133	1.133	1.238	1.091	1.211	1.073	1.145	0.962	0.830
62.47	1.125	1.185	1.324	1.066	1.296	1.064	1.224	1.006	0.878

PLAIN ROD IN CENTER D = 0.125 / DISKS S = 12.0 D = 0.750

RUN	R-3-A	R-3-B	R-3-C	R-3-D	R-3-E	R-5-	A	B	C	D	E
Z	H/HO	H/HO	H/HO	H/HO	H/HO	X	H/HO	H/HO	H/HO		H/HO
1.49	1.076	1.097	1.117	1.092	1.078	0.00	1.192	1.161	1.208		1.197
5.41	1.022	0.993	0.971	0.897	0.836	0.00	1.107	1.054	1.047		0.894
9.42	1.013	0.979	0.965	0.859	0.791	0.00	1.081	1.025	1.036		0.859
13.40	1.002	0.955	0.957	0.834	0.749	0.00	1.047	1.001	1.010		0.842
17.41	0.995	0.949	0.951	0.826	0.738	0.00	2.313	2.002	2.069		2.284
22.17	1.008	0.959	0.965	0.835	0.742	3.77	1.674	1.841	1.958		2.291
25.34	1.008	0.961	0.966	0.835	0.744	6.94	1.331	1.435	1.510		1.635
29.32	1.008	0.969	0.974	0.833	0.745	0.96	2.483	2.237	2.395		2.766
33.30	1.005	0.966	0.970	0.828	0.751	4.94	1.613	1.852	1.966		2.402
37.28	0.990	0.961	0.965	0.825	0.752	8.92	1.273	1.392	1.441		1.598
41.20	1.002	0.972	0.976	0.837	0.766	0.84	2.503	2.266	2.358		2.640
45.27	0.978	0.959	0.963	0.828	0.758	4.91	1.503	1.696	1.875		2.326
49.22	0.989	0.970	0.978	0.842	0.770	8.86	1.232	1.372	1.465		1.603
53.26	0.995	0.980	0.984	0.852	0.785	0.96	3.040	2.877	3.087		3.281
57.28	0.999	0.989	0.992	0.854	0.789	4.98	1.406	1.384	1.503		1.620
62.47	1.041	1.014	1.020	0.884	0.813	10.17	1.188	1.223	1.317		1.256

Note: This table was prepared directly from IBM cards, making it necessary to use all upper case letters. The term H/HO in the Table refers to h/h_0; the symbol D in the table refers to d; and the symbol S in the table refers to s.

TABLE XIII (CONT'D)

RUN Z	DISKS S = 12.0 D = 0.750 X	R-6-D H/HO	R-6-E H/HO	DISKS S = 8.0 D = 0.750 R-7- X	A H/HO	B H/HO	C H/HO	D H/HO	E H/HO
1.49	0.00	1.177	1.175	0.00	1.130	1.117	1.145	1.134	1.125
5.41	0.00	0.961	0.906	0.00	1.053	1.030	1.016	0.944	0.915
9.42	0.00	0.939	0.864	0.00	1.055	1.026	1.016	0.929	0.893
13.40	0.16	2.037	2.191	0.78	2.083	2.251	2.458	2.587	2.653
17.41	4.17	2.495	2.599	4.79	1.667	1.594	1.708	2.006	2.112
22.17	8.93	1.687	1.749	1.59	2.472	2.643	2.848	2.932	2.950
25.34	0.16	2.524	2.657	4.76	1.680	1.617	1.724	1.927	1.987
29.32	4.14	2.660	2.683	0.78	2.300	2.472	2.749	2.957	3.057
33.30	8.12	1.724	1.753	4.76	1.718	1.662	1.786	1.990	2.054
34.30	9.12	1.555	1.577	5.76	1.601	1.571	1.654	1.727	1.775
35.30	10.12	1.459	1.464	6.76	2.456	2.502	2.761	3.103	3.107
36.29	11.11	1.316	1.306	7.75	2.264	2.213	2.325	2.545	2.610
37.28	0.16	2.773	2.810	0.78	2.341	2.405	2.742	3.010	3.013
38.28	1.16	2.287	2.400	1.78	2.267	2.289	2.536	2.925	2.884
39.28	2.16	2.836	2.898	2.78	2.138	2.054	2.286	2.640	2.668
40.28	3.16	2.694	2.742	3.78	1.978	1.872	2.031	2.389	2.407
41.20	4.08	2.553	2.558	4.70	1.898	1.812	1.943	2.167	2.238
45.27	8.15	1.680	1.735	0.81	1.967	1.899	2.152	2.613	2.618
49.22	0.16	1.873	1.908	4.76	1.405	1.384	1.460	1.523	1.525
53.26	4.20	1.812	1.950	0.84	1.884	1.858	1.996	2.014	1.988
57.28	8.22	1.420	1.405	4.86	1.295	1.282	1.359	1.373	1.372
62.47	13.41	1.195	1.152	10.05	1.275	1.220	1.254	1.229	1.205
34.30*	9.12	1.618	1.661	5.76	1.765	1.670	1.775	1.926	1.955
36.29*	11.11	1.401	1.431	7.75	3.280	3.217	3.262	3.232	3.234
39.28*	2.16	2.608	2.665	2.78	2.572	2.684	2.980	3.173	3.153
34.30+	9.12	1.486	1.552	5.76	1.524	1.520	1.633	1.735	1.826
36.29+	11.11	1.323	1.364	7.75	2.374	2.124	1.969	2.143	2.220
39.28+	2.16	1.761	1.863	2.78	2.443	2.508	2.622	2.937	2.890

RUN Z	DISKS S = 4.0 D = 0.750 R-8- X	A H/HO	B H/HO	C H/HO	D H/HO	E H/HO	DISKS S = 12.0 D = 0.875 R-9- X	A H/HO	B H/HO	C H/HO	D H/HO	E H/HO
1.49	0.00	1.142	1.140	1.152	1.162	1.110	0.00	1.154	1.151	1.154	1.159	1.122
5.41	0.00	1.073	1.056	1.032	0.965	0.906	0.00	1.083	1.060	1.033	0.973	0.898
9.42	0.00	1.506	1.475	1.570	1.815	1.911	0.00	1.070	1.048	1.024	0.948	0.861
13.40	3.82	2.486	2.685	2.825	3.376	3.526	0.00	1.783	1.837	1.827	2.109	2.202
17.41	3.85	2.432	2.682	2.868	3.262	3.290	3.79	2.665	2.838	1.749	3.339	3.315
22.17	0.59	3.038	3.078	3.025	3.079	3.105	8.55	1.791	1.708	2.929	1.882	1.934
25.34	3.76	2.170	2.460	2.605	2.912	2.976	11.72	1.975	2.059	2.118	2.600	2.718
29.32	3.82	2.358	2.658	2.816	3.262	3.376	3.76	2.656	2.830	2.921	3.386	3.369
33.30	3.82	2.427	2.762	2.909	3.290	3.401	7.74	1.727	1.625	1.739	1.918	2.030
34.30	0.84	2.383	2.665	2.734	2.989	3.027	8.74	1.540	1.499	1.565	1.619	1.689
35.30	1.84	2.277	2.559	2.728	3.039	2.996	9.74	1.461	1.430	1.467	1.504	1.498
36.29	2.83	2.070	2.168	2.353	2.620	2.598	10.73	1.364	1.353	1.354	1.397	1.377
37.28	3.82	2.411	2.788	3.029	3.488	3.628	11.72	2.222	2.331	2.400	2.834	2.912
38.28	0.91	2.169	2.337	2.502	2.819	2.863	0.78	2.319	2.443	2.338	2.486	2.454
39.28	1.91	2.168	2.352	2.614	2.905	2.909	1.78	2.706	2.895	2.934	3.227	3.153
40.28	2.91	2.014	2.065	2.280	2.533	2.542	2.78	2.831	3.052	3.168	3.511	3.438
41.20	3.83	2.294	2.533	2.744	3.089	3.235	3.70	2.819	3.062	3.127	3.511	3.455
45.27	0.93	2.247	2.461	2.798	3.281	3.531	7.77	1.638	1.611	1.724	1.836	1.904
49.22	4.88	1.927	1.919	2.155	2.547	2.677	11.72	1.795	1.737	1.891	2.066	2.146
53.26	3.95	1.820	1.841	1.960	2.290	2.414	3.82	2.063	1.959	2.169	2.607	2.631
57.28	3.99	1.375	1.409	1.448	1.505	1.509	7.84	1.628	1.609	1.696	1.751	1.739
62.47	9.18	1.248	1.248	1.234	1.215	1.206	13.03	1.319	1.281	1.278	1.257	1.217
34.30*	0.84	3.603	3.629	3.466	3.436	3.421	8.74	1.654	1.572	1.644	1.686	1.755
36.29*	2.83	2.298	2.546	2.596	2.771	2.785	10.73	1.537	1.476	1.488	1.476	1.455
39.28*	1.91	3.531	3.641	3.445	3.423	3.430	1.78	4.999	4.426	4.102	4.097	3.811
34.30+	0.84	2.658	2.828	2.698	2.641	2.646	8.74	1.458	1.442	1.492	1.548	1.589
36.29+	2.83	2.073	2.168	2.334	2.555	2.577	10.73	1.347	1.324	1.353	1.405	1.403
39.28+	1.91	44444	2.792	2.657	2.601	2.586	1.78	3.643	3.416	3.246	3.141	2.978

RUN Z	DISKS S = 8.0 D = 0.875 R-10 X	A H/HO	B H/HO	C H/HO	D H/HO	E H/HO	DISKS S = 4.0 D = 0.875 R-11- X	A H/HO	B H/HO	C H/HO	D H/HO	E H/HO
1.49	0.00	1.152	1.163	1.163	1.150	1.128	0.00	1.123	1.141	1.151	1.109	1.114
5.41	0.00	1.074	1.070	1.043	0.948	0.913	0.00	1.033	1.030	0.998	0.921	0.882
9.42	0.00	1.080	1.071	1.042	0.927	0.880	0.00	1.030	1.023	0.988	0.894	0.845
13.40	1.90	2.878	3.030	3.038	3.027	3.147	0.00	1.017	1.011	0.979	0.882	0.827
17.41	5.91	2.040	2.196	2.396	2.684	2.888	0.00	2.163	2.284	2.422	2.562	2.763
22.17	2.71	3.601	3.742	3.703	3.663	3.764	0.72	4.539	4.489	4.518	4.192	4.317
25.34	5.88	1.964	2.018	2.167	2.441	2.504	3.89	3.052	3.257	3.532	3.578	3.680
29.32	1.90	2.800	3.073	3.183	3.299	3.484	3.89	3.851	4.028	4.446	4.608	4.849
33.30	5.88	2.109	2.152	2.276	2.573	2.655	3.89	3.449	3.501	3.753	3.836	4.147
34.30	6.88	1.902	1.936	1.927	2.180	2.251	0.91	2.976	3.007	3.097	2.918	3.037
35.30	7.88	2.593	2.622	2.848	3.237	3.432	1.91	3.358	3.497	3.682	3.525	3.697
36.29	0.91	2.797	2.986	3.030	2.957	3.037	2.90	3.162	3.335	3.564	3.645	3.792
37.28	1.90	2.742	3.014	3.198	3.328	3.476	3.89	3.548	3.570	3.822	4.092	4.448
38.28	2.90	2.644	2.951	3.207	3.524	3.563	0.91	3.071	3.164	3.295	3.184	3.311
39.28	3.90	2.474	2.674	2.920	3.303	3.373	1.91	3.238	3.408	3.670	3.597	3.754
40.28	4.90	2.291	2.367	2.545	2.928	3.043	2.91	2.906	3.055	3.261	3.283	3.475
41.20	5.82	2.162	2.204	2.238	2.570	2.718	3.83	3.324	3.516	3.778	3.861	4.183
45.27	1.93	2.353	2.479	2.693	3.121	3.346	3.92	3.590	3.953	4.415	4.601	5.021
49.22	5.88	1.928	2.060	2.088	2.368	2.528	3.89	2.224	2.394	2.631	2.686	2.822
53.26	1.96	2.176	2.297	2.383	3.052	3.214	7.93	1.456	1.507	1.566	1.539	1.559
57.28	5.98	1.734	1.766	1.777	1.869	1.885	11.95	1.233	1.263	1.262	1.218	1.221
62.47	11.17	1.329	1.327	1.309	1.320	1.368	17.14	1.206	1.213	1.187	1.094	1.071
34.30*	6.88	1.996	2.029	2.055	2.343	2.414	0.91	5.161	5.038	5.086	4.570	4.667
36.29*	0.91	5.218	5.343	4.910	4.742	4.699	2.90	3.549	3.654	3.880	3.801	3.976
39.28*	3.90	3.405	3.773	3.788	4.010	4.015	1.91	5.819	5.711	5.875	5.369	5.492
34.30+	6.88	1.760	1.820	1.835	2.101	2.229	0.91	4.361	4.434	4.595	4.232	4.340
36.29+	0.91	4.344	4.520	4.332	4.307	4.324	2.90	3.016	3.209	3.440	3.464	3.641
39.28+	3.90	3.090	3.461	3.607	3.869	3.926	1.91	4.769	4.880	5.160	4.878	5.093

RUN Z	DISKS S = 8.0 D = 0.625 R-12- X	B H/HO	C H/HO	D H/HO	E H/HO	DISKS S = 12.0 D = 0.625 R-13- X	A H/HO	B H/HO	C H/HO	D H/HO	E H/HO
1.49	0.00	1.118	1.141	1.147	1.082	0.00	1.124	1.114	1.126	1.121	1.108
5.41	0.00	1.041	1.004	0.940	0.869	0.00	1.049	1.023	1.005	0.948	0.891
9.42	0.00	1.032	1.004	0.920	0.842	0.00	1.049	1.026	1.003	0.930	0.858
13.40	1.90	1.944	2.152	2.259	2.164	0.00	1.348	1.358	1.375	1.572	1.639
17.41	5.91	1.442	1.469	1.585	1.564	3.17	1.523	1.523	1.606	1.842	1.857
22.17	2.77	1.963	2.184	2.233	2.110	7.93	1.528	1.445	1.430	1.464	1.475
25.34	5.94	1.420	1.456	1.514	1.488	11.10	1.489	1.472	1.487	1.675	1.738
29.32	1.90	2.081	2.405	2.530	2.379	3.14	1.507	1.530	1.521	1.782	1.839
33.30	5.88	1.421	1.480	1.548	1.481	7.12	1.265	1.255	1.300	1.338	1.340
34.30	6.88	1.367	1.408	1.464	1.385	8.12	1.240	1.215	1.266	1.299	1.286
35.30	7.88	1.959	2.285	2.533	2.433	9.12	1.265	1.220	1.263	1.274	1.255
36.29	0.91	1.930	2.117	2.343	2.307	10.11	1.204	1.163	1.204	1.212	1.187
37.28	1.90	1.924	2.179	2.401	2.280	11.10	1.451	1.447	1.509	1.586	1.598
38.28	2.90	1.702	1.782	2.055	2.007	0.16	2.023	2.071	2.249	2.168	2.150
39.28	3.90	1.539	1.599	1.761	1.748	1.16	1.563	1.765	1.606	1.972	2.089
40.28	4.90	1.451	1.521	1.638	1.583	2.16	1.489	1.605	1.556	1.811	1.918
41.20	5.82	1.452	1.509	1.585	1.509	3.08	1.478	1.531	1.527	1.654	1.757
45.27	1.99	1.720	1.821	2.093	2.212	7.15	1.197	1.179	1.231	1.290	1.289
49.22	5.94	1.283	1.329	1.394	1.336	11.10	1.359	1.334	1.432	1.436	1.414
57.28	5.98	1.185	1.191	1.216	1.194	7.22	1.128	1.186	1.109	1.116	1.141
53.26	1.96	1.644	1.714	1.780	1.642	3.20	1.210	1.350	1.213	1.264	1.281
62.47	11.17	1.180	1.156	1.134	1.085	12.41	1.171	1.152	1.115	1.080	1.054
34.30*	6.88	1.479	1.490	1.541	1.487	8.12	1.323	1.293	1.333	1.356	1.345
36.29*	0.91	1.908	1.831	1.889	1.874	10.11	1.317	1.273	1.287	1.289	1.260
39.28*	3.90	1.918	2.060	2.240	2.134	1.16	1.721	1.786	1.619	1.855	1.858
34.30+	6.88	1.357	1.409	1.481	1.410	8.12	1.219	1.222	1.242	1.285	1.281
36.29+	0.91	1.533	1.410	1.455	1.400	10.11	1.183	1.167	1.177	1.224	1.218
39.28+	3.90	1.762	1.778	1.881	1.794	1.16	1.196	1.220	1.145	1.263	1.300

TABLE XIII (CONT'D)

RUN Z	R-14- X	A H/HO	B H/HO	C H/HO	D H/HO	E H/HO	R-15- X	A H/HO	B H/HO	C H/HO	D H/HO	E H/HO
1.49	0.00	1.123	1.203	1.140	1.210	1.132	0.00	1.151	1.150	1.161	1.140	1.105
5.41	0.00	1.050	1.137	1.006	1.005	0.900	0.00	1.064	1.026	0.992	0.912	0.843
9.42	0.00	1.080	1.167	1.056	1.042	0.935	0.00	1.074	1.039	0.993	0.868	0.812
13.40	3.76	1.747	1.988	1.986	2.273	2.135	0.28	1.109	1.115	1.122	1.056	1.017
17.41	3.79	2.005	2.290	2.386	2.816	2.725	4.29	1.170	1.165	1.176	1.195	1.242
22.17	0.59	2.577	2.550	2.408	2.525	2.400	9.05	1.295	1.254	1.195	1.100	1.054
25.34	3.76	1.731	1.917	2.150	2.544	2.448	0.28	1.184	1.196	1.208	1.187	1.164
29.32	3.76	1.881	2.198	2.471	2.947	2.890	4.26	1.204	1.205	1.220	1.271	1.316
33.30	3.76	1.842	2.025	2.314	2.769	2.734	8.24	1.128	1.101	1.073	1.030	1.011
34.30	0.78	2.199	2.538	2.373	2.723	2.641	9.24	1.109	1.082	1.049	0.992	0.962
35.30	1.78	1.914	2.070	2.107	2.462	2.372	10.24	1.147	1.118	1.076	1.004	0.955
36.29	2.77	1.691	1.727	1.786	2.170	2.086	11.23	1.135	1.116	1.082	1.014	0.968
37.28	3.76	1.868	2.048	2.333	2.840	2.745	0.28	1.384	1.384	1.389	1.376	1.336
38.28	0.78	1.996	2.286	2.248	2.690	2.691	1.28	1.660	1.727	1.816	1.909	1.994
39.28	1.78	1.779	1.860	1.859	2.287	2.290	2.28	1.356	1.404	1.471	1.601	1.725
40.28	2.78	1.620	1.646	1.657	1.994	1.962	3.28	1.262	1.293	1.339	1.441	1.527
41.20	3.70	1.806	1.870	1.976	2.435	2.332	4.20	1.258	1.268	1.288	1.352	1.403
45.27	3.79	1.771	1.829	1.915	2.434	2.455	8.27	1.107	1.092	1.079	1.061	1.043
49.22	3.76	1.655	1.756	1.758	2.139	2.170	0.28	1.395	1.415	1.441	1.401	1.305
53.26	3.82	1.609	1.707	1.674	1.905	1.877	4.32	1.170	1.180	1.207	1.291	1.327
57.28	3.86	1.343	1.385	1.283	1.416	1.358	8.34	1.122	1.107	1.092	1.081	1.049
62.47	9.05	1.237	1.239	1.144	1.175	1.092	13.53	1.144	1.131	1.113	1.096	1.017
34.30*	0.78	2.419	2.507	2.256	2.391	2.305	9.24	1.196	1.158	1.111	1.037	1.004
36.29*	2.77	1.884	1.939	1.995	2.303	2.242	11.23	1.266	1.240	1.193	1.109	1.060
39.28*	1.78	2.314	2.481	2.285	2.423	2.320	1.28	1.764	1.791	1.831	1.836	1.852
34.30+	0.78	1.914	1.921	1.761	1.884	1.815	9.24	1.122	1.108	1.073	1.018	0.975
36.29+	2.77	1.719	1.719	1.789	2.104	2.016	11.23	1.137	1.130	1.109	1.063	1.017
39.28+	1.78	1.884	1.886	1.729	1.849	1.782	1.28	1.516	1.560	1.619	1.676	1.704

STREAMLINE S = 12.0 D = 0.750 (R-18); STREAMLINE S = 8.0 D = 0.750 (R-19)

RUN Z	R-18- X	A H/HO	B H/HO	C H/HO	D H/HO	E H/HO	R-19- X	A H/HO	B H/HO	C H/HO	D H/HO	E H/HO
1.49	0.00	1.193	1.175	1.183	1.165	1.139	0.00	1.192	1.184	1.213	1.281	1.144
5.41	0.00	1.114	1.077	1.033	0.946	0.883	0.00	1.122	1.076	1.051	1.054	0.911
9.42	0.00	1.105	1.062	1.014	0.879	0.826	0.00	1.115	1.068	1.032	0.997	0.849
13.40	0.47	1.851	1.809	1.866	1.724	1.644	2.71	2.075	2.103	2.297	2.547	2.523
17.41	4.48	1.400	1.421	1.486	1.554	1.635	6.72	1.264	1.261	1.293	1.439	1.376
22.17	9.24	1.170	1.141	1.121	1.088	1.117	3.52	1.886	2.016	2.212	2.597	2.484
25.34	0.47	2.000	1.915	1.951	1.905	1.949	6.69	1.256	1.251	1.293	1.426	1.325
29.32	4.45	1.446	1.455	1.506	1.607	1.682	2.71	1.869	1.990	2.141	2.417	2.448
33.30	8.43	1.195	1.161	1.141	1.110	1.126	6.69	1.248	1.239	1.268	1.396	1.310
34.30	9.43	1.174	1.137	1.102	1.055	1.057	7.69	1.274	1.265	1.294	1.424	1.339
35.30	10.43	1.190	1.145	1.104	1.039	1.029	0.73	1.955	2.058	2.155	2.370	2.263
36.29	11.42	1.253	1.220	1.190	1.126	1.124	1.72	2.304	2.367	2.576	2.769	2.637
37.28	0.47	2.072	1.953	1.968	1.993	2.028	2.71	1.941	2.083	2.256	2.530	2.515
38.28	1.47	2.287	2.309	2.467	2.509	2.604	3.71	1.635	1.696	1.827	2.155	2.097
39.28	2.47	1.901	1.921	2.088	2.315	2.550	4.71	1.421	1.456	1.541	1.786	1.682
40.28	3.47	1.632	1.677	1.761	1.967	2.108	5.71	1.328	1.344	1.400	1.598	1.464
41.20	4.39	1.477	1.500	1.573	1.707	1.799	6.63	1.275	1.278	1.321	1.487	1.390
45.27	8.46	1.173	1.148	1.137	1.138	1.168	2.74	1.871	1.983	2.139	2.529	2.467
49.22	0.47	1.871	1.828	1.813	1.761	1.735	6.69	1.265	1.265	1.301	1.478	1.368
53.26	4.51	1.457	1.474	1.541	1.658	1.718	2.77	1.891	1.961	2.109	2.476	2.342
57.28	8.53	1.232	1.206	1.203	1.205	1.229	6.79	1.301	1.302	1.344	1.527	1.403
62.47	13.72	1.238	1.184	1.146	1.078	1.055	11.98	1.251	1.216	1.209	1.271	1.103
34.30*	9.43	1.253	1.203	1.162	1.099	1.098	7.69	1.370	1.344	1.358	1.471	1.359
36.29*	11.42	1.411	1.367	1.336	1.259	1.248	1.72	2.316	2.326	2.448	2.503	2.397
39.28*	1.47	2.344	2.323	2.349	2.193	2.286	3.71	1.866	1.917	2.010	2.282	2.160
34.30+	9.43	1.181	1.144	1.131	1.106	1.110	7.69	1.280	1.280	1.313	1.463	1.358
36.29+	11.42	1.282	1.269	1.269	1.246	1.249	1.72	1.917	2.033	2.153	2.403	2.373
39.28+	1.47	1.963	1.933	2.051	2.162	2.312	3.71	1.588	1.634	1.730	1.973	1.905

STREAMLINE S = 8.0 D = 0.625 (R-16); STREAMLINE S = 4.0 D = 0.625 (R-17)

RUN Z	R-16- X	A H/HO	B H/HO	C H/HO	D H/HO	E H/HO	R-17- X	A H/HO	B H/HO	C H/HO	D H/HO	E H/HO
1.49	0.00	1.158	1.148	1.158	1.168	1.109	0.00	1.184	1.169	1.172	1.169	1.155
5.41	0.00	1.077	1.043	1.001	0.945	0.868	0.00	1.090	1.047	1.003	0.938	0.859
9.42	0.00	1.063	1.029	0.978	0.884	0.812	0.00	1.073	1.029	0.974	0.867	0.791
13.40	2.40	1.368	1.379	1.430	1.543	1.643	0.00	1.061	1.021	0.968	0.844	0.752
17.41	6.41	1.110	1.090	1.075	1.073	1.064	0.00	1.056	1.017	0.967	0.849	0.734
22.17	3.20	1.398	1.420	1.467	1.586	1.694	0.00	1.047	1.013	0.964	0.849	0.728
25.34	6.37	1.146	1.126	1.114	1.116	1.108	0.00	1.076	1.042	0.995	0.888	0.761
29.32	2.39	1.465	1.483	1.541	1.672	1.749	3.14	1.318	1.322	1.346	1.462	1.532
33.30	6.37	1.153	1.133	1.121	1.129	1.118	3.20	1.277	1.271	1.294	1.409	1.539
34.30	7.37	1.163	1.141	1.133	1.137	1.135	0.29	1.336	1.351	1.409	1.561	1.693
35.30	0.35	1.322	1.263	1.302	1.322	1.304	1.29	1.769	1.781	1.854	2.000	2.079
36.29	1.34	1.686	1.700	1.776	1.929	2.010	2.28	1.507	1.517	1.576	1.732	1.843
37.28	2.33	1.403	1.417	1.466	1.596	1.635	3.27	1.367	1.372	1.411	1.532	1.618
38.28	3.33	1.255	1.256	1.299	1.383	1.437	0.32	1.323	1.351	1.327	1.604	1.713
39.28	4.33	1.197	1.186	1.206	1.253	1.276	1.32	1.686	1.695	1.744	1.934	1.961
40.28	5.33	1.174	1.154	1.163	1.185	1.188	2.32	1.444	1.459	1.507	1.686	1.776
41.20	6.25	1.149	1.130	1.125	1.139	1.124	3.24	1.341	1.344	1.377	1.499	1.590
45.27	2.36	1.388	1.413	1.485	1.632	1.683	3.36	1.313	1.324	1.362	1.478	1.562
49.22	6.31	1.159	1.142	1.144	1.165	1.149	3.39	1.313	1.315	1.340	1.446	1.507
53.26	2.39	1.420	1.437	1.499	1.629	1.701	7.43	1.135	1.111	1.088	1.096	1.075
57.28	6.41	1.191	1.165	1.153	1.157	1.126	11.45	1.121	1.091	1.053	1.007	0.927
62.47	11.60	1.190	1.145	1.109	1.048	0.951	16.64	1.190	1.130	1.088	1.020	0.902
34.30*	7.37	1.262	1.217	1.198	1.184	1.171	0.29	1.497	1.509	1.559	1.705	1.845
36.29*	1.34	1.871	1.853	1.911	2.013	2.063	2.28	1.665	1.650	1.674	1.800	1.873
39.28*	3.33	1.424	1.403	1.436	1.508	1.536	0.32	1.606	1.620	1.675	1.835	1.923
34.30+	7.37	1.185	1.154	1.146	1.130	1.105	0.29	1.302	1.327	1.378	1.529	1.629
36.29+	1.34	1.525	1.532	1.597	1.710	1.723	2.28	1.413	1.422	1.457	1.612	1.719
39.28+	3.33	1.265	1.253	1.280	1.335	1.385	0.32	1.342	1.364	1.419	1.580	1.675

STREAMLINE S = 4.0 D = 0.750 (R-20); STREAMLINE S = 12.0 D = 0.625 (R-21)

RUN Z	R-20- X	A H/HO	B H/HO	C H/HO	D H/HO	E H/HO	R-21- X	A H/HO	B H/HO	C H/HO	D H/HO	E H/HO
1.49	0.00	1.155	1.154	1.165	1.159	1.095	0.00	1.187	1.176	1.178	1.213	1.141
5.41	0.00	1.072	1.043	0.992	0.945	0.860	0.00	1.110	1.074	1.037	0.989	0.882
9.42	0.00	1.060	1.025	0.967	0.882	0.798	0.00	1.100	1.061	1.013	0.927	0.818
13.40	0.00	1.046	1.016	0.959	0.864	0.761	0.53	2.400	2.470	2.470	2.357	1.935
17.41	0.00	1.046	1.015	0.964	0.872	0.761	4.54	1.860	1.877	2.014	2.132	2.387
22.17	0.00	1.041	1.011	0.966	0.878	0.765	9.30	1.335	1.333	1.324	1.388	1.466
25.34	0.00	1.127	1.108	1.075	0.992	0.872	0.53	2.706	2.856	2.852	2.915	2.693
29.32	3.45	1.687	1.743	1.873	2.017	2.091	4.51	1.692	1.742	1.854	2.172	2.361
33.30	3.45	1.596	1.655	1.772	1.928	1.988	8.49	1.275	1.259	1.261	1.385	1.477
34.30	0.47	2.198	2.192	2.183	2.177	2.129	9.49	1.233	1.203	1.196	1.285	1.356
35.30	1.47	2.119	2.184	2.322	2.357	2.417	10.49	1.239	1.206	1.181	1.254	1.287
36.29	2.46	1.727	1.801	1.931	2.063	2.093	11.48	1.331	1.316	1.307	1.382	1.430
37.28	3.45	1.593	1.651	1.786	1.936	1.997	0.53	2.978	3.093	3.066	3.188	2.927
38.28	0.47	1.961	1.941	1.974	2.037	2.095	1.53	2.781	2.723	2.815	3.114	2.870
39.28	1.47	2.028	2.104	2.246	2.358	2.460	2.53	2.495	2.617	2.921	3.415	3.566
40.28	2.47	1.722	1.786	1.925	2.084	2.163	3.53	2.112	2.241	2.517	2.843	3.037
41.20	3.39	1.566	1.616	1.747	1.901	1.988	4.45	1.841	1.994	2.148	2.343	2.561
45.27	3.48	1.424	1.626	1.768	1.967	2.034	8.52	1.307	1.326	1.350	1.438	1.504
49.22	3.45	1.462	1.498	1.587	1.698	1.673	0.53	2.981	3.059	3.075	2.944	3.020
53.26	7.49	1.194	1.174	1.180	1.190	1.168	4.57	1.751	1.841	2.123	2.348	2.499
57.28	11.51	1.159	1.120	1.102	1.054	0.993	8.59	1.301	1.300	1.374	1.522	1.568
62.47	16.70	1.198	1.144	1.120	1.041	0.938	13.78	1.246	1.198	1.152	1.172	1.138
34.30*	0.47	2.068	1.992	1.981	1.981	1.960	9.49	1.309	1.276	1.258	1.326	1.430
36.29*	2.46	1.920	1.944	2.024	2.094	2.080	11.48	1.511	1.496	1.463	1.555	1.606
39.28*	0.47	2.138	2.044	2.025	1.988	1.989	1.53	3.374	3.752	3.926	4.133	4.038
34.30+	0.47	1.984	1.907	1.844	1.797	1.773	9.49	1.222	1.201	1.201	1.287	1.388
36.29+	2.46	1.632	1.687	1.814	1.964	2.026	11.48	1.391	1.393	1.407	1.499	1.578
39.28+	0.47	2.032	1.978	1.964	1.939	1.873	1.53	3.001	3.277	3.542	4.012	3.895

TABLE XIII (CONT'D)

STREAMLINE S = 8.0 D = 0.625

RUN Z	R-22- X	A H/HO	B H/HO	C H/HO	D H/HO	E H/HO
1.49	0.00	1.185	1.197	1.203	1.208	1.136
5.41	0.00	1.105	1.080	1.034	0.989	0.882
9.42	0.00	1.099	1.072	1.017	0.931	0.821
13.40	2.33	2.703	2.878	2.975	3.469	3.340
17.41	6.34	1.610	1.786	1.843	1.830	1.913
22.17	3.14	2.659	2.788	2.936	3.298	3.385
25.34	6.31	1.538	1.665	1.819	1.911	1.979
29.32	2.33	2.730	2.838	2.978	3.482	3.663
33.30	6.31	1.454	1.596	1.713	1.813	1.805
34.30	7.31	1.582	1.708	1.814	1.937	1.988
35.30	0.35	3.491	3.696	3.659	3.638	3.142
36.29	1.34	3.420	3.524	3.329	3.626	3.593
37.28	2.33	2.607	2.797	3.045	3.435	3.506
38.28	3.33	2.137	2.358	2.800	3.189	3.372
39.28	4.33	1.787	2.026	2.350	2.600	2.662
40.28	5.33	1.616	1.801	2.037	2.201	2.273
41.20	6.25	1.500	1.659	1.852	2.006	2.021
45.27	2.36	2.496	2.654	3.024	3.358	3.459
49.22	6.31	1.404	1.480	1.666	1.624	1.831
53.26	2.39	2.654	2.904	3.273	3.664	3.823
57.28	6.41	1.470	1.577	1.674	1.781	1.783
62.47	11.60	1.253	1.267	1.266	1.243	1.185
34.30*	7.31	1.584	1.697	1.792	1.889	1.930
36.29*	1.34	3.663	3.564	3.245	3.369	3.259
39.28*	3.33	2.433	2.698	2.985	3.298	3.393
34.30+	7.31	1.500	1.646	1.800	1.950	2.032
36.29+	1.34	3.067	3.206	3.188	3.548	3.582
39.28+	3.33	2.171	2.443	2.840	3.162	3.221

STREAMLINE S = 4.0 D = 0.625

RUN Z	R-23- X	A H/HO	B H/HO	C H/HO	D H/HO	E H/HO
1.49	0.00	1.177	1.187	1.195	1.171	1.115
5.41	0.00	1.089	1.068	1.017	0.942	0.842
9.42	0.00	1.076	1.049	0.993	0.882	0.785
13.40	0.00	1.061	1.031	0.980	0.863	0.755
17.41	0.00	1.062	1.025	0.984	0.868	0.756
22.17	0.00	1.056	1.023	1.003	0.870	0.755
25.34	0.00	1.171	1.139	1.147	1.125	1.186
29.32	3.33	3.102	3.190	3.463	3.756	4.598
33.30	3.33	2.893	2.892	3.006	3.377	3.902
34.30	0.35	3.993	3.870	3.612	2.511	2.193
35.30	1.35	4.135	4.024	4.151	3.839	3.657
36.29	2.34	3.483	3.480	3.517	4.028	4.175
37.28	3.33	2.922	2.867	3.109	3.419	3.850
38.28	0.35	3.876	3.759	3.420	2.849	2.694
39.28	1.35	3.743	3.711	3.888	4.044	3.724
40.28	2.35	3.320	3.306	3.461	3.877	4.257
41.20	3.27	2.916	2.851	3.142	3.464	3.874
45.27	3.36	2.693	2.616	2.916	3.012	3.597
49.22	3.33	2.591	2.526	2.711	2.760	3.156
53.26	7.37	1.484	1.488	1.567	1.639	1.732
57.28	11.39	1.271	1.240	1.252	1.255	1.288
62.47	16.58	1.274	1.210	1.188	1.115	1.095
34.30*	0.35	4.278	4.084	4.018	3.832	3.937
36.29*	2.34	3.858	3.698	3.774	4.036	4.175
39.28*	0.35	4.460	4.110	3.964	3.937	3.805
34.30+	0.35	3.330	3.247	3.184	3.247	3.314
36.29+	2.34	2.902	2.938	3.186	3.462	3.560
39.28+	0.35	3.431	3.288	3.225	3.460	3.613

DISKS S = 2.0 D = 0.750

RUN Z	R-26- X	A H/HO	B H/HO	C H/HO	D H/HO	E H/HO
1.49	0.00	1.152	1.162	1.163	1.177	1.116
5.41	0.00	1.065	1.034	0.957	0.941	0.851
9.42	0.00	1.052	1.017	0.926	0.878	0.789
13.40	0.00	1.042	0.999	0.924	0.854	0.756
17.41	0.00	1.042	0.998	0.939	0.862	0.751
22.17	0.00	1.037	0.990	0.939	0.861	0.751
25.34	0.00	1.061	1.016	0.969	0.891	0.779
29.32	0.09	3.521	4.244	3.923	3.506	3.698
33.30	0.09	3.122	4.105	4.217	4.114	4.007
34.30	1.09	2.751	2.795	3.089	2.794	2.883
35.30	0.10	2.240	2.346	2.691	2.484	2.551
36.29	1.09	2.133	2.246	2.465	2.767	2.943
37.28	0.09	3.253	3.676	4.240	4.053	4.150
38.28	1.09	2.377	2.433	2.586	2.627	2.821
39.28	0.10	3.080	3.806	4.077	4.202	4.058
40.28	1.10	2.613	2.648	2.853	2.863	2.923
41.20	0.03	2.508	2.748	3.129	3.461	3.585
45.27	0.12	3.028	3.561	3.784	3.891	3.926
49.22	2.08	1.992	2.214	2.264	2.288	2.344
53.26	6.12	1.324	1.371	1.390	1.437	1.409
57.28	10.14	1.198	1.185	1.166	1.172	1.116
62.47	15.33	1.213	1.186	1.141	1.081	0.985
34.30*	1.09	3.507	3.930	3.748	3.432	3.265
36.29*	1.09	2.554	2.743	3.030	3.256	3.292
39.28*	1.09	3.172	3.568	3.613	3.349	3.168
34.30+	1.09	2.869	3.182	3.301	2.891	2.724
36.29+	1.09	2.180	2.394	2.681	2.790	2.874
39.28+	1.09	2.834	3.030	3.232	2.767	2.960

DISKS S = 8.0 D = 0.750

RUN Z	R-27- X	A H/HO	B H/HO	C H/HO	D H/HO	E H/HO
1.49	0.00	1.180	1.182	1.204	1.194	1.127
5.41	0.00	1.088	1.043	1.006	0.964	0.856
9.42	0.00	1.074	1.026	0.973	0.895	0.791
13.40	0.00	2.104	2.106	2.230	2.394	2.653
17.41	3.98	2.006	2.083	2.237	2.467	2.570
22.17	0.78	2.916	2.980	3.232	3.122	3.393
25.34	3.95	1.955	1.883	2.188	2.316	2.418
29.32	7.93	2.787	2.587	3.133	3.247	3.307
33.30	3.95	1.911	1.819	2.089	2.216	2.366
34.30	4.95	1.799	1.623	1.856	2.006	2.147
35.30	5.95	1.707	1.560	1.700	1.892	1.962
36.29	6.94	1.590	1.409	1.563	1.748	1.793
37.28	7.93	2.864	2.487	2.729	3.176	2.808
38.28	0.97	2.417	2.470	2.595	2.770	3.193
39.28	1.97	2.031	2.255	2.500	2.395	2.630
40.28	2.97	1.924	2.028	2.162	2.078	2.244
41.20	3.89	1.816	1.833	1.911	1.909	2.004
45.27	7.96	1.990	1.977	2.129	2.388	2.696
49.22	3.95	1.550	1.512	1.673	1.509	1.577
53.26	0.03	1.934	1.909	1.964	2.175	2.347
57.28	4.05	1.422	1.540	1.554	1.547	1.515
62.47	9.24	1.304	1.277	1.241	1.246	1.216
34.30*	4.95	1.974	1.838	2.096	2.162	2.309
36.29*	6.94	1.754	1.541	1.714	1.893	1.926
39.28*	0.97	3.419	3.219	3.311	3.328	3.475
34.30+	4.95	1.823	1.685	1.941	2.007	2.118
36.29+	6.94	1.542	1.401	1.606	1.770	1.845
39.28+	0.97	2.524	2.715	2.697	2.725	2.606

DISKS S = 2.0 D = 0.625

RUN Z	R-24- X	A H/HO	B H/HO	C H/HO	D H/HO	E H/HO
1.49	0.00	1.157	1.182	1.158	1.170	1.115
5.41	0.00	1.068	1.062	0.974	0.937	0.842
9.42	0.00	1.062	1.041	0.943	0.868	0.781
13.40	0.00	1.081	1.074	0.993	0.901	0.807
17.41	0.00	1.055	1.033	0.950	0.897	0.785
22.17	0.00	1.035	1.015	0.924	0.852	0.765
25.34	0.00	1.056	1.036	0.957	0.862	0.764
29.32	1.96	2.431	2.730	2.926	2.919	3.041
33.30	1.96	2.381	2.562	2.662	2.782	2.710
34.30	0.97	2.082	2.145	2.118	2.165	2.420
35.30	1.97	2.383	2.650	2.649	2.778	2.736
36.29	0.97	2.116	2.191	2.136	2.159	2.377
37.28	1.96	2.243	2.530	2.527	2.659	2.701
38.28	0.97	1.995	2.092	2.060	2.128	2.308
39.28	1.97	2.204	2.383	2.366	2.432	2.616
40.28	0.98	2.003	2.100	2.070	2.136	2.211
41.20	1.90	2.035	2.258	2.309	2.450	2.697
45.27	1.99	2.041	2.222	2.157	2.280	2.396
49.22	1.96	1.678	1.771	1.714	1.768	1.726
53.26	6.00	1.266	1.267	1.234	1.249	1.218
57.28	10.02	1.185	1.158	1.112	1.100	1.038
62.47	15.21	1.216	1.177	1.108	1.057	0.968
34.30*	0.97	2.443	2.512	2.487	2.380	2.372
36.29*	0.97	2.330	2.429	2.392	2.378	2.402
39.28*	0.97	2.377	2.500	2.434	2.353	2.366
34.30+	0.97	2.178	2.164	2.107	2.118	2.042
36.29+	0.97	2.141	2.208	2.155	2.162	2.141
39.28+	0.97	2.132	2.220	44444	2.151	2.119

DISKS S = 2.0 D = 0.875

RUN Z	R-25- X	A H/HO	B H/HO	C H/HO	D H/HO	E H/HO
1.49	0.00	1.197	1.190	1.179	1.171	1.108
5.41	0.00	1.077	1.054	0.998	0.943	0.861
9.42	0.00	1.062	1.037	0.968	0.878	0.800
13.40	0.00	1.050	1.024	0.956	0.845	0.752
17.41	0.00	1.052	1.025	0.961	0.851	0.743
22.17	0.00	1.049	1.021	0.983	0.850	0.741
25.34	0.00	1.067	1.037	0.978	0.872	0.765
29.32	0.00	1.068	1.040	0.981	0.880	0.780
33.30	1.65	4.041	4.481	4.729	5.304	5.584
34.30	0.66	4.392	4.367	4.024	3.827	3.849
35.30	1.66	3.660	3.760	4.258	4.975	4.811
36.29	0.66	4.794	4.743	4.174	4.014	4.068
37.28	1.65	3.719	3.630	4.084	5.066	5.177
38.28	0.66	4.404	4.591	4.080	3.968	4.013
39.28	1.66	3.834	3.957	4.756	5.240	5.551
40.28	0.67	4.307	4.375	3.831	3.838	3.902
41.20	1.59	3.327	3.272	3.843	4.028	4.326
45.27	1.68	3.516	3.578	4.104	4.500	4.994
49.22	3.64	1.801	1.788	1.870	2.071	2.140
53.26	7.68	1.300	1.270	1.257	1.297	1.294
57.28	11.70	1.193	1.153	1.123	1.081	1.038
62.47	16.89	1.224	1.169	1.135	1.040	0.935
34.30*	0.66	6.067	5.648	5.250	4.980	4.867
36.29*	0.66	5.917	5.673	5.622	5.207	5.091
39.28*	0.66	6.194	5.749	5.702	5.334	5.057
34.30+	0.66	4.397	4.563	4.504	4.473	4.216
36.29+	0.66	4.518	4.697	5.022	5.224	5.224
39.28+	0.66	4.461	4.658	4.959	5.077	5.057

PLAIN ROD IN CENTER D = 0.625

RUN Z	R-28-	A H/HO	B H/HO	C H/HO	D H/HO	E H/HO
1.49		1.832	1.778	1.710	1.596	1.389
5.41		1.754	1.662	1.480	1.277	0.940
9.42		1.734	1.649	1.455	1.179	0.810
13.40		1.723	1.648	1.483	1.171	0.723
17.41		1.707	1.642	1.487	1.227	0.665
22.17		1.700	1.640	1.492	1.242	0.626
25.34		1.737	1.680	1.535	1.286	0.624
29.32		2.202	2.164	2.114	1.965	1.258
33.30		1.840	1.805	1.727	1.642	1.356
34.30		1.816	1.737	1.652	1.558	1.301
35.30		1.828	1.862	1.623	1.490	1.273
36.29		1.799	1.707	1.586	1.449	1.217
37.28		1.785	1.718	1.575	1.411	1.168
38.28		1.723	1.631	1.515	1.345	1.108
39.28		1.729	1.634	1.525	1.340	1.161
40.28		1.739	1.651	1.547	1.353	1.075
41.20		1.716	1.655	1.536	1.333	1.041
45.27		1.698	1.666	1.564	1.373	0.936
49.22		1.738	1.704	1.607	1.433	0.899
53.26		1.760	1.734	1.643	1.481	0.899
57.28		1.810	1.781	1.688	1.533	0.943
62.47		1.964	1.915	1.812	1.648	1.049
34.30*		2.116	2.005	1.892	1.662	1.086
36.29*		2.095	1.965	1.835	1.638	1.228
38.28*		2.077	1.945	1.811	1.611	1.297
34.30+		1.816	1.742	1.694	1.610	1.351
36.29+		1.767	1.684	1.599	1.469	1.229
38.28+		1.767	1.699	1.600	1.432	1.159

PLAIN ROD IN CENTER D = 0.750

RUN Z	R-29- X	A H/HO	B H/HO	C H/HO	D H/HO	E H/HO
1.49		2.470	2.394	2.282	2.100	1.763
5.41		2.407	2.305	2.110	1.716	1.196
9.42		2.381	2.288	2.108	1.697	1.036
13.40		2.394	2.308	2.150	1.788	1.029
17.41		2.350	2.280	2.142	1.803	1.117
22.17		2.452	2.377	2.239	1.917	1.211
25.34		2.504	2.433	2.289	1.980	1.244
29.32		2.728	2.643	2.470	2.231	1.470
33.30		2.604	2.527	2.395	2.285	1.926
34.30		2.542	2.462	2.309	2.124	1.803
35.30		2.559	2.485	2.301	2.061	1.706
36.29		2.529	2.466	2.308	2.017	1.605
37.28		2.536	2.484	2.311	2.019	1.535
38.28		2.417	2.370	2.252	1.943	1.438
39.28		2.436	2.393	2.273	1.965	1.398
40.28		2.487	2.442	2.315	1.999	1.383
41.20		2.461	2.409	2.282	1.997	1.351
45.27		2.502	2.387	2.265	2.013	1.266
49.22		2.555	2.434	2.314	2.091	1.351
53.26		2.556	2.433	2.324	2.116	1.510
57.28		2.639	2.503	2.385	2.182	1.642
62.47		2.820	2.741	2.584	2.383	1.805
34.30*		3.048	2.931	2.674	2.345	1.904
36.29*		3.026	2.905	2.648	2.250	1.707
38.28*		3.031	2.919	2.676	2.269	1.613
34.30+		2.422	2.381	2.260	2.038	1.667
36.29+		2.440	2.401	2.275	1.999	1.572
38.28+		2.488	2.450	2.334	2.055	1.518

APPENDIX D

CALCULATIONS REQUIRED FOR EXAMPLE HEAT EXCHANGER DESIGN

The specified data were

$$W = 250{,}000 \text{ lb}_m/\text{hr}$$

$$Q = 10{,}000{,}000 \text{ BTU/hr}$$

$$\Delta T_m = 100 \text{ deg. F}$$

$$h' = 3000 \text{ BTU/hr - deg. F - ft}^2$$

$$C_F = 2.28 \times 10^{-3} \text{ dollars/ft}^{1.2} \text{ - hr}$$

$$C_E = 4.88 \times 10^{-7} \text{ dollars/BTU}$$

$$c = 1 \text{ BTU/lb}_m \text{ - deg. F}$$

$$\rho = 62.4 \text{ lb}_m/\text{ft}^3$$

$$k = 0.353 \text{ BTU/hr - deg. F - ft}$$

$$\mu = 2.42 \text{ lb}_m/\text{ft - hr}$$

Unless otherwise specified, all calculations will be made for a tube diameter of one inch. Values of calculated quantities corresponding to other diameters may be obtained by ratios.

$$Pr = \frac{c\mu}{k} = \frac{1 \times 2.42}{0.353} = 6.8555 \qquad (82)$$

$$Pr^{1/3} = 1.8995 \qquad (D\text{-}1)$$

Factors Needed to Calculate Fixed Cost

$$\frac{D}{k\,\Delta T_m} = \frac{1}{12 \times 0.353 \times 100} \qquad (D\text{-}2)$$

$$= 2.3607 \times 10^{-3} \text{ (BTU/hr ft}^2)^{-1}$$

$$\left[\frac{D}{k\,\Delta T_m}\right]^{0.6} = 2.6535 \times 10^{-2} \text{ (BTU/hr - ft}^2)^{-0.6} \qquad (D\text{-}3)$$

$$B_2 = (h' \, D/k)^{-1} \tag{113}$$

$$= \frac{0.353 \times 12}{3000 \times 1} \tag{D-4}$$

$$= 1.4120 \times 10^{-3}$$

$$Q^{1-m} = (10{,}000{,}000)^{0.4}$$

$$= 630.96 \; (BTU/hr)^{0.4} \tag{D-5}$$

$$\text{Fixed Cost} = \frac{C_F \; (D/k \; \Delta T_m)^m \; [1 + B_2 \; Nu]^m}{Q^{1-m} \; Nu^m} \tag{D-6}$$

$$\text{Fixed Cost} = \frac{(2.28 \times 10^{-3})(2.6535 \times 10^{-2})(1 + 1.4120 \times 10^{-3} Nu)^{0.6}}{(630.96) \; Nu^{0.6}} \tag{D-7}$$

For D = 1 $$\text{Fixed Cost} = \frac{0.98855 \times 10^{-7} \; (1 + 1.4120 \times 10^{-3} \; Nu)^{0.6}}{Nu^{0.6}} \tag{D-8}$$

For D = 0.5 $$\text{Fixed Cost} = \frac{0.63256 \times 10^{-7} \; (1 + 2.8240 \times 10^{-3} \; Nu)^{0.6}}{Nu^{0.6}} \tag{D-9}$$

For D = 0.25 $$\text{Fixed Cost} = \frac{0.41731 \times 10^{-7} \; (1 + 5.6480 \times 10^{-3} \; Nu)^{0.6}}{Nu^{0.6}} \tag{D-10}$$

The preceeding three equations were used to plot the fixed cost curves in Figure 48. The second equation was also used to plot the fixed cost in Figure 49.

The limiting fixed cost for $B_2 Nu >> 1$ was calculated as follows

$$\text{Limiting Fixed Cost} = \frac{C_F}{Q^{1-m} \; (h' \; \Delta T_m)^m} \tag{D-11}$$

$$= \frac{(2.28 \times 10^{-3})}{(630.96)(3000 \times 100)^{0.6}} \tag{D-12}$$

$= 1.8692 \times 10^{-9}$ (dollars/BTU)

Factors Needed to Calculate Pumping Cost for Empty Tube Geometry

$$f = C_1 \, Re^{-n_1} \qquad (81)$$

$$Nu = C_2 \, Re^{n_2} \, Pr^{1/3} \qquad (80)$$

$C_1 = 0.079$; $C_2 = 0.027$; $n_1 = 0.250$; $n_2 = 0.80$

$$p = \frac{3 - n_1}{n_2} = \frac{3 - 0.25}{0.80} = 3.4375 \qquad (111)$$

$$B_1 = \frac{C_1}{2\,(C_2)^p} = \frac{0.079}{2\,(0.027)^{3.4375}} = 0.97453 \times 10^4 \qquad (112)$$

$$B_3 = \frac{\mu^2}{J_c \, g_c \, \rho^2 \, D^2 \, c \, \Delta T_m} \qquad (114)$$

$$= \frac{(2.42/3600)^2}{(777.5)(32.2)(62.4)^2 \, (1/12)^2 \, (1)(100)} \qquad (D\text{-}13)$$

$$= 6.675 \times 10^{-15}$$

$$Pr^{(p/3-1)} = (6.8555)^{0.14583} = 1.3241 \qquad (D\text{-}14)$$

$$\text{Pumping Cost} = \frac{C_E \, B_1 \, Nu^{p-1} \, (1 + B_2 \, Nu) \, B_3}{Pr^{(p/3-1)}} \qquad (D\text{-}15)$$

$$\text{Pumping Cost} = (4.88 \times 10^{-7})(0.97453 \times 10^4) \, Nu^{2.4375}$$

$$\times \frac{(1 + 1.4120 \times 10^{-3} \, Nu) \times 6.675 \times 10^{-15}}{1.3241} \qquad (D\text{-}16)$$

For D = 1.0 $\quad$ Pumping Cost $= 2.3275 \times 10^{-17} Nu^{2.4375} (1 + 1.4120 \times 10^{-3} \, Nu)$ (D-17)

For D = 0.5 Pumping Cost = $9.5900 \times 10^{-17}\ Nu^{2.4375}\ (1 + 2.8240 \times 10^{-3}\ Nu)$ (D-18)

For D = 0.25 Pumping Cost = $38.360 \times 10^{-17} Nu^{2.4375}\ (1 + 5.6480 \times 10^{-3}\ Nu)$ (D-19)

The preceding equations were used to plot the pumping cost curves in Figure 48; the second equation was used to plot the pumping cost for the empty tube in Figure 49.

Factors Needed to Calculate Design Parameters from Optimum Nusselt Numbers

$$N_{tube} = \frac{4\ W\ (C_2\ Pr^{1/3})^{1/n_2}}{\mu\ \pi\ D\ Nu^{1/n_2}} \quad (120)$$

$$= \frac{(4)(250{,}000)(0.027 \times 1.8995)^{1.25}}{(2.42)(3.14159)(D/12)\ Nu^{1.25}} \quad (D\text{-}20)$$

$$= \frac{0.38522 \times 10^5}{D\ Nu^{1.25}} \quad (D\text{-}21)$$

For D = 1 $\quad N_{tube} = \frac{0.38522 \times 10^5}{(1)(600)^{1.25}} = 13$ (D-22)

For D = 0.5 $\quad N_{tube} = \frac{0.38522 \times 10^5}{(0.5)(330)^{1.25}} = 55$ (D-23)

For D = 0.25 $\quad N_{tube} = \frac{0.38522 \times 10^5}{(0.25)(175)^{1.25}} = 241$ (D-24)

$$L = \frac{Q\ \mu\ D}{4\ W\ k\ \Delta T_m}\ \frac{[1 + Nu/(h'D/k)]}{(C_2\ Pr^{1/3})^{1/n_2}}\ Nu^{(1/n_2 - 1)} \quad (122)$$

$$L = \frac{(10^7)(2.42)(D/12)}{(4)(250{,}000)(0.353)(100)}\ \frac{[1 + Nu/(0.353/3000\ D)]}{(0.027 \times 1.8995)^{1.25}}\ Nu^{0.25} \quad (D\text{-}25)$$

$$= 2.3408\ D\ (1 + 1.4120 \times 10^{-3}\ Nu)\ Nu^{0.25} \quad (D\text{-}26)$$

For D = 1 $L = 2.3408 \times 1 \times (1 + 1.4120 \times 10^{-3} \times 600) \times (600)^{0.25}$ (D-27)

$= 21.4$ ft.

For D = 0.5 L = 9.6 ft. (D-28)

For D = 0.250 L = 4.2 ft. (D-29)

Factors Needed to Evaluate Turbulence Promoting Geometries

All factors are for D = 0.50 inch

Pumping Cost

Geometry I Disks d = 0.625 s = 4

$C_1 = 0.06724;\ C_2 = 0.17134;\ n_1 = -0.0425;\ n_2 = 0.6941$

$$p = \frac{3 + 0.0425}{0.6941} = 4.3834 \quad \text{(D-30)}$$

$$B_1 = \frac{0.06724}{2(0.17134)^{4.3834}} = 0.76717 \times 10^2 \quad \text{(D-31)}$$

$$Pr^{(p/3-1)} = (6.8555)^{0.46113} = 2.4295 \quad \text{(D-32)}$$

Geometry II Disks d = 0.875 s = 8

$C_1 = 0.72954;\ C_2 = 0.22708;\ n_1 = -0.0066;\ n_2 = 0.6888$

$$p = \frac{3 + 0.0066}{0.6888} = 4.3650 \quad \text{(D-33)}$$

$$B_1 = \frac{0.72954}{2\ (0.22708)^{4.3650}} = 2.362 \times 10^2 \quad \text{(D-34)}$$

$$Pr^{(p/3-1)} = (6.8555)^{0.4550} = 2.4699 \quad \text{(D-35)}$$

For Geometry I

$$\text{Pumping Cost} = 4.1144 \times 10^{-19}\ Nu^{3.3834}\ (1 + 2.8240 \times 10^{-3}\ Nu) \quad \text{(D-36)}$$

This equation was used to plot the pumping cost curve in Figure 49.

$$N_{tube} = \frac{5.175 \times 10^5}{Nu^{1.4407}} \quad \text{(D-37)}$$

$$= \frac{5.175 \times 10^5}{(300)^{1.4407}} = 142.6 \quad \text{(D-38)}$$

$$L = 0.17424 \ (1 + 2.8240 \times 10^{-3} \ Nu) \ Nu^{0.4407} \quad \text{(D-39)}$$

$$= 0.17424 \ (1 + 2.8240 \times 10^{-3} \times 300)(300)^{0.4407} \quad \text{(D-40)}$$

$$= 3.958 \text{ ft.}$$

For Geometry II

$$\text{Pumping Cost} = 12.461 \times 10^{-19} \ Nu^{3.3650}(1 + 2.8240 \times 10^{-3} \ Nu) \quad \text{(D-41)}$$

This equation was used to plot the pumping cost curve in Figure 49.

$$N_{tube} = \frac{4.7025 \times 10^5}{Nu^{1.4518}} \quad \text{(D-42)}$$

$$= \frac{4.7025 \times 10^5}{(245)^{1.4518}} = 158.8 \quad \text{(D-43)}$$

$$L = 0.19172 \ (1 + 2.8240 \times 10^{-3} \ Nu) \ Nu^{0.4518} \quad \text{(D-44)}$$

$$= 0.19172 \ (1 + 2.8240 \times 10^{-3} \times 245) \ (245)^{0.4518} \quad \text{(D-45)}$$

$$= 3.859 \text{ ft.}$$